UNIVERSITY OF NAIROBI

PETROLOGY AND IRON ORE MINERALIZATION IN THE NEOPROTEROZOIC MOZAMBIQUE BELT ROCKS OF MUTOMO – IKUTHA AREA, KITUI COUNTY, S.E. KENYA.

BY

AARON KUTUKHULU WASWA

REG. I80/83941/2012

A THESIS SUBMITTED IN FULFILLMENT FOR THE REQUIREMENT FOR THE AWARD OF THE DEGREE OF DOCTOR OF PHILOSOPHY IN GEOLOGY OF THE UNIVERSITY OF NAIROBI

NOVEMBER 2015

Declaration

I declare that this thesis is my original work and has not been submitted elsewhere for examination, award of degree or publication. Where other people's work or my own work has been used, this has been properly acknowledged and referenced in accordance with the University of Nairobi's requirements.

Signature ……Date……

Aaron Kutukhulu Waswa

I80/83941/2012

Department of Geology

School of Physical Sciences

University of Nairobi.

This thesis is submitted for examination with our approval as research Supervisors:

	Signature	Date
1. Dr. Christopher M. Nyamai Department of Geology University of Nairobi P.O. BOX 30197-00100, Nairobi, Kenya cnyamai@uonbi.ac.ke.	……	……
2. Prof. Eliud M. Mathu Department of Geological Sciences South Eastern Kenya University (SEKU) P.O. BOX 170-90200 Kitui emathu@seku.ac.ke	……..	……..
3. Dr. Daniel W. Ichang'i Department of Geology University of Nairobi P.O. BOX 30197-00100, Nairobi, Kenya dichangi@uonbi.ac.ke	…….	……

Appendix I Declaration Form for Students

UNIVERSITY OF NAIROBI

Declaration of Originality Form

This form must be completed and signed for all works submitted to the University for Examination.

Name of Student: AARON KUTUKHULU WASWA

Registration Number: I80/83941/2012

College: BIOLOGICAL AND PHYSICAL SCIENCES

Faculty/School/Institute: SCHOOL OF PHYSICAL SCIENCES

Department: GEOLOGY

Course Name: Ph.D. in Geology

Title of the work: PETROLOGY AND IRON ORE MINERALIZATION IN THE NEOPROTEROZOIC MOZAMBIQUE BELT ROCKS OF MUTOMO – IKUTHA AREA, KITUI COUNTY, S.E. KENYA.

DECLARATION

1. I understand what Plagiarism is and I am aware of the University's policy in this regard

2. I declare that this _____ (Thesis, project, essay, assignment, paper, report, etc.) is my original work and has not been submitted elsewhere for examination, award of a degree or publication. Where other people's work, or my own work has been used, this has properly been acknowledged and referenced in accordance with the University of Nairobi's requirements.

3. I have not sought or used the services of any professional agencies to produce this work

4. I have not allowed, and shall not allow anyone to copy my work with the intention of passing it off as his/her own work

5. I understand that any false claim in respect of this work shall result in disciplinary action, in accordance with University Plagiarism Policy.

Signature _____

Date _____

Dedication

Dedicated to my beloved Father Willington Kutukhulu and My Mother Rebecca Kutukhulu

Acknowledgement

I wish to thank our Almighty God for the care, knowledge and wisdom He granted me during the entire time of this research.

I am greatly indebted to my supervisors; Dr. Christopher M. Nyamai, Prof. Eliud M. Mathu and Dr. Daniel W. Ichang'i who constantly followed this work and for their invaluable advice, encouragement, and useful criticisms. I express my gratitude to them for sparing their time to read this thesis and suggesting useful comments, and above all their sense of humor and understanding. I also express my profound gratitude to the Chairman of the department of geology and the entire teaching staff for their support and encouragement during my research. My special gratitude goes to Dr. Franziska Wilke, Potsdam University for analyzing some of the samples. I also wish to thank Brucker Elemental Company for providing me with mobile XRF machine through Dr. Lydia Olaka. It is with pleasure and gratitude that I thank the University of Nairobi to have given me a fee waiver for my doctorate studies. I wish to appreciate the hospitality and effective services of the technical and administrative staff without singling out names, of the Department of Geology at the University of Nairobi, Mines and Geology (the ministry of Mining) and the institute of Nuclear science in the University of Nairobi.

I also wish to thank the district commissioners of both Mutomo and Ikutha and the local chiefs for their kind support during the fieldwork.

I wish to acknowledge my parents "the KUTUKHULUS" and my wife Stela for their encouragement and prayers. As ever, the major inspiration and encouragement comes from my daughters; Miriam, Grace, and Martha. Their encouragement, understanding, and patience, even during hard times, is highly appreciated.

May the good Almighty God abundantly bless whoever participated directly or indirectly to the success of my research and compilation of this thesis.

Abstract

The research area, which occurs within the Neoproterozoic Mozambique belt (NMB) in Kenya, is located in Mutomo-Ikutha area, in South Kitui district, Kitui County. The study area is bounded by longitudes 38° 04′E to 38°20′E and latitudes 1°48′S to 2°10′S. The area can be accessed from the Nairobi-Thika-Kitui/ Nairobi-Machakos-Kitui roads, or from Nairobi – Mombasa Road –Kibwezi – Ikutha-Mutomo road. An enigmatic problem within the polyphase and highly deformed NMB is lack of better understanding of the geology, tectonic structures and metamorphism that affected the formation, occurrence and genesis of the iron ore deposits and other related minerals in the study area. In order to decipher the aforementioned problem, this study undertook a geological, geochemical and geophysical study with the aim of having a better understanding of the petrology, tectono-metamorphic setting, genesis and distribution of iron ore deposits and related mineralization in the study area.

Ground magnetic and geochemical surveys were carried out to establish the spatial distribution and potential reserves of iron deposits in the study area. Investigation using remote sensed data has established prevalent geological structures, lithology and mineral alteration zones. This study has provided a comprehensive understanding of the tectono-thermal scenario and its associated economic mineralization. One of the key findings of this study is the realization that Mutomo–Ikutha gneisses and migmatites represent a thick sequence of meta-sedimentary rocks. The entire protolith sequence was marked by the alternation of thin pelitic, psammitic and limey layers, together with minor thin basic meta-volcanic rocks that were deposited under deep marine conditions. The entire paragneissic sequence was subsequently subjected to multiple phases of successive deformation and metamorphism, which was accompanied by shearing, faulting and folding. Three phases of folding (F_1, F_2 and F_3) were accompanied by medium- to high-grade amphibolite-facies metamorphic conditions. The mean attitude of F_1 hinges plunges between 10^0 and 25^0 to N320^{0}W, F_2 plunges between 12^0 and 70^0 to S140^{0}E, and F_3 plunges 15^0 and 25^0 to 270^{0}W. From these data, it is apparent that the F_1 and F_2 had dominantly NW–SE striking axial surfaces, with gently plunging hinges, whereas the superimposed F_3 folds generally have W-E orientations. The geometrical relationships between D_1 and D_2 structures suggest that the Mutomo – Ikutha structures were mainly developed in response to a NE–SW compressional stress regime. The deformation sequence (D_1, D_2 and D_3) clearly indicate that the iron mineralization in Mutomo–Ikutha was controlled by tectonics and high-grade metamorphism. Shearing of the hornblende gneiss host rocks took place during the D_3 episode where the main reef of iron deposition took place during D_3 deformation phase. The iron ore deposit is structurally controlled by shear zone and is hosted in the hornblende gneiss. Shearing along the western part of the area, especially within Tiva gneisses created room for iron ore deposition.

Metamorphism affected iron formation in two ways. Two sets of metamorphism (M_1 and M_2) took place in Mutomo – Ikutha area. Iron mineralization took place during M_1 as evidenced by the replacement of hornblende by iron. M_1 resulted from the collision of East and West Gondwanaland that was accompanied by magmatism and hydrothermal processes. Iron ore formed during M_1 episode from late stage magmatism and hydrothermal process. Two sets of metasomatism took place in the area. The first metasomatism led to the formation of calc – silicates while the second set of metasomatism led to the formation of iron in pegmatites. Petrographic evidence have shown the occurrence of the iron ore deposit in Mutomo – Ikutha

area to be associated with the rocks whose mineral assemblage is of Hornblende + Quartz + Biotite + Magnetite + Apatite ± Plagioclase. Petrological studies have shown that Mutomo–Ikutha area occurs in an ophiolitic suite and mimics similar lithological and geochemical signatures as those reported in other ophiolite suites occurring in Kenya like in Moyale, Sekerr in West Pokot and in Voi, SE Kenya. The field occurrence of this suite has been documented by the lithological and stratigraphic sequence of serpentinite, sheeted dykes, gabbro, limestone and remnants of pillow lava found in the type area. The field occurrence of this suite is an indication of the remnants of the obducted oceanic crust during the closure of the palaeo-Mozambique Ocean and collision of the East and West Gondwanaland.

Geochemical evidence indicate that the iron ore deposit of Mutomo – Ikutha area contain between 48 – 93 % Fe_2O_3, 0.2-5.9% P_2O_5, 0.05 – 1.9 % TiO_2 and 0.007% - 1.3% V. The characteristic chemical signatures of Ikutha deposits closely resemble the Apatite – Iron ores of the Kiruna type. The Fe_2O_3 has positive Pearson correlation of 0.59 with P_2O_5 and shows negative correlation with other elements found within the host rock. This shows that the mode of delivery of the two elements into the area were similar. Fe_2O_3 and P_2O_5 are interpreted to have been introduced into the area through hydrothermal/ magmatic fluids.

The iron ore deposits in Ikutha area cover an area of 5 sq km with a reserve tonnage of 250 million tons of magnetite. Besides the occurrence of iron ore deposits in the study area, this study has also established the presence of other minerals of economic importance like manganese, garnets, copper, magnesite, graphite and marbles. It is envisaged that mining and subsequent beneficiation of these minerals will bring a great economic growth in Kitui County and the country as a whole. This study recommends that drilling works should be done to establish the actual tonnage and quality of the iron deposits.

TABLE OF CONTENTS

List of tables

List of figures

CHAPTER 1

CHAPTER 2

CHAPTER 3

CHAPTER 4

CHAPTER 5

List of papers published in peer reviewed journals

List of appendices

List of acronyms, symbols and initials

2D.....Two dimensional

3D.....Three dimensional

AAS.....Atomic absorption spectrophotometer

ANS.....Arabian Nubian Shield

Ar .....Argon

BIF .....Banded iron formation

By.....Billion Years

D1.....Deformation 1

D2.....Deformation 2

D3.....Deformation 3

DEM.....Digital elevation model

DN.....Digital Number

EMBS .....Eastern Mozambique belt segment

ENE.....East North East

F1 .....Folding 1

F2 .....Folding 2

F3 .....Folding 3

GIS .....Geographical Information system

IGRF .....International geomagnetic reference field

IOCG.....Iron ore ±copper,gold

ISSC .....International Subcomission on Stratigraphic Classification

IUGS .....International Union of the Geological Sciences

K.....Potassium

M1.....Metamorphic 1

M2.....Metamorphic 2

Ma .....Million years

NACSN.....North American Commission on Stratigraphic Nomenclature

NNW .....North North West

NW .....Northwestern

NWMBS .....Northwestern Mozambique belt segment

P1 .....Principle analysis 1

P2 .....Principle analysis 2

P3 .....Principle analysis 3

SEDEX.....Sedimentary exhalative

SSE.....South South East

SWMBS .....Southwestern Mozambique belt segment

USGS .....United States geological society

W .....West

WSW.....West south west

XRF.....X –ray florescence

Hbl.....Hornblende

% .....Percentage

< .....Less than

TAS.....Total alkali – silica

T .....Total anomalous field magnetic anomaly

SI.....Structural index

CHAPTER ONE: INTRODUCTION

1.1 BACKGROUND INFORMATION

Industrialization is one of the economic pillars in the Kenya Vision 2030 (Government of Kenya, 2007). The *Kenya Vision 2030* is the country's new development blueprint covering the period 2008 – 2030. It aims to transform Kenya into a newly industrializing, "middle-income country providing a high quality life to all its citizens by the year 2030". The Vision was developed through an all-inclusive and participatory stakeholder consultative process. In order to achieve this vision, iron and associated steel products will play a prominent role in the industrialization process. Currently, Kenya relies heavily on the importation of manufactured goods with iron and steel products forming some of the bulk of the raw materials. World production statistics (USGS, 2013) shows that China was the leading Iron ore produced in 2013 (Figure 1.1).

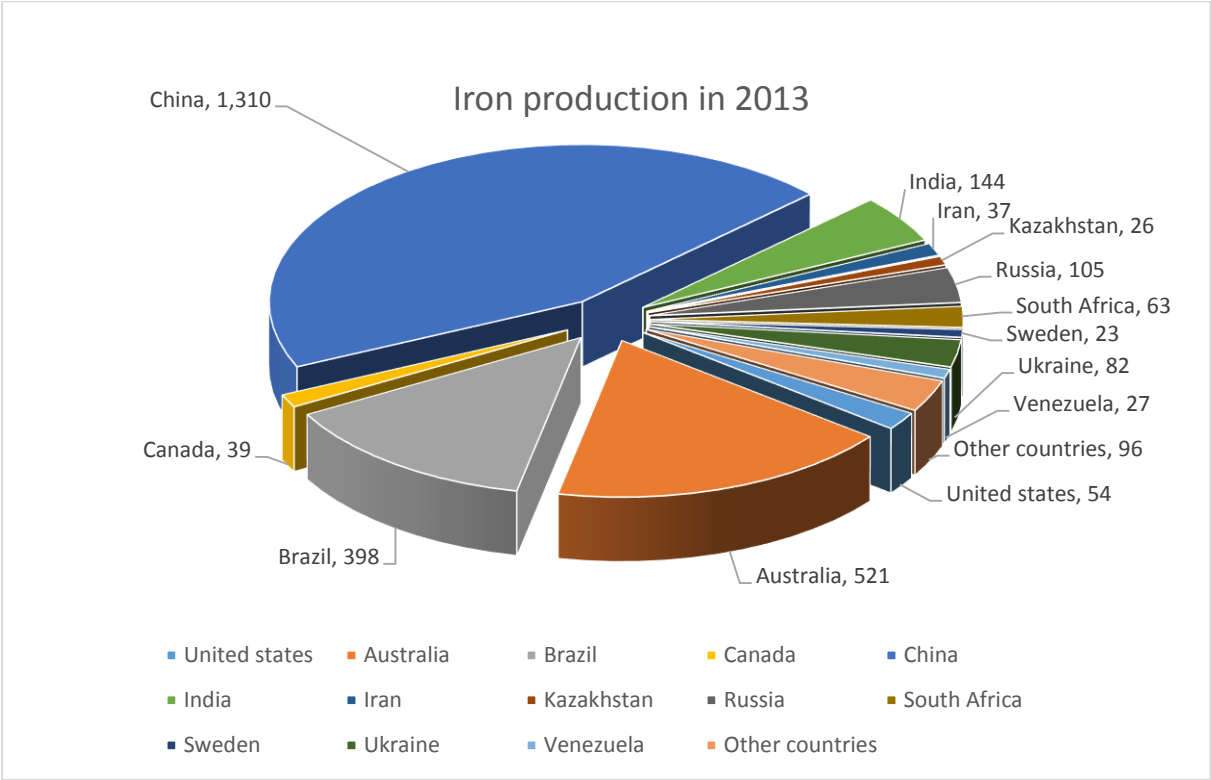

Figure 1.1: Global iron ore production statistics for the year 2013 in million metric tons (adopted from USGS, 2013**).**

Mineral deposits in Kenya occur in different geological settings. Although some economic deposits are associated with Paleocene rocks (e.g. fluorite, diatomite, barite, galena, oil and gas etc.) and the Archaean craton (gold, copper, nickel etc.), most of the deposits located within the Kenyan Neoproterozoic Mozambique Orogenic Belt (gemstones, marble, wollastonite, iron ore, graphite) have not been adequately studied and evaluated. In order to more readily study mineral deposits and explore them more effectively, it is helpful to first subdivide them into categories. This subdivision, or classification, can be based on a number of criteria, such as minerals or metals contained, the shape or size of the deposit, host rocks (the rocks which enclose or contain the deposit) or the genesis of the deposit (the geological processes which combined to form the deposit). Since there is considerable debate among geologists as to the exact mode of formation (genesis) of most mineral deposits, it has been recommended that we stick to features that we can first of all agree on, namely, the physical description of the deposits and ore genesis (Eckstrand, 1984; Evans, 1993; Roberts and Sheahan, 1989).

Even though no two mineral deposits are exactly alike, most of them normally fall into one or another of a small number of categories that coincides with a generally accepted hypothesis as to how the mineral deposits were formed. It has therefore been found useful to define a small number of terms used in mineral classification which have a genetic connotation (Evans, 1993; Suleiman, 1999). Evans (1993) has classified mineral deposits into (1) mineral deposits that originate due to internal processes i.e. magmatic segregation, hydrothermal, lateral secretion and metamorphic processes; and (2) mineral deposits that originate due to surface processes i.e. mechanical accumulation, sedimentary precipitates, residual processes, secondary supergene enrichment and volcanic exhalative deposits.

A comparative classification given by Suleiman (1999) has classified mineral deposits into: (1) Magmatic deposits which include apatite, feldspar, tourmaline and/or beryl-bearing pegmatites, and sapphire-bearing monzonitic pegmatoids, (2) metamorphic deposits which are as the result of isochemical or sub-isochemical metamorphism. They include a wide range of deposits of gemstones such as kornerupine, moonstone, tourmaline, garnet, ruby and sapphire, (3) metasomatic deposits which produce gemstones of high quality. They are the result of interactions between various lithologies and fluids under metamorphic conditions. (4) Hydrothermal deposits that include tanzanite and amethyst deposits.

Iron ore deposits are formed by three geological processes according to Evans (1993), namely: i) through direct sedimentation process that forms bedded sedimentary deposits resulting into

two types of iron formation: banded iron formation and ironstones; ii) Iron ore deposits of igneous origin that are formed through magmatic segregation of iron-bearing minerals that occur as veins and tabular replacement bodies of magnetite and hematite; and iii) Iron-ore deposits that are formed by surface or near surface enrichment as less resistant minerals were removed. In this process, chemical and physical weathering by soil forming processes of pre-existing iron-bearing minerals results in progressive concentration of iron oxides to form iron-rich deposits.

As noted above, the formation of iron deposits occurs in a wide range of P-T conditions. These deposits are usually associated to particular lithologies. Structural controls play important role in mineralization in areas where basins do not exist as is the case in the present study area. For example, large scale structures such as faults and shear zones are often the place of heat and fluid transfers that are favorable to the formation of mineral deposits.

In order to address a key pertinent need regarding industrialization of the Republic of Kenya as projected in "*Vision 2030*", the present research study was carried out with a view to investigate the iron ore mineralization deposit occurring in Mutomo - Ikutha area. The studies were to investigate its tectonic setting, mode of occurrence, quantity and associated structural controls. This new added knowledge, placed within the context of the geological history of the Mozambique Belt in Kenya, will greatly assist in future exploration, appraisal and exploitation of the deposit itself and the associated minerals e.g. manganese magnetite, graphite, marbles, vermiculite, copper and garnets deposits found elsewhere within similar terranes.

1.2 STATEMENT OF THE PROBLEM

The relationship between iron ore mineralization, metamorphism and tectonic processes in Mutomo – Ikutha area has never been investigated. This has led to poor mining techniques by artisanal mining due to poor understanding of structural controls and petrology of the lithologies hosting these deposits. The Mozambique Belt where the project study area occurs, has a long and complex history marked by a succession of major tectonic events (Key et al., 1989; Muhongo, 1994). There is a need of connecting the formation of iron deposits to these events, and to the structures that are associated with them in order to gain a better understanding

of the content, the surface extent and genesis of iron ore deposits that are found within Mozambique belt.

The last documented geological mapping in the study area was done in late 1950's. Since then, with advent of new mapping techniques and plate tectonic theories relating to mineral formation and genesis, it is necessary to critically review the geology and mineral potential of the study area. (Drury, 1993; Goldstein *et al.,* 1981 ; Litchte *et al.,* 1987*;* Nicol, 1995; Peters, 1983; Reid *et al.,* 1990*;* Thompson, 1982;) rock (Hutchison 1974; IUGS 1996; Jones 1987;), (Evans, 1993; Pearce et al.,1984; Pohl and Prochaska, 1983).

Mutomo – Ikutha area is part of the Mozambique mobile belt which has been partially investigated by previous researchers of the Mozambique mobile belt. These include researchers (Key *et al.,* 1989*;* Mathu *et al.,* 1991*;* Mathu and Tole 1984; Mosley, 1993; Nyamai, 1995; Nyamai *et al.,* 1993; Nyamai *et al.,* 1999, 2000a, 2000b, 2002, 2003*;* Saggerson, 1957; Sanders, 1954; Suwa *et al.* 1979; Suwa, 1981; Vearncombe, 1983; Walsh, 1963). None of the previous researchers characterized the iron ore deposit found in the study area in terms of its genesis.

1.3 OBJECTIVES

1.3.1 Main Objective

The main research objective of this project was to investigate the petrology, tectonometamorphic setting, the genesis and size of iron deposit in the Mutomo – Ikutha area with a view to understanding the geological processes that led to the formation of such a deposit.

1.3.2 Specific Objectives

1. To investigate the petrology and geochemical signatures of the rocks hosting the iron ore and associated minerals in order to characterize their tectonic setting.

2. To determine the surface and subsurface extent of the iron deposits in the project area and associated alteration zones so as to establish their quantity and economic potential.

3. To identify major and minor geological structures occurring in the project area in order to establish the deformation history and tectonic controls of the iron mineralization.

4. To investigate the tectono-metamorphic setting and genesis of the iron deposit occurring in the Mutomo-Ikutha area.

1.4 JUSTIFICATION AND SIGNIFICANCE OF THE RESEARCH

Iron production form the structural basis of modern civilization. No other commodity is so necessary to assure a growing, viable economy and society. Iron appears in many forms in modern civilization, sometimes obvious, but often concealed. When not used directly, Iron is usually found in the equipment used in the extraction, production, shaping and fabrication of other materials. Its most frequent form is as products made from carbon and alloy steel.

Iron ore plays an important role in the global and Kenyan economy, hence there's need to carry out a scientific research to understand its mode of occurrence, content and genesis in this segment of the Mozambique belt. Kenya plans to put up mini steel mills to drive the economy according to vision 2030. The mini steel mills are a key driver of the manufacturing sector of the country's vision 2030 that will supply industrial machines and equipment. These mini steel mills will require iron ore as raw material in their processing. The research findings will significantly contribute towards the setting up of such steel mills to drive the economy of Kenya.

The outcome of this research will be useful to policy formulators, iron ore prospectors, scientists, and investors who might have interest in the Kenya mining industry. This study will provide a model for exploration of similar deposits elsewhere within the Neoproterozoic Mozambique mobile belt. Mining of iron ore will provide employment to Kenyans and boost the economy by reducing on importation of steel.

1.5 GEOGRAPHICAL SETTING OF THE STUDY AREA

1.5.1 Location and Communication

The study area is located in the S.E. Kenya region in the Kitui county and is bounded by longitudes 38º 4´E to 38º 20´E and latitudes 1º 48´S to 2º 10´S and cover an approximate area of 1200 Km^2. The area is accessed from Nairobi through Thika-Kitui – Mutomo road or Machakos – Kitui - Mutomo road, or from Mombasa road – Kibwezi – Ikutha – Mutomo road (Figure. 1.3). The railway line passes through Kibwezi which is located about 40 Km in the southwestern part of the study area.

1.5.2 Vegetation

The area is occupied by African savannah vegetation. The type of vegetation cover is predominantly of the *Mimosoideae* family of Acacia trees (Figure 1.2). Common Acacia species found in the project area include the Yellow fever tree and the Whistling thorn. Other common tree species in the area includes baobab and *Tamarindus indica* (muthithi) whose fruits are eaten. Nzoani forest which is located in Mutha area is one of the natural forests gazetted by the Government of Kenya. There is also extensive grass cover in some parts of the area. Grasses include the *Tetrapogon bidentatus* and *Chrysopogon ancheri* species.

Figure 1.2: Vegetation cover in the iron ore mineralized zone. *Mimosoideae* family of acacia trees are observed in the background.

1.5.3 Land use and land resources

Land use activities are very limited and vary in the project area being governed by factors such as climate (rainfall and temperature), soil conditions, altitude, and limited use of farm inputs such as pesticides and fertilizers. Crop farming in the project area is mainly for subsistence purposes. The main food crops grown include maize, beans, pigeon peas, cowpeas, sorghum and cassava (Survey of Kenya, 1980). Livestock farming in the area include domestication of goat, sheep, rabbits, and cattle. Other commercial activities in the area include wood curving, bee hive making and bee keeping. Wildlife found in the area includes Baboons, Monkeys and Mongoose.

1.5.4 Climate

The study area is generally hot and dry, with two rainy seasons; the long and short rains. The long rains start at the end of March and continue to the end of May, and the short rains start at the end of October and continue to the end of December. The average rainfall in the project area varies from 500 to 1300 mm per year with high altitude areas receiving more rain (Survey of Kenya, 1980). This type of rainfall pattern is referred to as bimodal rainfall pattern. The project area is classified as semi-humid to semi-arid area. The mean average maximum temperature is 25°C and the average minimum temperature is 12.3°C. The coldest months being July to August, while October and March are the hottest.

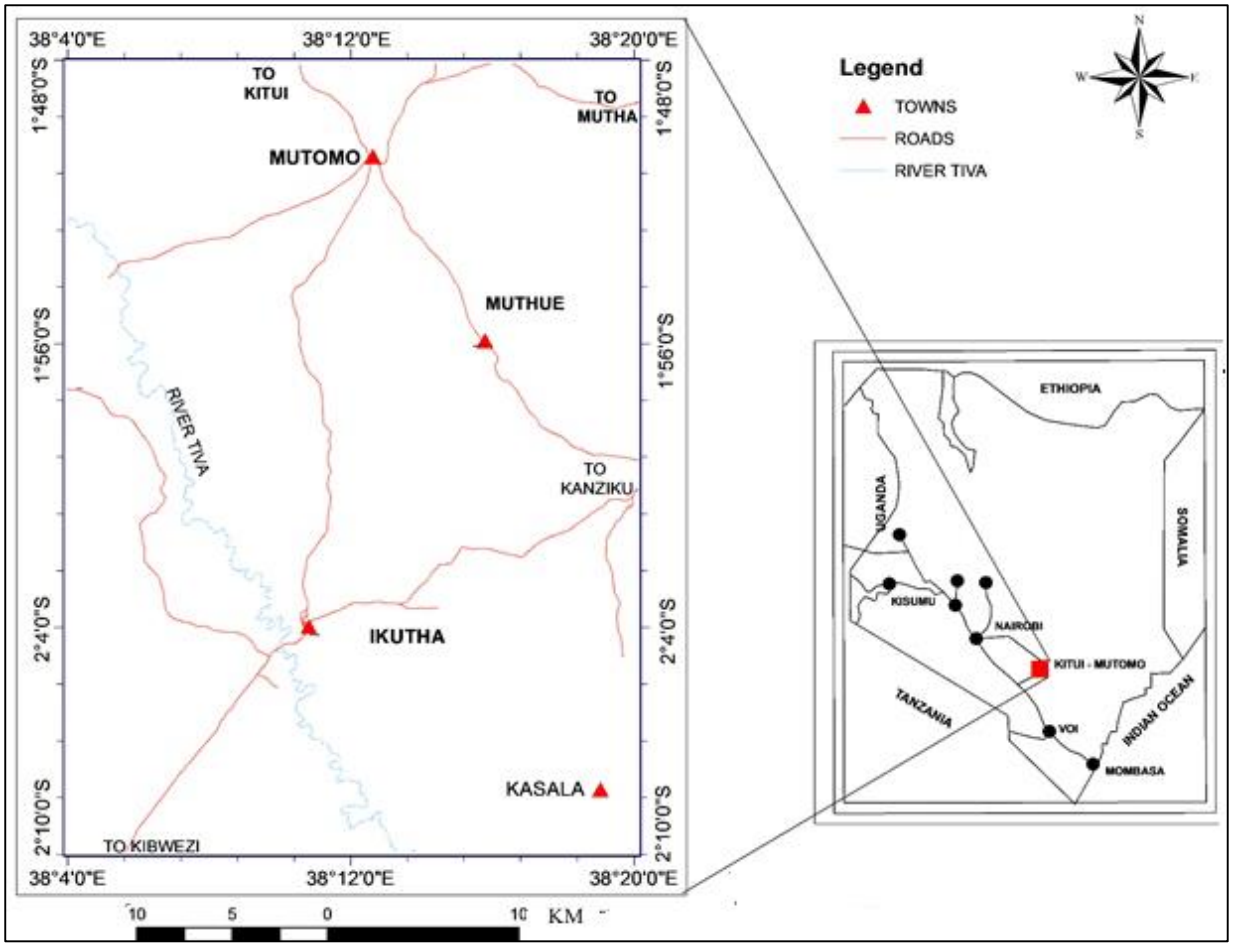

Figure. 1.3: The map showing the area of the project. Major towns within the area include Mutomo and Ikutha.

1.5.5 Physiography and drainage

The geology of the study area has greatly influenced the topography. The area is dominated by a series of parallel ridges that form part of the Kitui anticline. The ridges swings to a NW-SE trend in the present area, which gradually decrease in height as they pass south-eastwards toward Mutomo, Kanziku and, Nzamba (see Figure 1.4). Prominent hills that influence topography in the study area include; Kenze, Kapoponi, Nzoani and Kanyunga hills. The elevation of the hills ranges from 750 meters to 1000 meters. River Tiva is the major river observed in the area, flowing from NW to SE direction.

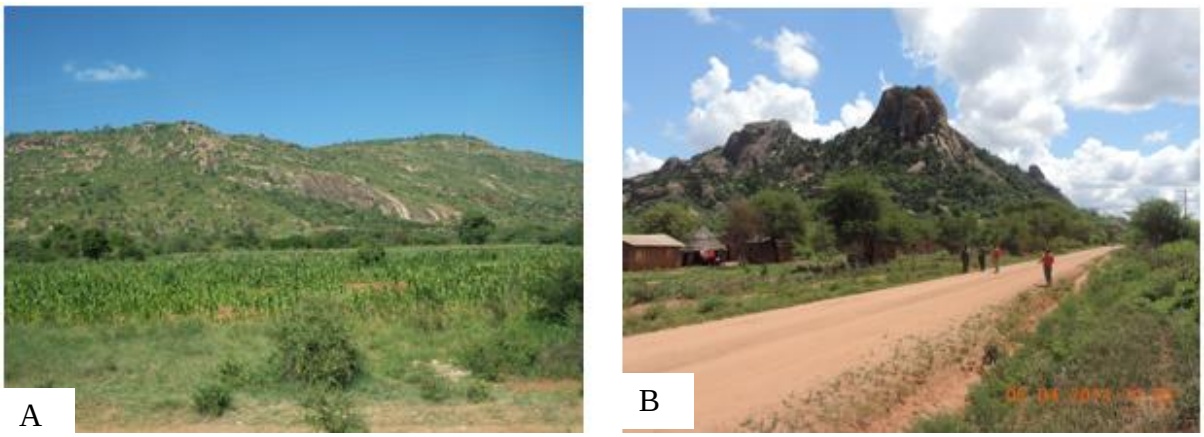

Figure 1.4: Physiography of Mutomo – Ikutha area, (A) Nzamba - Miusiani hill, a view taken from Ngotheni area, (B) Mutomo hills, along Mutomo – Mutha road.

1.5.6 Geological setting of the project area

The project area occurs within the Kenyan Mozambique belt (MB), (see Figure 1.5). The MB itself runs for over 5,000km from Egypt through Ethiopia, Sudan, Kenya, Uganda, Tanzania, Malawi and ends up in Mozambique. The study area consists of high grade metamorphic rocks of igneous and sedimentary origin (Saggerson, 1957). The grade of metamorphism is largely regional and has affected large areas. The Mozambique belt rocks found in the area belong to the Ukamba group (Mosley, 1993). The major tectonic deformation in the Mozambique belt includes folding and faulting. This has produced structural features like foliations, joints and lineations. The general strike directions within the belt are NE–SW and N–S.

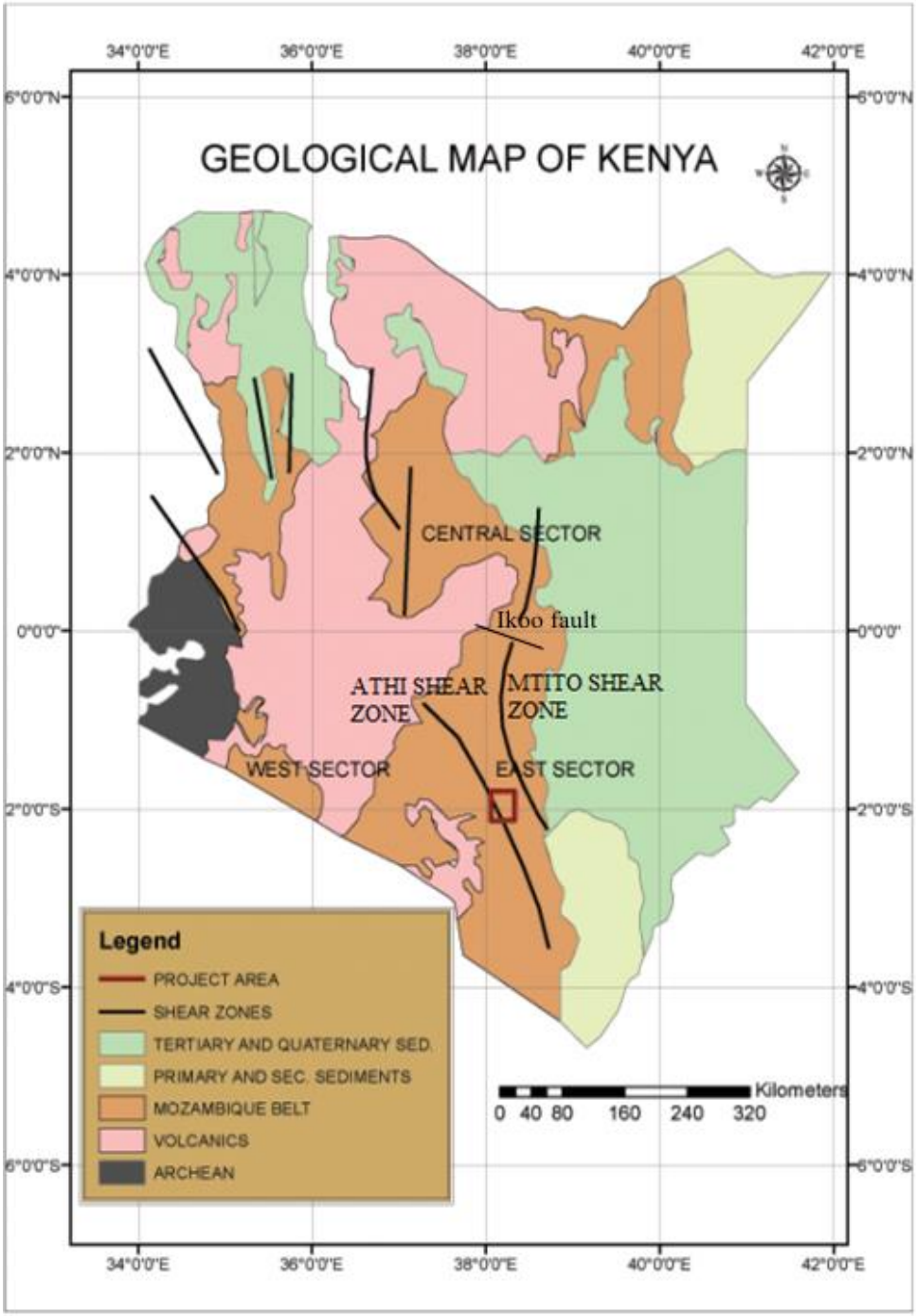

Figure 1.5: Geological setting of Mozambique mobile belt relative to other rock units in Kenya (after Mosley, 1993).

1.6 THESIS LAYOUT

This thesis is based on a number of papers published or under review in peer review international journals.

Chapter 1: Introduces the general information on the iron ore, problem statement, objectives of the research, geographical and geological setting of the area, and the general layout of this thesis.

Chapter 2: Provides literature review of Mozambique belt and general information on the genesis of Iron ore.

Chapter 3: Presents the methods and materials used to achieve the objectives of this research. The methods discussed are geological survey, geochemical survey, remote sense investigation and ground magnetic survey.

Chapter 4: Gives the results obtained from the research and discussion. This chapter gives the results and discussion on petrology, stratigraphy, geochemistry and ground magnetic survey.

Chapter 5: Presents the conclusion and recommendation. This chapter also gives the contribution of the research carried out to knowledge and economy of the country as well and the county where the research was done.

CHAPTER TWO: LITERATURE REVIEW

2.1 GEOLOGY OF MOZAMBIQUE MOBILE BELT ROCKS

The rocks of the Mozambique mobile belt in the study area were considered to be of the Archean by Walsh (1963) and Saggerson (1957). Sanders (1965), through his Ph.D. work proved that the Mozambique belt is mobile belt cutting cratons and older mobile belt. The rocks of the southern part of the area have been classified by Walsh (1963) as; Metamorphosed psamittic sediments, Metamorphosed semi-pelitic sediments, metamorphosed pelitic sediments, Metamorphosed calcareous sediments, migmatites and Igneous rocks that have intruded into the Mozambique mobile belt. Saggerson (1957) classified the rocks in the northern part of the area into; Calcareous, Pelitic, Semi-pelitic, Psamattic, Migmatites, Anatectic or Palingenetic and Meta-intrusives.

The Mozambique Belt is a major N-S trending metamorphic and lithotectonic domain that extends along the Eastern Coast of Africa (Figure 2.1), as well as in Saudi Arabia, Madagascar, India and Sri Lanka. It was first defined by Holmes (1951) on the metamorphic and structural criteria. Mozambique mobile belt is a Neoproterozoic belt (900 to 550 Ma). It was affected by the Pan African tectono-thermal event about 650 Ma (Cartier, 2009; Kazmin, 1972; Kennedy, 1964, and Kröner, 1977). The events between 900 – 650 Ma were polycyclic. The Pan African event encompasses a wide time span from 650 to 500 Million years. Mozambique Belt is considered as an orogeny resulting from the collision between the east and west Gondwanaland (Burke and Derwey, 1972; Gass, 1977; Key *et al.*, 1989; Kröner, 1991). Stern (1994) has proposed its name to be changed to East African Orogeny. The oblique collision of east and west Gondwanaland resulted in the development of large shear zones parallel to the direction of the orogeny after the main collision phase due to tectonic escape phenomena. The geology and tectonic history of the Mozambique Belt in Kenya has been reviewed by various researchers, (Biyajima *et al.,* 1975; Gaciri *et al.,* 1993; Key *et al.,* 1989*;* Mathu and Tole, 1984; Mathu, 1992; Mathu *et al., 1991*; Mosley, 1993; Opiyo-Aketch and Nyambok, 1984; Hackman *et al., 1989*; Nyamai *et al*., 1999, 2000a, 2000b, 2002, 2003; Suwa *et al.,* 1979). Mozambique belt also on the eastern part of Uganda according to Schlüter (1997). The undifferentiated Cherangani meta-sediments spreads over from Kenya to the eastern part of Uganda.

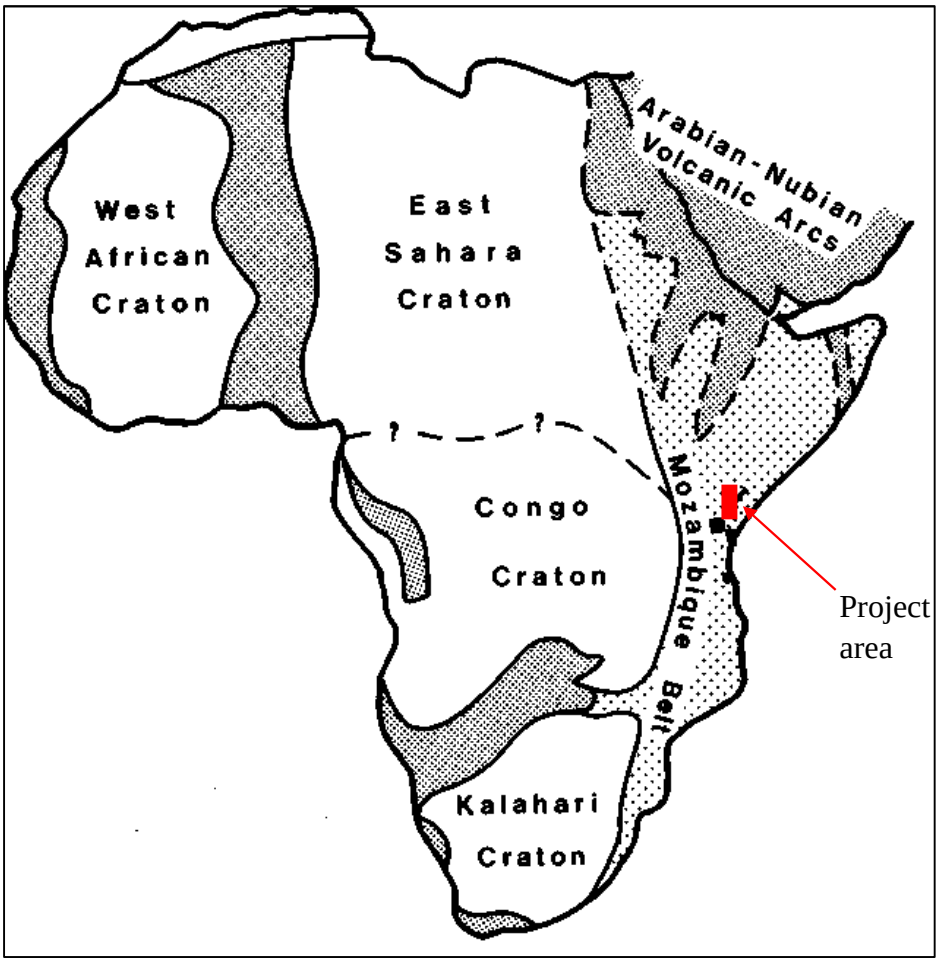

Figure 2.1: Location of the project area in Mozambique mobile belt in Africa (modified from POHL et al., 1980).

2.1.1 Major segments of Mozambique mobile belt in Kenya

The Mozambique belt as exposed in Kenya occurs in four major segments according to Nyamai *et al.,* (2003). The two Mozambique belt segments to the west of the Rift valley have been referred to as the north western Mozambique belt segment (NWMBS) and the south western Mozambique belt segment (SWMBS) respectively as shown in Figure. 2.2. The other two Mozambique belt segments located to the east of the Rift Valley are the north – east Mozambique belt segment (NEMBS) and the eastern Mozambique belt segment (EMBS). The western segments are characterized by W to NW verging thrust sequences. In all the segments stretching lineation represent the initial thrusting stage. Metamorphism culminated in granulite facies (about 10 Kbar and 700ºC), with a high pressure of carbon dioxide underlined by the ubiquity of graphite (Key and Hill, 1989). Pressure - temperature - composition paths are clockwise owing to crustal thickening resulting from the Mozambiquian collision. The study

area is bounded between the Yatta Shear Zone to the West and the Mutito Shear Zone to the East (Mathu, 1992; Nyambok *et al.*, 1993) as shown in Figure. 2.2

Early structures have been transposed within upright ductile shear zones during two related tectonothermal events (Mathu, 1992). Associated metamorphism is of high temperature, with sillimanite and cordierite. Lineation is mostly plunging gently to the north, parallel to the direction of the shear zones. The Eastern Sector of the Mozambique belt is less understood than the western sector owing to inadequately recent study and occasional lack of exposures in Eastern Kenya.

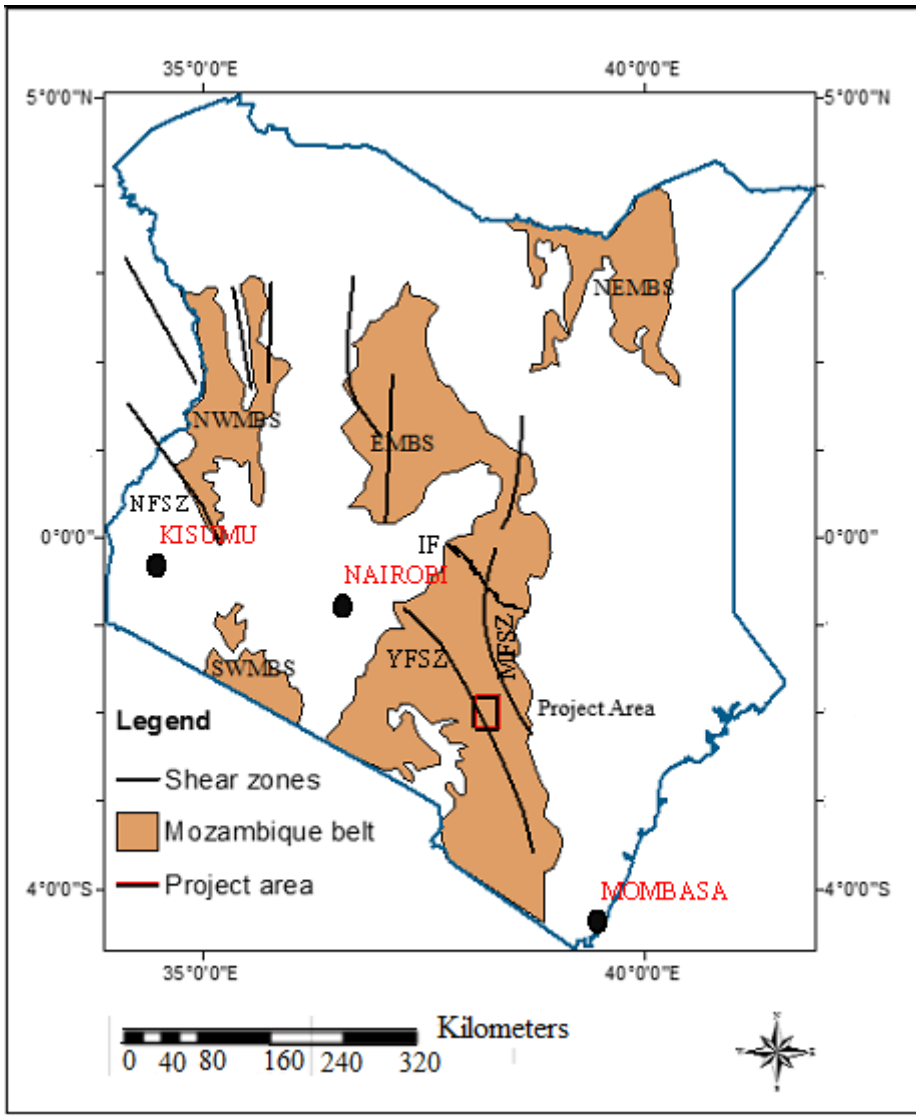

Figure. 2.2: Map of Kenya showing the location of Mozambique Belt Segments (Modified from Nyamai *et al.*, 2003). NFSZ = Nandi fault shear zone, IF= Ikoo fault, MFSZ=Mutito fault and shear zone, YFSZ = Yatta fault shear zone (also referred to as Athi shear zone).

2.1.2 Formation of Mozambique mobile belt

Several major phases in the post-Kibaran evolution of the Mozambique Belt in Kenya, linked to the oblique collision between two east and west fragments of Gondwana have been discussed (Biyajima *et al.*, 1975; Burke and Derwey, 1972; Key *et al.*, 1989; Kröner, 1991; Mosley, 1993; Muhongo, 1994; Nyamai, 1995 and Simonet, 2000). Stern, (1994) summarized the evolution of Mozambique mobile belt. According to Stern (1994), erosion and crustal extension occurred before 820Ma due to the Kibaran Orogeny. This was accompanied with limited construction of oceanic crust in supra-subduction basins that is witnessed by ophiolitic remains throughout Kenya (Behre, 1990).

The main deformation and metamorphism of the Neoproterozoic Mozambique belt in East Africa occurred at about 840 Ma. However this date is not well defined (Cahen *et al.*, 1984). It was apparently followed by tectonothermal events around 744 ± 140 Ma (accompanied by granite intrusion) and 540 Ma. The Mozambique Belt contains numerous ultramafic bodies, frequently associated with mafic rocks. The ultramafic bodies are either discordant or concordant with the country rocks. These occurrences form long pearl-strings in south eastern Kenya, which are interpreted as marking thrusts or sutures (Pohl and Niedermayr, 1979). These rocks have been deformed and metamorphosed to the same degree as their host country rocks. Some of them are tectonically reduced ophiolites (Horkel *et al.,* 1979; Pohl and Niedermayr, 1979; Shackleton, 1976; Vearncombe, 1983), while others that are associated with granulites are possible fragments of sub-continental mantle (Pohl and Prochaska, 1983). In the absence of distinctive geological features, petrochemical methods have been used for a tentative genetic attribution of these rocks as exemplified by (Nyamai *et al.,* 2003).

In summary, Stern (1994) who has proposed a change of the name from Mozambique belt to East African Orogeny states that the belt began by rifting of the supercontinent Rodinia (Figure 2.3), at about 900 -850 Ma. Rifting led to the development of passive margin and an aulacogen like suture which evolved into a narrow ocean basin (Mozambique Ocean). The passive margin is preserved in the West, where it has severally been deformed and metamorphosed. The poorly developed margins in the East as compared to the West may be due to poor exposure, extensive deformation and metamorphism. It may also be that the eastern margin of Mozambique belt developed later as an Andean type convergent margin. The hypothesis that the Mozambique belt began by rifting, with the implication that Rodinia block broke up into West Gondwanaland and East Gondwanaland about 870-650 Ma, is consistent with global consideration (Figure 2.3). The volume of Juvenile crust which formed during the internal

process suggest that a pacific sized ocean (Mozambique Ocean) was opened and closed. Accretion of juvenile arcs and a few older continental fragments continued during this interval. The continental collision first led to crustal thickening and uplift, beginning perhaps as early as 750- 700 Ma. The collision continued with Orogenic collapse and escape tectonics until the end of Precambrian (Stern, 1994).At least as far as Mozambique belt is concerned, this dates the consolidation of East and West Gondwanaland. Thickening of the crust and uplift propagated with time eastwards and now marked by zones of granulites in south on the parts of most India, Sri Lanka, and Madagascar. Tectonic escape led to the development of major rift basins in the northern Mozambique belt and its environs which led directly to sea floor spreading and formation of passive margin on the remnants of Gondwanaland basin to the north, at about 550 Ma (see Figure 2.3).

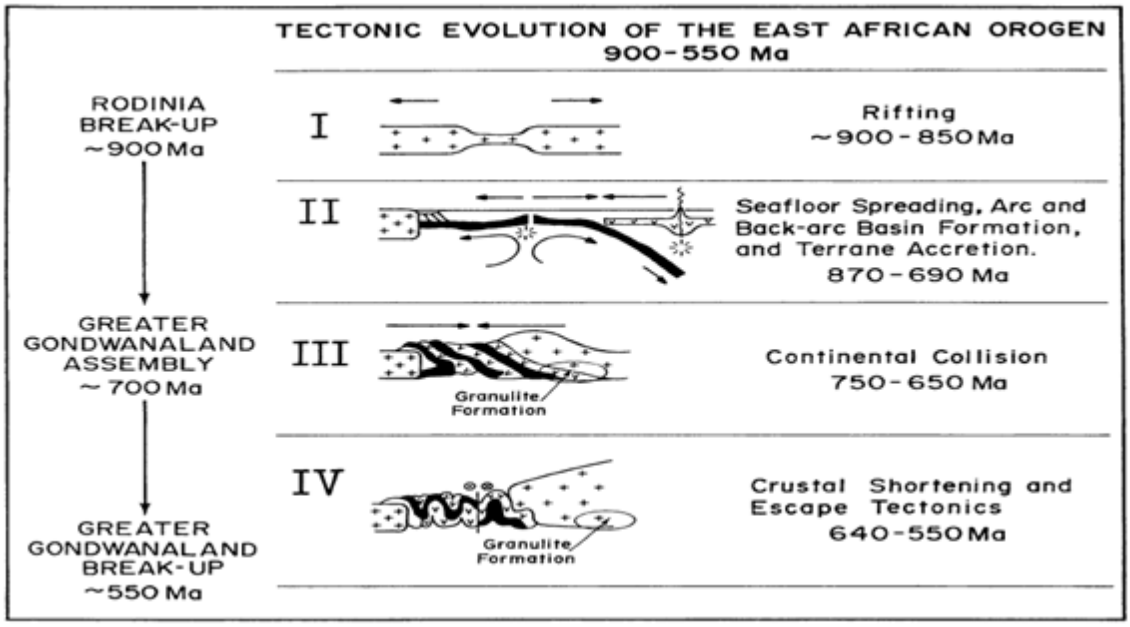

Figure 2.3: The tectonic evolution of Mozambique belt using a Wilson cycle model 900 – 550 Ma (after Stern, 1994).

This episode supports arguments that modern plate tectonic system had begun by about 1000 Ma (Bogerand Miller, 2004*;* CollinsandPisarevsky2005; Collins, 2006; Davies, 1992). In contrast to crust produced between 1.0 and 1.8 Ga, Pan African Juvenile crust preserves most of the evidence of modern plate tectonics regime. This evidence includes abundant ophiolites, calc- alkaline batholiths and volcanic sequences and immature clastic sediments according to Meert, 2003 and 2007.

The Neoproterozoic Era consisted a protracted Orogenic cycle referred to as "Pan African" Orogenic Cycle as proposed by Stern (1994). Kröner (1984) redefined Pan-African as involving a protracted orogenic cycle from 950 to 450 Ma. This tectonism was not limited to African diastrophic events. Similar age and style of tectonism is common throughout Gondwanaland (Figure 2.4) and many parts of Laurasia.

Horizontal tectonic displacement is proved by ophiolites and nappes which travelled at least several kilometres. In many instances, Pan African metamorphism resulted in granulites formation, suggesting crustal over-thickening due to continent – continent collision, (Burke and Derwey, 1972). McWilliams (1981) argued that Gondwanaland assembled during the Neoproterozoic era from two fragments of East and West Gondwanaland along the Pan-African Mozambique Belt of East Africa (Figure 2.4).

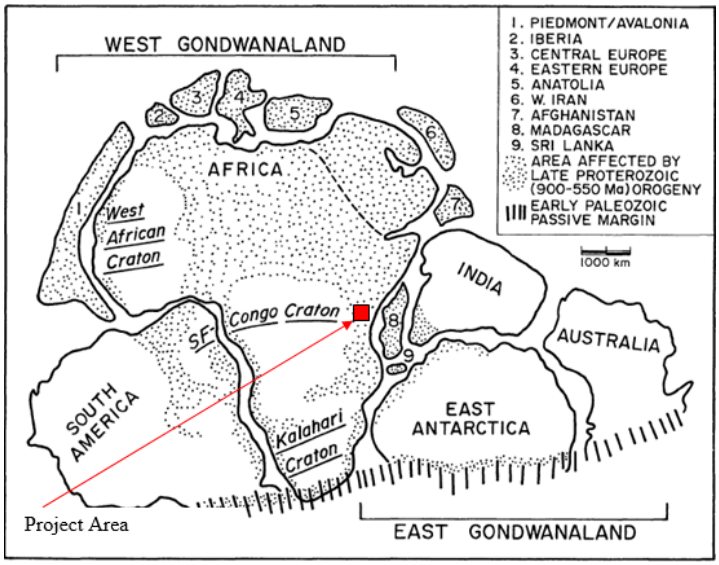

Figure 2.4: Assemblage of East Gondwanaland and West Gondwanaland (after Stern, 1994).

This argument is supported by lithological associations characteristic of the Mozambique Belt to the north referred to as the Arabian-Nubian Shield (ANS). Following the arguments, Behre (1990) noted that the ophiolites decorated meridian sutures traced in East Africa. The ophiolites, granulites, and structures of Mozambique Belt are fossil fragments of Neoproterozoic Wilson Cycle. They represent the opening and closing of an ocean basin (Mozambique Ocean) that occurred between the East and West Gondwanaland. This Mozambique Ocean is proposed to have closed in a fan-like manner with a fulcrum in the south and this supports the abundance of the Juvenile crust in the north (Saudi Arabia, Sudan and Egypt known as the Hijaz magmatic Arc (Stern, 1994).Shackleton, 1996 also proposed a model

of the closure of the Mozambique Ocean and the collision between the East and West Gondwana which dates between 680 Ma and 550 Ma.

Structurally the Kenya-Tanzania is characterized by meridianal foliation trend but local detailed studies have shown that the generalization is an oversimplification of the structural picture (Cahen and Snelling, 1966). Each metamorphic event within the Mozambique belt was accompanied by folding movement according to Nureki *et al.,* (1977). Muhongo *et al.,* 2003 took into account the structures and ages within Tanzania to highlight events of Kibaran (1400 Ma - 1000 Ma), and dated the peak granulite metamorphism that was associated with the EAO to 640 Ma. Direct evidence for rifting has been preserved in sedimentary succession in the Mozambique belt that has been interpreted as passive margin deposits in the Mozambique belt of Kenya. Key *et al.,* (1989) argued that the Kenya sediments were deposited during a period of crustal extension sometimes between 840 and 770 Ma. The geochemical analysis of rocks has made it possible to characterize and define the evolution of the continental crust in some parts of Mozambique belt. The geochemical analysis distinguishes three areas for ages as; a Neoproterozoic craton, a set of Archean crust reworked to Neoproterozoic and crust juvenile Neoproterozoic (Key *et al.,* 1989*;* Mosley 1993; Stern, 1994; Stern, 2002; Stern, 2008 and Vearncombe, 1983).

2.2 IRON ORE MINERALIZATION

Iron ores can occur in different forms depending on the mode of genesis and environments in which it forms. Iron element is the most widely distributed and abundant metallic element in the earth's crust. It constitutes 4.6% of the elements in the earth's crust. The chief ores of Iron are; magnetite, Fe_3O_4 (containing 72.4 percent Fe); hematite, Fe_2O_3 (containing 70 per cent Fe; limonite, $2Fe_2O_3.3H_2O$, containing 59.9 percent Fe; and the carbonate siderite, $FeCO_3$, containing 48.3 per cent Fe.

2.2.1 Iron Ore Genetic models

I. Syngenetic Models

Syngenetic (iron ore) deposit is an iron ore deposit formed contemporaneously with, and by essentially the same processes as the enclosing rocks. Epigenetic deposits form later after the host rock has already formed. Banded Iron Formations (BIF) are examples of synegenetic deposits. On a global scale, most of the iron ore that is mined in the world currently comes

from large deposits of massive hematite formed by the in situ enrichment in iron, most commonly from Banded Iron Formations (BIFs). Most significant resources are the Banded Iron Formation (BIF) preserved in the remnants of old sedimentary basins of Archean age. These occurred as shelf type sedimentation which also yielded carbonates, quartzites and meta-pelitic schist (Trendall, 1983). Examples include BIFs in the Hamersley Basin in Western Australia, Lake Superior Region in North America, Transvaal Region in South Africa, Krivoy Rog Region in the Ukraine and Minas Gerais Region in Brazil. The world's resources are, however, dominated by low-grade ore in the form of magnetite. The genetic model for BIFs include;

1 SiO_2 and Fe associated with volcanism were poured out on the seafloor from springs.
2 SiO_2 and Fe are brought from landmasses through erosion, carried in solution, and dumped in shallow basins. Deposition took place in a rhythmic fashion due to some seasonal variations (similar to that responsible for the formation of varves). Blue green algae may have played a role in the precipitation of the Fe.
3 Deposition as thickly bedded ferruginous tuffs. These were then diagenetically oxidized and silicified under the influence of solutions that were partly volcanic in origin.
4 Deposition as final products of carbonate sedimentary cycles.
5 Archean seas were acidic with pH of 6, and Eh of 0, in equilibrium with an atmosphere rich in CO_2. These conditions kept the Fe in solution as Fe^{2+}. As the CO_2 level in the atmosphere was depleted, the pH of seawater increased, and Fe was precipitated as siderite and magnetite.
6 Upwelling of cold, deep seawater onto a warm continental shelf. Cold water saturated in CO_3^{-2}, Ca^{2+}, and Fe^{2+}, as well as amorphous silica. All would precipitate as these waters mixed with warmer waters.

II. Hypogene Models

Hypogene (iron ore) deposit are iron ore deposit formed below the surface, commonly by ascending fluids. In their studies on Magmatic Ti-Fe±V oxide deposits in British Columbia, Gross *et al.*, (1998) found that such deposits occur as, hemo-ilmenite, Ilmenite titaniferous magnetite accumulations as cross-cutting lenses or dike-like bodies, layers or dissemination within anorthositic/gabbroic/noritic rocks e.g. Lac Tio in Canada

Iron ore can hosted by massive, layered or zoned intrusive complexes. These complexes constitute; anorthosite, norite, gabbro, diorite, diabase, quartz monzonite and hornblende

pyroxenite. These complexes can further be subdivided into an ilmenite subtype (anorthosite-hosted titanium-iron) and a titaniferous magnetite subtype (gabbro-anorthosite-hosted iron-titanium. They are commonly associated with anorthosite-gabbro-norite-monzonite (mangerite)-charnockite granite (AMCG) suites that are conventionally interpreted to be an orogenic and/or extensional. Some of the iron-titanium deposits occur at continental margins related to island arc magmatism followed by an episode of orogenic compression. In layered intrusions the titaniferous magnetite seams are commonly within the upper stratigraphic levels and in marginal zones of complex intrusive bodies. Titaniferous magnetite deposits are commonly associated with magnesian, labradorite phases of anorthositic intrusions or gabbroic phases near the margins of the stock.

Apart from the Marimante titaniferous magnetite deposit in Kenya which occur within the Mozambique mobile belt, other examples are the titaniferous magnetite deposits associated with zoned ultramafic complexes in Alaska and British Columbia such as Lodestone Mountain and Tanglewood Hill. Titanomagnetite ores are among the leading types of commercial iron ore deposits and the main provider of vanadium, while ilmenite-titanomagnetite variety of these ores is an important source of titanium. The ores of the titanomagnetite deposits are complex, with Ti, V and Fe proportions varying over a wide range; they may be essentially titaniferous or essentially iron-vanadium ones.

According to Gross *et al.,* (1998), titaniferous magnetite deposits can be considerably large, ranging up to a billion tonnes with grades between 20 to 45% Fe, 2 to 20% TiO_2 and less than 7% P_2O_5 with V contents averaging 0.25%.

Hypogene ore deposits can be broadly divided into two groups: -

(a) Vein/stockwork systems, in which solutions have deposited ore minerals in brittle open structures or cavities;

(b) Replacement ore deposits. These are ore deposits in which solutions have reacted with host rocks, leading to the replacement of silicates and carbonates by new gangue and ore minerals.

Primary dispersion patterns associated with these types of deposits are related to the movement of hydrothermal fluids. Hydrothermal fluids move through the host rocks carrying with them mineral elements. Element transfer to the host rocks is by fluid-related diffusion, fluid flow through fractures and pore spaces or a combination of these processes.

III. Supergene (metamorphic models)

In Supergene model, iron ore deposit forms near or at the surface, commonly by descending fluids. Laterite which is a low quality iron ore forms by this process.

2.2.2 Occurrence of iron ore deposits in Kenya

Kenya has been known to have iron ore deposits in several parts of the country in places such as Taita-Taveta, Meru, Kitui, Embu, Homa Bay, Machakos, Lolgorien, Migori, Samburu, Samia Hills and Mrima Hill, among others. These deposits occur either as oxides: (magnetite, hematite, martite, goethite and limonite); carbonates (siderite and ankerite) or sulphides (pyrite and Pyrrhotite). Ochieng (1993) described large bodies of titanium-vanadium-magnetite-bearing layered norite-gabbro suite to the S.E. of Mt. Kenya in the Marimante area. He analyzed the ilmenomagnetite and found it to contain between 31.2 and 58.61% Iron oxide (Fe_2O_3), 14.2 to 35.16% titanium (TiO_2) and 0.84 to 0.88% Vanadium.

The Bukura and Mbesa massive sulphides described by Ichang'i (1983) are examples of hydrothermal deposits. Ichang'i observed that the ore consisted of pyrite, pyrrhotite, chalcopyrite and sphalerite. He suggested that hydrothermal fluids associated with the adjacent Mumias Granite were responsible for the mineralization. Huddleston (1954) also described the Bukura massive sulphide and observed that the body had been traced for more than one and a half kilometres. He estimated that the ore reserve was about 17 million tonnes down to a depth of 90 metres but suggested that it may exceed this figure since lateral extensions are known to exist. Magnetite deposits associated with amphibolite bodies similar to the Wanjala deposit in Taita-Taveta are likely to occur in the West Pokot area where similar tectonic environment prevailed during the Proterozoic. In this area, Vearncombe (1983) described a dismembered ophiolite sequence that includes podiform chromite. The possible sheeted dyke complex and manganiferous meta-cherts in the Marich-Ortum region associated with the ophiolite are; andesitic agglomerates, crystalline limestones, mica schists and psammites. All are indicative of island arc and continental margin environment. The coastal parts of Kenya have sedimentary iron-manganese deposits especially in the Kilifi area. Schissel and Aro (1992), referred to the Wilson cycle plate subduction of the early Proterozoic and the amalgamation of a Proterozoic supercontinent from 2000 to 1800 Ma to propose a tectonic setting of the large sedimentary basins, which host large resources of iron and manganese in the very large Superior-type banded iron-formations. They deduced that this tectonic setting is consistent with the favoured geological model in which huge iron and manganese deposits form. These deposits form on

shallow continental margin shelves. Their continuous lateral bands also support a stable tectonic setting. The Kurase Group in the Taita-Taveta area comprises miogeosynclinal lithologies such as marble, quartzite, graphite, sillimanite and kyanite-gneiss and schists; biotite-hornblende gneiss; and amphibolites. Amphibolites of the Mwatate Formation, being part of the Kurase Group, reveal the characteristics of tholeiite. Thoeliites within-plates may occur at continental margins near spreading centres (Nyamai *et al.,* 2003). Pohl and Horkel (1980) suggested that the Wanjala magnetite deposit in Kurase group is a metamorphosed submarine exhalative mineralisation associated with basic volcanics. Hydrothermal fluids have formed mineral deposits in this group.

Ore deposits formed from submarine exhalations commonly are surrounded by laterally more extensive non-ore exhalites. During regional metamorphism, these may form metamorphosed exhalites that have distinctive mineral assemblages that will include magnetite, silicate- and phosphate-bearing iron formations, garnet-quartz rock, quartz-gahnite rock, barite-rich rocks and tourmaline. Mineralogy and geochemical variations in the meta-exhalites relate to primary zoning in the exhalite and may be useful in the exploration of the ore. Mineral assemblages of; Fe, Mn, B, P and Zn indicate a hydrothermal-exhalative source while Al and Ti a clastic source. Association of the ore with some elements (e.g., Cr, Sr, Cu, Pb, Zn, Ag, Cd, Co, Mo, Ni, Sb, S, Se, Te, Ti, and Mo) are suggested as useful geochemical indicators of mineral ore proximity. Metamorphosed hydrothermal alteration regions show metamorphic mineral assemblages that reflect to the elemental composition of the original alteration pattern.

2.2.3 Industrial application of Iron ore

The earliest documented use of iron was about 2000 B.C. by the Egyptians, who used meteoric iron in some of their weapons. Iron ore smelting was discovered during the same time. Iron brought industrial revolution in Europe during the invention of steam engines and railway line. The main industrial application of iron ores is in the production of steel and cement processing. Iron may also be employed in the form of castings, wire, rod, and sheet (USGS, 2013). Material forms of iron and steel is used to produce various automobile and truck parts. Machinery and equipment for industrial, mining and agriculture are made from iron. Iron is also used in making storage tanks for petroleum products and packaging materials like metal cans for food, beverage, motor oils and various drug and chemical products.

CHAPTER THREE: MATERIALS AND METHODS

This chapter presents the materials and the methods used to achieve the objectives documented in chapter one of this thesis. The research involved both field investigations, and laboratory analysis which are discussed in the next subsections of this thesis. The methods used to acquire data in this research included; geological survey, ground magnetic survey, geochemical survey and remote sensing studies as outlined in the research design (see Figure 3.1). Field studies were carried out in the years 2011 to 2014 in Ikutha – Mutomo area. Laboratory analysis was done in the University of Nairobi (Departments of Geology and Nuclear Science), Potsdam University and Ministry of Mining (Mines and Geology Department).

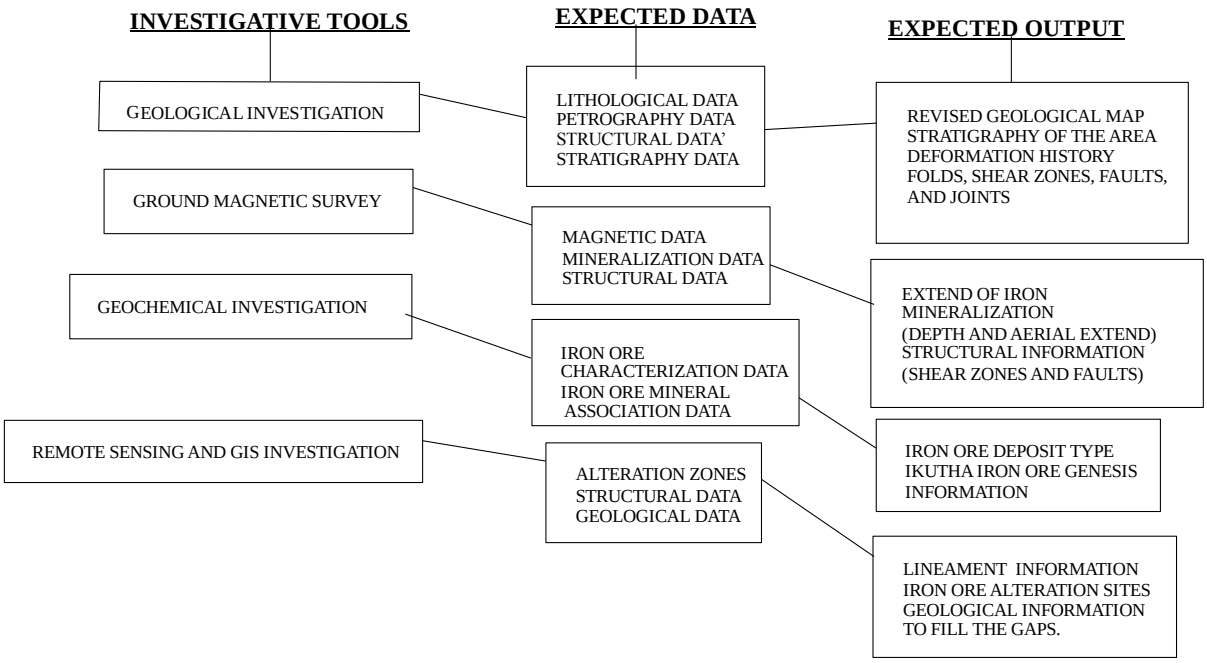

Figure 3.1: Research design flow chart. The research design shows the steps followed to accomplish the research carried out and discussed in this thesis.

3.1 GEOLOGICAL INVESTIGATION

3.1.1 Geological field studies

Geological field studies involved mapping of the various rock units and geological structures (e.g. Figure 3.2). Preparation of detailed sketch maps, cross-sections and vertical stratigraphic sections were done in order to understand the meso-structures, boundary relationships, and

lithological variations in defined rock units. Detailed structural/kinematic analysis of suitable outcrops were also carried out in order to establish deformational and tectonic history.

Figure 3.2: Measurement of geological structures on the biotite gneiss of Mutomo – Ikutha area.

Rock types, mineral assemblages, and geologic relationships were mapped and described in the field. Samples were collected from various stations (Figure 3.3) for petrological and structural analysis. Collection of samples was done across the strike to be able to cover as much lithology as possible within the study area. Structural data, including orientations of tectonic foliation, stretching and intersection lineation, folds, faults, and crosscutting relationships, were collected on foot. Macroscopic shear-sense e.g. pressure shadow indicators were recorded in the field, laying down a kinematic framework for later analysis.

3.1.2 Petrographic investigations

About 120 thin sections were prepared from the rock samples collected during the fieldwork. The detailed petrographic and microstructural analysis of the thin sections cut from the rocks obtained from the study area were carried out at the mineralogical laboratories, Department of Geology, at the University of Nairobi. Petrographic studies included; mineralogical, metamorphic, textural and microstructural features. The sections were all cut parallel to the mineral stretching lineation and perpendicular to the main foliation in the rock sample; a direction parallel to the shear direction, and perpendicular to the finite shortening plane. All necessary marks from the oriented samples were transferred to the thin-section glass during preparation. The information obtained supplemented the field data and facilitated the

establishment of lithostratigraphy, iron ore genesis and tectonometamorphic histories of the project area.

Structural analysis of the foliation and mineral stretching lineation of metamorphic rocks were done using stereographic projection techniques. These techniques involved the preparation of stereograms using Schmidt net lower hemisphere projection. The structural data was computed using the stereo net utility of Rockworks version 2002 software developed by Rockware Inc. in order to determine the dominant orientations for these structural elements.

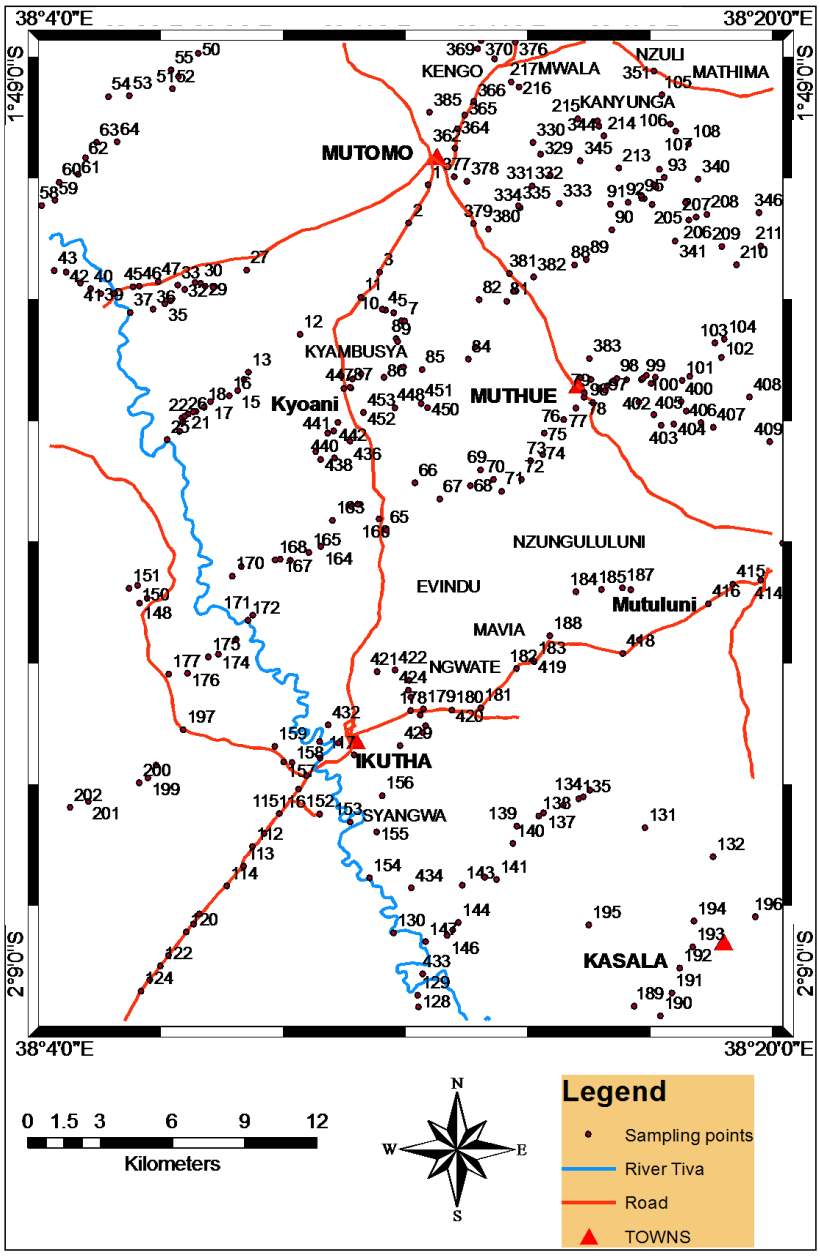

Figure 3. 3: The Map showing sample collection stations in Mutomo – Ikutha area.

3.2 GROUND MAGNETIC SURVEY

Geophysical investigation utilizes the measurements of physical quantities made at or above the ground surface and were used to investigate concealed geology. Proton magnetometer was used in this investigation. Ground magnetic survey was carried out in the southern part of Ikutha based on the results obtained from remote sensing and geological field investigations which had indicated the presence of mineral alterations. The subsurface structures were estimated by the interpretation of ground magnetic data. Magnetic survey was used to delineate magnetic lineaments, analyze its relationship to tectonic fabric and to estimate the depth of iron ore mineralization.

3.2.1 Magnetic data acquisition

Total intensity magnetic field measurements in the study area were carried out with MP2 SCINTREX proton precession magnetometer (Figure 3.4). The same magnetometer was used for base station recordings, to apply the diurnal variation correction as well as taking field measurements. Magnetic surveys are based on the premise that a target is limited in space and has a different physical property (e.g. magnetic susceptibility) from the surrounding formation. Unlike gravity surveying, however, the variation in magnetic susceptibility for various rock types is in orders of magnitude greater than the variation in density for the same rock types. Thus, even knowing the types of rocks in a specific area does not provide sufficient information to constrain susceptibilities. Like density contrast, variations in susceptibility tradeoff strongly with other model parameters. Therefore, if susceptibility, or other model parameters, cannot be constrained from different observations, it is difficult to make quantitative estimates of the geologic structure based on magnetic observations alone.

In this survey, additional constraints were applied that allowed the magnetic observations to be used in a quantitative fashion. This information was derived from other separate data sets, for example, mineral alteration zones obtained from geological mapping. The general trend of the rock units was in the northwest direction. A magnetic survey was designed to estimate the spatial extent of the structure and its susceptibility by in-lab forward modeling. In planning the magnetic survey, the noise was predicted from sources not of interest in the survey, estimated the standard deviation of the random (operator and instrument) noise, calculated the shape of the signal (the theoretical anomaly produced by the assumed source), then decide whether the signal generated by the target of interest is above the noise level that allowed a meaningful interpretation to be conducted.

The Magnetic survey profile orientation were in the northeast – southwest direction, across the general strike of the rock units in the area. Survey was carried out at an interval of 28.3 m along each profile and 700 m from one profile to the next profile (Figure 3.5). MP2 SINTREX proton precession magnetometer was used to carry out the survey. Readings taken included position coordinates, altitude, time and magnetic variations in nT.

Figure 3.4: Ground Magnetic survey in the project area using Proton precession Magnetometer

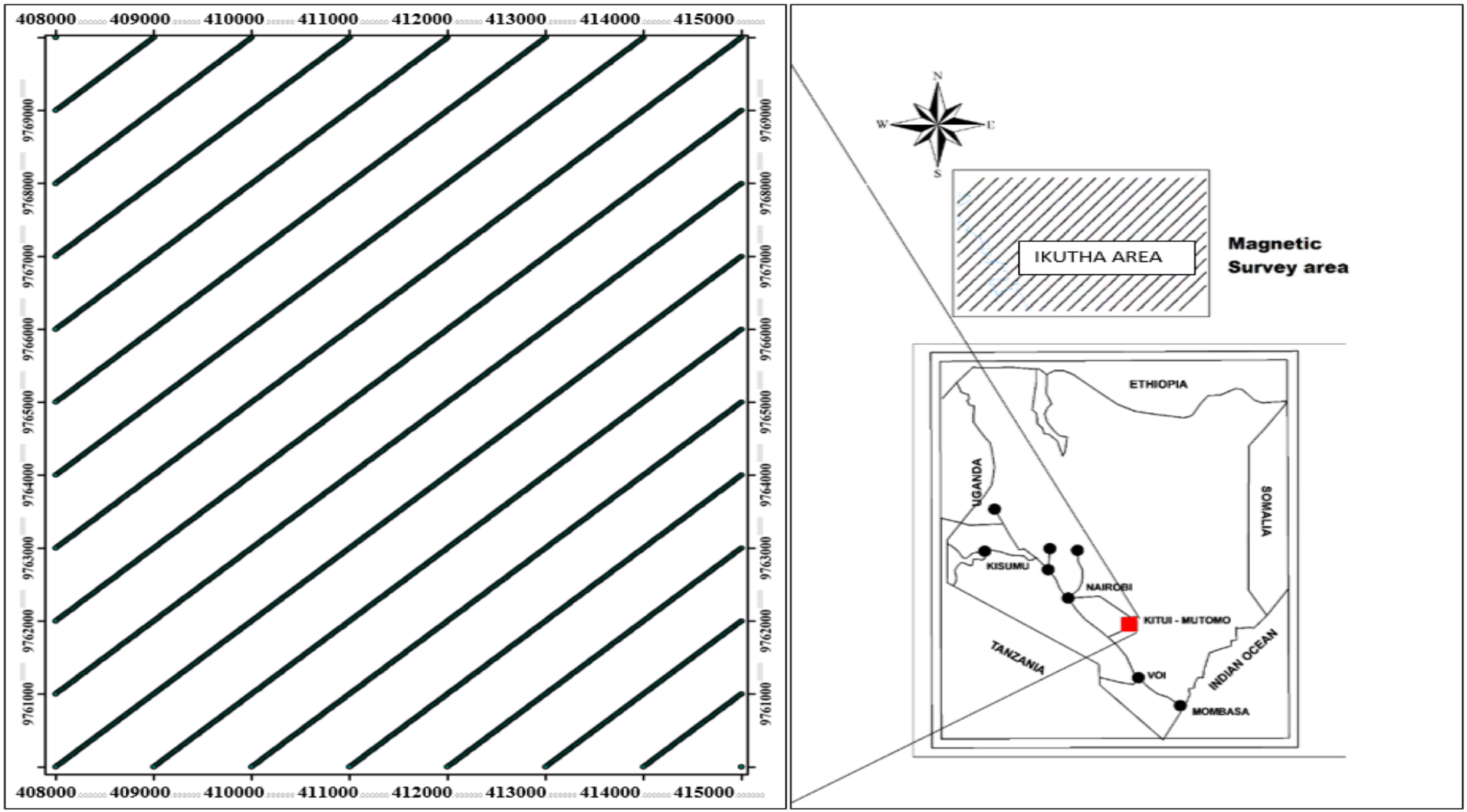

Figure 3.5: The map showing the location of ground magnetic profiles.

3.2.2 Magnetic data processing

The various steps taken in processing the magnetic data obtained in the field is summarized in Figure 3.6. The obtained values were corrected for the normal gradient of the earth's magnetic field (IGRF); the corrected magnetic values were plotted using Euler 2D and Oasis Montaj. The envisaged output of the data processing is a total intensity magnetic map showing the anomalies noted in the study area. The steps in data processing involved interpolation of the field data with the base station data. This data was then corrected for diurnal variation. The corrected data was plotted into a map showing the anomalies using Oasis Montaj.

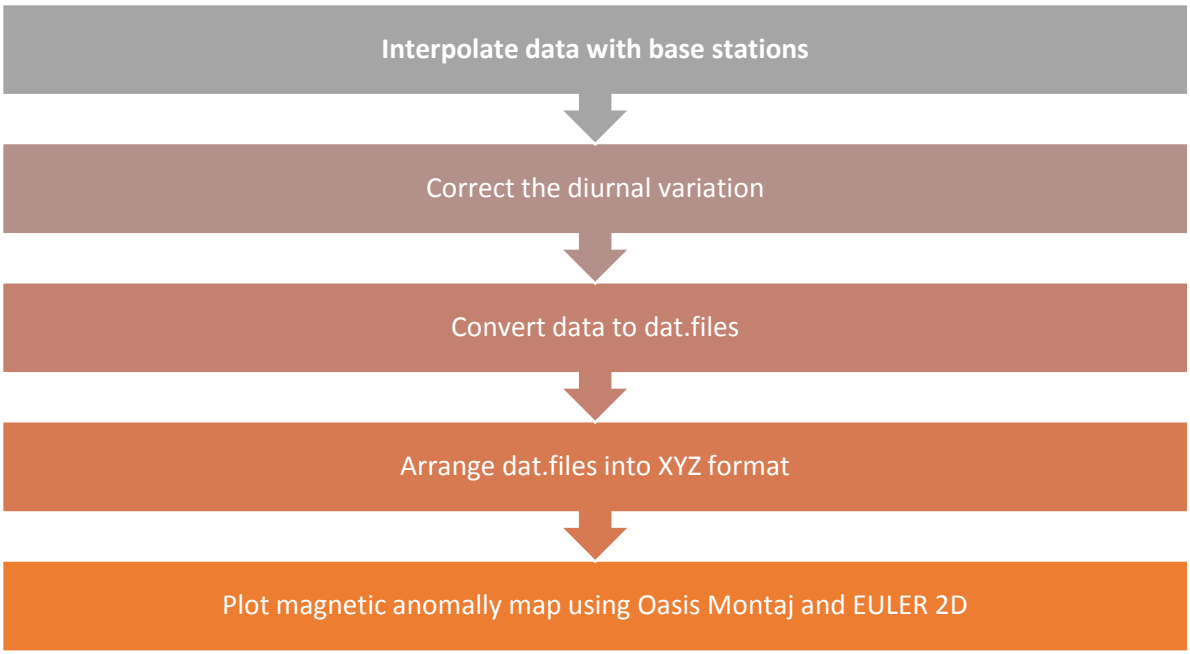

Figure 3.6: Stages involved in processing Magnetic data obtained in the study area.

3.2.3 Data reduction and analysis

a. Diurnal variation correction

Variation of earth's magnetic field with time, due to the rotation of the earth and with respect to the solar wind, which may last for several hours to one day, is called diurnal variation (Riddihough, 1971). In order to correct for drift or diurnal effect in the magnetic readings, a base station within the area of the survey and free from magnetic interference was selected. Repeated readings were taken approximately after every one hour of the magnetic

measurement for the diurnal correction. After the data collection, the diurnal effect was calculated and the magnetic data were filtered by using equation 3.1:

$$\text{Drift} = \frac{\text{B base,f} - \text{B base,i}}{\text{tbase,f} - \text{tbase,i}} \quad \ldots\ldots\ldots\ldots\ldots\ldots\ldots\ldots \quad (3.1)$$

Where, Drift is the drift of measurement in a loop. B base,f and B base,i are the final and initial total magnetic field at the base station. tbase,f and d base,i are the final and initial time at the base station.

The drift corrected field at any station in the loop for a given day was calculated from:

$$\text{Bdrift,n} = \text{Bn} - \text{drift}\ (\text{tn} - \text{tbase}) \quad \ldots\ldots\ldots\ldots\ldots\ldots\ldots\ldots (3.2)$$

Where Bdrift,n is corrected magnetic field at the nth station in the loop. Bn is the total magnetic field at the nth station. tn is the measuring time at the nth station. tbase is the measuring time at the first station of the loop.

b. Removal of geomagnetic field

The regional magnetic field, often referred to as geomagnetic field requires to be subtracted from the acquired total magnetic field to obtain the magnetic field anomaly caused by the local source. After subtracting the diurnal effect from the original magnetic data observed, the geomagnetic field was calculated using the mathematical model of earth magnetic field called International Geomagnetic Reference Field (I.G.R.F) model 2000-2015 in potent software, a product of Geosoft Oasis Montaj software. This model is calculated based on the dates, elevation and geographical locations (latitudes and longitudes) of the observed magnetic data with the generated average geomagnetic field of 33000 nT, inclination of -25.3° and declination of 0.4°. The IGRF values were subtracted from the observed magnetic values for each station to determine the residual magnetic field due to anomalous contribution from local magnetic sources in the area.

3.3 GEOCHEMICAL INVESTIGATIONS

3.3.1 Analytical methods

Amongst the instrumental methods used in analysis included atomic absorption spectrometry (AAS) and X-ray fluorescence (XRF). The model of AAS used in the analysis is VARIAN. Atomic absorption spectrometry (AAS) is an analytical technique that measures the concentrations of elements. Atomic absorption is so sensitive that it can measure down to parts per billion of a gram in a sample. The technique makes use of the wavelengths of light specifically absorbed by an element. They correspond to the energies needed to promote electrons from one energy level to another, higher, energy level. In AAS, the sample is atomized – *i.e.* converted into ground state free atoms in the vapour state – and a beam of electromagnetic radiation emitted from excited lead atoms is passed through the vaporised sample. Some of the radiation is absorbed by the lead atoms in the sample. The greater the number of atoms there is in the vapour, the more radiation is absorbed. The amount of light absorbed is proportional to the number of lead atoms. A calibration curve is constructed by running several standards of known lead concentration under the same conditions as the unknown. The amount the standard absorbs is compared with the calibration curve and this enables the calculation of the lead concentration in the unknown sample. Details of the operation of the AAS equipment are discussed by Rose et al., (1979). UV visible spectrophotometer model PG node T80+ was used to analyze the phosphorus content in the samples.

3.3.2 Field work

Field work involved trenching in areas having high total magnetic intensity readings. The areas for trenching were also selected based on the remote sensed data in chapter 4 of this thesis). Sampling was also done on rock outcrops and soils on a grid as shown in Figure 3.7. Samples were collected from trenches and pits that were dug manually to a maximum depth of one meter (Figure 3.8). About 1kg of the sample collected was packed in polythene papers and taken for analysis.

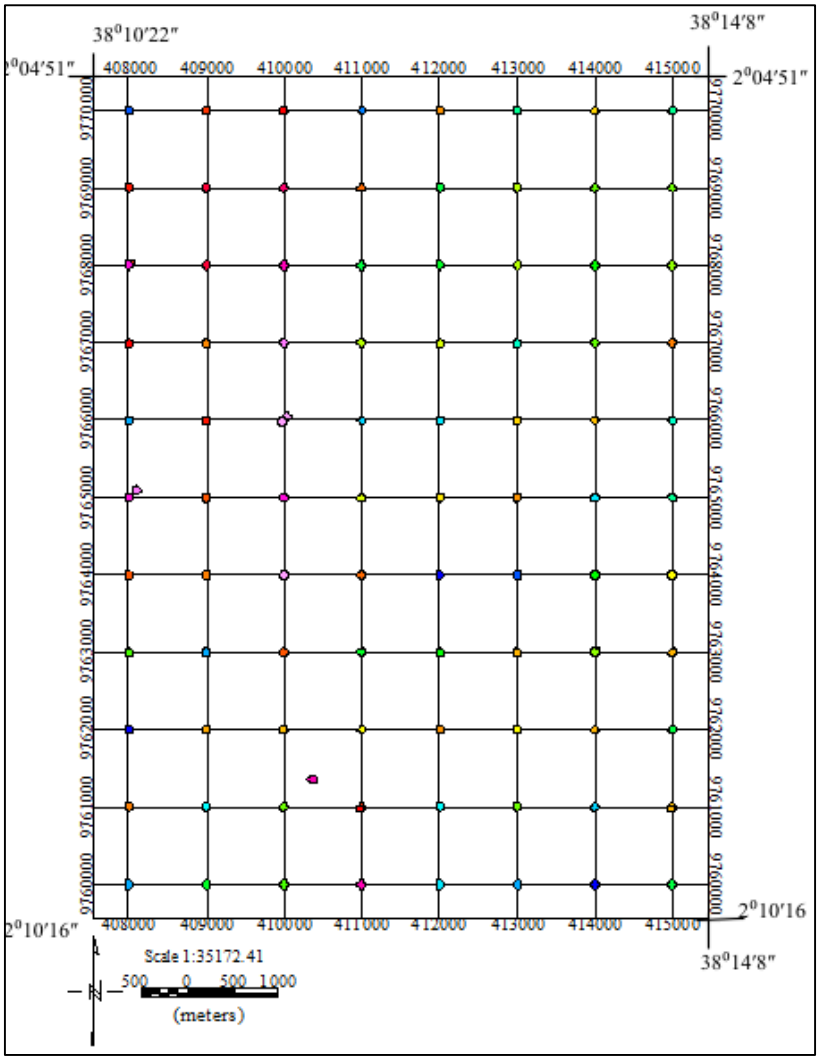

Figure 3.7: The geochemical sample collection stations. The samples were collected along the ground magnetic profiles.

Figure 3.8. Pitting and trenching to collect samples in Mutuluni (a) and Katokolo (b) areas, east of Ikutha town.

3.3.3 Precision and accuracy

There are many sources of errors in chemical analyses. Therefore, precision and accuracy are necessary to determine the range of these errors. These errors probably occurred in the:

- method of analysis,
- instruments
- tools of analysis,
- preparation of the analyzed sample

Precision is the agreement of values among frequent readings for particular content from the sample. It is the reproducibility of the data obtained from the particular analysed sample. The accepted value was specified in confidence level measurement at 95%. According to Maxwell (1968), precision can be obtained using equation 3.3

$$P\% = \frac{2SD}{X} * 100 \ldots\ldots\ldots\ldots\ldots\ldots \text{(95 confidence)} \qquad (3.3)$$

Where; P% = precision percentage

$$SD = \sqrt{(X1 - X)^2 + (X2 - X)^2 + (X3 - X)^{2/N}}$$

Where;

X1, x2, x3 ..... are the actual readings of analyses of the same sample.

N: the number of readings (number of analyses).

X: the average of readings for each element.

SD: standard deviation.

Formulae 3.3 was used in this research to establish precision.

Accuracy is the closeness of the results to reality, using international standards, these Standard materials are to be used for estimating the accuracy of the analysis of the various elements. British chemical standard reference number 393 was used during the geochemical analysis.

3.3.4 Major element characteristics

Major element data was used to distinguish between hydrothermal and sedimentary deposits. Correlation of data from separate stations of the study area was calculated and plotted using a geochemistry extension on Oasis montaj software to demonstrate apparent positive and negative dependences between the major chemical components of elements. Various geochemical discriminant diagrams were used. These plots included AFM ternary diagrams and XY plots. AFM (alumina – ferrous – magnesia) diagrams were used to infer the tectonic environment in which the rocks of the study area formed. XY plots were used for correlation of different elements in the iron ore and the host rocks which showed dependence of some elements that co – exists. Such dependences was used to interpret the data in terms of the likely components (e.g. hydrothermal fluids, detrital material, and alteration) that deliver these elements to the site of deposition.

3.4 REMOTE SENSING AND GIS INVESTIGATIONS

Remote sensing is the collection of information about an object or area without being in physical contact with it. Satellite imagery application technique was used in geological mapping and research as well as in mineral exploration. In this project exploration imagery was used to provide basic geological map and to produce map of local fracture patterns, which controlled mineralization. Image analysis was done using PCI GeomaticaV9.1. Several techniques were used digitally to enhance the images for lineaments analysis, band ratios, linear stretching, and edge enhancement. The procedure of these techniques are summarized in Lillesand and Kiefer (1979).

3.4.1 Data sources

The digital satellite imagery used for structural analysis and mapping in this study was Landsat ETM+ captured on 11th April 2003, (USGS (http:/www.earthexplorer.gov).

3.4.2 Processing method

A flowchart depicting the general steps adopted to obtain a modified geologic map from remote sensing data is given in Figure 3.9. The process involved georeferencing of satellite images using ArcGIS 10.1 software The next step involved application of PCI GeomaticaV9.1 and ArcGIS software in interpretation of spectral signatures in true color composite for available

Landsat images of the area. This was done to create a base map for mapping iron ore and structures in the area. The Least Square method was used to identify details of lithology (rock formation) in order to map iron ore prospects. Digital image processing techniques which included principal component analysis were carried out to detect faults and lineaments of the study area. This was later followed by ground verification, analysis and interpretation.

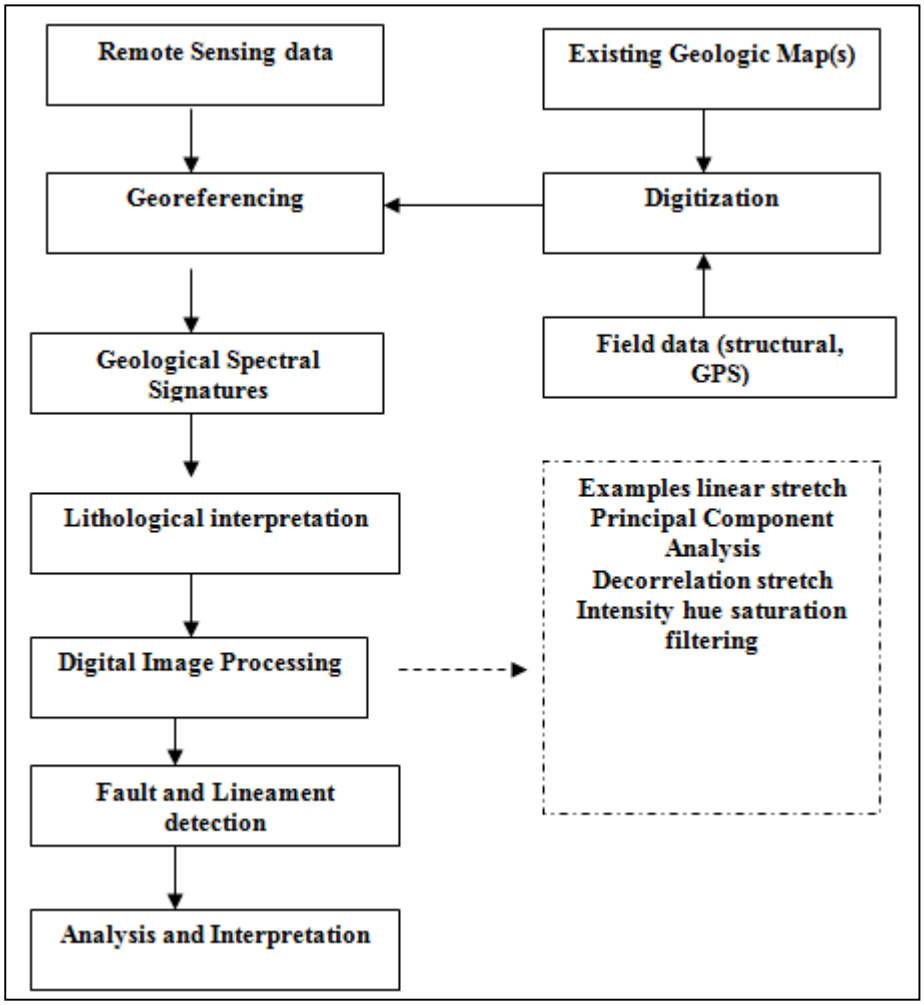

Figure 3.9: Flow chart for analysis and interpretation of satellite images.

Using LANDSAT 7 ETM+ satellite image, it was possible to map major geological features, recognize and classify certain rock types, delineate unconsolidated rocks and soils, map volcanic surface deposits, map geologic landforms, identify indicators of iron mineral resources and determine regional geologic structures. The acquired images were interpreted using Geomatica 9.1 software. Primary access to Geomatica 9.1 was through Geomatica Focus, an all-in-one tool that incorporates PCI Geomatics technologies for remote sensing, image processing map publishing, GIS and spatial analysis in one operating and viewing setting.

Geomatica Focus offers a proficient and comprehensive tool for image rectification, data analysis and visualization, and it works easily with several geospatial data formats. The software Algorithm Librarian provides more than 300 practical algorithms, which are essential for data processing. The supported data processing functions embrace; image filtering, image classification, data interpolation, spatial analysis and Digital Elevation Model (DEM) analysis. It displays the algorithm results in the Focus view or saving them to an appropriate storage medium.

The Ortho Engine interface is a powerful photogrammetric tool designed to perform basic and advanced geometric corrections as well as geospatially mosaic remotely sensed imagery. Production of ortho rectified or geometrically corrected images, DEMs, 3-D vectors and mosaics is simple and accurate. The latest spatial analysis operations in Geomatica 9.1 provide useful tools for a wide range of GIS applications. Fundamental GIS tasks such as overlay, identify, assemble, derive, extract, store, manipulate, import, export and display geographical referenced vector and raster data can be performed without any difficulties. Image processing operations involved the following steps;

a. Image enhancement

The purpose of image enhancement was to render the images more interpretable, i.e. some features should become more visible, which generally occurs at the cost of some other features which may be relatively unimportant in that specific context.

b. Linear contrast stretching

Generally, the number of actually recorded intensity levels in a scene is rather low and the full dynamic range of the digital image (256 levels) is not utilized, so linear contrast stretching expanses the old grey range to occupy the full range of grey levels in the new scale. In this study, linear stretching was used to expand the entire maximum-minimum range in the DN's values. This allowed greater contrast in the entire image.

c. Edge enhancement

The edge enhancement is a typical local operation in which the DN-values at a particular pixel in the new image depend also on the DN-values at neighbouring pixels in the old image. The high-frequency variations of DN-values correspond to local changes from pixel to pixel in an

image. It is influenced mainly by terrain properties, vegetation and solar elevation. Thus, edge enhancement is basically a sharpening process whereby borders of objects are enhanced. Edge enhancement tries to bring out variations in DN values in neighbouring pixels or high-frequency spatial changes, and is also called high pass filtering or textural enhancement.

d. Textural enhancement

Texture analysis is defined as the classification or segmentation of textural features with respect to the shape of a small element, density and direction of regularity. Texture is one of the important characteristics used to identify objects or regions of interest in an image. Unlike spectral features, which describe the average tonal variation in the various bands of an image, textural features contain information about the spatial distribution of tonal variations within a band. Textural analysis produces several output images in which the grey levels represent textural measures of the input image. These textural measures are derived from a grey level co-occurrence matrix or difference vector computed for each rectangular window of user specified dimensions and spatial relationships of the input image. The texture measure is put at the center of the window at the appropriate position in the output image. This technique was used to obtain a sharper image showing more details. The details could be related to differences in some fracture systems. The technique is also used to enhance linear systems, fractures and joints.

e. Directional edge enhancement

This is done by using a first derivative edge enhancement filter that selectively enhances image features having specific direction components (gradients). The sum of the directional filter kernel elements is zero. The result is that areas with uniform pixel values are zeroed in the output image, while those that are variable are presented as bright edges. This method was mainly used to detect the boundaries or lineaments in the study area.

CHAPTER FOUR: RESULTS AND DISCUSSION

This chapter presents the details of the results of the research carried out on the Mutomo – Ikutha area. Results and discussions on the petrology (rock types and their properties), stratigraphy, geological structures, remote sensing investigations, petrochemistry, geochemistry of magnetite ores, ground magnetic survey and iron ore genesis of Mutomo – Ikutha area are given in the following sections.

The geology of Mutomo – Ikutha area is presented in Figure 4.2. Mutomo – Ikutha area is dominated by Metasediments, marbles and meta- igneous rocks that have been affected by metamorphism and tectonism. The rocks affected by tectonism are clearly noticeable on a satellite image of the area trending in the NW-SE direction. Folds and faults are also clearly observed on the satellite images. The project area has ophiolite suits which represent the remnant of oceanic crust which has been obducted on to the continental crust. The area is composed of rocks of the following sequence; Meta sediments (gneisses and Marbles), Metabasalts (pillow lavas) Sheeted dike complex, Metagabbros, Dunites, and peridotite which is atypical ophiolite suite.

The lithostratigraphy of Mutomo – Ikutha area indicate that the Ukamba group (Mosley, 1993) is renamed as Ukamba Super group. The groups under the Ukamba Super include; Ikutha group, Mutomo group and Kapoponi group.

Mineral chemistry shows that Mutomo – Ikutha area is composed of apatite – rich iron ore which resembles the Kiruna type iron ore deposit. The deposit trends in the NW – SE direction for more than 10 Km with a width of I Km – 3Km as observed from ground magnetic survey.

SUB-CHAPTER 4.1: GEOLOGY, METAMORPHISM AND ASSOCIATED MINERALIZATION IN MUTOMO – IKUTHA AREA

This sub-chapter shows an updated geology of Mutomo – Ikutha area. The gaps left by the previous geologists who missed out some of the geological details that have been noted during the current survey. The gaps found in the reports produced by previous researchers included; (1) missing lithology in some sections, (2) discontinuity of the lithologies from the map produced by Saggerson (1957) to the one produced by Walsh (1963). The current survey has managed to establish continuity of these lithologies (Figure 4.78).

The Mutomo – Ikutha area is identified as a medium to high-grade metamorphic terrain having Gabbroic intrusions and Meta volcanic rock units. The area can be subdivided into three zones with different metamorphic characteristics: (1) the Mutomo area extending to the north east and south east, (2) the Ikutha area extending to the northwest and southwest, (3) the Kapoponi area in the north eastern part of the research area. A Gabbroic intrusion and meta-volcanics intercalation occur in the Ikutha and Kapoponi area. The Ikutha area is composed of Ikutha group (see Table 4.1) which comprises predominantly of amphibolite-grade metasediments (metamorphosed psammitic sediments, metamorphosed semi-pelitic sediments, and metamorphosed calcareous sediments)

The rocks of the Mozambique mobile belt in Mutomo – Ikutha area are considered to be the metamorphosed equivalents of originally sedimentary rocks, the sedimentary pattern being retained. The field repetition of certain psammitic and semi-pelitic beds (Figure 4.1 and 4.2), the meta-calcareous horizons in the area which indicates the presence of originally carbonaceous limestone and stratiform succession are considered proof of sedimentary origin.

Figure 4.1: Preserved repeated beds of Metasediments that indicate the original sedimentary facies in Mutomo – Ikutha area.

The sedimentary rocks were tilted and metamorphosed due to the collision of east and west Gondwanaland which made them to trend in NW-SE direction. Evidence of lateral variation is observed in this area. The pelitic gneisses grade into rocks which do not contain the higher-grade index mineral like garnets and staurolite. An example of lateral variation is seen south of Mutomo area where the biotite gneisses grade imperceptibly into biotite-hornblende gneisses. Another lateral variation is noted in Ikutha area where biotite gneiss grades gradually into biotite hornblende gneiss

Rock units of Mutomo-Ikutha area have been classified based on field relation, lithology and colour into groups and formation. These groups include; Ikutha, Kapoponi and Mutomo groups. The formations and members of these groups have been subsequently discussed in the following sections of this thesis.

The new geological map produced show the repetition of some rock units on the western part of the area. The unmapped geological area that had been left out by Saggerson (1957) and Walsh (1963) has now been studied and new information added to fill the missing gaps.

4.1.1 Ikutha group

The lithologies of the Ikutha group which take its name from Ikutha town, is well exposed on the southern and southwestern part of the research area. These gneisses are confined to the western part of the research area. Ikutha gneisses have been categorized based on the field relation, lithology and colour. The boundary between them and the adjacent Mutomo gneisses is gradational. The rock units of this formation strike in the northwest to southeast direction, with dips ranging from general dips range between 30 – 80 degrees in SW direction.

The Ikutha group consist of a paragneissic suite consisting essentially of thick bedded:

(i) Leucocratic meta-psammites (quartzo-felspathic gneisses)
(ii) Mesocratic gneisses (hornblende gneiss, hornblende biotite gneisses),
(iii) Amphibolites

The following mineral assemblages are represented by the lithologies within Ikutha gneisses;

- Hornblende + Quartz + Biotite + Magnetite + Apatite ± Plagioclase, Microcline found in mesocratic rocks.
- Quartz + Plagioclase ± hornblende, biotite, muscovite, Magnetite and apatite (which consists Leucocratic meta-psammites)
- Hornblende + Quartz + Plagioclase + Biotite ± Epidote, apatite, Iron ore, Garnet, Zircon (found in Mesocratic rocks)
- Hornblende + Hypersthene + Quartz + Plagioclase + Diopside + Apatite + Biotite + Magnetite (occur in Mesocratic rocks)
- Hornblende + Quartz + Plagioclase + Myrmekite + Biotite + Diopside ± Apatite, zircon, sericite, iron ore (occur in Mesocratic rocks)
- Plagioclase + Hornblende ± Biotite, Diopside, Hypersthene, Calcite, Sphene, Apatite, Magnetite (occur in Amphibolites)

Table 4.1. Classification of the rock units in the study area based on the current fieldwork

SUPPER GROUP	GROUP	FORMATION	TYPE OF THE LITHOLOGY
UKAMBA SUPER GROUP	IKUTHA GROUP	• Quartz-feldspathic gneiss • Feldspathic gneisses • Granitoid gneiss	• Metamorphosed psammitic sediments
		• Hornblende gneiss • Hornblende biotite gneiss • Hornblende diopside gneisses , Amphibolites	• Metamorphosed semi-pelitic sediments
		• Marbles	• Metamorphosed calcareous sediments
		• Olivine norites, Pyroxenites	• Intrusives
	MUTOMO GROUP	• Biotite gneisses • Biotite hornblende gneisses	• Metamorphosed semi-pelitic sediments
		• Migmatites	• Anatectic rocks
		• Marbles	• Metamorphosed calcareous sediments
	KAPOPONI GROUP	• Oligoclase porphyroblast gneisses • Quartz- feldspathic gneisses	• Metamorphosed psammitic sediments
		• Biotite-garnet gneisses • Garnet enriched rocks	• Metamorphosed semi-pelitic sediments
		• Calc-silicate granulites	• Metamorphosed calcareous sediments
		Meta-basalts, meta-gabbro, Gabbro ,Melagabbro, Pyroxenite, Peridotite Dunites	• Metamorphosed and un-metamorphosed Volcanincs and Intrusives

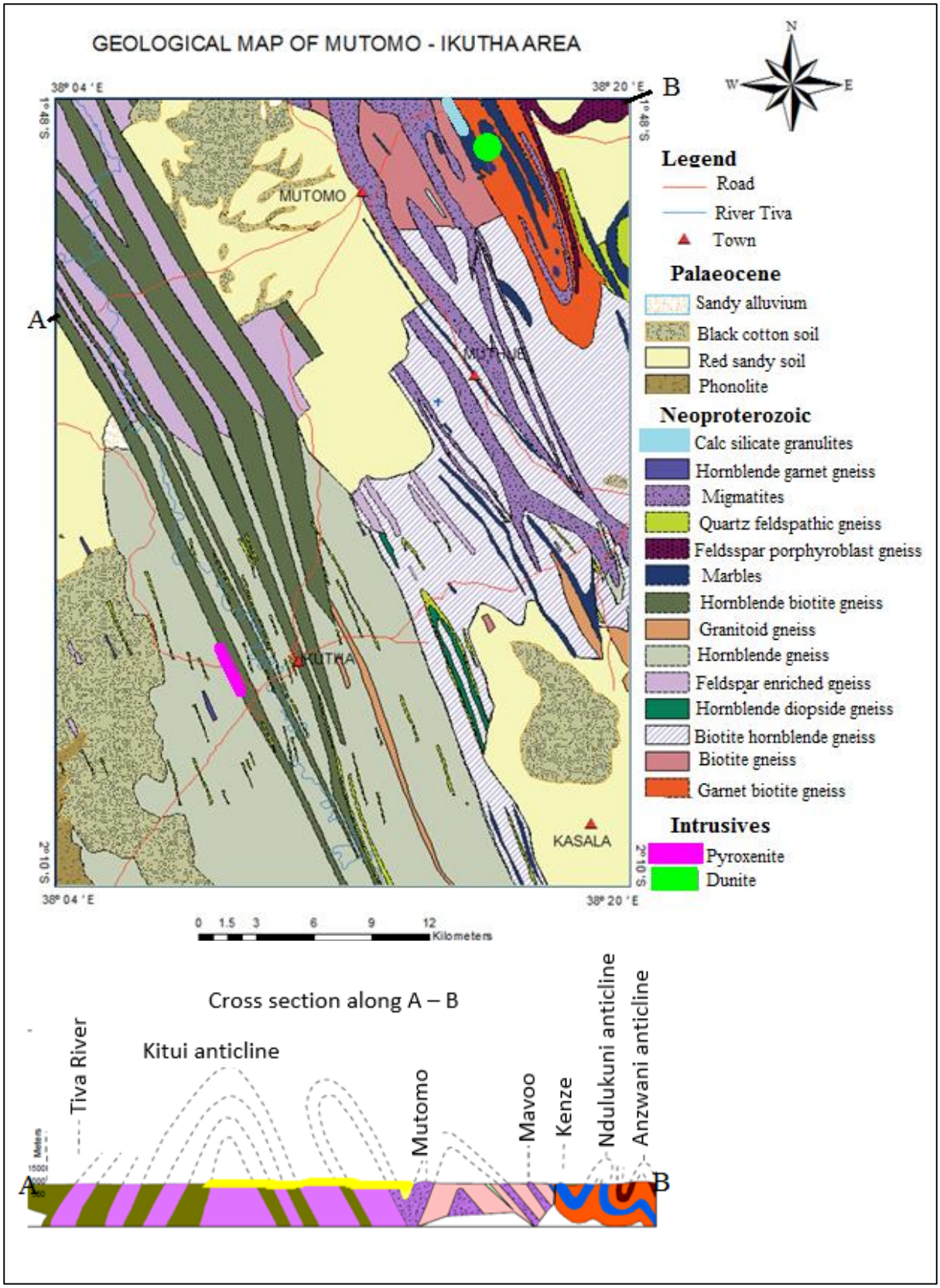

Figure 4.2: New Geological map of Mutomo – Ikutha area. A copy of the A0 size of this map is attached at the back of this thesis. (Remapped and updated from Saggerson, 1957; Walsh, 1963).

I. Quartz-feldspathic gneisses

These vary in colour from cream to pink or red. Quartz-feldspars are coarse grained with stretched quartz grains. They show good foliation marked by alignment of mafic accessory minerals. The rock formation trend in the N320W. These rocks outcrop on the southern part of Ikutha town.

Under the transmitted light microscope interstitial recrystallization of quartz and feldspars is noted, as observed in specimen 153 (Table 4.2) from Katokolo. Plagioclase feldspars are all of the composition of oligoclase. Accessory minerals include hornblende, biotite, muscovite, Magnetite and apatite. The rocks have undergone shearing and mylotization (figure 4.3A) to form microfolds (figure 4.3B) in some areas as noted from recrystallization of the quartz and feldspars. Garnet crystals have been rotated indicating dextral shearing (Figure 4.3B).

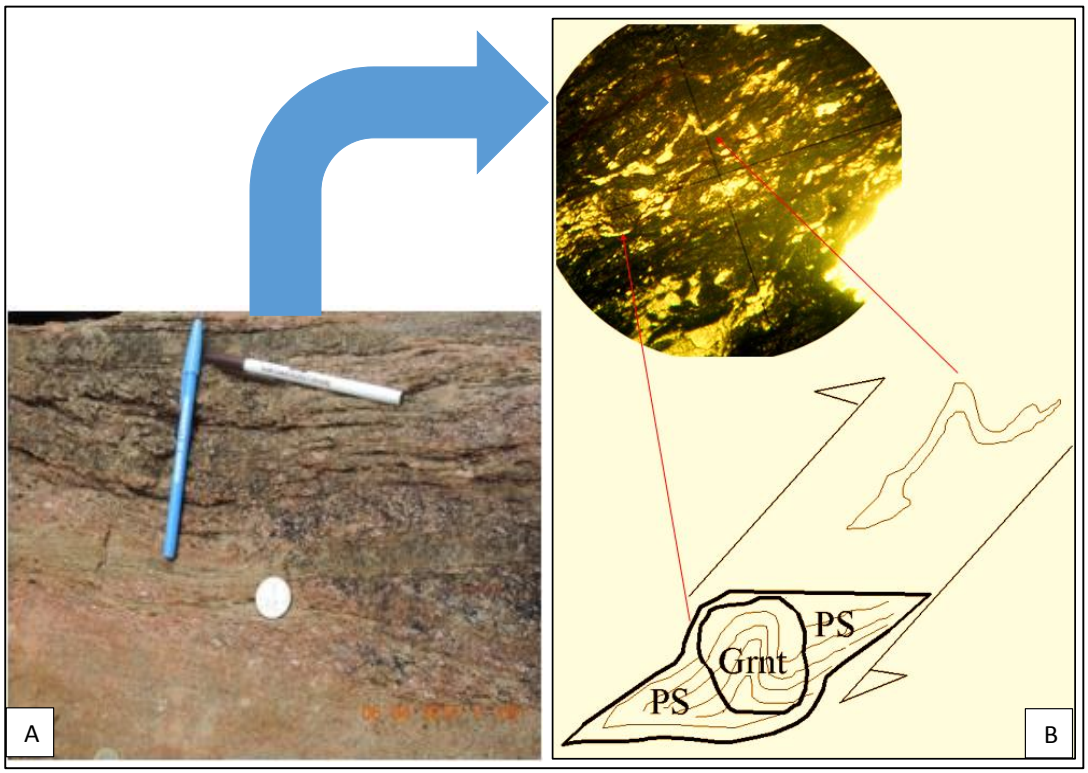

Figure. 4.3 (A): Photograph of: Mylonitized quartz – feldspathic gneiss (sample 147 in situ) on the eastern part of river Tiva, (coordinates- 0411047/ 9765477). (B): Photomicrograph of quartz – feldspathic gneiss showing dextral shearing of the Ikutha rock formations. (PS - are the pressure shadows developed as result of the rotation of Garnet crystal (Grnt)).

Table 4.2: Modal composition of the quartz - feldspathic gneiss from Ikutha formation

Mineral	147	153	178	182
	(Vol. %)	(Vol. %)	(Vol. %)	(Vol. %)
Quartz	50	45	45	50
Plagioclase	48	51	53	49
Accessories	1	3	1	1
Total	99	99	99	100

NB: Reference coordinates

147 -411624/9763274; **153**-408498/9768275; **78**-411009/9772953; **182**-415405/9774706

II. Hornblende gneisses

Hornblende gneisses are exposed in a broad band flanking the Tiva River on the south western part of the research area. Their resistance to erosion is minimal, and they outcrop in river sections (Figure 4.4). They vary in colour from buff to almost black, according to their content of mafic minerals in situ. These rocks have also undergone wall rock sericitisation. Where exposures are continuous, the colour index changes rapidly over short distances and in some places the rocks are clearly banded. Along the Tiva River north-west of Ikutha the gneisses contain bands of reddish quartzo-felspathic gneiss, perfectly conformable with the strike and can be traced for several kilometers as they cut successive meanders of the river.

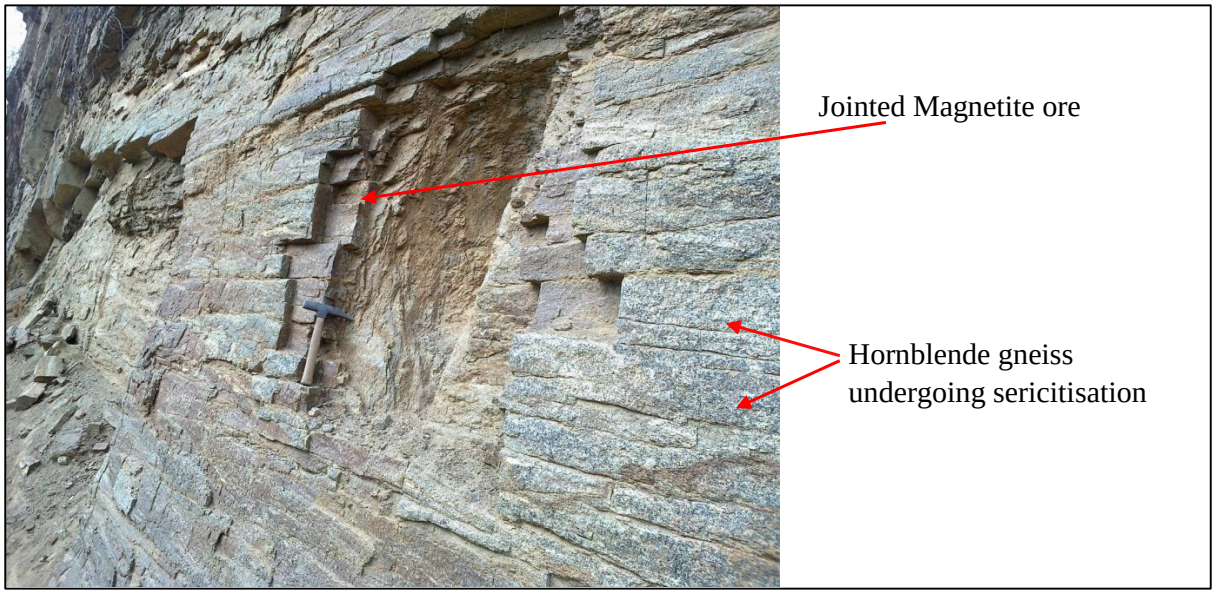

Figure. 4.4: Hornblende gneiss which host magnetite in Tiva area, west of Ikutha town (Sample number 430, UTM coordinates; 408009/9715192). The hornblende is undergoing sericitisation due to the alteration process.

In thin section hornblende is strongly pleochroic in shades of olive green to blueish. (Figure 4.5). Quartz and feldspar has undergone recrystallization. Biotite and apatite, show shattering and strain effects, as a result of strong shearing. Hornblende has undergone replacement by iron ore due to metasomatism. Microcline feldspar is dominant in some thin sections while others have plagioclase as a dominant feldspar. Other accessory minerals observed include apatite, magnetite and biotite. The mineralogical composition of this rocks is presented in Table 4.3.

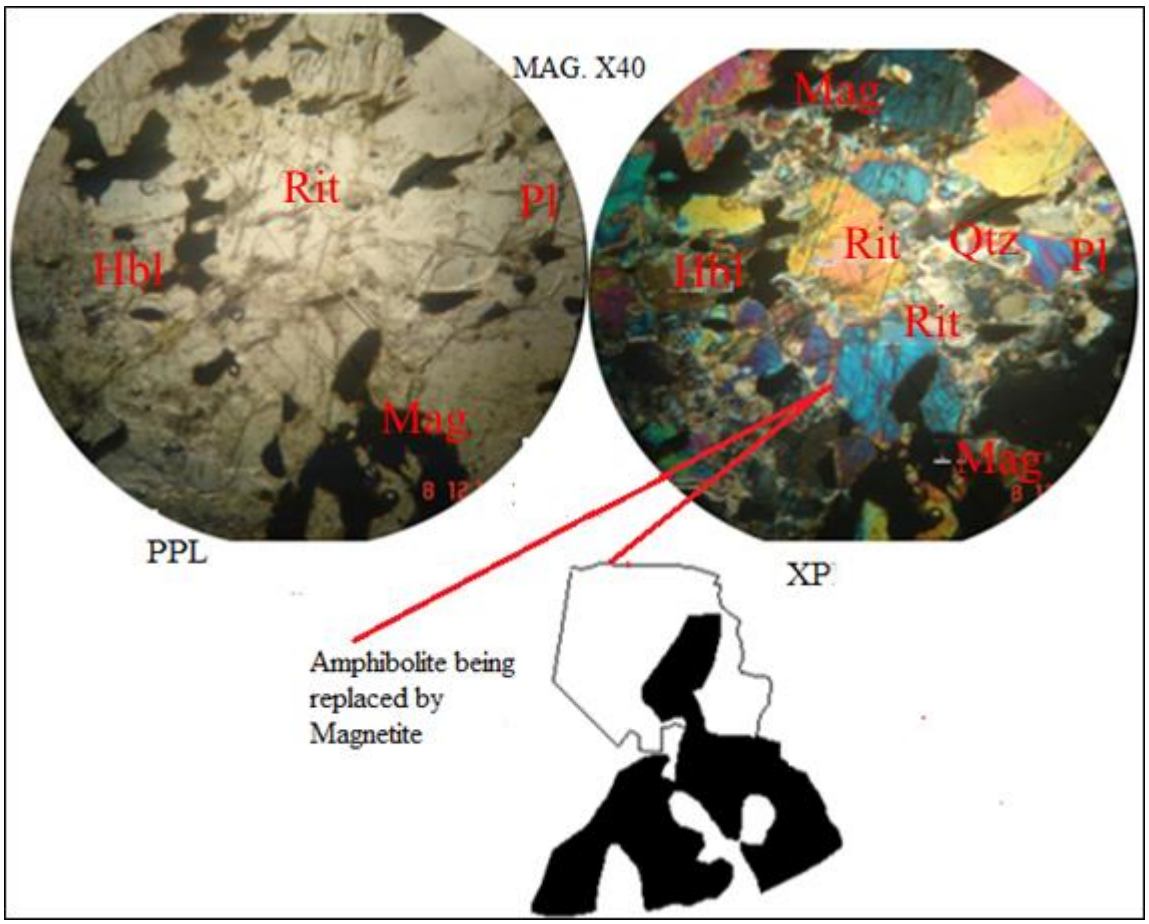

Figure 4.5: Photomicrograph of the hornblende gneiss showing replacement of hornblende by magnetite in Mutomo – Ikutha area. Hbl=hornblende, Mag=Mag, Pl= Plagioclase , Qtz = Quartz, Rit = Richterite. The thin section was cut from sample number 430 (UTM coordinates X= 408009, Y= 9715192).

Table 4.3: Modal composition of hornblende gneiss of the Ikutha group.

Mineral	430	434	437	449
	(Vol. %)	(Vol. %)	(Vol. %)	(Vol. %)
Hornblende	20	25	20	25
Quartz	9	9	14	9
Microcline	-	-	49	-
Plagioclase	50	50	-	45
Apatite	10	9	5	10
Biotite	1	1	1	1
Magnetite	9	5	10	9
Total	99	99	99	99

NB: Reference coordinates

430 – 408009/9715192; **434** – 411037/9765522; **437** – 407853/9783531; **449** – 410715/9787328

III. Hornblende-biotite gneisses

These rocks occur in Tiva River and in Kasala area where they intercalate with hornblende gneisses (Figure 4.6), the transition from one to the other being gradual. Hornblende biotite gneiss is mesocratic, medium to coarse grained rock with feldspars, quartz, amphibole and mica occurring as essential constituents (Table 4.4). It is characterized by typical gneissic banding with varying trends from N320°W to N340°W and steep dips of 50° to 70° along the contacts with the hornblende gneisses. In some cases, the gneisses are xenoblastic with a weak gneissose structure. Many slides indicate that shearing has taken place, imparting a stronger foliation to certain rocks along river Tiva.

Figure 4.6: Banded Hornblende biotite gneisses at location 142. The rock unit trends in the NW-SE direction.

Under the microscope, hornblende and biotite noted as mafic constituents. The felsic constituents are plagioclase and quartz. The hornblende is deep green to light green while biotite is yellow to brown. Epidote, apatite, hypersthene, Iron ore, Garnet, Zircon occur as common accessories. Hornblende is pleochroic from light to very olive green, and biotite dichroic from yellow to dark greenish brown. Hypersthene shows zoning as noted in Figure 4.7.

Table 4.4: Modal composition of the minerals in the hornblende biotite gneiss

Mineral	142	422	425	434
	(Vol. %)	(Vol. %)	(Vol. %)	(Vol. %)
Hornblende	10	8	9	10
Quartz	19	20	21	20
Plagioclase	60	64	64	63
Biotite	5	5	5	5
Accessories	5	2	1	1
Total	99	99	100	99

NB: Reference coordinates **142** – 414081/9765977; **422** – 410351/9774643; **425** – 411021/9773506; **434** – 411037/9765522

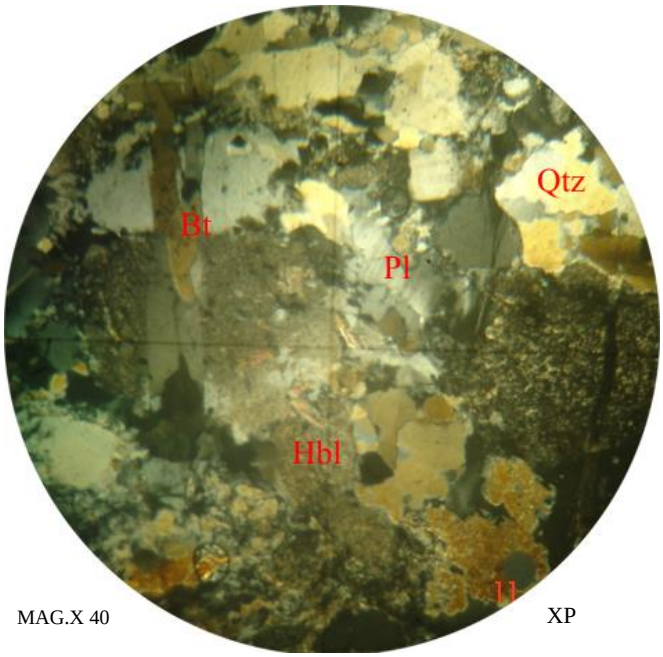

Figure 4.7: Photomicrograph of a hornblende biotite gneiss. Hbl = hornblende, Qtz = quartz, BT=biotite, Pl=plagioclase.

IV. Hornblende-diopside gneisses

The hornblende-diopside gneisses are dark grey in colour, of medium to coarse grain. They are foliated on a fine scale by the concentration of the melanocratic minerals in marked layers as observed in situ and hand specimen. This rock unit occurs along river Tiva and Katokolo area, south of Ikutha town. They trend in the NW – SE direction and are conformable to other neighboring rock units. The rock's mineral modal composition is shown in Table 4.5.

Table 4.5: Modal composition of hornblende – diopside gneisses

Mineral	51 (Vol. %)	55 (Vol. %)	56 (Vol. %)	68 (Vol. %)
Hornblende	20	25	30	25
Hypersthene	5	5	2	5
Quartz	5	5	2	5
Plagioclase	50	50	50	45
Diopside	15	10	10	15
Apatite	1	1	1	1
Biotite	1	1	1	1
Magnetite	3	3	3	3
Total	100	100	99	100

NB: Reference coordinates
51- 401370/979490; **55** – 401064; **56** – 406305/9801393; **68** – 413481/9782363

Under the microscope, hornblende is seen to be pleochroic from light green to dark olive green while diopside is faintly pleochroic in light blue to green. Diopside undergoes replacement to magnetite as exemplified in sample 56 from Katokolo area (Figure 4.8).

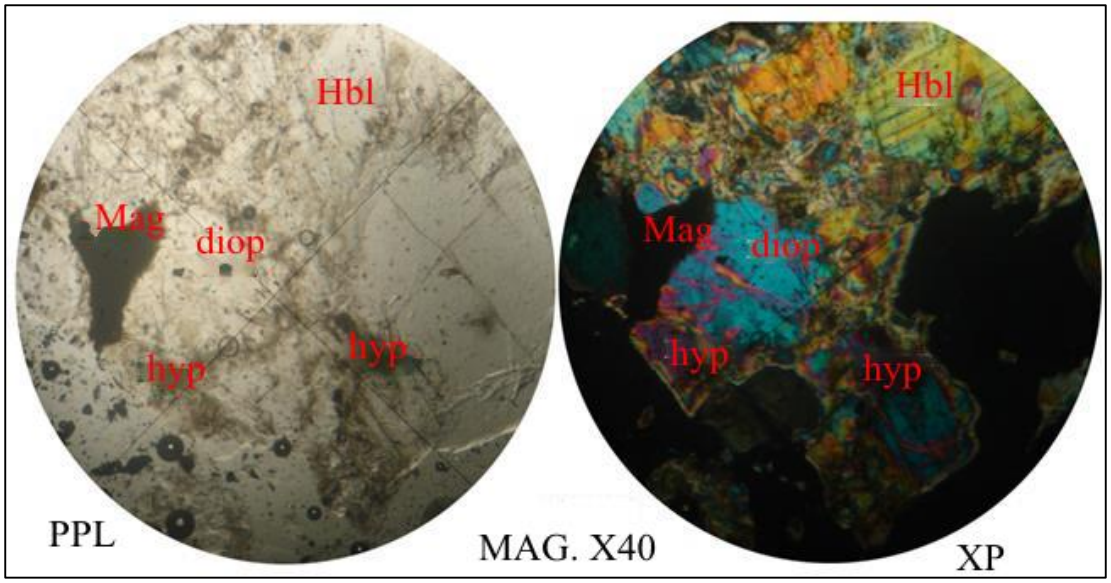

Figure 4.8: Photomicrographs of hornblende – diopside gneiss. Hbl=hornblende, diop = diopside, hyp = hypersthene, Mag = magnetite

V. Plagioclase Feldspar enriched gneisses

Reddish-pink outcrops alternate with the biotite-hornblende gneisses in the area of the Tiva River (Figure 4.9). They are impure psammitic bands within the semi-pelitic series and are characterized by the nature of their outcrop, their striking colour and by gradations to the darker interbanded rocks. Near the hornblende biotite gneisses, the feldspar enriched gneisses form an alternating series of dark and light bands occasionally showing graded bedding. Porphyroblastic felspars occur in the mafic bands and as they increase in number, the rocks becomes more coarse-grained and enclose impersistent and lenticular folia of hornblende biotite gneiss. Towards their centers the lighter bands are more homogeneous, leucocratic, often coarse-grained, with fewer mafic lenses or minerals. Specimens are medium-grained and have a crystalloblastic texture.

Under the microscope plagioclase is relatively common (Table 4.6). Myrmekite and staurolite are relatively common in the samples collected (Figure 4.10). Small pale green hornblende crystals are associated with the biotite, both being irregular and the former showing alteration and iron-staining. In addition small diopside crystals slightly replaced by magnetite. Apatite, zircon, sericite and iron ore are common accessories.

Figure 4.9: The geological contact of the feldspar enriched gneisses and hornblende gneisses at River Nzeo.

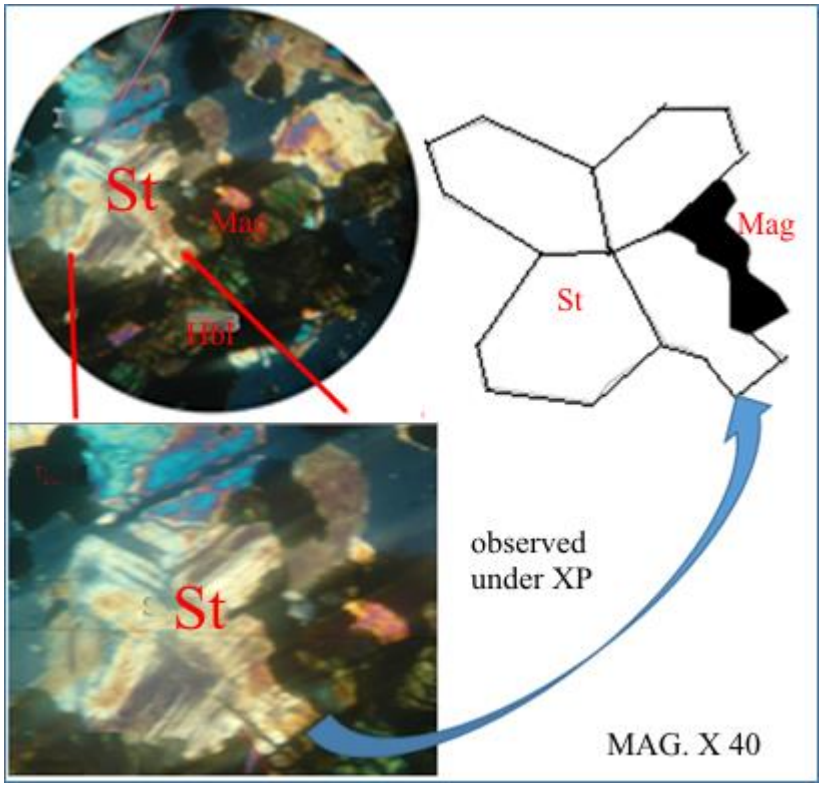

Figure 4.10: Staurolite displaying interpenetration twinning. St = Staurolite, Mag = Magnetite, Hbl = Hornblende. Part of the hornblende crystal has been replaced by magnetite.

Table 4.6: Estimated modal composition of feldspar enriched gneisses.

Mineral	59 (Vol. %)	61 (Vol. %)	62 (Vol. %)	64 (Vol. %)
Hornblende	5	10	4	5
Quartz	17	5	5	15
Plagioclase	68	74	79	70
Myrmekite	1	3	1	0
Biotite	5	2	5	1
Diopside	-	-	-	5
Accessories	3	5	5	4
Total	99	99	99	100

NB: Reference coordinates
59- 396244/9794320; **61**- 397211/9795403; **62** – 397510/9796093; **64** – 398817/9796765

VI. Amphibolite

The field relationships of the amphibolite were determined with some degree of certainty, and proved that they are unconformable with the trend of the rocks in their vicinity, or are found in discordant contact with other rocks. Rocks included in this category are those with high amphibole/pyroxene content and a fairly calcic plagioclase. All are of fairly coarse grain, dark grey-green to black in colour, speckled with white or pale pink feldspars (figure 4.11).

In thin section the hornblende is found to be pleochroic in olive green, and sometimes shows clear evidence of being replaced by hypersthene (Figure 4.12). No quartz was found in any of the slides and the only feldspar is plagioclase.

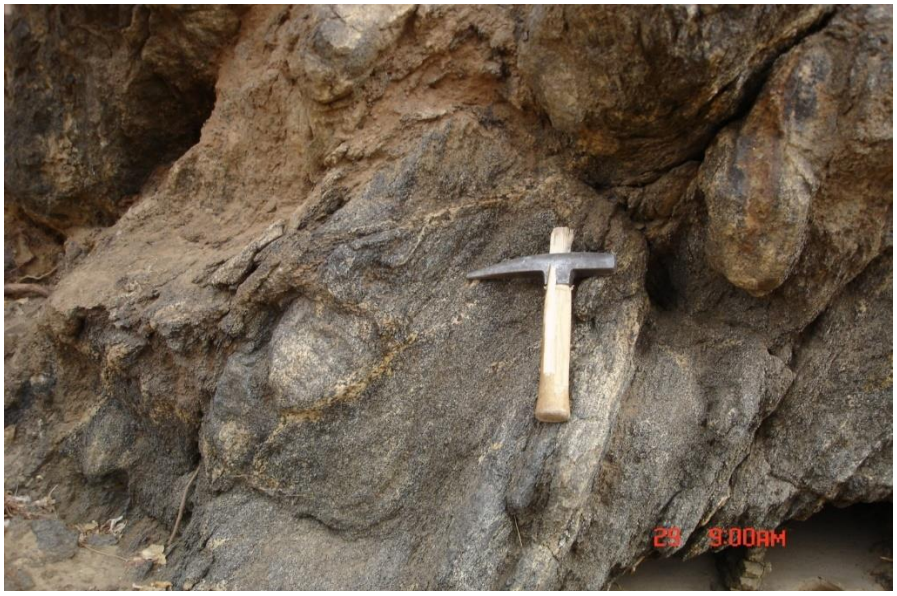

Figure 4.11: Amphibolite found in along the banks of River Tiva

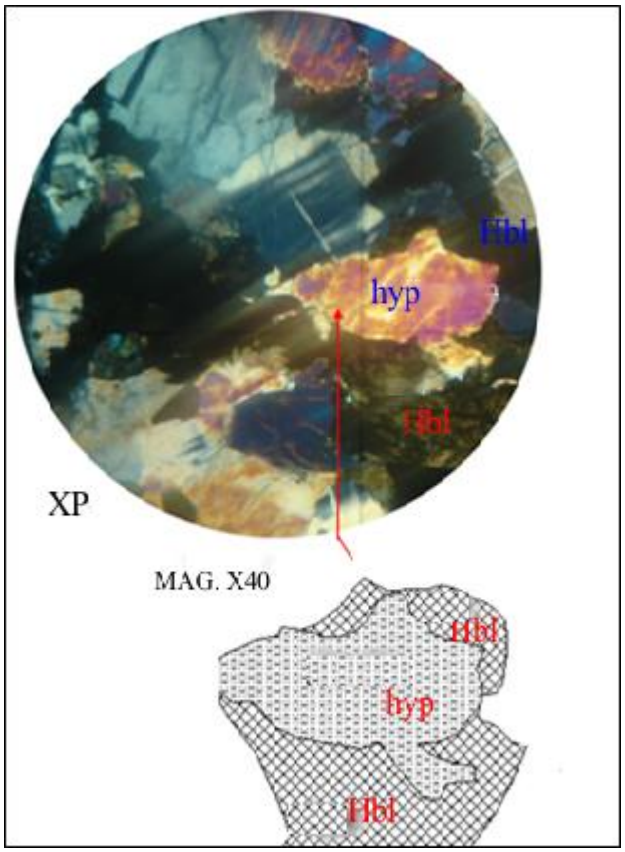

Figure 4.12: Photomicrograph of showing the breakdown of hornblende (an amphibole) which gets replaced by hypersthene (a Pyroxene) defines the lower boundary of the upper amphibolites facies. Hbl = hornblende, hyp = hypersthene .

VII. Olivine Norite

Olivine norite occurs in Muangeni area, 5 Km south western part of Ikutha town. Typical outcrops are elliptical in shape measuring 50 meters by 80 meters. In hand specimen, the rock is very coarse, dark grey and unfoliated (Figure 4.13). Under the microscope Olivine occurs in large anhedral crystals rimmed by hypersthene. Plagioclase feldspar displays the characteristic albite twinning. The mineral modal composition is shown in Table 4.7.

Table 4.7. The modal composition of Olivine Norite under the microscope.

Mineral	(Vol. %)
Hypersthene	20
Olivine	40
Plagioclase	18
Biotite	20
Apatite	1
Iron	1
Total	100

Figure 4.13: Olivine norite at UTM coordinates 409297/9765939 south western part of Ikutha town.

VIII. Pyroxenite

This is an ultramafic rock unit found 2 km west of Ikutha town having about 200 meter length and 50 meters wide. It is non – foliated, medium grain size and dark blue - grey in colour, speckled with white feldspars (Figure 4.14).

Under the microscope, the rock is dominated with hedenbergitic diopside that is pleochroic from yellow to medium blue-green. The feldspars are plagioclase having strong albite twinning. Epidote and sphene occur as small irregular grains, while anhedral magnetite anhedral grains are in contact with diopside. Other minerals noted in this rock include enstatite - which is pleochroic from pale green to pink, hornblende and biotite.

Figure 4.14: Pyroxenite outcrops in situ at west of Ikutha town (Coordinates 406085/9770773)

4.1.2 Mutomo group

The Mutomo group is developed in the central part of the study area and derive their name from the sub – county headquarter town called Mutomo. The main outcrop areas are Mutomo, Muthue, Kasala, Simisi and Mutuluni. This formation consists of;

1. Biotite gneisses
2. Biotite hornblende gneiss
3. Migmatites
4. Marbles

Mutomo formation has been affected tectonically by ductile shearing, folding and faulting. Folds identified within these gneisses include, Yamumu fold, Kimathena and Imiwa – Kaivisi folds. Folding has also affected the gneisses near Mutomo town as indicated by Mutomo anticline. The western part of the study area occupied by these gneisses is affected by major episode of folding whose imprint is exemplified by the Kitui anticline.

The following mineral assemblages are represented by the lithologies within Mutomo gneisses.

(i) Quartz + Plagioclase ± hornblende, biotite, muscovite, magnetite, hematite, apatite, plagioclase

(ii) Quartz + hornblende+ biotite + hypersthene + apatite + zircon + sericite +calcite +sphene

(iii) Quartz + microcline + oligoclase + biotite ± magnetite, hornblende, sphene, zircon

I. Biotite gneisses

They are pale brown in colour, often strongly sheared and foliated, and flecked with small brown biotite flakes which are occasionally concentrated into dark bands (Figure 4.15). They grade into leucocratic granulitic varieties relatively poor in biotite. The biotite gneisses trend in the NW – SE direction, conforming to the general trend of the rocks of the region being investigated.

In thin sections dark brown biotite flakes are associated with quartz and plagioclase (Table 4.8), forming medium-grained heteroblastic texture. Microcline has replaced by oligoclase and quartz, forming deep lobe-like embayments into these minerals, whilst it also contains quartz as small grains in some specimens. Iron ores, rounded apatites, sphene and rare zircon occur as accessory minerals.

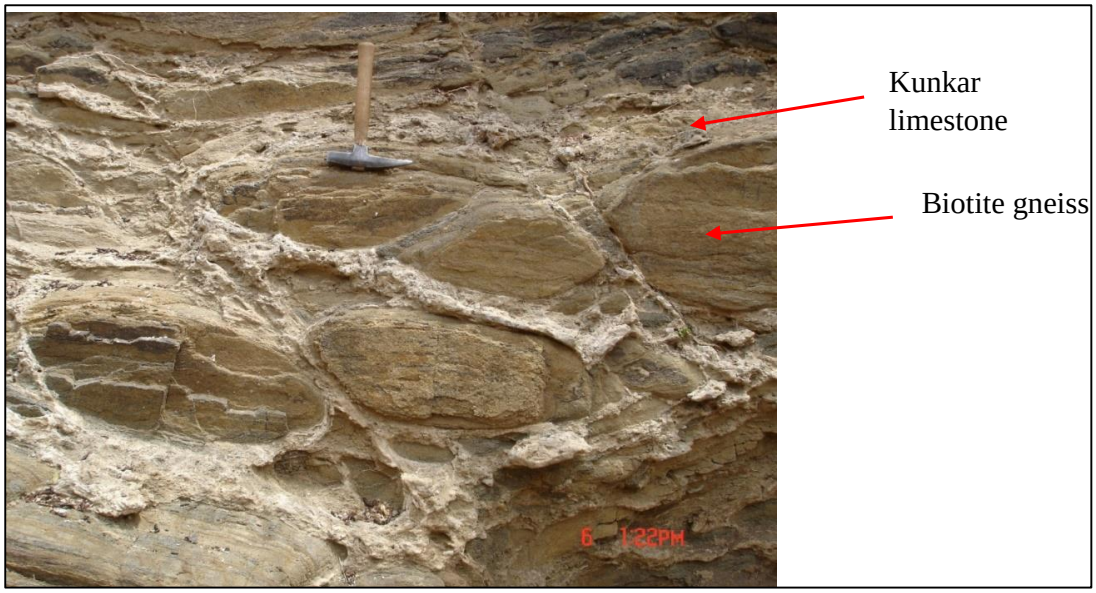

Figure 4.15: Strongly sheared and fractured biotite gneiss that is cemented by secondary kunkar limestone.

Table 4.8: Modal composition of biotite gneiss found in Mutomo formation.

Mineral	8	338	5	7
	(Vol. %)	(Vol. %)	(Vol. %)	(Vol. %)
Hornblende	-	8	-	10
Quartz	14	10	5	5
Plagioclase	80	72	83	74
Biotite	5	7	11	5
Microcline	-	-	-	5
Accessories	1	3	1	1
Total	100	100	100	100

NB: Reference coordinates
8 – 410410/9788531; **338** – 421198/9794858; **5** – 410305/9789600; **7** – 410748/9789256

II. Biotite-hornblende gneisses

These rock type were mapped east of the Mutomo-Kanziku road where they form lower ground between migmatite ridges. They outcrop chiefly towards Ndulukuni, and grade into banded biotite gneisses to the north east of Mutomo town.

The biotite-hornblende gneisses are melanocratic or mesotype rocks generally exposed in river courses only, and are often found to be extremely friable due to the ease with which they

weather. Sometimes they grade into black granulitic varieties, when they form resistant bands in which there is little biotite to be seen. Similar rocks have been described by Saggerson (1957).

Hornblende blades (pleochroic from yellow-green to green to dark brownish green) are intimately associated with pale or dark brown biotite flakes. Specimens from river Kathini show crude preferred mineral orientation. The biotite flakes, which interfinger with muscovite are, seen to wrap round the plagioclase crystals (Figure 4.16). In sheared specimens the mafic minerals are ragged and broken and often wisp-like near the edges of the more euhedral feldspar crystals. Iron ore, including blood-red hematite, prismatic apatite, zircon, sericite, calcite and sphene are minor constituents (Table 4.9).

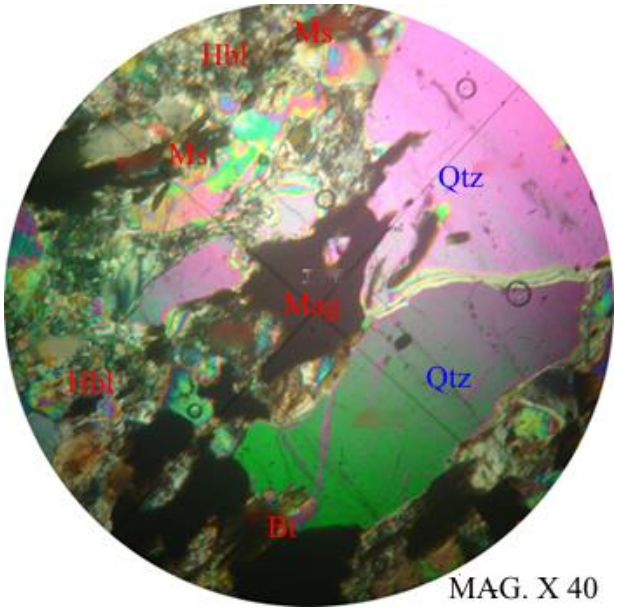

Figure 4.16: Microphotograph of biotite hornblende gneiss. Bt = Biotite, Ms= Muscovite, Mag= Magnetite, Hbl = Hornblende

Table 4.9: Modal composition of the biotite hornblende gneiss

Mineral	75	81	84	57
	(Vol. %)	(Vol. %)	(Vol. %)	(Vol. %)
Hornblende	23	10	10	15
Quartz	50	63	67	60
Plagioclase	8	5	5	5
Biotite	14	9	10	15
Myrmekite	1	1	2	1
Hypersthene	1	8	2	1
Accessories	2	3	4	3
TOTAL	99	99	100	100

NB: Reference coordinates
75 – 416552/9784570; **81** - 415001/9790075; **84** – 413403/9787666; **57** – 395476/9794075

III. Migmatites

Migmatites are composite silicate metamorphic rocks, pervasively heterogeneous on a mesoscopic to megascopic scale. It typically consists of darker and lighter parts. The darker parts usually exhibit features of metamorphic rocks whereas the lighter parts are of igneous-looking appearance. They are composite igneous and metamorphic high grade rocks that record crustal flow processes at the roots of orogens (Whitney *et al.*, 2004). Migmatite petrology gives insights into the composition and differentiation of the middle to upper crust, while migmatite structures register the deformation that is active during orogenesis (Ashworth, 1985).

The petro-structural characteristics of migmatites (Figure 4.17) have been studied and classified for over thirty years (Mehnert, 1968). Quantitative (Blumenfeld and Bouchez, 1988; Leitch and Weinberg, 2002), and qualitative (Brown and Rushmer, 1997; Weinberg and Mark, 2008) work was extensively employed, encompassing field mapping, melt topology and fabric analysis to characterise the structure and reconstruct the emplacement and strain history and their relationships with large-scale crustal deformation. However, the inherently complex geometry at the outcrop scale constantly renders tectonic interpretations uncertain or ambiguous. Due to both their igneous and metamorphic nature, migmatites behave as two-phase materials enhancing strain localisation in the liquid (magma) phase and promoting strain hardening in the solid (host rock) phase; textures are commonly divided into solid-state in the

metamorphic host and magmatic microstructures in the leucosomes or magma (Vigneresse *et al.*,1996; Vernon, 2000).

Migmatite outcrops are characterized by the intermixing of mineral aggregates of very marked contrast, taking the form of leucocratic host-rocks enclosing lenses and schlieren of melanocratic character. They are characterized by acute contortions on a small scale, indicative of tight folding whilst in a semi-plastic state. Where such rocks are weathered to smooth pavements or low rounded erosion residuals, as is often the case, it is usually possible to determine their overall strike and dip, which always prove to be in good accord with the regional pattern. The melanocratic components of these rocks are biotite and hornblende.

In Mutomo - Ikutha area, the rocks in the north-western part of the area and on the ridges immediately adjacent to the Mutomo-Kanziku road are considered to be migmatites. They are highly granitized gneisses derived partly from semi-pelitic rocks in which veins, lenses and laminae of granitic material exhibit crude parallelism concordant with the original sedimentary pattern or occur as ptygmatic veins. Unorientated feldspar porphyroblasts indicate the initial stages of grantization and the rocks grade into augen gneisses (near the locus of greatest grantization, as noted on the Mutomo ridge) in which oligoclase and microcline porphyroblasts are more frequent and orientated.

Mutomo – Ikutha migmatites can be classified using Mehnert (1968) structural classification based on the relationship between the leucosome and melanosome as follows;

a. **Vein-type migmatites:** The leucosome forms a fairly random network of distinct veins that separate irregular blocks of melanosome (Figure 4.18A).
b. **Stromatic migmatites:** The most common type, in which the leucosome forms concordant layers that are commonly parallel to the schistosity of the melanosome. The layers are rarely continuous, however, and typically die out and/or cross-cut the melanosome at some point along their length (Figure 4.18B).
c. **Nebulite:** The leucosome occurs as irregularly-shaped patches that grade into the melanosome (Figure 4.19A).
d. **Agmatite:** Numerous blocks of paleosome are surrounded by subordinate and relatively narrow veins of leucosome (Figure 4.19B). Agmatites are typically enclave-rich zones marginal to granitoid intrusions.

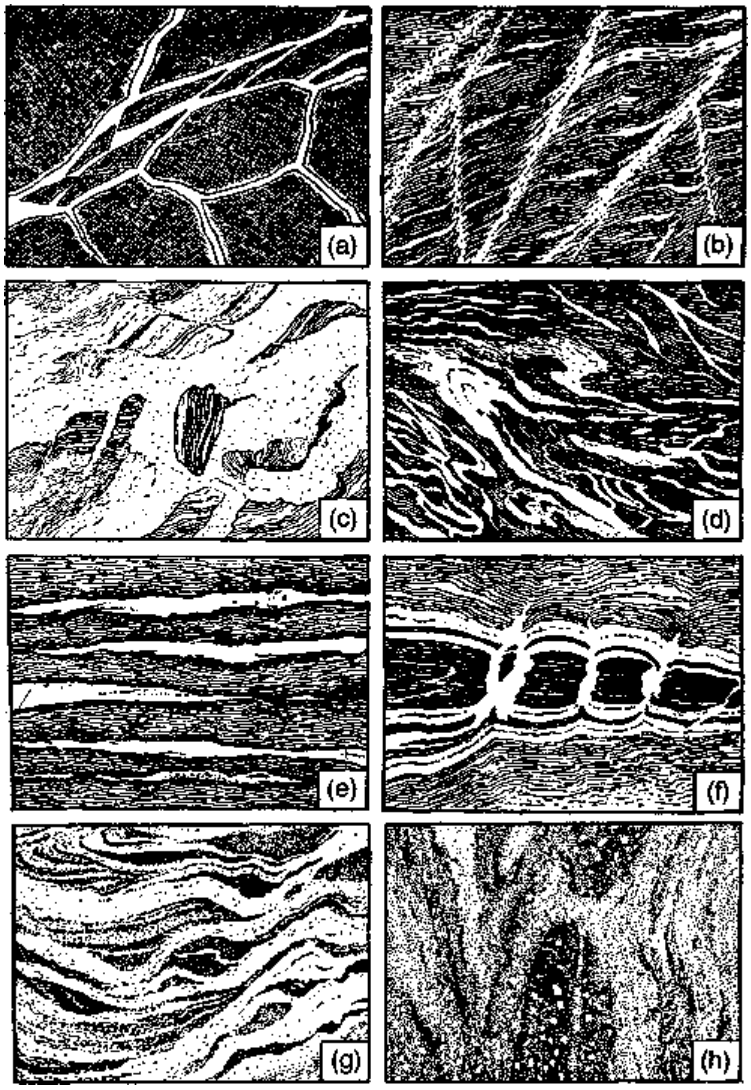

Figure 4.17: Some textures of migmatites. (a) Breccia structure in agmatite. (b) Net-like structure, (c) Raft-like structure. (d) Vein structure, (e) Stromatic, or layered structure, (f) Dilation structure in a boudinaged layer, (g) Schlieren structure. (h) Nebulitic structure. From Mehnert (1968).

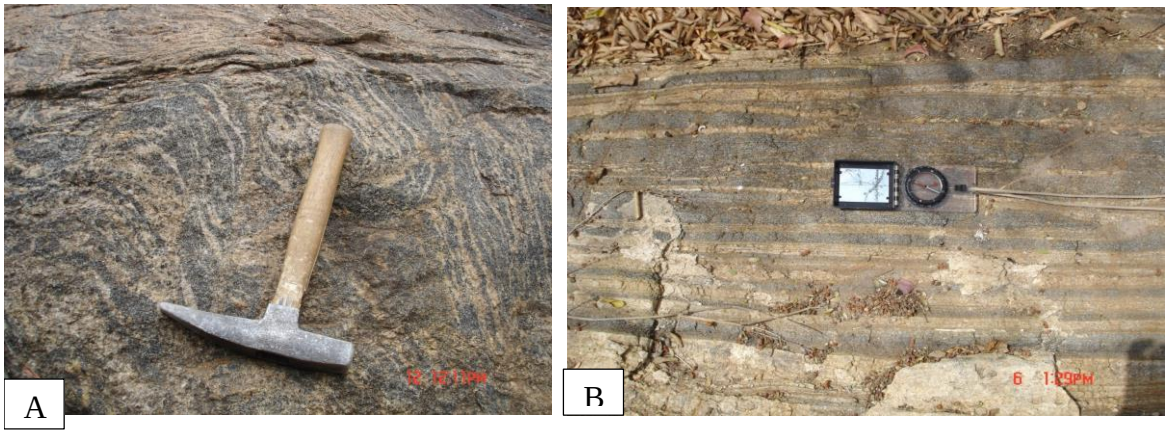

Figure 4.18: (A), Vein structure migmatite located at station 351 of coordinates 421108/9799730. (B) Stromatic, or layered structure migmatite located at station 344 of UTM coordinates 418824/9797410.

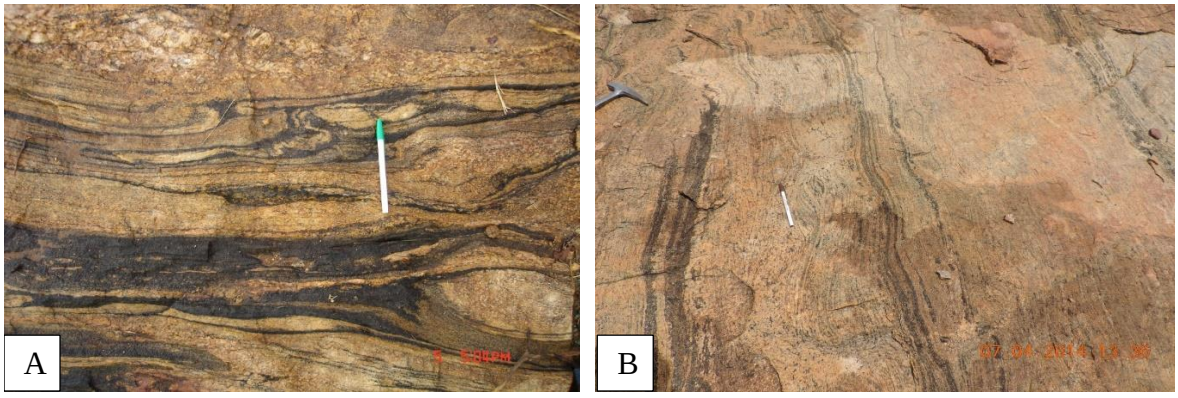

Figure 4.19: (A), The Schlieren and Nebulite structure migmatite showing leucosome that are irregularly-shaped and grade into the melanosome at station 99 of UTM coordinates 420652/9786864. (B), Agmatite structure located at station 212 of coordinates UTM 420573/9794517.

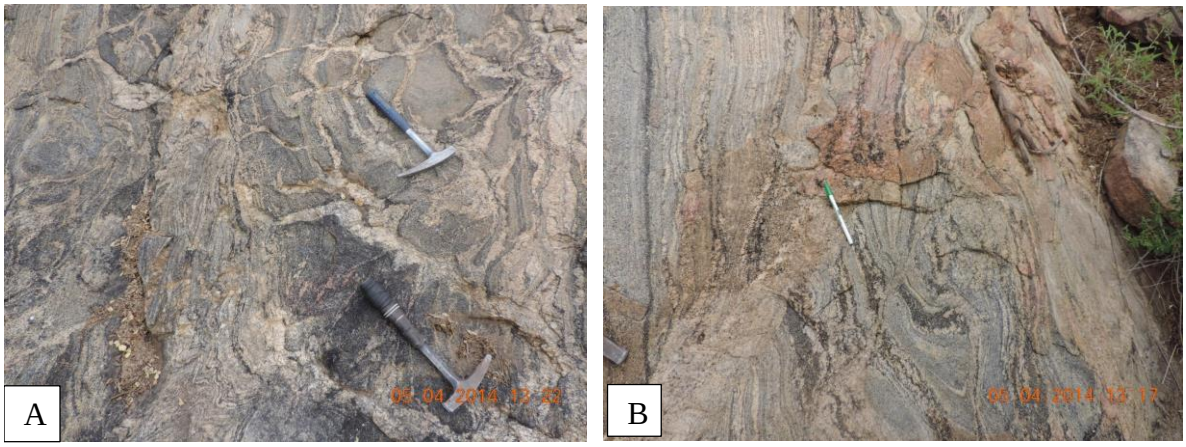

Figure 4.20: (A) Vein migmatite structure. The migmatite has also undergone shearing as noted from the folded veins. (B), Raft-like structure. The migmatite has undergone shearing as depicted by shear band (located where the pen is placed).

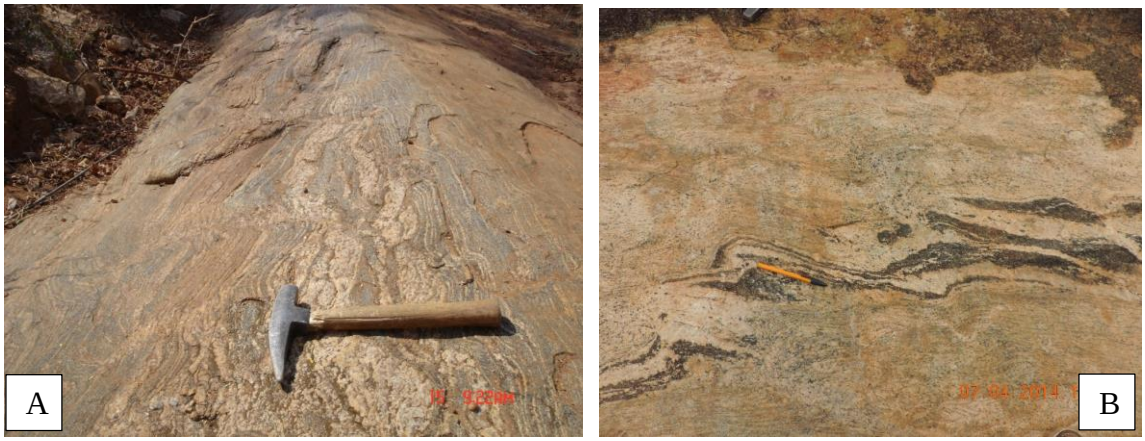

Figure 4.21: (A), Dilation structures in a migmatite as classified by Mehnert (1968), and observed in Mutomo formation. (B) Schlieren structure, South of Mutomo town at UTM coordinates 413033/9795188

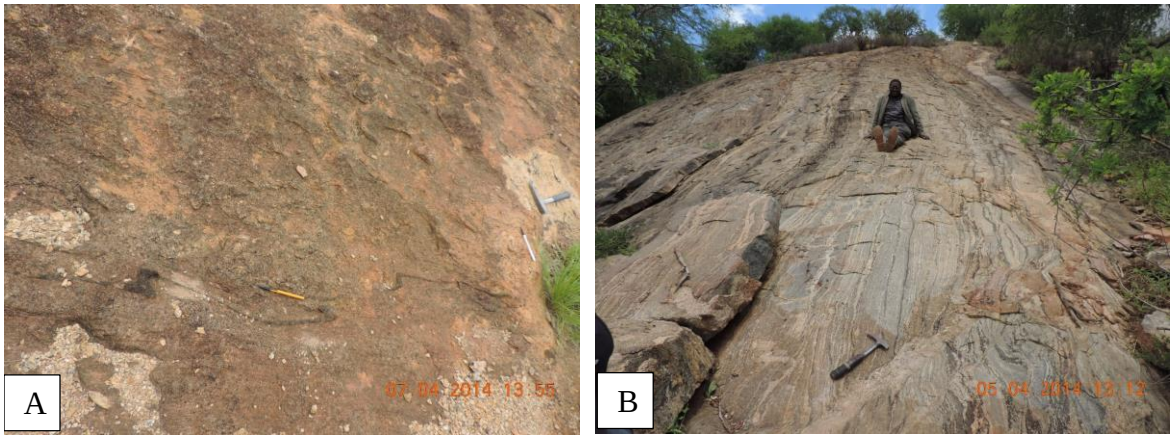

Figure 4.22: (A), Snake structure in migmatites, South of Mutomo town at UTM coordinates 413030/9795168. (B), Banded migmatite along Mutomo – Mutha road, UTM coordinates 419376/980059.

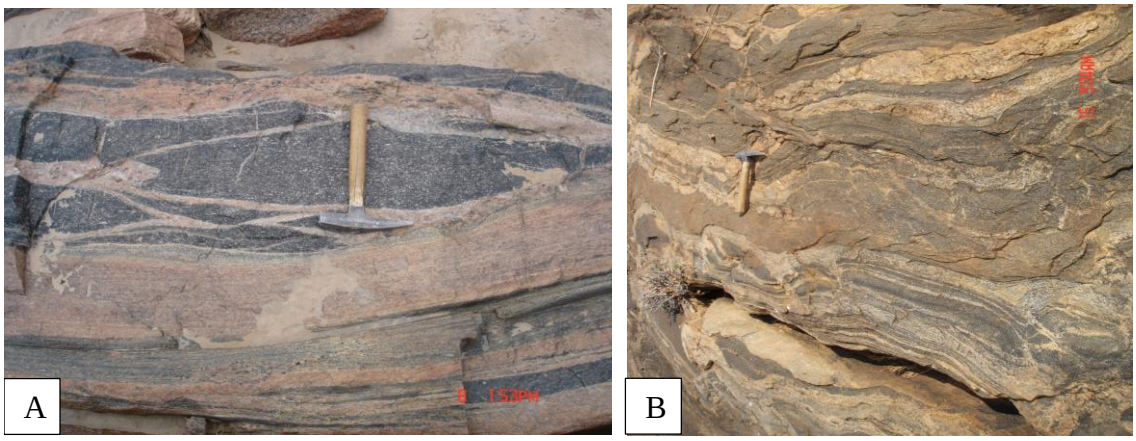

Figure 4.23: (A), Breccia structure at station 95 of location UTM coordinates 418562/9785845. (B) Migmatite with granoblastic aggregated of feldspars and quartz

Other common structures are net-like structures similar to veins, but accompanied by shear (Figure 4.20A); raft structure that are similar to agmatite, but commonly sheared (Figure 4.20B); dilation structure, in which the leucosome fills openings in stretched competent layers (Figure 4.21A; and schlieren, stretched or sheared irregular streaks of melanosome that taper at the ends (Figure 4.21B), snake structure (Figure 4:22A), Banded structure (Figure 4.22B) and breccia structure (Figure 4:23A). For a more detailed classification, and a discussion of migmatite structures and textures, see Mehnert (1968) and Ashworth (1985).

Along the Mutomo - Kanziku road, strongly banded migmatitic gneisses (Figure 4.22B) grade into homogeneous leucocratic rocks in which a faint wavy foliation is visible. Other typical examples of the biotite migmatites is found in Kemwa and Chamusia area, west of Kasala.
The leucocratic component is mineralogically fairly typical biotite gneiss, except that the plagioclase is rather basic, being of the composition of andesine. It usually shows albite twinning. Biotite, dichroic from yellow-brown to black, makes up 12 % of the rock and quartz and orthoclase are important constituents. In the melanocratic components biotite makes up only 2 per cent against 65 per cent of hornblende. Plagioclase feldspar here is mostly untwined, again andesine. Small amounts of orthoclase and quartz also occur. Faintly twinned oligoclase, hornblende and biotite are associated with ragged pale-green diopside partly altered to hornblende. Magnetite, ilmenite, sphene, epidote and large prismatic apatites are accessory.

Ptygmatic veins are considered by Wilson (1980) to be of primary or secondary origin. He classifies the veins into three structural groups. In Mutomo - Ikutha area, examples of veins in which the contortions have resulted from primary buckling during injection into static country-rock were seen. Other veins, however, are considered to have some tectonic significance and to be the product of combined primary injection and country-rock movement. In these cases the direction of injection was at right angles to the strike, whilst the traces of the axial planes of the ptygma parallel the strike of the migmatites and the axes of the major folds.

The leucocratic bands are a granoblastic aggregate of feldspar and quartz with subordinate hornblende and biotite (Figure 4.23B). Epidote, calcite, muscovite and iron ore are accessory minerals and are commonly confined to the crushed margins of the feldspar. In more homogeneous types local banding is still present and hornblendic granitoid foliation swell and pinch between thinner parallel melanocratic bands, which contain varying proportions of

biotite and hornblende. Some of them have a preponderance of biotite towards their edges whilst their centres are composed of meso-type rock.

Granitic veins invade the main gneissic host-rocks, particularly around Mutomo area. The veins are faintly sinuously banded but the banding does not conform to that in the host rock, whose foliation wraps round the intrusions. These veins exhibit a more typical granitic hypidiomorphic-granular texture than the host rocks which commonly have xenomorphic-granular textures. Some of the granitic material that have invaded host rocks form ptygmatic veins as observed in Nzeveni (Figure 4.24). Migmatites in the area form part of the Mutomo anticline which is observed in the vicinity of Mutomo town.

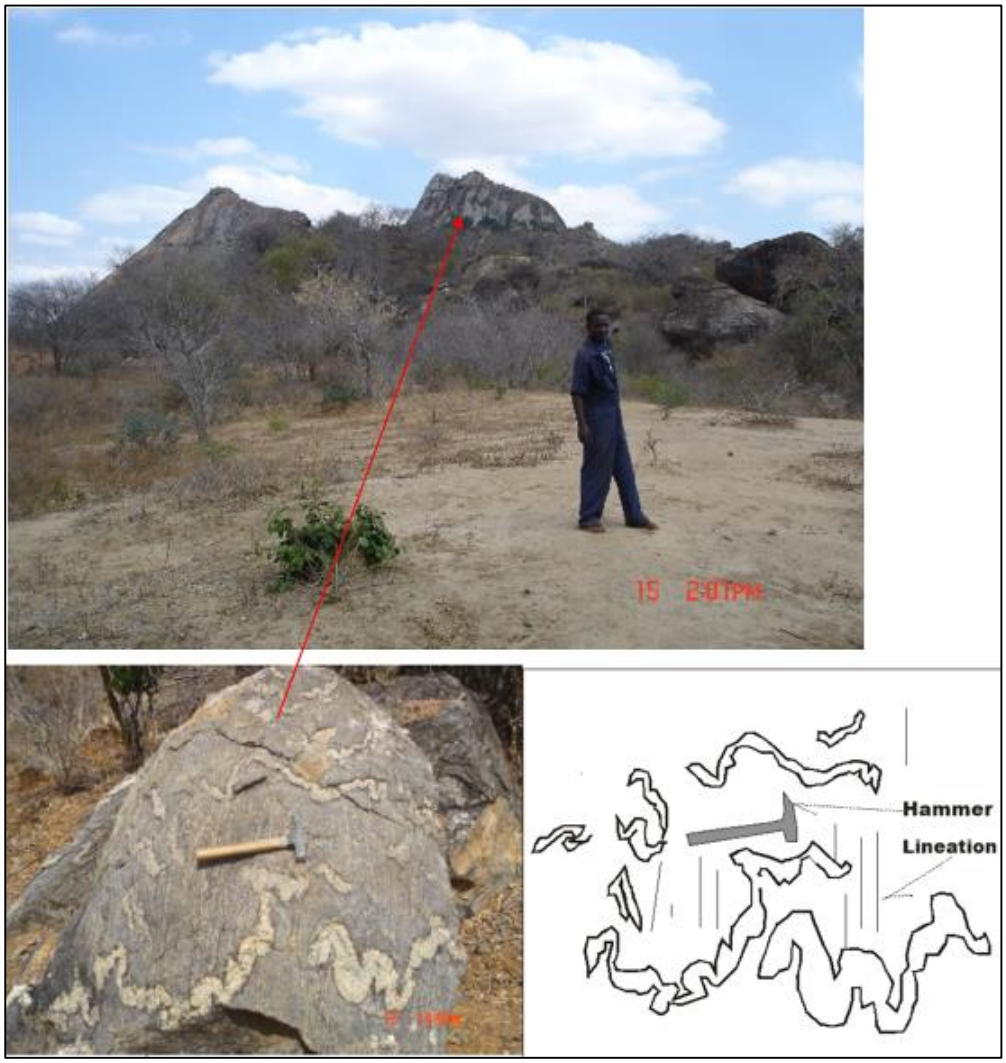

Figure 4.24: Ptygmatic folds in a Migmatite at way point 104, Nzeveni area (X = 0424022, Y = 9788499). The granitic materials cut across the lineation.

IV. Granitoid gneisses

These are coarse-grained rocks, varying in colour from cream to pink, and often carrying very small amounts of mafic minerals, usually magnetite, hornblende and biotite. Major minerals are Quartz, Microcline, and Plagioclase (Table 4.10). Foliation is usually only poorly marked, and shows itself by alignment of mafic crystals and sometimes by the flattening and elongation of quartz and feldspar grains. Accessories include magnetite, hornblende, biotite, muscovite, garnet, epidote, sphene and zircon. Replacement of richterite by iron ore (magnetite) is noted in some slides (Figure 4.25).

Table 4.10: Modal composition of the granitoid gneiss

Mineral	100	101	98	89
	(Vol. %)	(Vol. %)	(Vol. %)	(Vol. %)
Quartz	55	40	27	25
Microcline	36	40	55	60
Plagioclase	8	15	15	12
Accessories	1	3	3	3
Total	100	98	100	100

NB: Reference coordinates for samples.
100 – 420791/9786985; **101** – 422279/9786774; **98** – 419562/9786847
89 – 418301/9791831

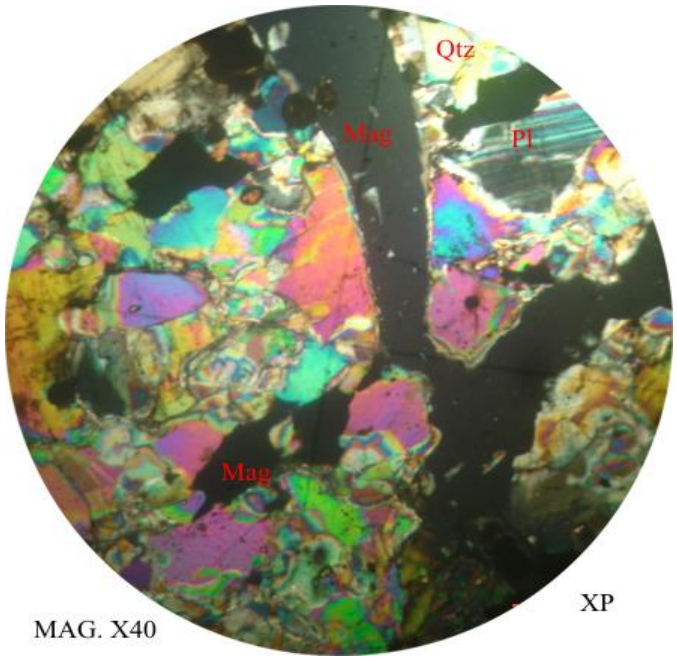

Figure 4.25: Photomicrograph of granitoid gneisses showing replacement of Quartz by Iron ore. Mag=Mag, Pl= Plagioclase , Qtz = Quartz.

V. Marbles

Bands and lenses of marbles sometimes reaching three hundred meters in width of outcrop are found in Mutuluni (Figure 4.26), Kasala and Simisi. Colours range from pure white to light red and shades of grey and blue-grey. There are colour variations in different parts of the same outcrop, and could not be used as a criterion for identifying discontinuous outcrops of the same hand specimens from all the larger outcrops which contain a small percentage of dolomite. Graphite occurs in some of the exposures examined, as single flakes disseminated throughout the rock, but occasionally in large lenses enclosed in and marginal to the limestone.

Figure 4.26: White marble outcrops in Mutuluni, north of Kasala area, about 8 Km from Ikutha in the NE direction.

4.1.3 Kapoponi group

Kapoponi formation occurs in the north-eastern part of the area. The name Kapoponi is derived from the hills found in the area where these rock units occur. Kapoponi formation consists of: Oligoclase porphyroblast gneisses, biotite garnet gneisses, garnet enriched rocks, quartz-feldspathic gneisses. This formation also contains intrusives and deformed pillow basalts. The intrusive rock units include: Gabbro, melano gabbro, pyroxenite, peridotite, and serpentinite.

I. Oligoclase porphyroblast gneisses

Oligoclase porphyroblast gneisses form prominent ranges of hills from Mathima to a few kilometers north of Ndulukuni. They have conspicuous orientated feldspar porphyroblasts (Figure 4.27). Biotite and hornblende are the common mafic minerals whilst garnet is developed in thin bands. The modal composition of the oligoclase porphyroblast gneisses is presented in Table 4.11.

Figure 4.27: The photograph showing Oligoclase porphyroblast gneiss. The porphyroblasts can be seen near the top edge of the hammer. The photograph was taken at station 394, whose coordinates in UTM are; 419967/9786798.

Table 4.11: Modal composition of oligoclase porphyroblast gneisses

Mineral	85	80	61	394
Type	(Vol. %)	(Vol. %)	(Vol. %)	(Vol. %)
Hornblende	2	1	1	1
Quartz	15	10	15	16
Plagioclase	59	65	60	65
Microcline	15	18	15	10
Biotite	7	4	5	5
Garnet	1	1	-	-
Iron ores	1	1	2	3
Total	100	100	98	100

NB: Reference coordinates for samples: **85** - 411486/9787227; **80** – 415268/9790498; **61** – 397211/9795403; **394** – 419967/9786798

II. Biotite-garnet gneisses

They are dark-grey meso type rocks, often well foliated, the foliation being emphasized by melanocratic bands rich in biotite. They outcrop mainly in stream sections and are interbedded with, or grade into, flaggy biotite gneisses and hornblende granulite and gneisses. A horizon occurs in the Ndulukuni syncline where the gneisses show good foliation, but the garnets are larger and generally confined to the darker bands. Specimen 91 (Table 4.12), from the Kapoponi area, contains small euhedral pale pink garnets, up to 0.5 mm in diameter. The garnets are associated with variably orientated dark brown and greenish-brown biotite flakes in a fresh granoblastic mosaic of plagioclase and quartz (Figures 4.28 and 4.29). The plagioclase which encloses small rounded blobs of quartz is mostly oligoclase, finely albite-twinned and in one case pericline-twinned.

Figure 4.28: Pink coloured Biotite garnet gneiss in situ (X = 419306, Y= 9794150). It is a medium to coarse grained rock. Light brown to dark coloured minerals.

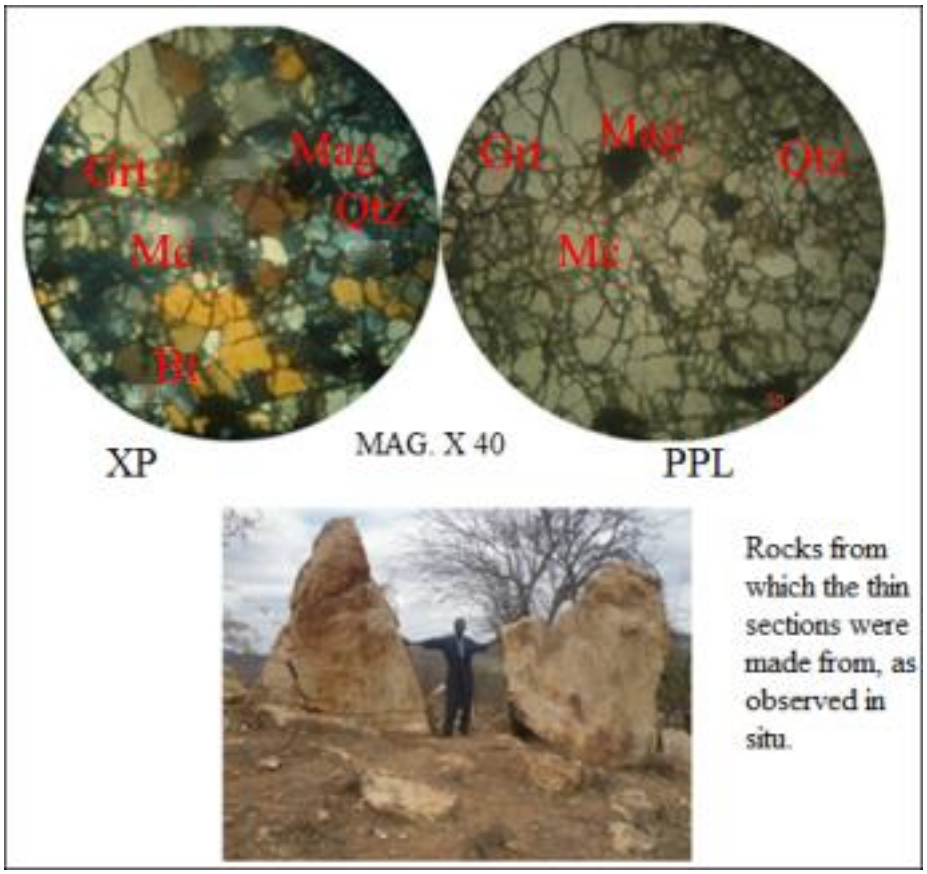

Figure 4.29: Light coloured Biotite garnet gneisses Way point 216 (415505/9799060). Grt = Garnet, Mag =Magnetite, Mc=Microcline, Qtz= Quartz, Bt=Biotite

Table 4.12: Modal composition of biotite garnet gneiss

Mineral	210	208	91	216
	(Vol. %)	(Vol. %)	(Vol. %)	(Vol. %)
Hornblende	1	-	-	1
Quartz	10	6	10	15
Plagioclase	65	65	70	60
Biotite	20	25	15	20
Garnet	3	3	4	4
Accessories	1	1	1	1
Total	100	100	100	100

NB: Reference coordinates
210 – 424527/9791610; **208** – 423300/9793713; **209** – 423920/9792378
216 – 415505/9799060

III. Garnet-rich gneissic rocks

A deep red massive garnet-rich rock with a distinct gneissose texture forms Magongo hill, on the northern side of one of the dunite pipes at Ndulukuni. This rock has been reconstituted from the garnetiferous biotite gneisses in which the dunite was emplaced. Garnets which are almandine are randomly distributed in the host rock (Figure 4.30). The diameter of the garnet crystals is in the range of 0.1 mm to 1 cm.

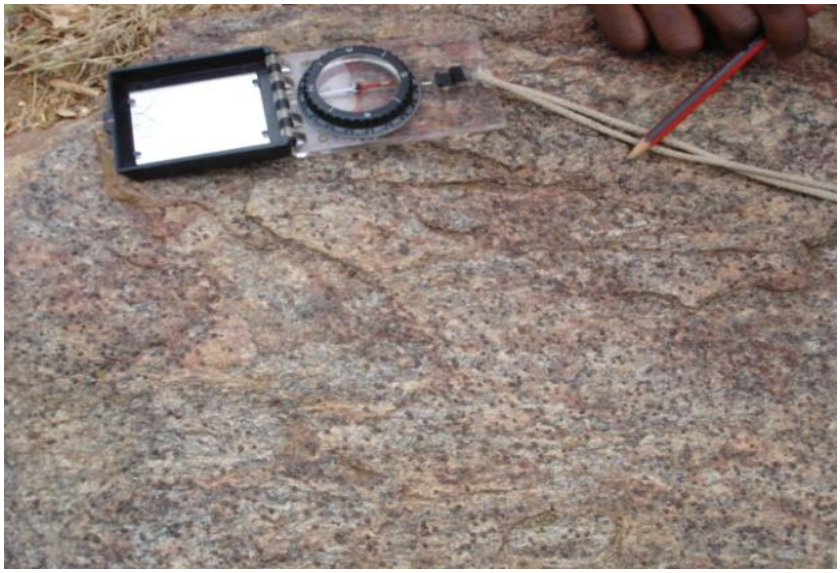

Figure 4.30: Unevenly distributed garnets in garnet enriched rock.
The garnets are of almandine variety. Outcrops occur west of Mutomo town.

IV. Quartz-feldspar gneisses

Leucocratic quartz-feldspar gneisses form the hills of Kanziku, Nzwani and Mutha. They are mostly homogeneous, white or buff, coarse- to medium-grained rocks containing minor hornblende and/or biotite, which have a random orientation. Melanocratic lenses occur as bands in the rocks. These rocks are found in Ndilili north of Kanziku area. The rocks are considered to be metamorphosed psammitic sediments which had original interbanded semi-pelitic material, and pass into the semi-pelitic series.

The quartz-feldspar gneisses are heteroblastic rocks in which microcline is often common and is seen to replace plagioclase. Quartz forms irregular, re-crystallized grains but is rarely contained as droplets within the feldspar and occasionally forms a graphic intergrowth with biotite flakes. Oligoclase shows the greatest alteration, being clouded by sericite flakes, and is associated with myrmekitic growths. Rare muscovite flakes were seen in some specimens. Like the quartz-feldspar granulites these rocks contain perthite (Figure 4.31). Near the darker bands there is a greater proportion of hornblende and biotite which occur as unorientated blades and flakes. The hornblende which is sample 427 (Table 4.13) occur as dark olive green variety is commonly altered to chlorite, whilst the biotite has a pale pinkish brown to greenish brown colour.

Table 4.13: Modal composition of quartz-feldspathic gneiss

Mineral	**426**	**427**	**424**	**428**
	(Vol. %)	(Vol. %)	(Vol. %)	(Vol. %)
Hornblende	-	1	-	-
Quartz	10	4	14	10
Microcline	40	30	10	15
Perthite	-	-	-	3
Oligoclase	54	60	70	66
Biotite	3	3	3	3
Accessories	2	1	2	3
Total	99	99	9	100

NB: Reference coordinates
426 – 411397/9772770; **427** – 411621/9772314; **424** – 410914/9773802
428 – 411513/9772028

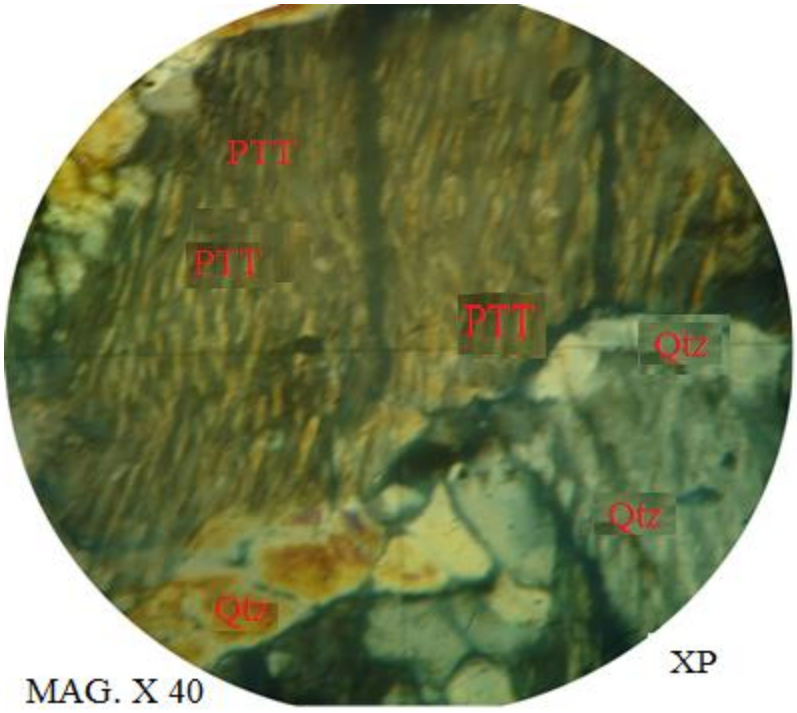

Figure 4.31: Perthite feldspar in quartz feldspar gneisses. Perthite indicates high temperature metamorphic zone (PTT=Perthite, Qtz=Quartz).

V. Intrusive rocks

Four ultra-basic intrusives and associated rocks occur near, the axis of the Ndulukuni anticline. Three of these intrusives include ; Kapoponi, Magongo and Mukono-outcrop occur as small knolls, 5 km north of the Ndulukuni peak whilst the fourth, Kenze, is 7 Km north of ndulukuni. The intrusions are dunite pipes which are rarely seen outcropping at the surface, but in most places are covered by large black boulders of basic rocks, the boulders often being so massive as to suggest that they are in situ.

At Kapoponi and Kenze, a pit of magnesite quarry show that dunites are underlain by soft yellowish green serpentinized material and have been formed by the weathering of the dunite. The serpentine alters to form magnesite which is being mined (Figure 4.32). Where exposed in the trenches the dunite is cut in every direction by Magnesite veins varying in width from a fraction of a centimeter to two meters.

Figure 4.32: The photo showing alteration of serpentinite to form magnesite in Kapoponi area

Asbestos, talc and vermiculite are also associated with the basic intrusions but good exposures of the vermiculite are associated with the magnesite veins. On the southern side of Kapoponi, large patches of nearly pure pyroxene (enstatite) rock were seen and probably represent a differentiation product of the original intrusion. At Magongo hill the dunite is the principal rock of the intrusions in which olivine altered to serpentine and antigorite forms about 95 per cent, the remainder consisting of clinopyroxene, pyrrhotite and iron ore. The boulders that overlie the intrusions in these areas are melanocratic, heavy rocks medium-grained but occasionally fine-grained, and vary considerably in mineral composition. Dykes and sills that were intrusive into the Neoproterozoic rocks before metamorphism are numerous in the area. The outcrops vary from a few centimeters to over ten meters in width. The metamorphosed intrusive rocks include amphibolites, plagioclase and pyroxene amphibolites, hornblende-pyroxene gneisses and a pyroxenite. The presence of dunites, serpentinites, sheeted dikes, pillow lavas, Gabbros and sediments indicates that this area is an ophiolite suite as proposed by Vearncombe (1983).

(a) Amphibolites

These rocks grade from plagioclase and pyroxene-bearing amphibolites to amphibolites with increased in hornblende content. Coarse-grained dark green amphibolite occurs in contact with the quartz-feldspar gneisses south of Nzoani (Figure 4.33), whilst the remaining types were seen in the semi-pelitic series. The accessory minerals in these amphibolites are magnetite and titanite.

Figure 4.33: An amphibolite at location 419306/9794150. The rock out crop is intrusive that has undergone some metamorphism.

(b) Pyroxenites

The pyroxenite outcrops in the river Kathini (Figure 4.34). It is an intrusion, green in colour, occurring as irregular patches in gneisses. It is a nearly monomineralic rock and is composed of pale green diopside partly replaced by pale green hornblende, and calcite. Pyroxenites have small felspar content and pyroxene is the dominant mineral, associated with hornblende which pseudomorphoses it in part, and pale green chlorite. Specimen from Magongo contains abundant green spinel in addition. Brown oxidised ilmenite is scattered throughout the rock.

Figure 4.34: The photo shows pyroxenite rocks unit in Kathini River near Kenze area.

(c) Gabbros

The gabbros range from fine-grained rocks to more coarse-grained types generally exhibiting a hypautomorphic granular texture in which the felspars are rarely idiomorphic (Figure 4.35 and 4.36). Pale to emerald green pyroxene is associated with a pale pink augitic type and is little altered to hornblende. Primary green hornblende, strongly pleochroic in shades of green, is tabular in habit but usually sub-idiomorphic (Figure 4.37). The ferromagnesian minerals are associated with granular iron ore which in some cases is enclosed entirely within the hornblende. All the samples analyzed have plagioclase and pyroxene (Table 4.14)

Figure 4.35: Gabbro rocks near Kanyunga at way point 93 (X=0421537, Y = 9795267)

Figure 4.36: Sheeted gabbroic dykes around Mutomo area. The dykes are in a biotite gneiss located 3 km south of Mutomo town

Table 4.14: Modal composition of Gabbro

Mineral	93	94	95	96	97	98
	(Vol. %)	(Vol. %)	(Vol. %)	(Vol. %)	(Vol. %)	(Vol. %)
Plagioclase	60	40	15	20	40	35
Pyroxene	20	60	74	77	10	15
Hornblende	18	-	5	-	50	50
Garnet	-	-	-	3	-	-
Iron ore	2	-	2	-	-	-
Accessories	1	-	4	-	-	-
Total	100	100	100	100	100	100

NB: Reference coordinates
93: 418768/9797456; **94**: 418767/9797639; **95**: 421980/9792606; **96**: 418765/9797550
97: 418765/9794860; **98**: 418824/9797410

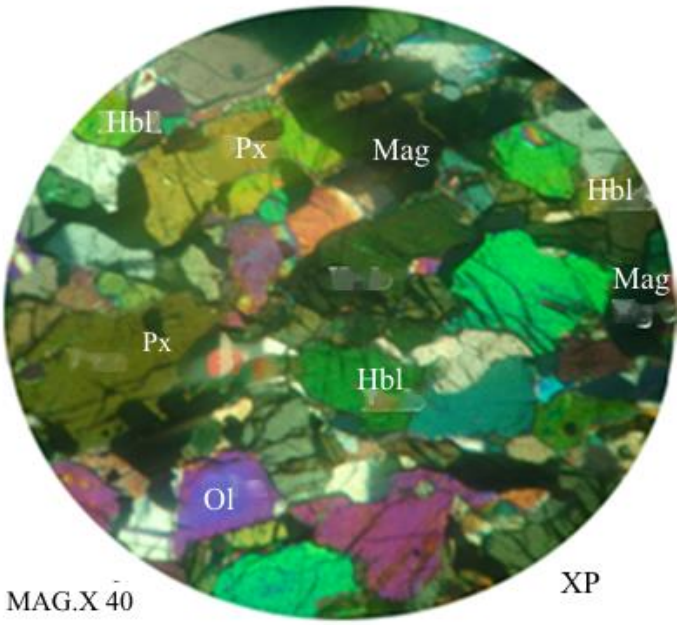

Figure 4.37: Photomicrograph for a gabbro at Kenze area, way point 93 (X = 421537, Y = 93957267). Px = Pyroxene, Hbl = Hornblende, Ol = Olivine, Mag=Magnetite

(d) Melagabbros

The Melagabbros are similar to the gabbros except that they contain less plagioclase feldspar, with a corresponding increase in pyroxene content. A single example of melagabbro was picked up at Magongo and like the rocks previously described appears granulitic in the hand-specimen. A thin section however shows that its grain size varies from 0.5 mm. to 3 mm. Brown pleochroic hornblende is associated with fairly fresh augite, whilst pale pink euhedral garnet is accessory. The amphibole contains occasional rounded inclusions of augite and in certain cases is clearly replacing pyroxene. A little labradorite, occurring interstitially between the other minerals, is present but is not abundant. Rare iron ore is the 'only other accessory.

(e) Hornblende Gabbro

Basic intrusive in which hornblende is the predominant and ferromagnesian mineral are rare. Pyroxenes are less than 5 %. Three slides of such rocks were examined and in these the hornblende is predominant mineral, there being a marked reduction in the pyroxene content. The hornblende shows slight replacement by brown biotite, whilst larger tabular crystals have ragged borders unlike the amphiboles of the gabbros. The plagioclase, like that in the gabbros, is calcic with a composition about that of bytownite. Rounded apatites occur in these rocks.

(f) Peridotite

The peridotite from Kapoponi is a more coarse-grained rock in which little alteration was observed. Abundant and fairly fresh olivine, hypersthene, and green spinel are the common minerals and iron ore is present more rarely. Slight serpentinization of the olivine occurs along fine cracks, whilst granular iron ore is scattered throughout the crystals. Characteristically the pleochroic hypersthene occurs as subhedral crystals up to 2.5 mm. in length.

VI. Pegmatites

Pegmatitic intrusion accompanied granitization in the migmatitic parts of the area and in the quartzo-felspathic gneisses in the east. The larger bodies are sheets and veins averaging half a meter to one meter in thickness. Though some of the pegmatites may have been formed by replacement, in general their intrusive character is shown by the cross-cutting nature of the veins which often branch from the concordant sheets. These intrusions have clear-cut margins and invade all rock types within the Migmatites. Fine-grained quartzo-felspathic aplites are frequently seen as narrow anastomosing veinlets and are found in areas where pegmatites are numerous. At least two stages of pegmatitisation are recognized. Pegmatites of the first stage, which cut and are thus later than the conformable granitoid gneisses, are assumed to have been emplaced during the main phase of granitization. A second, late stage occurred after the migmatites had resumed some rigidity, as shown by the veins that have been emplaced in fault-planes, the faults being small strike-slip movements associated with drag-folding.

The pegmatites are white, pink or brown in colour and are either uniform or variable in texture. In the coarser varieties large six-inch flesh-coloured felspars occur within a coarse quartz-felspar matrix with few or no mafic minerals. Magnetite-bearing quartz segregations occur at the southern foot of Mutha, south of Mwanavya, southeast of Kanziku and south of Ikutha (Figure 4.38). These occur within an area of metamorphosed psammitic sediments. Schoeman (1948) draws attention to mafic aureoles surrounding segregation pegmatites, suggesting that the enrichment in mafic minerals is due to subtraction of felsic material required to form the segregations. Such aureoles were commonly seen in the present area, as at Kanyunga near Mathima, the mafic constituents being biotite and hornblende.

Figure. 4.38: Pegmatite in a hornblende gneiss at location 0400180/9761681. South of Ikutha town.

4.1.4 Results on Metamorphism

Both field and petrographic studies of the metamorphic rocks have shown that the rocks in Mutomo – Ikutha area underwent at least, two-distinct metamorphic events, M1 and M2. M1 event was associated with NE-SW compressional accompanied by SE extension. M2 followed and was associated with the NW-SE compression and NE-SW extensional during the exhumation of the rocks.

M1 Metamorphism

The first phase of metamorphism is a more regional event and pervasive throughout the metamorphic rocks of the study area. It is associated with S1 regional foliation in the metasediments. The field, petrographic, and textural evidence from the metasediments and microstructures of deformed grains in the gneisses are used to estimate the metamorphic conditions that prevailed during M1 metamorphism; the data are all consistent in indicating that the M1 metamorphism reached upper amphibolite facies conditions with associated partial anatexis.

The determination of metamorphic grade prevailed during the M1 metamorphism is largely based on the use of the index minerals. It is realized that the precise determination of

metamorphic grade using the index minerals of the Barrovian zonal assemblages is possible particularly when aluminosilicate minerals such as Staurolite, are present. There are examples worldwide that these minerals are absent although the pressure and temperature conditions would favour their growth; in such cases, the absence of these minerals are attributed to the composition of protolith rocks where semi-pelitic and/or calcsilicate rocks have unsuitable composition for aluminosilicate minerals to form (Winchester, 1972; Yardley 1989). Green diopside, hypersthene, hornblende, garnet and plagioclase are found in the rocks in Mutomo – Ikutha area, although all are not necessarily present together, and mineralogical disequilibrium is indicated in those rocks. Although such assemblages would usually be considered as indicative of the pyroxene hornfels facies or the granulite facies, it is undesirable in the present case to include them in either of those facies as the area is one of intense granitization. Sillimanite, a high-grade index mineral of regional metamorphism, is present in the northern part of area in biotite gneisses and biotite garnet gneisses. The sillimanite has developed in originally pelitic sediment in a restricted zone of probably high alumina content. The assemblages formed indicate the high-grade sillimanite-almandine sub-facies of the amphibolites facies of metamorphic rocks. In the southern part of the study area, the metamorphic grade is high, and is characteristic of the almandine-diopside-hornblende sub facies of the amphibolite facies, a typical mineral assemblage is hornblende-plagioclase-hypersthene-diopside with or without quartz and orthoclase. The presence of stromatic migmatites with local granitic leucosomes developed parallel to the regional S1 foliation strongly suggests that partial anatexis took place during peak M1 metamorphism and that the M1 metamorphism have reached upper amphibolite zone (Yardley, 1989).

M2 Metamorphism

A post-M1 phase of retrograde metamorphism can be recognized in the rocks of the study area. It is termed M2 metamorphism and is associated with the development of S2 shear band foliation overprinting the earlier S1 foliation. Along S2, foliation retrogressive processes are characteristic. It is expressed by the development of retrogressive chlorite replacing biotite and hornblende within the iron rich areas. In the metasediments, sporadic development of chlorite can also be attributed to this phase. The M2 retrogressive metamorphism in the project area is also indicated by olivine –→ serpentinite –→talc–→ magnesite and plagioclase –→sericite.

Retrogressive processes suggest metamorphic reactions under greenschist facies conditions. In addition to pervasive ductile deformation microstructures, the deformed grains in the gneisses exhibit evidence for brittle deformation through fracturing of feldspars and quartz grains,

suggesting temperatures below 300°C (Pryer, 1993). The brittle deformation fabrics/microstructures become dominant towards the structurally upper parts of the hornblende and quartzo-feldspathic gneisses. The brittle fabrics are attributed to decreasing metamorphic grade during exhumation as a function of depth where D1 fabrics developed under upper amphibolite facies conditions have suffered cataclastic deformation under low greenschist facies conditions. This, in turn, may reflect the transition of deformation from ductile to brittle during exhumation. The retrogressive M2 metamorphism is therefore characterized by replacement textures developed under the conditions of declining temperature and pressure, presumably during the uplift of the metamorphic complex. The latter effect of D2 deformation and associated M2 metamorphism overprinting the early D1/M1 fabrics are consistent with the extensional exhumation of metamorphic rocks.

4.1.5 Discussion on the geology, metamorphism and associated mineralization

Rock units in the Mutomo – Ikutha area have a general trend of NW – SE direction conforming to the general trend of Neoproterozoic Mozambique belt rock units. Mozambique rock units formed between 950 – 550 Ma according to Holmes (1951). These rocks were affected by Pan African tectonothermal events about 650 Ma according to Kennedy (1964). Since the rocks in the Mutomo – Ikutha area occur in the same orogeny, it is interpreted that they were also formed in the same period.

Occurrence of an ophiolites suite (metasediments, gabbroic sheeted dikes, peridotites, pillow lavas and serpentinite) in Mutomo – Ikutha area shows that this area was once part of an oceanic crust that was obducted onto continental crust during the collision of east and west Gondwanaland.

According to a detailed petrographic work carried out in the present study, results show that the area contains gneisses, migmatites, meta-volcanics (meta-basalts), meta-intrusives (meta-gabbros), marbles, and calc-silicates. From field observation which include, bedding relics and banding of biotites, it is concluded that the parent rocks of the gneisses, marbles and migmatites were sedimentary with minor volcanic intercalations. The primary rock types would have included, in order of abundance, pelites, greywackes, sandstones, volcanic intercalations, and calcareous sandstones. This interpretation is based on the following observations: (1) preserved relict bedding revealing intercalated pelitic, semi-pelitic, and calcareous layers; and (2) abundance of biotite, defining the argillaceous parent sedimentary rocks. The quartzo-feldspathic gneiss, calc-silicate rocks, biotite gneiss, and hornblende-biotite gneiss are derived

from arenaceous, arenaceous–limey, pelitic, calcareous–pelitic or marly, and limey sediments. The higher quartz contents in the quartzo-felspathic gneiss and calc-silicate rocks indicate their arenaceous nature. The argillaceous nature of the biotite gneiss is evidenced from the higher volume percentage of biotites and feldspars. The occurrence of iron oxides surrounded by thick clusters of titanite in the Kapoponi group amphibolites suggests that they are of igneous origin (e.g. Williams *et al*., 1982). These oxides may also be a result of simple reaction products as seen in many metamorphosed pelitic rocks. It is observed that the area experienced regional amphibolite facies metamorphic conditions. Metasomatic processes affecting the gneisses belt took place in two stage which involved early phase of medium-grade regional metamorphism, followed by a highly metasomatic phase.

The first early event led to the formation of calc-silicates in the area while the last one led to the formation of iron ore. These two stages were related to one cycle of metamorphism and were intervened by different tectonic events. The micro-structures show evidence of gradual changes in the metamorphic conditions as the deformation progressed. The metamorphic units of the area show the effects of two successive phases of regional amphibolite-facies metamorphism (M1 and M2), followed by a later thermal overprint. Specific mineral assemblages, fabric orientations and compositions characterize each metamorphic phase.

Although some migmatitic rocks in the Mutomo – Ikutha area are located near the Kapoponi and Kenze intrusive bodies (like the gabbros), the degree of partial melting is not controlled by distance from the pluton contacts and is very irregular. Instead, it seems that the melt fraction and migmatite type were determined by several factors. These factors include the chemical composition of parent rocks, the presence of deformation and the fluids in high strain zones. In the neighbouring layers within an outcrop, the degree of partial melting is variable and produced different types of migmatitic structures discussed in section 4.1.3 of this thesis.

The variety of migmatites noted in the study area is due to changes in parent rock compositions and availability of high strain zones that enabled the movement of fluids. The formation of thin leucosomes, in the migmatites of the project area, was noted. This formation was controlled by short-range melt movement along grain boundaries to form melt-rich layers constrained by pre-existing compositional layering (Marchildon & Brown 2003). Leucosomes in stromatic migmatites of Mutomo - Ikutha area is parallel to bedding planes in some parts. The parallel leucosomes may have formed by sub-solidus processes and in situ melting in a closed system. Melt transfer from grain-scale sites where melting occurred controlled the leucosomes. The

formation of Leucosomes was also controlled by the spatial distribution of pre-existing compositional layering and foliation formed by metamorphic segregation or in situ partial melting (i.e. showing pinch and swell structures). Other leucosomes with mafic edges were generated by metamorphic differentiation or in situ partial melting. Accumulation of melt in the hinge zones of folds, shear zones, fault zones and boudin necks is common in the migmatite zone of the Mutomo - Ikutha area. Bedding and foliation planes have also been important for the movement of melts/fluids in the parent rocks.

The petrographic, textural, microstructural and field evidence all reveal two major metamorphic events in the study area. The first is a regional alpine-type metamorphism M1 which reached upper amphibolite facies conditions. During the M1 peak, crustal anatexis occurred, and a granitic melt was produced in the northern part of the study area, (i.e. Mutomo area). A second localized metamorphism M2 took place during the exhumation of the metamorphic rocks in a shear zone at presumably low grade greenschist facies conditions during declining temperature and pressure in the southern part of Ikutha town.

According to the evidence from mineral assemblages, explained in this research work and the previous works, the metamorphic-magmatic history of Mutomo - Ikutha area is:

1) A medium pressure to high-pressure alpine-type metamorphism. Metamorphism that involved a sequential development of various minerals that include chlorite, biotite, garnet (almandine-rich), Staurolite, and K-feldspar. It involved the development of synmetamorphic quartz- feldspar bearing veins as well as the emplacement of the mafic suites in felsic rocks and regional migmatization.

According to Zwart(1967) and Pitcher(1979), alpine-type metamorphism is characterized by;

a. High pressure, thick metamorphic zones

b. Metamorphism of many facies and is dependent on decrease in pressure

c. Migmatites

d. Ophiolites with ultramafic rocks

e. Relatively narrow orogeny with large and rapid uplift

f. Nappe structures

2) The post - tectonic intrusion of younger gabbros, olivine gabbros, melano gabbros, pyroxenites and peridotites around Kenze, Ikutha and Kapoponi. These bodies generated very limited low grade contact metamorphism and alteration zones in the previously metamorphosed rocks and older plutonic rocks.

The alpine-type metamorphism can be deduced from the migmatites, ophiolites and nappe structures found in Mutomo – Ikutha area. Migmatites and rocks that form ophiolite suite in Mutomo – Ikutha area have been discussed under the Mutomo group in section 4.2 of this thesis. The study area has one major nappe structure (F2) found on the south-eastern part of Mutomo (see structural map under section 4.3).

Petrographical and field study information shows that iron ore mineralization took place in two phases. The first phase was immediately after shearing. Shearing opened room for emplacement of the ore by the magmatic hydrothermal fluids. The second mineralization involved replacement by metasomatic processes that lead to the formation of iron in the pegmatites (Figure 4.39 A and B, Figure 4.40A - C).

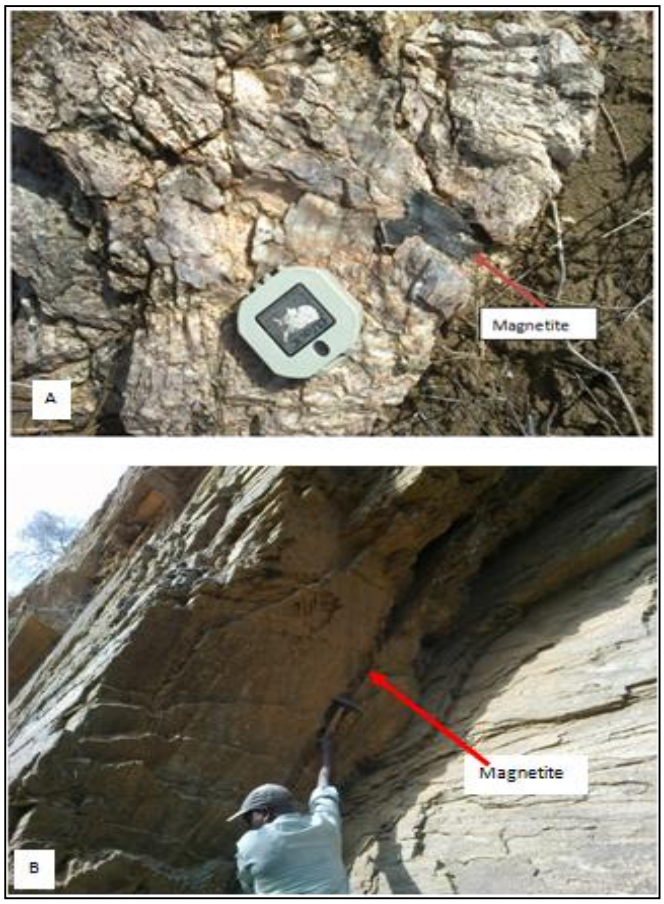

Figure 4.39: Magnetite iron in pegmatite in A, while in B it is Magnetite sill in hornblende gneisses

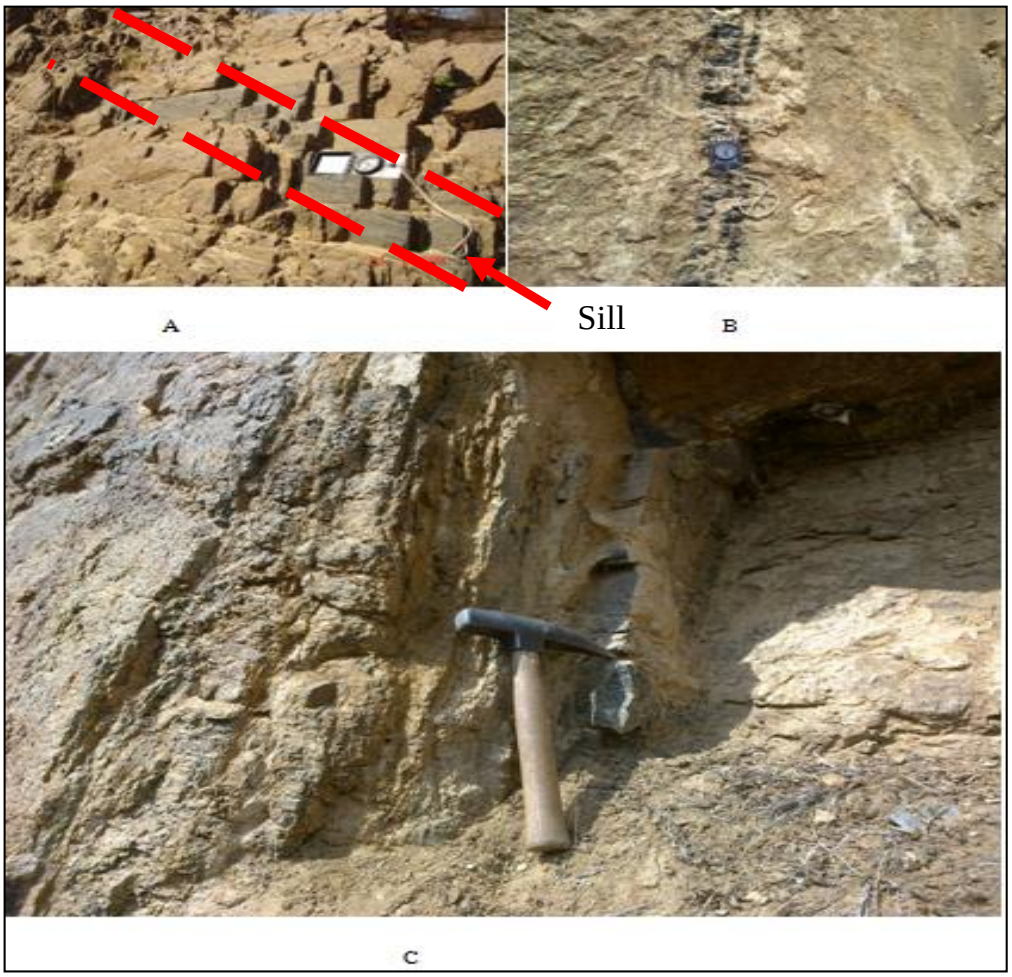

Figure 4.40: Veins of Apatite-iron ores of Kiruna type characteristics occurring in Mutomo – Ikutha area. Iron in A is a magnetite inform of a sill while in B and C. They are in the form of dikes within hornblende gneisses.

(A). Tectonometamorphic evolution of Mutomo – Ikutha segment of Mozambique belt

The Wilson cycle model postulates the formation of the Mozambique belt. This model postulated the initial splitting of the major Precambrian Rodinia into super continent Gondwanaland. The Gondwanaland was then split into two major continents, the east and west Gondwanaland and a new ocean basin (the Mozambique Ocean) was generated between them. The ocean widened and thinned edges where the two continents used to be joined cooled, became denser and sunk below the sea level. This process culminated in eruption of pillow lavas and the interaction of the cold sea waters and warm basalt.

The activity similar to the closure of ocean basin as explained by the Wilson cycle model is adopted to explain the Mozambique Ocean closure. Technically the closing phase of the

Wilson cycle was over when collision had occurred and the only thing left was the foreland of one continent (overriding continent plate) and the eroded material of the sea bed. With the collision, eroded material rose and eventually got to the earth's surface. This resulted in the formation of the Mozambique belt. The Mozambique belt presents experimental and thermodynamics evidence for the operation of high pressures in Proterozoic metamorphism.

The Mozambique belt segment of Mutomo – Ikutha area is interpreted in Tibetan style i.e. continent - continent collision between east and west Gondwanaland. Shackleton (1986) and Stern (2008) suggested that collision with NW to SE motion was followed by a stage of post collision ductile shearing parallel to the plate boundary. The area occurring in the north central Kenya has six tectonothermal events of evolution of Mozambique belt between 900-470Ma (Key et. al., 1989). Three tectonothermal events listed below have been recognized in the Mutomo –Ikutha area. The signatures indicating that indeed there was collision of the West and East Gondwanaland includes presences of thrusts, napes, and mineral lineation occurring in the Mutomo, Ikutha and Kapoponi groups discussed earlier in this thesis.

(B). Tectonothermal events in the Ikutha – Mutomo research area

Based on the mineral assemblages, Metamorphism and tectonic processes, Mutomo – Ikutha area can be classified in the following tectonothermal events;

1. ***Kapoponi tectonothermal event***
   This is indicated by folding and faulting. The Ndulukuni anticline runs from NE to SW through Kenze area. Intrusion of gabbroic rocks in Kenze has accompanied this event.
2. ***Ikutha tectonothermal event***
   This event is indicated by brittle and semi ductile shearing in Tiva – Ikutha area on Tiva gneiss which has been described elsewhere in this thesis. Intrusion of Olivine norite south of Ikutha accompanies this event.
3. ***Mutomo tectonothermal event***
   Mutomo event is recognized by intense migmatization south of Mutomo area. This event is also accompanied by folding and faulting as well as ductile shearing.

SUB-CHAPTER 4.2: STRATIGRAPHY AND MINERALIZATION OF MUTOMO – IKUTHA AREA

This section presents the interpreted stratigraphy of Mutomo – Ikutha area. It also gives a new account on iron mineralization as controlled by stratigraphy of the area. Stratigraphy nomenclature applied to Mozambique mobile belt in Kenya has led to inconsistencies in the application of stratigraphic terms to rock sequences within the belt. In consequence, the stratigraphy of the rocks found in the Mutomo –Ikutha area had been poorly understood. The chronostratigraphic terminology like Neoproterozoic and lithostratigraphic terminology like Mozambique mobile belt possess a great confusion in stratigraphic nomenclature of the area. A re-evaluation of stratigraphic terms and usage is now appropriate and a new stratigraphic framework required providing a better approach in geological mapping and mineral exploration in this area.

The available evidence used to work out lithostratigraphy of Mutomo – Ikutha area include the following; Field observation of the rock units along well designed sections which involved the main principles of stratigraphic classification, Petrographic investigations discussed elsewhere in this thesis and Petrochemical investigation. Stratigraphy of Mutomo – Ikutha area is largely classified on the basis of the lithology of the rocks. According to the regulation of the international Subcomission on Stratigraphic Classification (ISSC, 1976) of the international Union of the Geological Sciences (IUGS), the stratigraphy of Mutomo – Ikutha area is interpreted to be composed of the lithostratigraphic rock units in Table 4.1.

4.2.1 Lithostratigraphy of Mutomo – Ikutha area

Lithostratigraphy is the element of stratigraphy that deals with the description and nomenclature of the rocks of the earth based on their lithology and their stratigraphic relations. Lithostratigraphic units are bodies of rocks, bedded or unbedded, that are defined and characterized on the basis of their lithologic properties and their stratigraphic relations. These units are the basic units of geologic mapping. These units are defined and recognized by observable physical features and not by their inferred age, the time span they represent, inferred geologic history, or manner of formation. The geographic extent of a lithostratigraphic unit is controlled entirely by the continuity and extent of its diagnostic lithologic features.

The main aspects considered in describing a new formal unit include:

i. A clear and complete definition, characterization, and description of the unit so that any subsequent investigator can identify it.
ii. The proposal of the kind, name, and rank of the unit.
iii. The designation of a stratotype (type section) or type locality on which the unit is based and which may be used by interested scientists as a reference and Publication in a recognized scientific medium.

The stratigraphic descriptions of the study area starts with Ukamba super group, which was referred to as Ukamba group by Mosley (1993). Ukamba super group comprises Mutomo group, Ikutha group and Kapoponi group. These groups are farther subdivided into formations depending on the distinguishing properties of each formation. The rocks of the Mozambique mobile belt in this area are classified lithostratigraphically as group, formation, and members (Table 4.15). Iron ore in Ikutha is found within the hornblende gneisses. Hornblende gneisses are part of the Mutomo group which is also part of the main Ukamba super group.

In designing nomenclature of the rocks in the study area, the North American Stratigraphic code prepared by the North American Commission on Stratigraphic Nomenclature (NACSN) and the rules for naming geological units in Norway (Nystuen,1989 and modified by Mathu,2000), have been used (Table 4.16). It involves a general description of the unit, origin of its name and where possible to its earlier work, areal distribution, including the best exposed areas and stratotype; the contact relations and thickness estimates; the division of the unit into sub-units and origin of the unit based on the available evidence (Laajoki, 1991).

Table 4.15: Lithostratigraphy of Mutomo – Ikutha area

SUPER GROUP	GROUP	FORMATION
UKAMBA SUPER GROUP	IKUTHA GROUP	• Quartz-feldspathic gneiss • Feldspathic gneisses • Granitoid gneiss
		• Hornblende gneiss • Hornblende biotite gneiss • Hornblende diopside gneisses , Amphibolites
		• Marbles
		• Olivine norites, Pyroxenites
	MUTOMO GROUP	• Biotite gneisses • Biotite hornblende gneisses
		• Migmatites
		• Marbles
	KAPOPONI GROUP	• Oligoclase porphyroblast gneisses • Quartz- feldspathic gneisses
		• Biotite-garnet gneisses • Garnet enriched rocks
		• Calc-silicate granulites
		Meta-basalts, meta-gabbro, Gabbro ,Melagabbro, Pyroxenite, Peridotite, Dunites

Table 4.16: Stratigraphic classifications and unit hierarchies (adopted from Mathu, 2000)

ROCK CLASS	SEDIME-NTARY	Increasing metamorphic grade METAMORPHIC			IGNEOUS		
		METASEDIMENTARY		UNDETER MINED ORIGIN	META-IGNEOUS	MASSIVE	STRATIFIED
		METASEDIMENTS	PARA-GNEISSES & SCHIST				
CRITERIA	LITHOLOGY AND SUPERPOSITION		TRANSITIONAL	LITHOLOGY			LITHOLOGY & SUPERPOSITION
STRATIGRAPHIC CLASS	LITHOSTRATIGRAPHIC (STRATOSTRATIGRAPHIC)			LITHODEMIC			LITHOSTRATIGRAPHIC (stratostratigraphic)
UNIT HIERARCHY	GROUP FORMATION MEMBER BED, FLOW			SUITE LITHODEME Informal { Layer, Band etc}			GROUP FORMATION MEMBER BED, FLOW
	COMPLEX (two or more rock classes involved)						

4.2.2 Discussion on Stratigraphy and mineralization in Mutomo – Ikutha area

Stratigraphy has played a role in mineralization in the project study area. Magnetite, apatite and copper were found to be hosted in the Ikutha group rock units. Magnetite is mostly hosted in the hornblende gneisses of the group. Mutomo group is rich in hematite, ferro-manganese and ilmenite. Kapoponi group is rich in Manganese, Iron, Magnesite, Vermiculite, Talc, Calcite and almandine garnets. The Kiruna apatite type magnetite ore in Ikutha group is strata-bound ore body.

SUB-CHAPTER 4.3: GEOLOGICAL STRUCTURES OF MUTOMO – IKUTHA AREA

This section describes, correlates, and analyses the field orientation data of the mesoscopic and mineralogical scale structures in the rocks of the Mutomo – Ikutha area in order to interpret the tectonic evolution of the area. The area contains a continuous highly deformed, stratigraphic sequence repeated numerous times by complex folds. Based on the overprinting relations between the different fold systems, three successive phases of folding, F1, F2, F3 have been distinguished. F1 orients in the NW, F2 orients in the SE, while F3 orients in the Eastern direction (see Figure 4.41).

4.3.1 Foliation planes

Gneissic foliation S1 (Figure 4.42), is the most penetrative set of foliation plane observed in Mutomo – Ikutha area. Intersection and transposed crenulation lineations define S2 foliation plane and in this area, they are axial-planar to the folds. Field studies show that this area has undergone multiple folding.

Crosscutting relationships between foliations, folding and veins that cut them are used to derive the relative ages of different generations of structures. However, some veins are cut by the S2 foliation and are also folded, indicating their formation after F1 and prior to or during the second F2 folding phase. Gneissic foliations in the area are generally defined by medium- to coarse-grained minerals that form compositional banding with a preferred planar orientation of platy, tabular, or prismatic minerals, and by subparallel lenticular mineral grains and grain aggregates. The compositional banding occurs at all scales from thick, continuous bands and layers that can be mapped across the entire field area, to discontinuous laminae that pinch out within individual outcrops, hand specimens, or thin sections . Some mesoscopic structures also are associated with thin layers and pods of granitic material, forming migmatites in the area. Foliation planes of F1 strike mainly NW–SE, roughly parallel to the elongation of the belt, with varying dip directions. The variation in strike and the dip of foliations throughout the Mutomo – Ikutha area reflects the effect of fold overprinting.

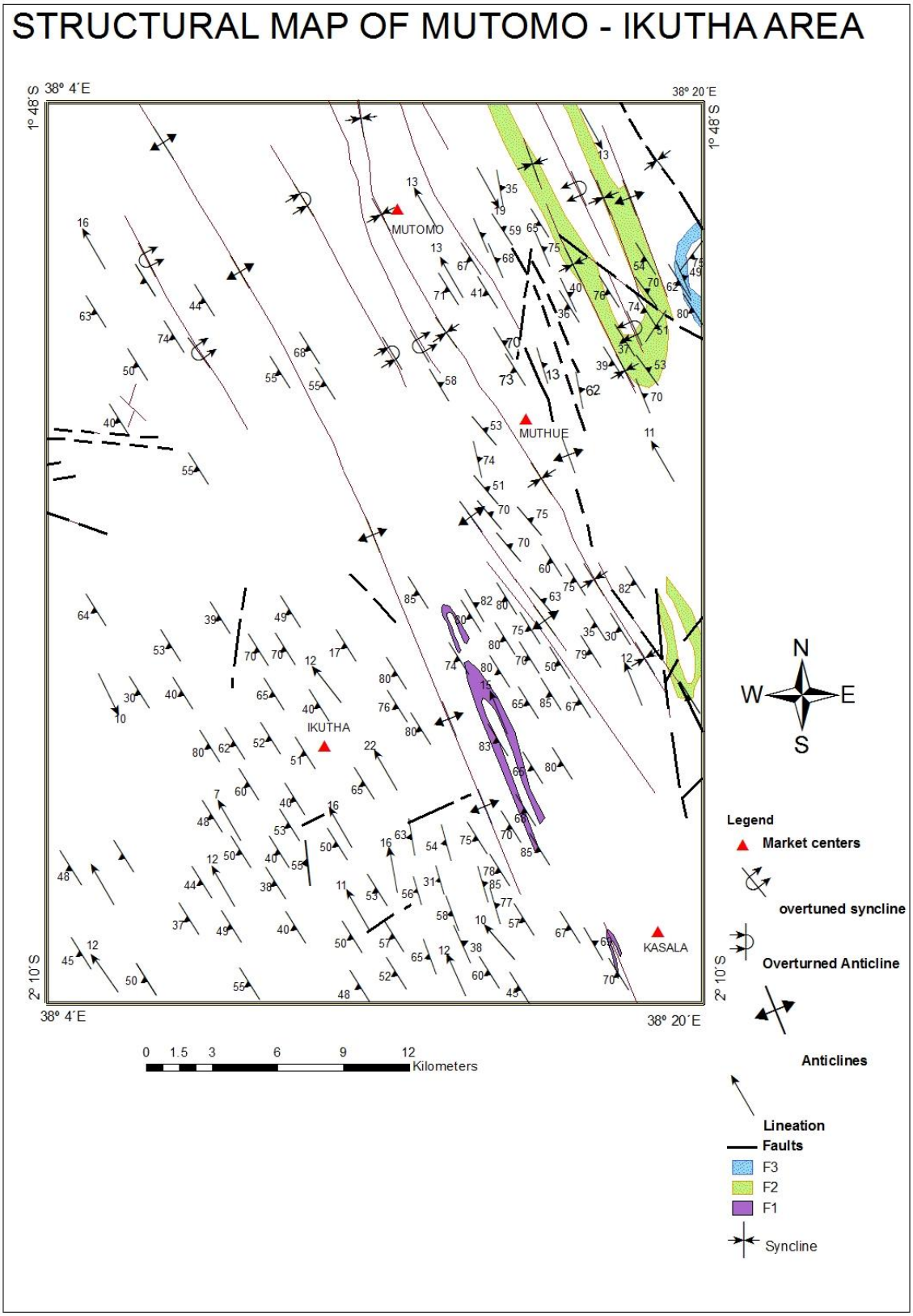

Figure 4.41: Structural map of Mutomo – Ikutha area, F1, F2, F3 are the folding events.

Figure 4.42: Typical field views from the main regional foliation (S_1) developed on (a) a biotite hornblende gneisses at location 041987/9785453; (b) migmatites composed of alternating dark (mesosomes) and light (neosome) layers. (c) Biotite –garnet gneisses. (d) S1 foliation on a biotite hornblende gneisses along Ikutha Kasala road, east of Tiva River.

Foliations are most pronounced in the metamorphosed and to a lesser extent in other rocks with exception of the granitoid gneiss, which commonly show no foliation. The foliation is paralleled by the boundaries between distinct rock types, by mineralogical banding and by preferred orientation of flaky minerals.

200 readings were collected from the area south of Ikutha town. These readings were projected on the stereo net which showed that foliation have imperfect monoclinic symmetry with fairly high degree of homogeneity. The fold axis plunges at 10^{o}, in a direction of 330^{o} (Figure 4.43). When 157 readings collected from Muthue area were plotted, the plunging of the fold was at 15^{0} and direction of 330^{0} (Figure 4.44).

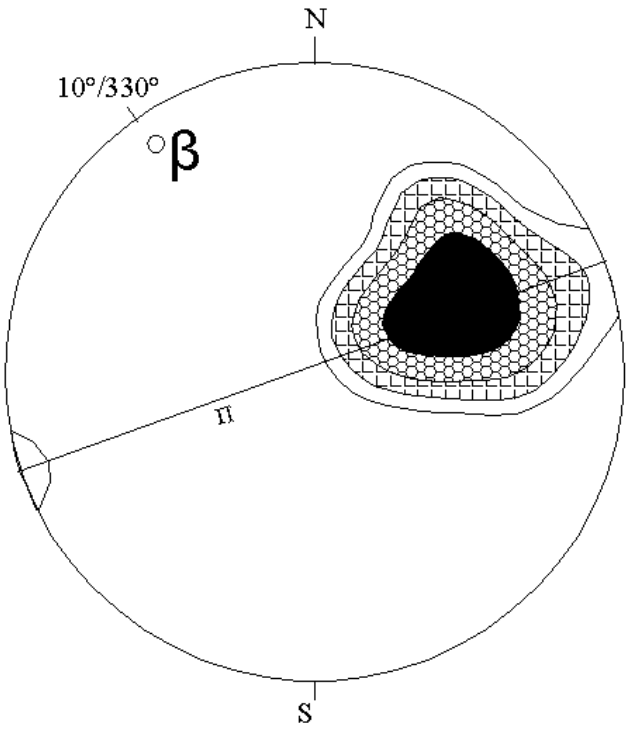

Figure. 4.43: 200 Poles to foliation planes of the hornblende gneisses, quartzo – feldspathic gneisses and biotite hornblende gneiss, south of Ikutha town projected from the lower hemisphere. Density contours are at 8%, 4%, 2% and 1 % per 1% area.

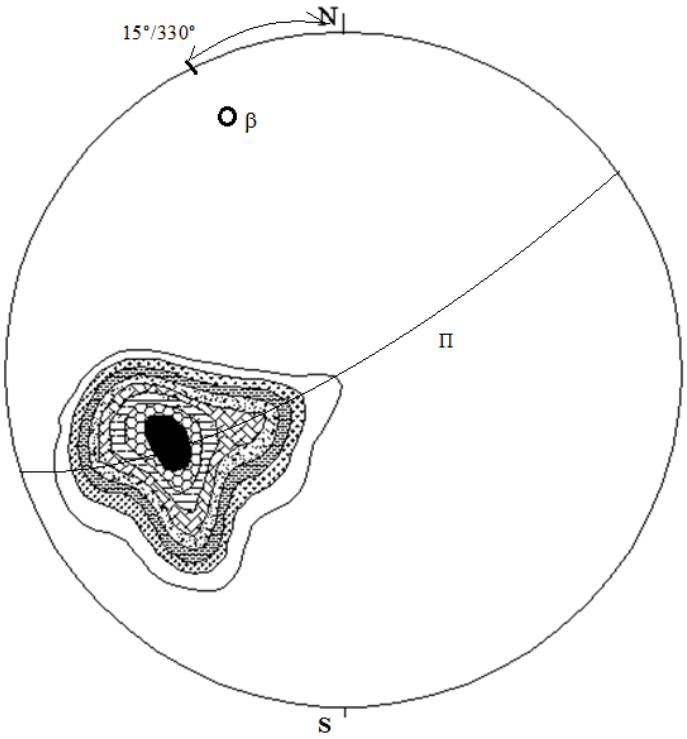

Figure 4.44: 157 poles of foliation planes projections on biotite hornblende gneisses west of Muthue town, projected from the lower hemisphere. Density contours are at 8%, 4%, 2% and 1 % per 1% area.

4.3.2 Lineations

The mineral lineation in the area is shown by alignment of mineral grains in a preferred direction. The general trend of lineation is 320 NW with a plunge of 15 degrees which almost coincides with the fold axes as seen in Figure 4.45. Linear structures are well developed throughout the area. They have been divided into the following types: intersection lineations, fold hinge lineations, boudin lineations, and mineral lineations. They are found in nearly all rock types, but are generally best developed in migmatites, biotite gneisses and hornblende gneisses especially in the crests and troughs of the macroscopic folds.

The mean geometric orientation of intersection lineations is parallel to that of the major fold axes (F2). The preferred orientations of mesoscopic folds define fold hinge lineations. The measured mesoscopic fold axes are treated geometrically as a regionally penetrative lineation. They show the presence of clusters on the stereonets that are related to the observed macroscopic fold axes. Boudins display a wide variety of shapes in the area. Leucocratic plagioclase-rich layers are commonly segmented forming boudins, while the surrounding melanocratic material flowed in between them. In this type of boudinage, the necks between boudins are smoothly curved.

The existence of pinch-and-swell structures is strong evidence for non-linear flow in the stiff layer (e.g. Hudleston and Lan, 1993). Some boudins are rotated about their long axes showing right-lateral sense of shearing. The long axes of most boudins are aligned parallel to the F2 macroscopic fold axes (recumbent folds). Some other boudins are oriented normal to the F2 axes, and these groups are related to post-F2 folding (i.e. parallel to F3 macroscopic folds). Comparisons of the orientation of layers that have been shortened versus those that were lengthened and boudinaged were used to infer the sense of shear during boudin formation (Davis and Reynolds, 1996). Mineral lineations in the area are developed in the plane of the foliation and are typically marked by a streaky, fiber-like linear appearance, composed of aligned crystals of quartz, feldspar and hornblende. This mineral fabric (stretching lineation) is parallel to the geometric axes of the macroscopic F1 (plunges 10-25 west of north, (see Figure 4.45)) and F2 (plunges 12-70 east of south) folds.

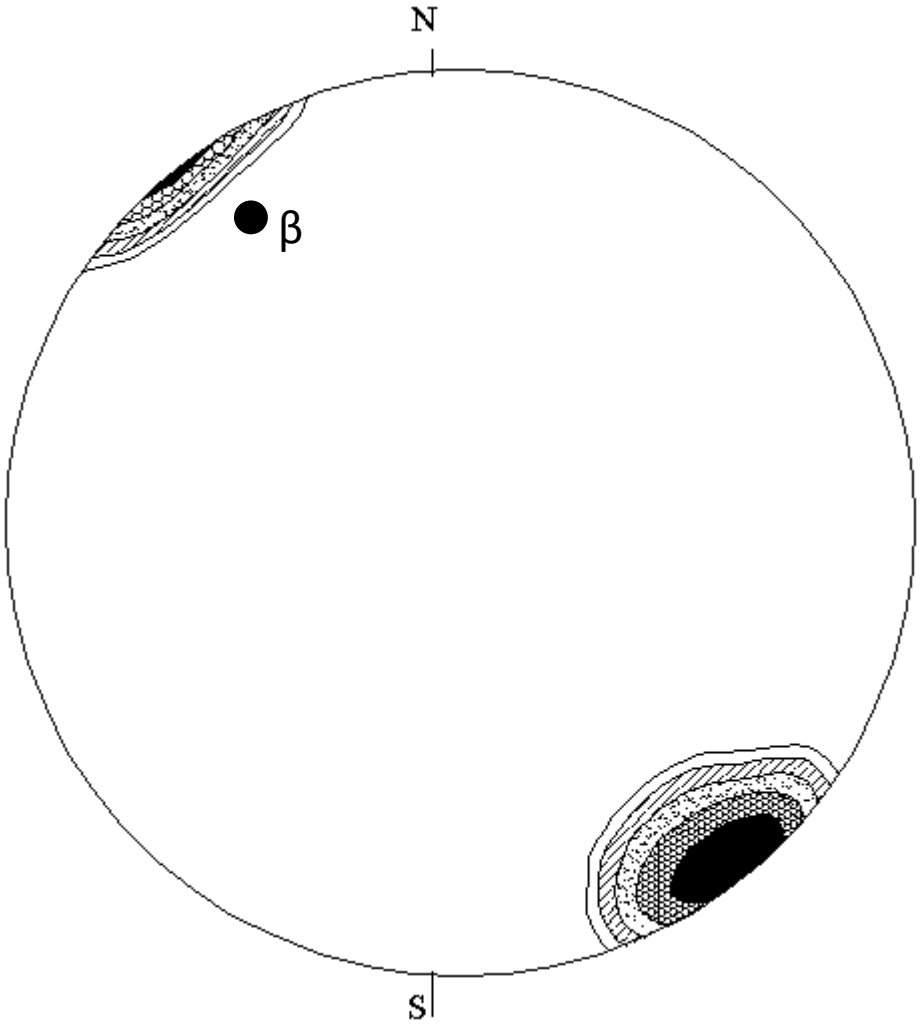

Figure 4.45: 180 readings of mineral grains lineation from the hornblende gneiss, quartzo – feldspatic gneisses and biotite hornblende gneiss, south of Ikutha town projected from the lower hemisphere. Density contours are at 20%, 10%, 5% and 1 % per 1% area.

4.3.3 Fold style, orientation, and overprinting relationships

Mesoscopic folds with wavelengths of tens of centimetres to a few meters and variable styles and orientations are numerous in the Mutomo – Ikutha area. Most folds in area belong to Class 2 and 1B types (Ramsay 1987; Fleuty, 1964; Ramsay, 1967; Ramsay and Huber, 1987; Hudleston, 1973; Twiss, 1988; Hudleston and Lan, 1993).

Mesoscopic folds were analysed in the field and grouped according to style, orientation, and overprinting relationships. NW- and SE-trending folds characterize the Mutomo – Ikutha area. NW-trending folds generally are more steeply plunging than those with a SE trend. SW - trending folds occur only in Kivyuni area on marbles and quartz feldspathic gneiss and are rare in other parts of Mutomo – Ikutha area. The number of SE-trending folds increases at the

expense of the NW-trending folds, both of which have moderate to steep axial plunges. The earliest folds (F1) exhibit variability in attitude from region to region throughout the area, but show considerable similarity of style (i.e. they are isoclinal), intensity of folding, and associated planar and linear mineral growth. The axial planes of the isoclinal folds are parallel to the regional foliation, which in turn is roughly parallel to the trend of the belt. This suggests a strong NE–SW flattening normal to the trend of the gneiss belt at this stage of deformation. Some folds show broad rounded hinges, suggesting a low ductility contrast during folding equivalent to Model A of Ramsay, 1967; Ramsay and Huber, 1987), where the thickness ratio of the competent to incompetent layers is low.

Elsewhere, both competent and incompetent layers are thickened in the fold hinge zone and are thinned in the fold limbs (Model B of Ramsay, 1967 ;). Some folds show highly attenuated limbs as a result of progressive strain. Ptygmatic folds were also encountered in most of the metamorphic units. However, some mesoscopic folds display the effect of a simple shear mechanism as indicated by the presence of sigmoidal "drag" folds. Other mesoscopic folds show the effects of flattening by ductile shearing.

The younger fold sets show a progressively more uniform orientation throughout the metamorphic rock sequence, and they are nearly identical in terms of style and orientation. F2 fold sets are characterized by tight to recumbent folds, and are encountered predominantly in the biotite hornblende gneiss. F2 fold sets have a strong and consistent sense of asymmetry; virtually all verge towards the SE and are S-shaped when viewed down-plunge. F2 folds refolded the F1 structures and the variability of their geometry is ascribed to progressive development of folds and the original orientation of F1 folds. F3 open folds occur on marbles and quartz feldspathic gneisses. Z-shaped folds are recognized in many parts of the study area and are used together with S-shaped folds to locate the large scale ones.

4.3.4 Geometry and mechanics of superimposed mesoscopic folds

Fold overprinting relationships are clearly recognized within the metamorphic rock units of the Mutomo – Ikutha area. The resulting outcrop pattern of three successive folding events depends entirely on: (a) the style, orientation, and scale of the individual fold sets, including the shapes of the earlier folds and the inclination of their axial planes; (b) the orientation and intensity of the F2 fold formation; and (c) the amount of flattening which accompanies the formation of F2 folds and the orientation of the outcrop surface (e.g. Ramsay, 1962 and 1967; Huddleston and Lan, 1993) as shown in Figure 4.46. Domes occur in the southern part of the area (Figure 4.47)

showing that the area had compressional forces on all sides making the rock units to dip in opposite direction from the centre of the dome towards the periphery.

The metamorphic rocks of Mutomo – Ikutha area show interference patterns between F1 and F2 folds, and among F1, F 2, and F3 folds. F1 folds are characterized by overturned isoclinal folds on small scale that resulted in the development of a strong gneissocity (S1), which is defined by mafic minerals in metapelites. Broadly spaced cleavage is developed in more competent lithologies such as quartzofeldspathic gneisses. The orientation of F1 planar and L1 linear fabrics varies according to their positions with relation to F2 major folds. The second set of folding (F2) is the main fold set of tight, recumbent and local similar fold styles. The mesoscopic folds of these sets show different geometries.

The axial trends of F2 folds consistently plunge between 12° and 70° towards the SE and the associated planar fabric with this phase of deformation consists mainly of axial crenulations and spaced cleavage, which strikes SE and dips 25–80° towards the NE. L2 lineations within the area are mainly boudins and intersection lineations, and plunge 25–50°NW. F3 is a local mesoscopic fold set, characterized by broad, open fold.

In the Mutomo – Ikutha area, the axial surfaces of similar type of folds show slight rotation or "rearrangement" of the inferred principal shortening direction. The geometry of structures indicates that flattening played a major role in the deformational history of the rock units in the area. Flattening probably dominated in the early stages and gave way to local simple shear in the later stages. The planar and linear fabrics in the metamorphic rock units display a close geometric relationship with the coeval larger-scale folds (i.e. outcrop-scale lineations are parallel to map-scale fold axes).

This study area is dominated by folding trending in the NW – SE direction. Kitui anticline passes trends NW – SE in the central part of the area. In south west of Ikutha the folds dip SW direction between 220 and 240. Overturned folds occur at Ndulukuni.

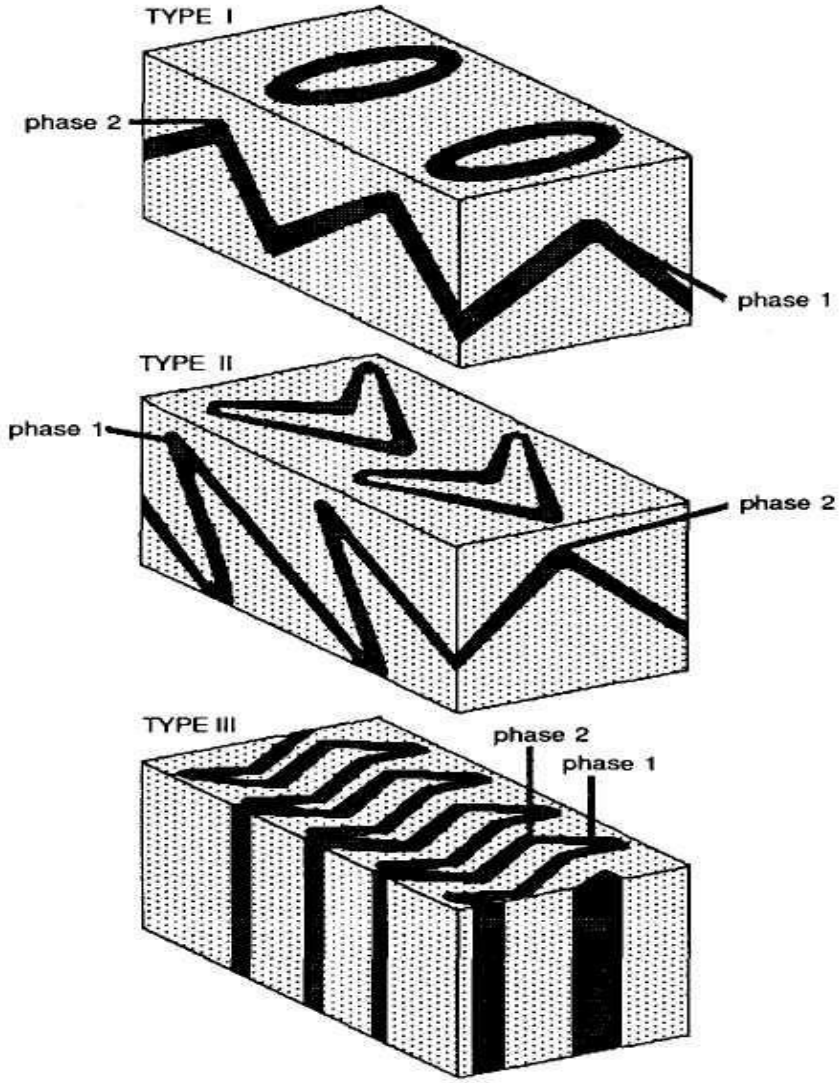

Figure 4.46: Fold interference patterns formed by two phases of folding, defined by Ramsay (1962). Type I - dome-and-basin structures; Type II - mushroom-shape folds; Type III - refolded folds with subparallel fold axes.

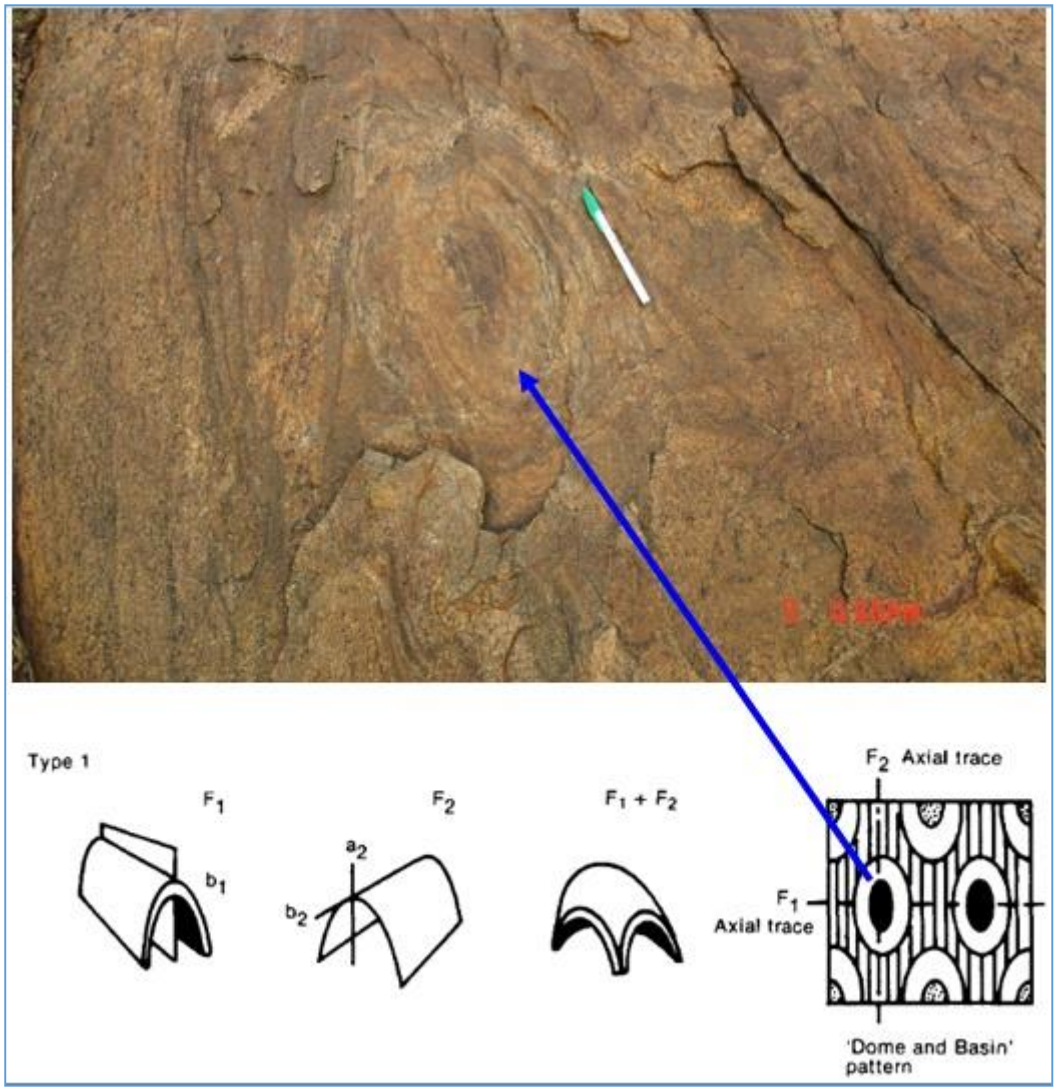

Figure 4.47: Type 1 fold, showing domes and basins pattern developed in the southeastern part of the area

I. F1 Folding

The widespread occurrence of F1 folds (Figure 4.48) encountered in migmatites is one of the most diagnostic structural elements formed during the D1 deformation and can be attributed to the bending and buckling produced by the collision of East and West Gondwana . The folding of migmatitic leucosomes may suggest that lecuosomes may (1) pre-date the folds, (2) form syn-tectonically or (3) form post-tectonically by selective reconstitution of layers of appropriate composition (cf. Mehnert 1968). The style of folding observed in the migmatites − thickened crests and thinned limbs in these folds − may suggest that mobilization and deformation were simultaneous processes and that the folding has originated during the main act of mobilization rather than before or after.

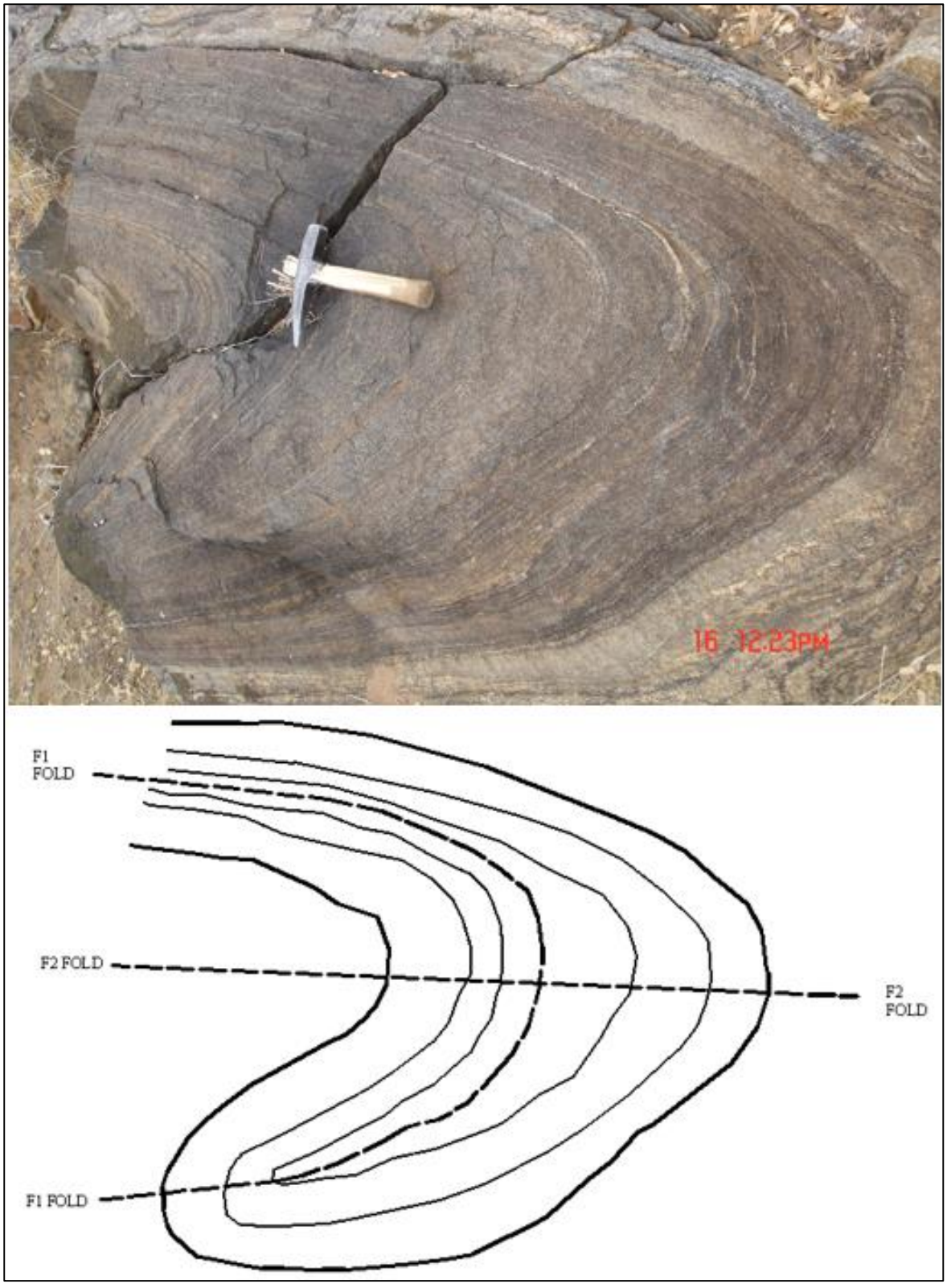

Figure 4.48: Folded and refolded biotite garnet gneiss at way point 107 (0422008/9797207)

I. F2 Folding

A regional-scale F2 fold with NW−SE-trending axes are observed within the study area. These are open folds that refolds the earlier S1 regional foliation in the metamorphic rocks of the study area. The general trend of these type of folds is consistent with an approximately NE−SW-directed compression, which is perpendicular to the general direction of NW-trending extension in the study area. F2 folding is observed on Kapoponi and Mutomo gneisses (Figure 4.49 and 4.50). In Kapoponi, the fold plunges to the SE. Ngwate fold in the Mutomo gneisses plunges SE and has undergone faulting. Kapoponi fold plunges SSE and occurs on Kapoponi gneisses.

Folds with axes parallel to the NW-trending mineral stretching lineation in the metamorphic rocks tend to have important bearing on the evolution of the extensional tectonics in Mutomo – Ikutha area. The general trend of these folds indicates horizontal shortening in a NE−SW direction at a high angle to the mineral stretching lineation as well as extension direction to general trend of NW-trending lithologies. The folds are interpreted as the result of a deviation from plane strain deformation on a regional scale due to an extra component of NE−sub-horizontal shortening during the development of the NW shear zones both in Ikutha and Mutomo.

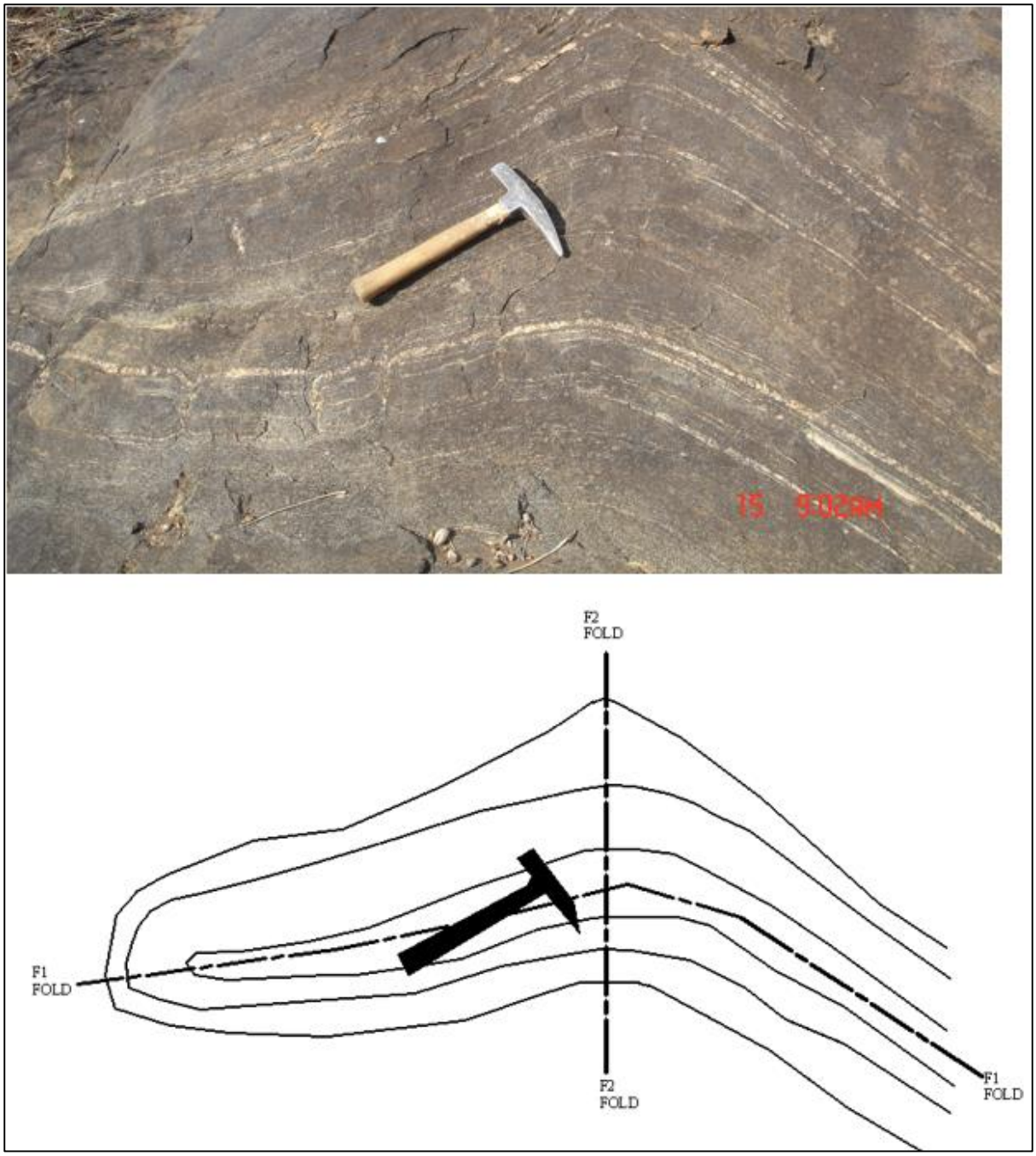

Figure 4.49: Superimposed fold at way point 96 (0418562/9785845) on a biotite hornblende gneiss. F1 is fold one while F2 is fold two.

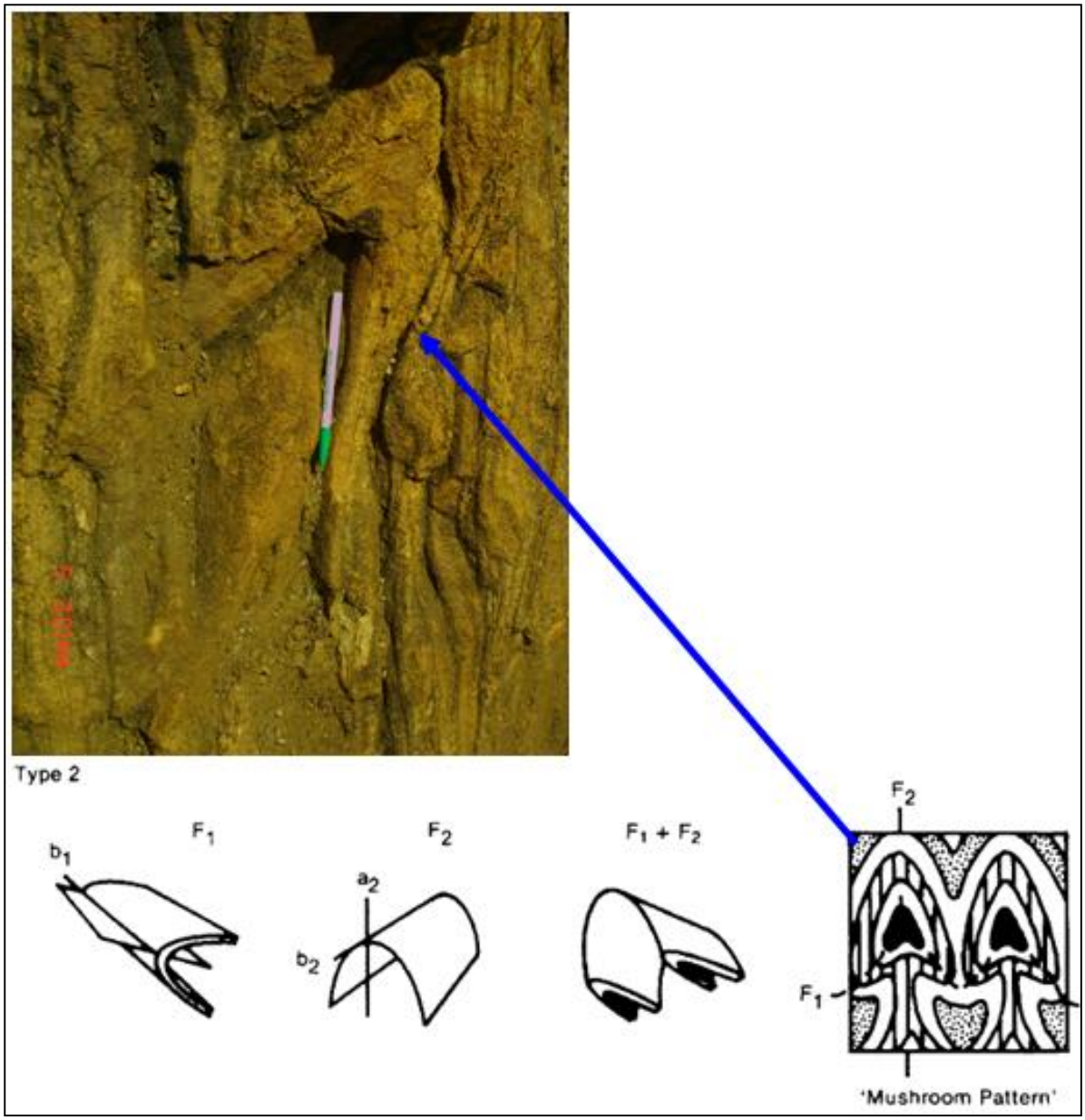

Figure. 4.50: Type 2 fold, showing Mushroom pattern in Mutomo – Ikutha area

II. F3 Folding

This type of folding took place in Kivyuni on marbles and Quartz-feldspathic gneisses. The fold plunges to the west contrary to the general trend of the belt. From field observations, F3 folding is the youngest of all the three folding events that took place within Mutomo – Ikutha area. Type 3 folds formed by refolding of F1 and F2 and were observed on the migmatites occurring south of Mutomo town (Figure 4.51, 4.52, 4.53).

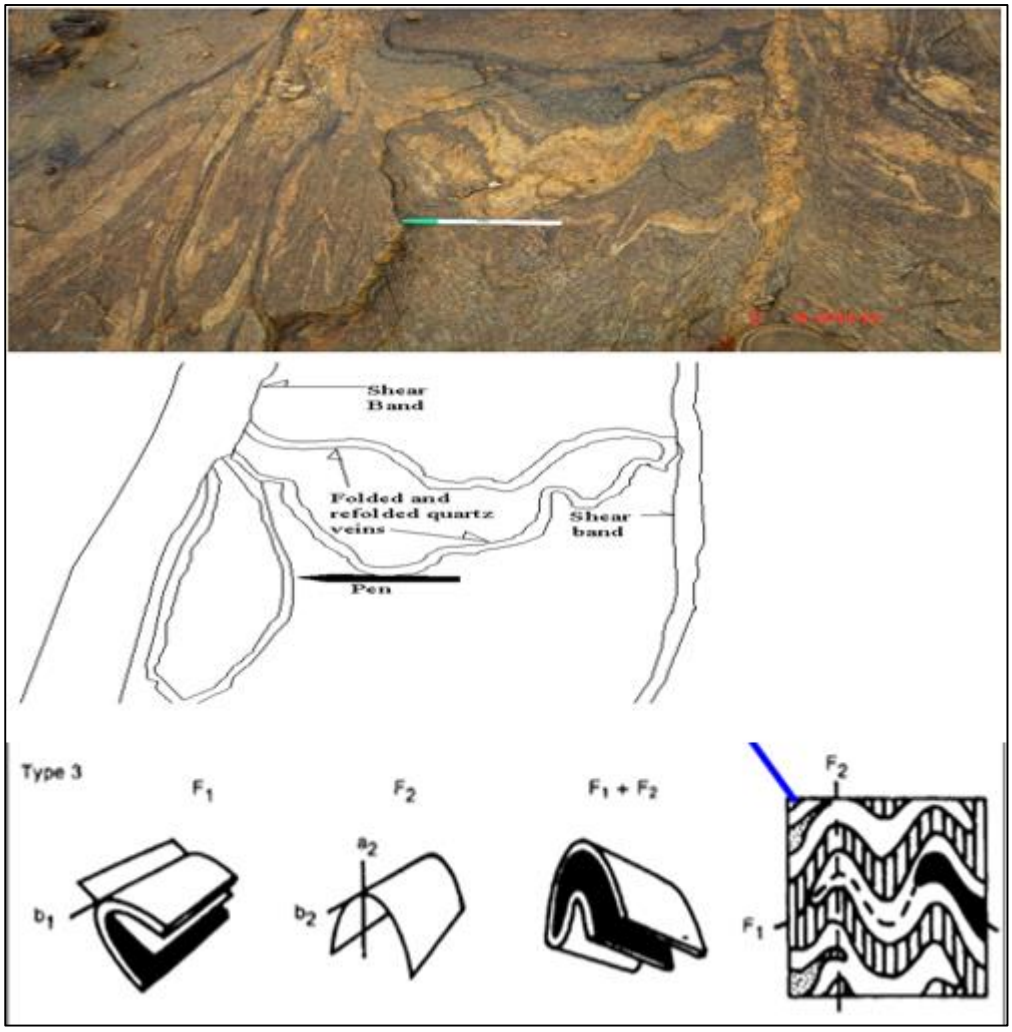

Figure 4.51: Type 3 fold, showing refolding of types 1 and 2 in Mutomo-Ikutha area

Figure 4.52: Open F3 refolded (recumbent) fold on migmatites in Mutomo – Ikutha area

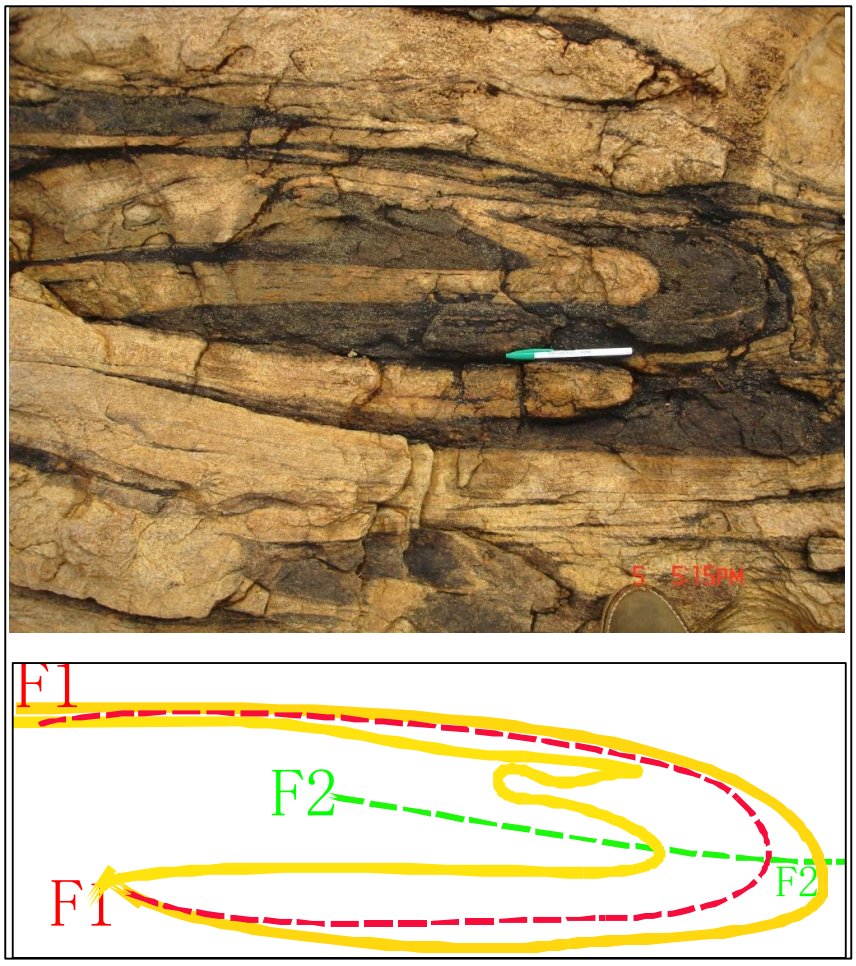

Figure 4.53: Intrafolial isoclinal folds of a quartzo – feldspathic layer in a gneiss. The folds are contained within the gneissic foliation

4.3.5 Joints and tectonics evolution of Mutomo – Ikutha area

Jointing in the northern part of the area is developed in the migmatite rocks. The joints comprise longitudunal joints, cross joints,diagonal joints and foliation joints (Figures 4.54,4.55, and 4.56) . Longitudinal joints are dominant in Kanziku- Mathima – Mutomo area while cross joints are dominat in Ikutha – Tiva area. During the period of compression stretching took place along the crest of the anticlines producing longitudinal tension joints parallel to the axes of the folds. A rose diagram for 82 data sets was plotted and indicate that most of dilation joints are oriented in the NW –SE direction (Figure 4.57). These joints deveoped due to folding.

Figure 4.54: Vertical joints trending 212 degrees south west on a Hornblende Gneiss at waypoint 0404434/9767251

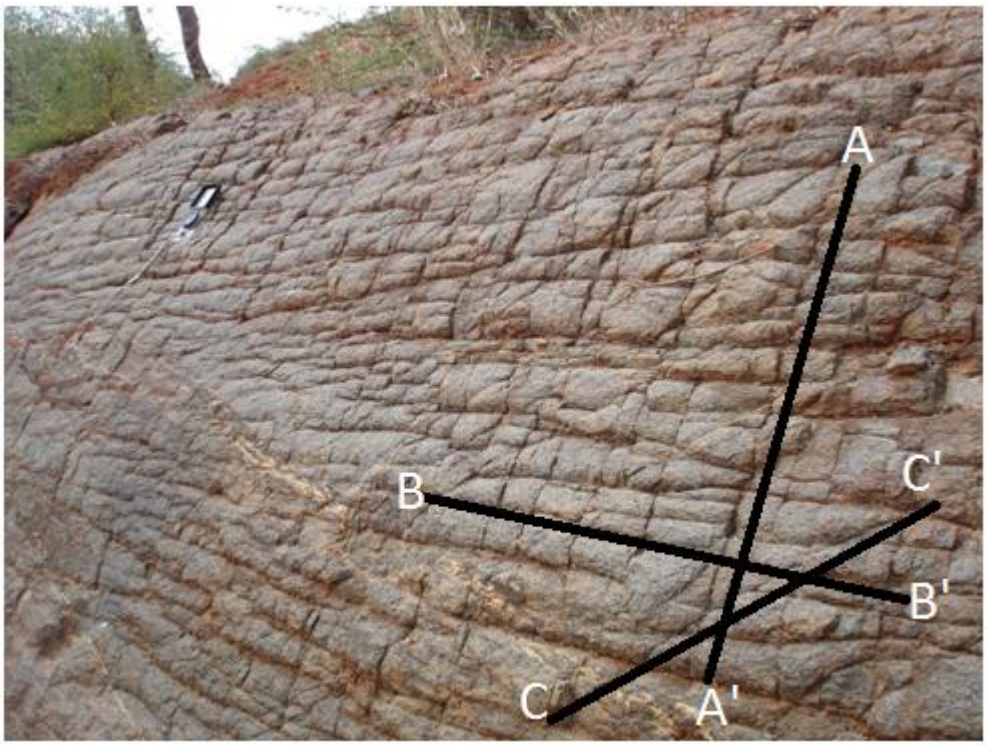

Figure 4.55: Tectonic joints: A-A’ = cross (joints), B – B’ = longitudinal joints, and C-C’ = oblique joints on Hornblende Gneiss along Tiva river

Figure 4.56: Horizontal extensional joint system in a quartzo-feldspathic gneiss joined by vertical cross joints producing H and T intersection patterns.

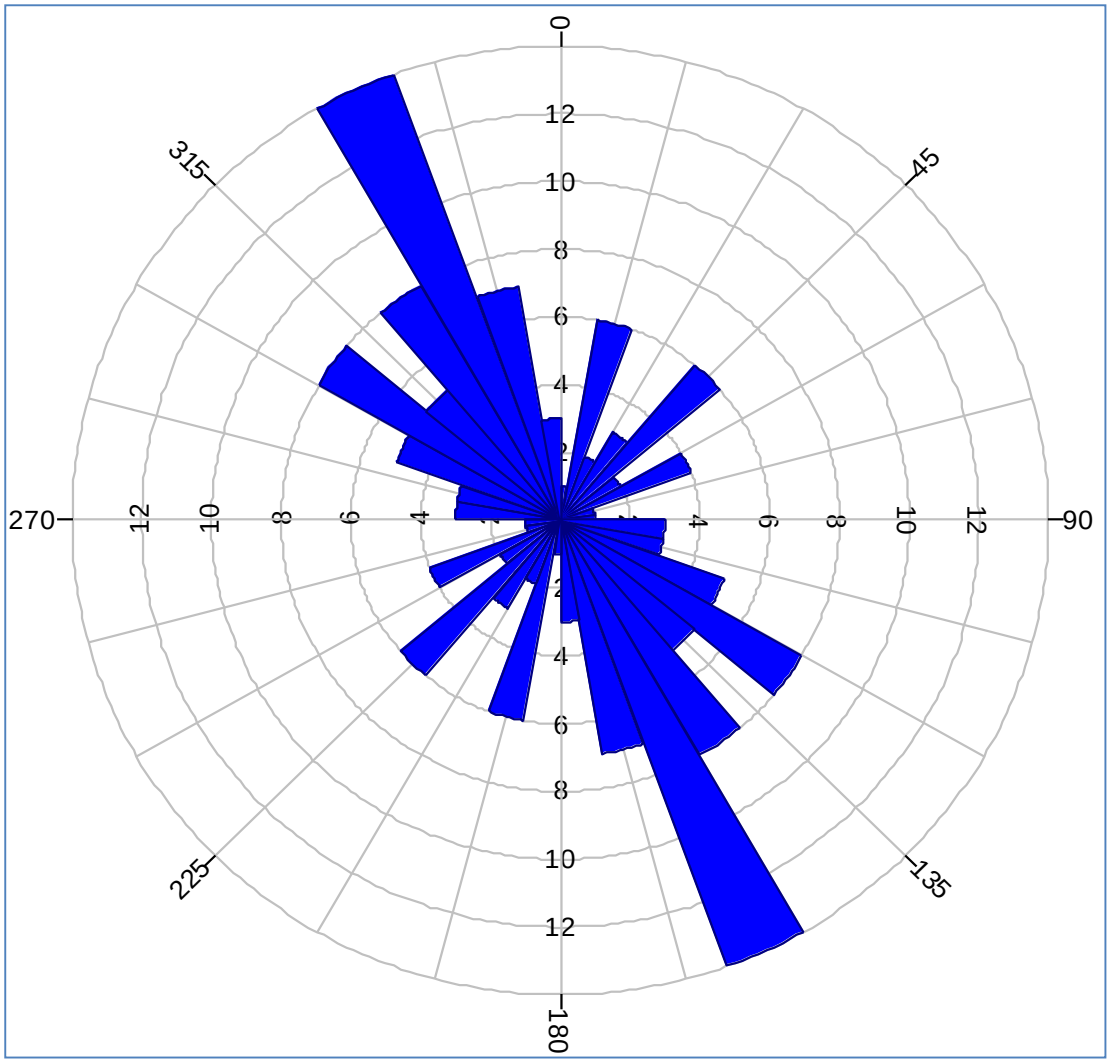

Figure 4.57: A rose diagram for data collected south of Ikutha town, within Tiva gneisses. This shows majority of the joints are longitudinal joints running parallel to the fold axes. Few are cross joints and others are oblique joints.

4.3.6 Shearing of the lithologies in Mutomo – Ikutha area

Shear zones, also sometimes called ductile faults, are intensely strained zones that separate less severely deformed units.

Shear zones occur;

- At the base of some thrust sheets
- At the base of fold nappes - large recumbent folds in orogens.
- Transform faults and other strike-slip zones where erosion has removed the brittle upper crust and exposed ductile rocks below.

- Core complexes - extensional zones within orogens that have stripped off the brittle upper crust exposing deeper metamorphic rocks originally in the lower crust.

Shear zones are the locus of large amounts of mineralization. They are characterized by extreme grain-size reduction and mylonite. Grain size reduction is the result of recrystallization, promoted by strain-induced crystal defects.

Mutomo – Ikutha area has undergone ductile and brittle shearing. Brittle shearing has taken place south of Ikutha, along river Tiva while ductile shearing took place in Mutomo and north east of the area. One of the main goals in studying shear zones is to determine the sense of shear (the direction one side of a shear zone is displaced laterally relative to the other side). Shear-sense indicators are those features that show the sense of shear for a deformation and includes; offset Markers, Foliation Patterns, Shear Bands, S-C Fabrics, Mica Fish, Inclusions, Pressure Shadows, Porphyroclasts and Porphyroblasts, Foliation Fish, Fractured and Offset Grains, Veins and Folds.

I. Porphyroblast as sense of shear indicators in Mutomo – Ikutha area

Porphoryoblast shear indicators were observed on quartzo – feldspathic rocks (Figure 4.58) and in migmatites at Mutomo town (Figure 4.59). Both shear indicators show that the rock units have undergone ductile shearing. Figure 4.59 shows that there was formation of quartz veins, the quartz vein formed boudins when extensional forces affected the rock units. This was followed by compression and rotational forces which led to sinistral shearing indicated by the arrows in figure 4.57. Sheared porphyroblasts can undergo second phase of shearing as indicated by figure 4.60.

Figure 4.58: Shearing observed on a Quartzo-feldspathic gneiss at waypoint 0406356/9769663 ear Ikutha town.

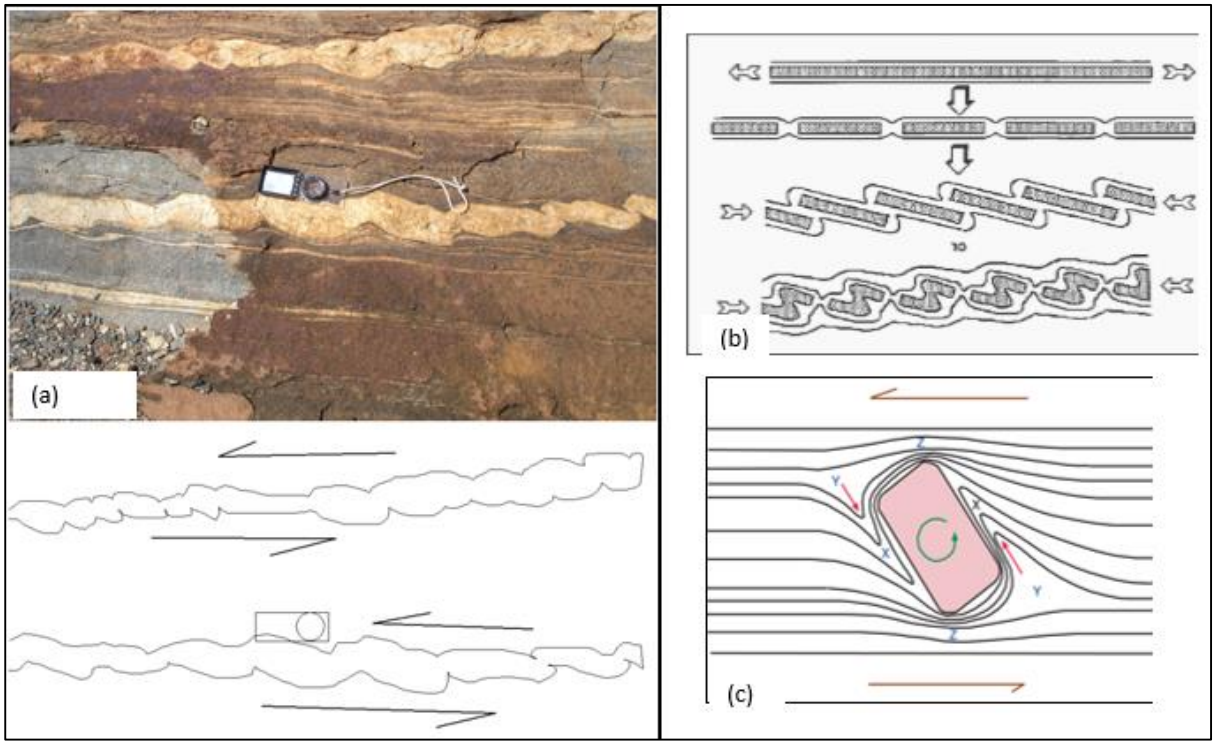

Figure 4.59: (a) sheared quartz in Mutomo biotite gneisses. (b) Stages involved in formation was ;1- extension, 2- formation of boudins, 3- compression, 4- shearing. (c) Sketch showing structural feature ideally developed around a rotating porphyroblast in a biotite gneiss flowing by simple sinistral shear. Compression of the flow layers occurs at X, expansion occurs at Y, and deflection around the porphyroblast occurs at Z. The small arrows show the direction of closure of the microfolds and the sense of rotation of the porphyroblast. The overall sense of shear is indicated by the large top and bottom arrows.

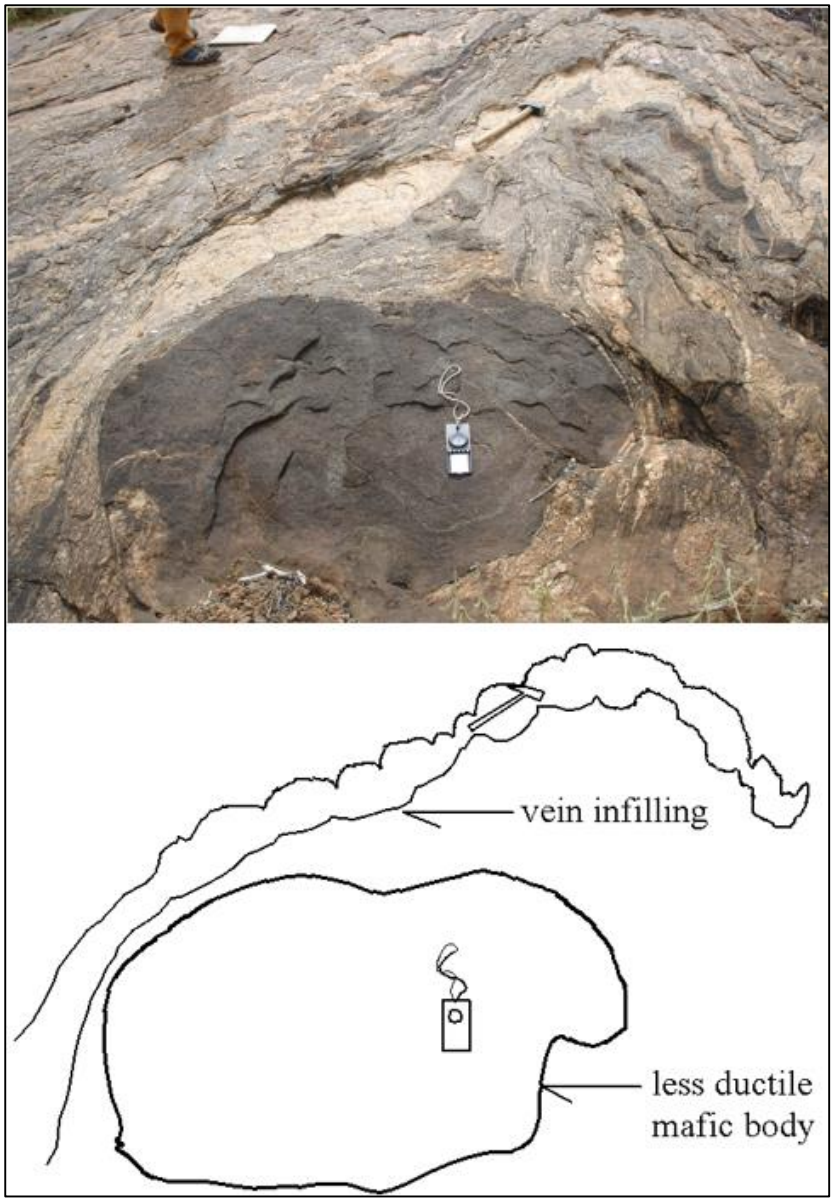

Figure 4.60: The less ductile mafic rock that has not undergone major deformation in semi ductile sheared gneiss which is fractured and has vein in filling at Way point 369 (X=413935, Y= 9801009)..

II. Folds and veins as shear indicators

Folded and sheared veins were observed on migmatites (Figure 4.61A). These sheared veins indicate that the rocks were in plastic status at the period of shearing. The forces that acted on this rock unit were compressional and led to the sinistral shearing which was ductile. Pillow lavas whose chemistry are discussed elsewhere in this thesis have also been deformed by shearing and are used as shear indicators (Figure 4.61B).

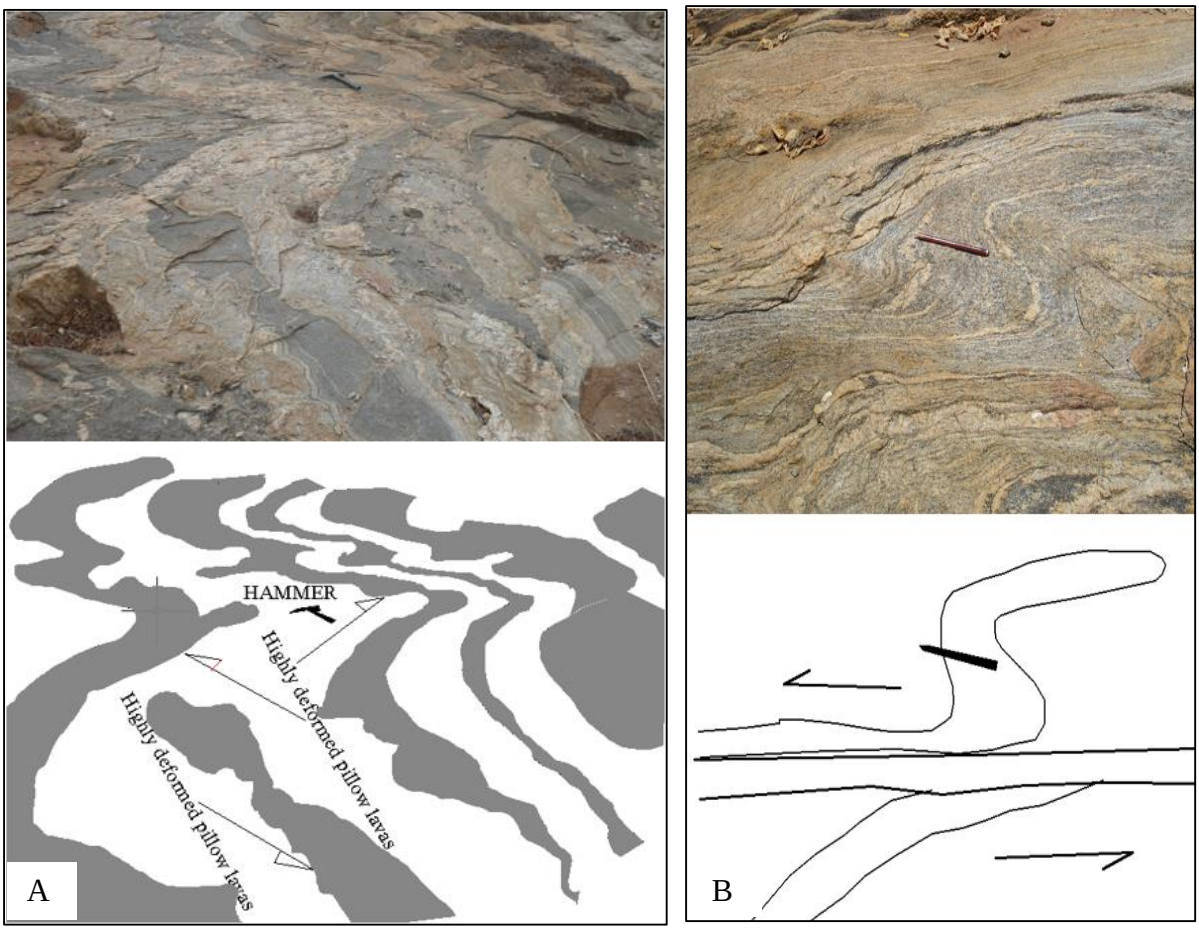

Figure 4.61 A: Folded and sheared Metamorphosed pillow basalts at way point 217 (X=415182, Y= 9799264). The mafic (pillow lavas) have undergone progressive metamorphism, ductile flowage and folding. These pillow lavas are hosted in the gneissses in mutomo – Ikutha area. The pillow lavas were sheared then compressed later. (B), Folded and sheared veins of quartz at Way point 329 (0416397/9796241) near Muumba river in Mutomo. The area has undergone ductile shearing as noted from the pressure shadows located near the pencil. The ultramafic rock has undergone compression of 58%.

III. Mica fish

Mica fish shear indicators also known as pressure gashes were observed on migmatites (Figure 4.62). Their presence on migmatite indicate ductile shearing.

Figure 4.62: Complex Schlieren Migmatitic structures (Mica – fish indicator) showing shearing and high plastic deformation at way point 328 (0416306/9795354).

IV. S-C fabrics as shear zone indicator

S – C fabrics were observed on migmatites south of Mutomo town. Shearing was dextral as indicated by the arrows on figure 4.61. S – C fabric shear indicators showing sinistral shearing were also observed near Mutomo town (Figure 4.63). The C plane has an extensional geometry with respect to the sense of shear. *S–C* fabric consisting of two simultaneously developed foliations serves as an indicator of sense of shear during noncoaxial deformation in a ductile shear zone.

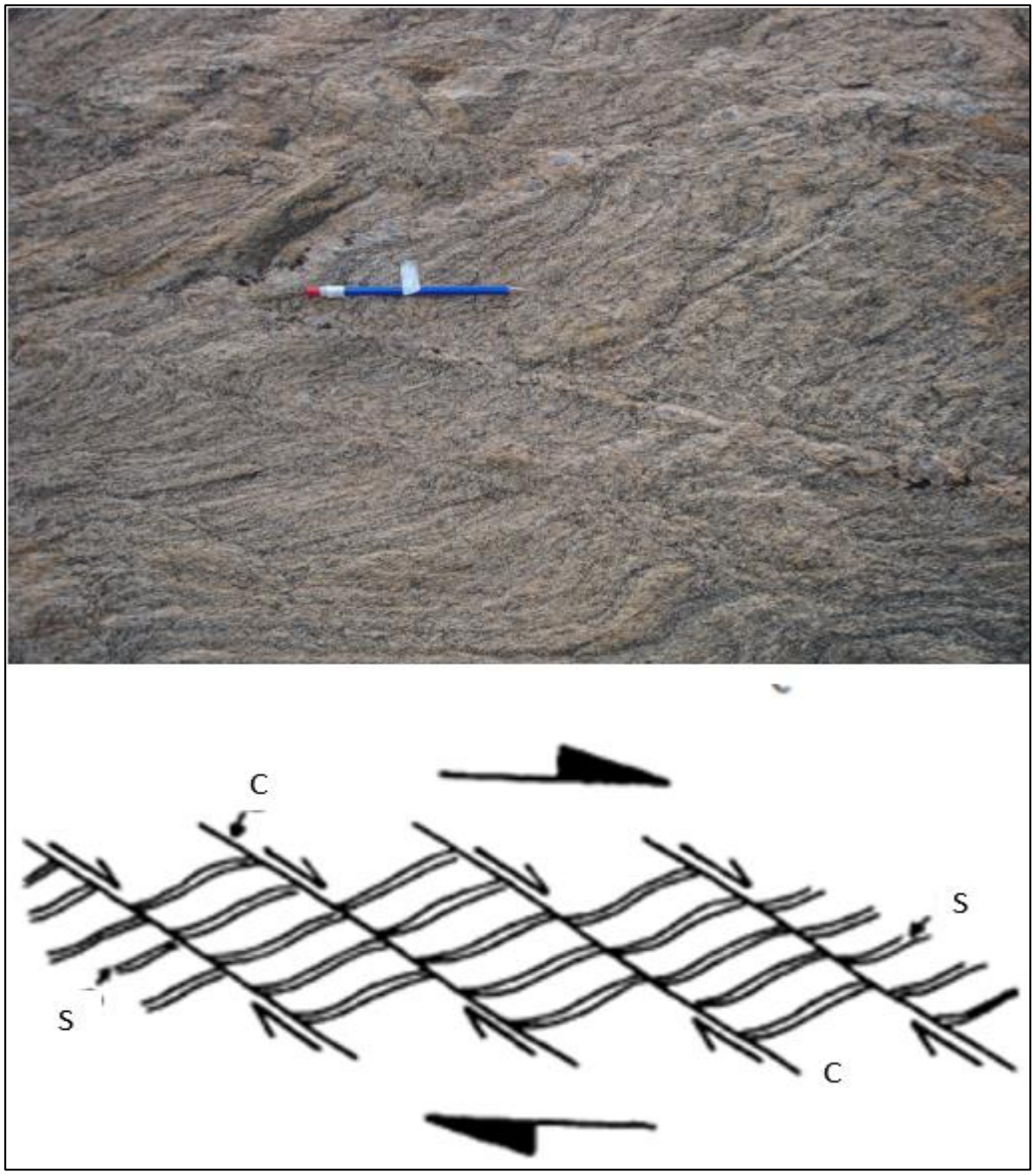

Figure 4.63: The C and S fabrics at Way point 329(0416397/9796241) at Muumba river, southern part of the study area on biotite gneiss. The C plane is the shear plane and S is the schistosity plane.

V. Shear bands as shear zone indicator

Shear bands were observed along Kanziku - Ikutha road on migmatites (Figure 4.64). The shear bands indicate dextral shearing that took place on the migmatites.

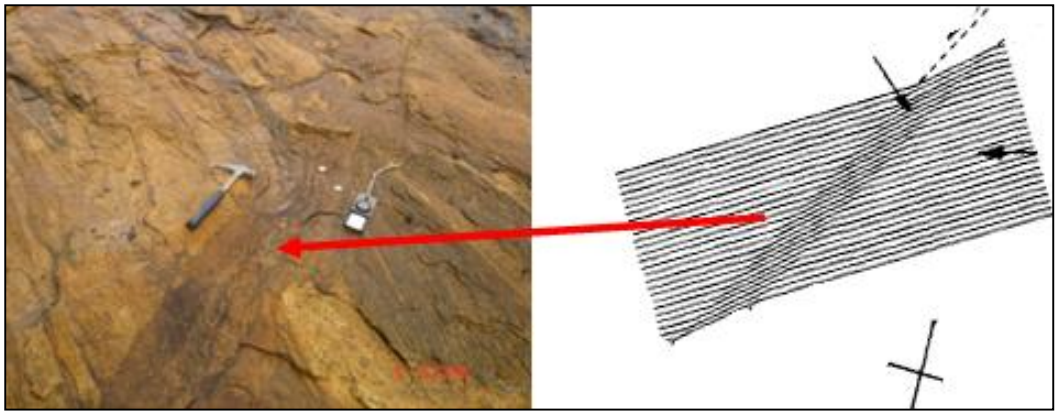

Figure 4.64: The shear bands observed east of Ikutha town showing dextral shearing.

VI. Offset markers as shear zone indicator

Offset markers includes the faulted veins and faulted pretectonic inclusion that was obeserved in the area. Tectonic history indicates that the rocks formed by sedimentary processes, metmaorphosed, sheared and then faulted. Mineral infilling indicates the last stage of the formation of this indicator(Figure 4.65A). This indicaor was observed near Mutomo town and it shows that the rocks have undergone semi – brittle shearing which is sinistral.

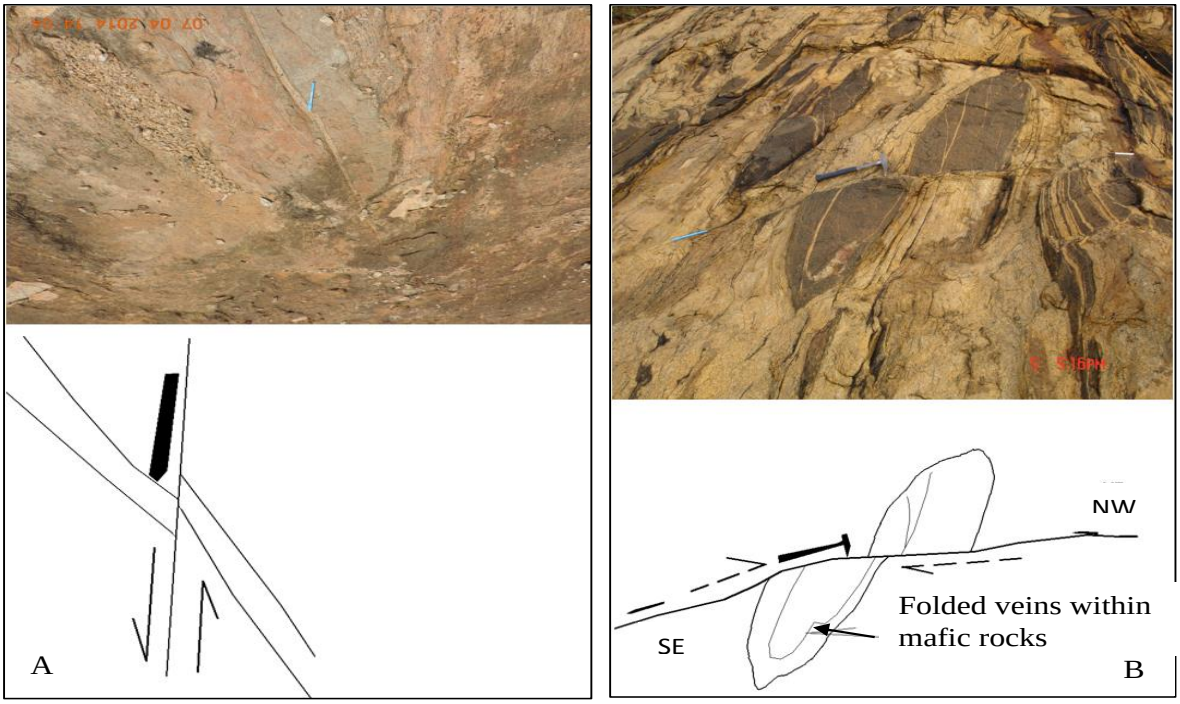

Figure 4.65: (A), Sheared quartz vein in NE – SW direction at location X=413033 and Y=9795188. (B), Faulted and folded mafic rock within the migmatite (initially a mélange) depicted by isoclinally folded vein in mafic body at way point X=0421122 and Y=9776279.

Brittle to semi brittle shearing was also observed in Simis found in the southern part of Muthue. The mafic inclusion have been sheared and faulted (Figure 4.65B) . It is presummed that this is melange because of the rubbled mafics in the felsic rock. The melange are the unsorted sediments formed when two plates collide (continent and ocean plate). The unsorted sediments are scrapped off the oceanic plate and deposited on the accretional wedge. The sediments then underwent metamorphism which was followed by shearing and faulting.

Other offset markers are flattened dike (Figure 4.66A) and deformed dike (Figure 4.66B). Dikes in figures 4.67A and 4.67B postdates the shearing and metamorphism as indicated by the veins cutting across the dikes.

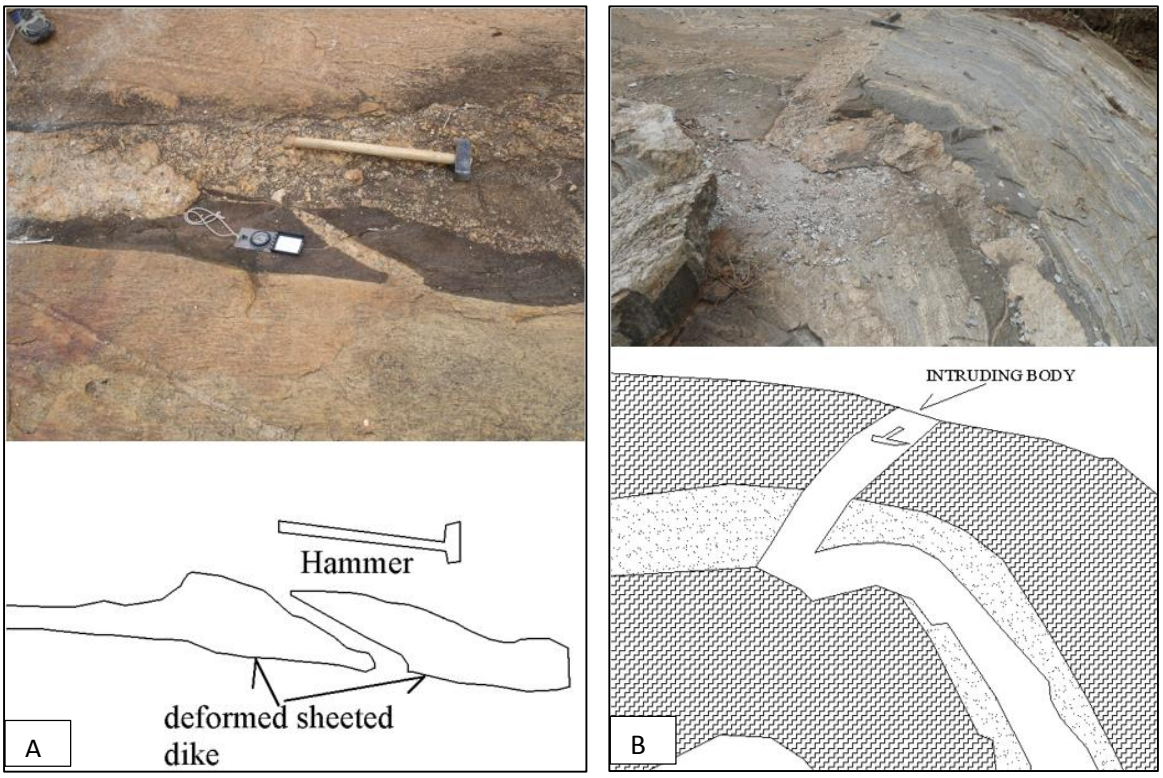

Figure 4.66: (A) Deformed sheeted dike observed on the eastern part of Mutomo town. The deformation was due to brittle shearing that has fractured the dike and given room for infilling of quartz and feldspar material as a vein. (B)Shear related fault on Way point 217 (415182/9799264).

Figure 4.67A: Sheeted dikes at way point 377 (X=0412810, Y = 9795302) south east Mutomo town. (B), Quartz veins (shear extensional components of movement) showing development of capillary quartz porphyroblast as infilling at Waypoint 216 (X=415505, Y= 9799060).

VII. Pressure shadows as shear zone indicator

Pressure shadows indicated the extensional and shortening forces acting on an inclusion. This was noted on the southern part of the research area showing dextral shearing. Mafic accidental xenolith have been extended in the NW –SE direction, conforming to the general trend of the belt (4.68).

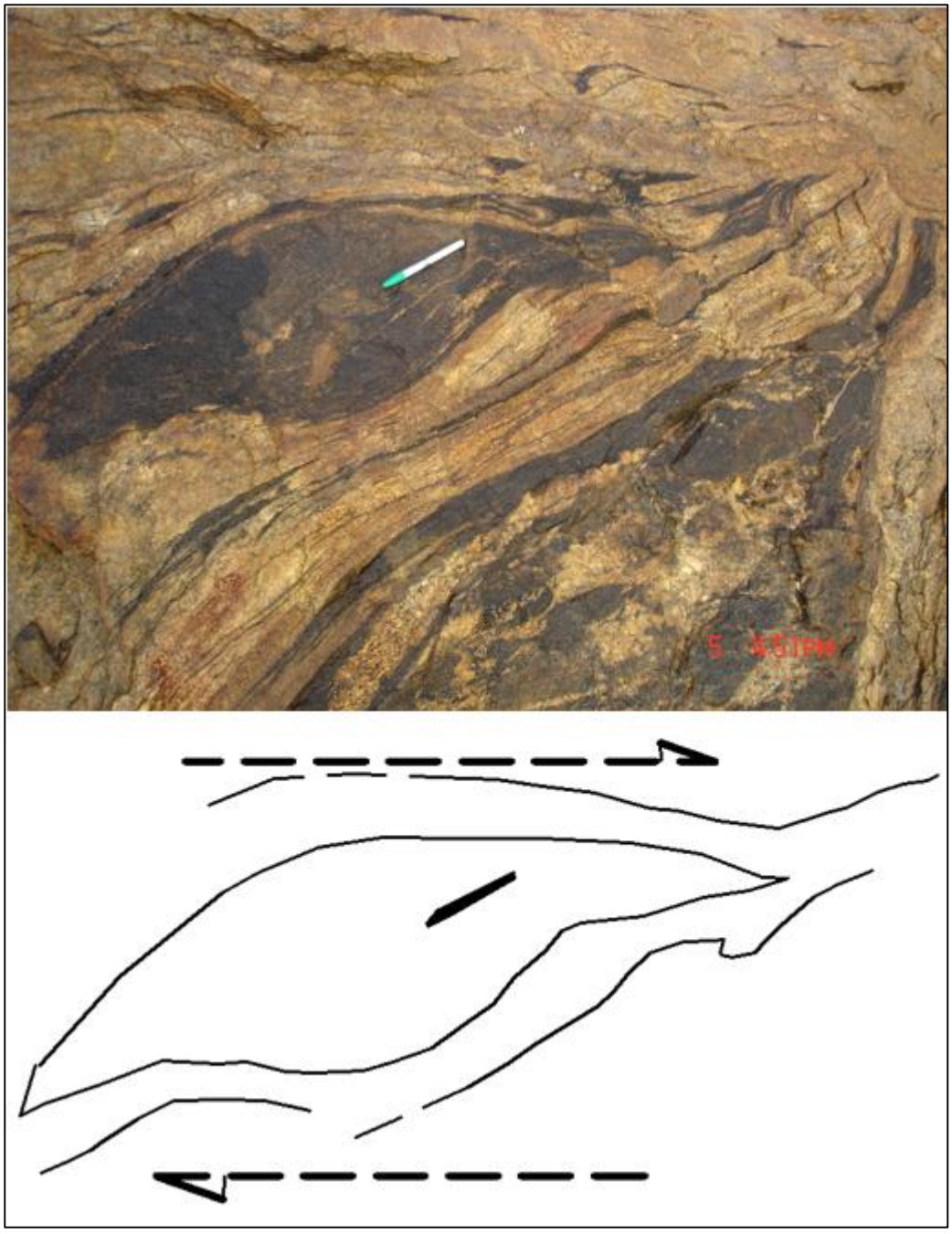

Figure 4.68: Pressure shadow indicator forming sigmoidal structure on way point 329 (0416397/9796241) at Muumba river in Mutomo. The area has undergone ductile deformation.

4.3.7 Faults

Faulting perpendicular to the axial trend of the folds is developed particularly in Maimu south-eastern part of the research area. Diagonal faulting has caused displacement of the limbs along the Ndulukuni anticline where the beds have been downthrown to the south – west. Other faults parallel to the axes of the folds, and also near their axes. Three faults were mapped west of Nzaia in the Mutomo anticline (Figure 4.69). These faults occur where maximum folding of the rocks has taken place and together with the strong jointing seen on these rocks.

Figure 4.69: Faulting on the western part of Mutomo, parallel to Mutomo anticline.

4.3.8 Deformation sequence in Mutomo – Ikutha area

Both the field and microstructural studies of the metamorphic rocks of the study area have shown that these rocks have experienced, at least, three-distinct phases of deformation associated with metamorphism: (1) a NNW D1 deformation, (2) a N-NNE D2 deformation, and late (3) brittle faulting (D3 deformation).

I. D1 deformation

The effect of deformation (D1) and associated M1 metamorphism is commonly observed within the metamorphic rocks of the study area and is expressed by the penetrative pervasive regional foliation (S1) and invariably associated approximately NNW-trending mineral elongation/stretching lineation (L1) that lies in the plane of the foliation.

Asymmetric micro- and meso-folds (F1) with axial plane foliation parallel to S1 are common structures associated with these rocks; they are particularly common in the migmatites. Various kinematic indicators are all consistent with a top-to-the-NNW sense of movement during this phase.

The other important point realized from the structural analysis of the Tiva gneisses is that the mineral elongation lineation trends approximately NNW and does not change its orientation across the lithological contacts throughout Tiva and Ikutha. This observation suggests that the mineral lineation and associated penetrative regional foliation and deformation is a common phenomenon and are all genetically related. This phase of deformation was synchronous with M1 regional Barrovian type metamorphism (main Ikutha metamorphism, MIM) that reached upper amphibolite facies conditions. The progressive increase of metamorphic grade towards the structurally northern parts of the Mutumo - Ikutha area is indicated by migmatization and anatexis observed on the biotite gneisses.

The NNW deformation associated with M1 metamorphism is an important observation and its significance with respect to the origin and evolution of the main Ikutha iron mineralization and metamorphism needs to be discussed. The main Ikutha metamorphism has long been attributed to collision of east and west Gondwanaland. This was later followed by shearing that opened up spaces for iron mineral deposition. Shearing along in Tiva gneisses contributed immensely in the formation of the main vein of iron that trend in the NNW in line with D1 deformation.

In conclusion, the D1 deformation and associated upper amphibolite facies M1 metamorphism is the result of a compressional deformation within a crustal-scale shear zone.

II. D2 deformation

The D2 deformation is expressed by the widespread development of S2 shear band foliation and L2 mineral elongation/stretching lineation (Figure 4.70). The present day configuration of shear bands is consistent with a non-coaxial flow during the-NNW shearing. This phase was

associated with M2 retrogressive metamorphism possibly at greenschist facies conditions. The microstructures of deformed grains in the gneisses are broadly consistent with fabrics developed under greenschist facies conditions at temperatures below 300°C (Pryer, 1993). The S2 foliation is well expressed and best preserved in the gneisses. The detailed fieldwork and microstructural studies of deformed grains in the gneisses demonstrate that the metamorphic rocks of the study area are affected by both ductile and brittle deformation mechanisms. The progressive deformation through first ductile phase in Mutomo area produced migmatite, while brittle shearing mechanisms are exposed in Tiva gneiss.

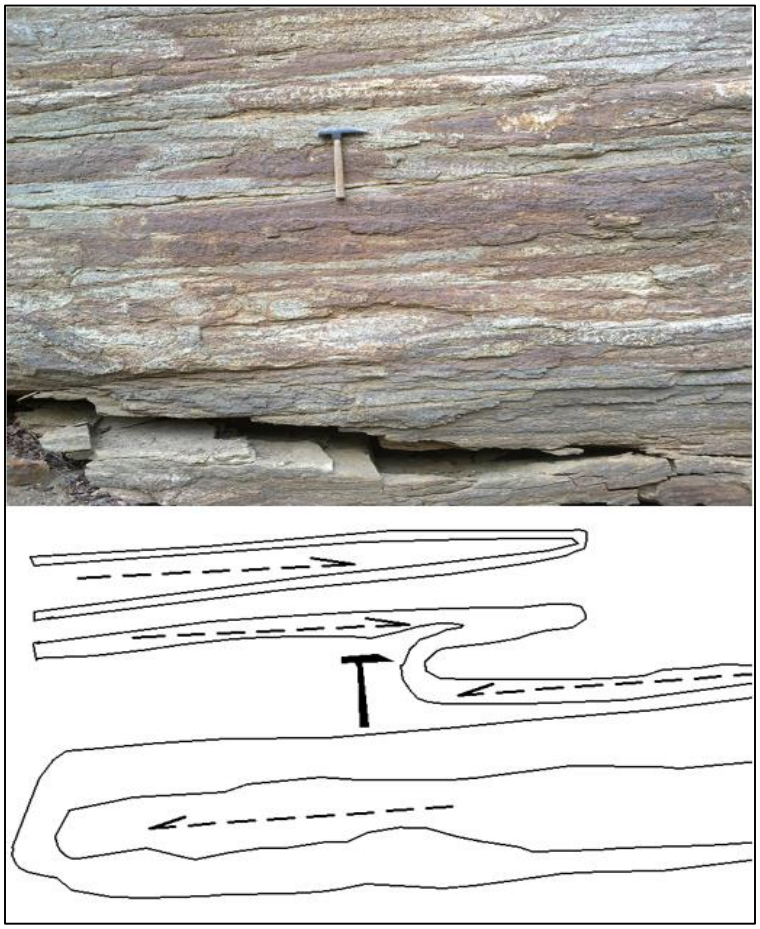

Figure 4.70: Sheared hornblende gneiss in Tiva area

III. D3 deformation

The high-angle (63−89°) faults of diverse size form the other conspicuous feature of the study area and form the boundaries between various rock associations of the study area. The faults brought the mineralizing fluid in contact with the metamorphic rocks, suggesting that faulting

must have predated the iron mineralization and deposition in the area. Fault plane-related features such as slickensides lines and tension cracks characteristically occur on the fault planes (Figure 4.71).

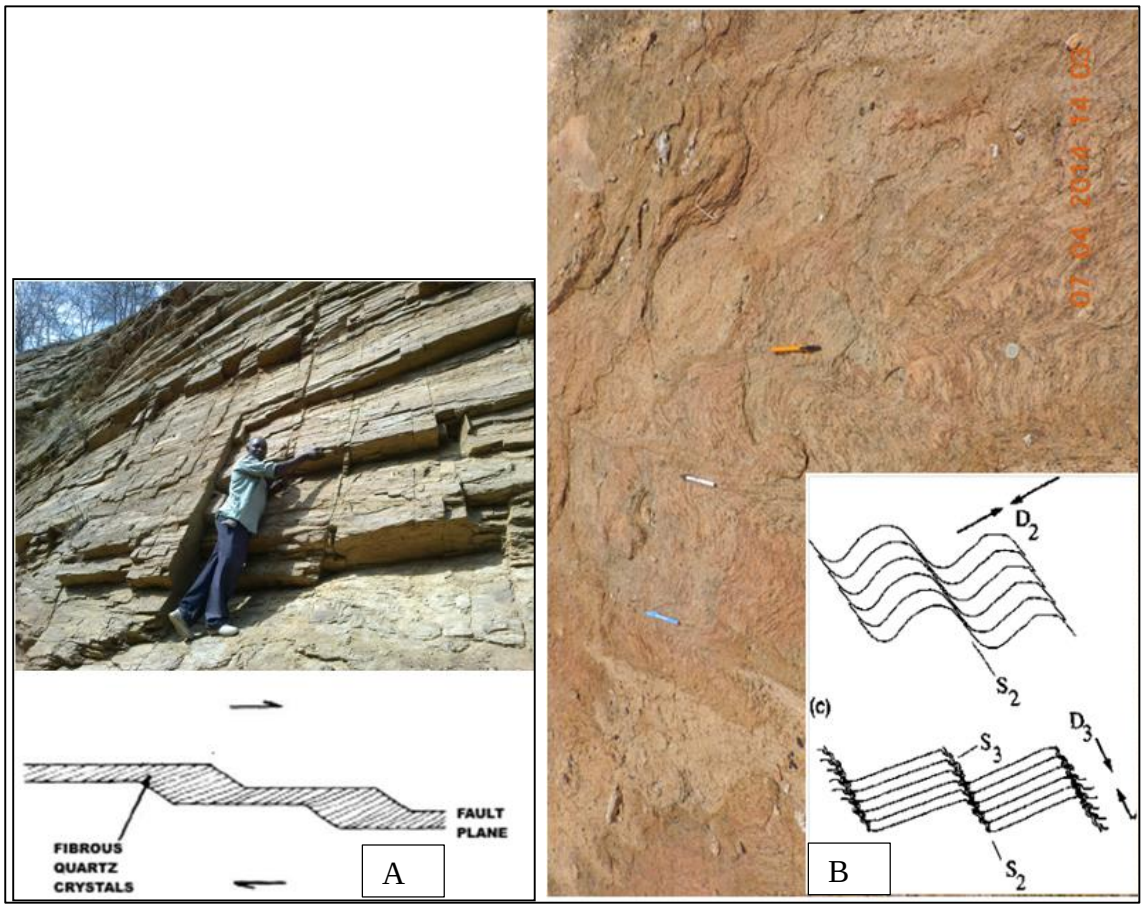

Figure 4.71: (A), Slickensides developed as fibrous crystals of quartz joining opposite sides of a stepped fault plane along Tiva River, western part of the study area. (B) Asymmetric crenulation cleavage (S2) developed over *S1* cleavage. *S2* is folded, as can be seen in the dark sub-vertical *S2* bands. Field width ~ 2 mm, sequential analysis of the development of the textures.

The E−W-directed compression suggested by dextral strike-slip motion is consistent with the inferences about the origin and significance of F2 folding in the study area (Figures 4.72A and B). This, in turn, suggests that the fault was operating as a dextral strike-slip fault under approximately E−W compression during the later stages of NNW ductile-brittle extension along presently low-angle fault and that approximately E−W sub-horizontal shortening accompanied the shear zone deformation during its later stages.

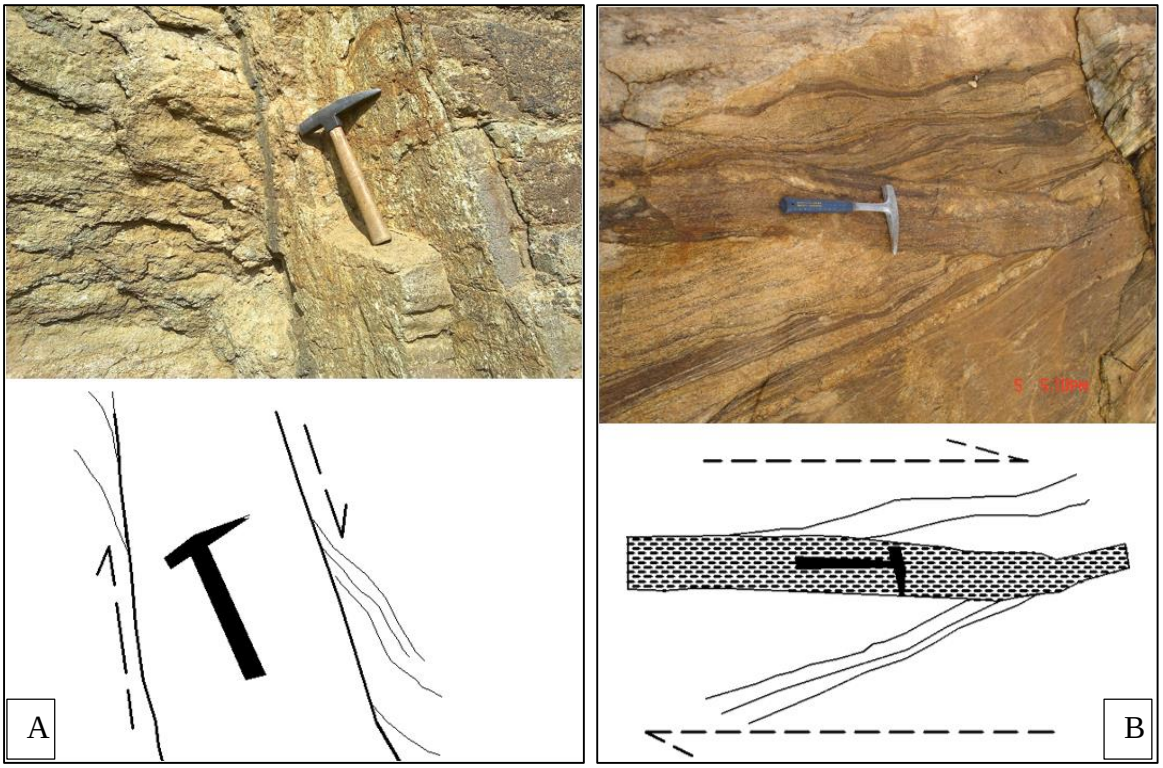

Figure 4.72: Faulted hornblende gneiss in Tiva river (X = 4109648, Y = 9765712).The hammer is placed on the fault plane. (B), Faulting and dextral shearing in location (0421107/9776279). The hammer is placed parallel to fault and shear zone.

4.3.9 Discussion on Geological structures of Mutomo – Ikutha area

(i) Fold style, orientation, and overprinting relationships

Mesoscopic folds with wavelengths of tens of centimetres to a few meters with variable styles and orientations are numerous in the Mutomo – Ikutha area. Most folds in the area belong to Class 2 and 1B types according to the classifications given by Fleuty (1964), Ramsay(1967), Hudleston, (1973), Twiss (1988), Hudleston and Lan (1993).

Mesoscopic folds were analysed in the field and grouped according to style, orientation, and overprinting relationships. W -trending fold occurs only in Kivyuni area on marbles and quartz feldspathic gneiss and are rare in other parts of Mutomo – Ikutha area. The number of SE-trending folds increases at the expense of the NW-trending folds, both of which have moderate to steep axial plunges. The earliest folds (F1) exhibit variability in attitude from region to region throughout the area, but show considerable similarity of style (i.e. they are isoclinal), intensity of folding, and associated planar and linear mineral growth. The axial plane of the

fold is parallel to the regional foliation, which in turn is roughly parallel to the trend of the belt. This suggests a strong NE–SW flattening normal to the trend of the gneiss belt at this stage of deformation. Some folds show broad rounded hinges, suggesting a low ductility contrast during folding (Model A of Ramsay, 1967; see also Ramsay and Huber, 1987), where the thickness ratio of the competent to incompetent layers is low.

Elsewhere, both competent and incompetent layers are thickened in the fold hinge zone and are thinned in the fold limbs (Model B of Ramsay, 1967 ;). Some folds show highly attenuated limbs as a result of progressive strain. Ptygmatic folds were also encountered in most of the metamorphic units. However, some mesoscopic folds display the effect of a simple shear mechanism as indicated by the presence of sigmoidal "drag" folds. Other mesoscopic folds show the effects of flattening by ductile shearing. The younger fold set (F3) show a progressively more uniform orientation through marble and quartzo-feldspathic rock sequence. F2 fold set is characterized by tight to recumbent fold, and is encountered predominantly in the biotite hornblende gneiss. The F2 fold sets have a strong and consistent sense of asymmetry. It is observed that F2 folds refolded the F1 structures, and the variability of their geometry is ascribed to progressive development of fold and the original orientation of F1 folds. F1 open folds are locally developed at outcrop scale and regional scale in the western part of Ikutha town. These were the earliest folds to form in Mutomo - Ikutha area during the collision of East and West Gondwanaland.

(ii) Geometry and mechanics of superimposed mesoscopic folds

Fold overprinting relationships are clearly recognized within the metamorphic rock units of the Mutomo – Ikutha area. The resulting outcrop pattern of three folding events depends entirely on:

(a) The style, orientation, and scale of the individual fold set, that include the shape of the earlier formed fold and the inclination of their axial planes;

(b) The orientation and intensity of the F2 fold formation;

(c) The amount of flattening accompanying the formation of F2 fold and the outcrop surface orientation (e.g. Ramsay, 1962; Hudleston and Lan, 1993). The Mutomo - Ikutha area metamorphic rocks show interference patterns between F1 and F2 folds, and among F1, F 2, and F3 folds. F1 folds are encountered on migmatites and resulted in the development of a strong gneissocity (S1), which is defined by mafic minerals in metapelites. Broadly spaced cleavage is developed in more competent lithologies such as quartzo-felsdpathic gneisses.

The orientation of F1 planar and L1 linear fabrics varies according to their positions with relation to F2 major folds in the area. The second set of folding (F2) in the area, is the main fold set of tight, recumbent and local similar fold styles. The mesoscopic fold of this set shows different geometries. The axial trends of this fold consistently plunge between 13 and 19°towards the SE. This is associated with a planar fabric of axial crenulations and spaced cleavage, which strikes NW and dips 39–65◦ towards the SW. L2 lineations within the area are mainly boudins and intersection lineations and plunge 13–19° SE. F3 is a local mesoscopic fold set, characterized by broad, open fold on marbles and gneisses. In the Mutomo – Ikutha area, the axial surfaces of similar type folds show rotation or "rearrangement" of the inferred principal shortening direction. The geometry of structures indicates that flattening played a major role in the deformational history of the rock units in the area. Flattening probably dominated in the early stages and gave way to simple local shear in the later stages. The planar and linear fabrics in the metamorphic rock units display a close geometric relationship with the coeval large-scale folds of the area (i.e. outcrop-scale lineations are parallel to large - scale fold axes).

(iii) Implications of geology and geological structures to the closure of the Mozambique Ocean

The Mutomo – Ikutha assemblage of metamorphosed pelitic, semi pelitic, calcareous and psammiticrocks suggests that the sequence may have been deposited in a shallow to deep marine environment. Metavolcanic intercalations are also present but rare within the sequence. From the observation made in the field, these metavolcanic intercalations might have been emplaced before the end of metamorphic episodes, and therefore they do not form an integral part of the original stratigraphy. The original sedimentary sequence may have been turbidites that were complexly folded by early NW striking intrafolial isoclinal folds and D1 recumbent tight to isoclinal folds while being shredded during subduction accretion into an accretionary wedge. Similar fabrics and structural styles are known from many younger accretionary prisms (e.g. Kusky *et al*., 1997; Kusky and Bradley, 1999).

(iv) Significance of D1, D2 and D3 deformations to iron ore formation

Iron ore localization requires room created by fracturing or extension. This extensions have contributed significantly to the iron ore localization in Mutomo – Ikutha area. They have provided room for the deposition of magnetite. The results of present study suggests that the rocks of the study area have experienced three distinct phases of extension: (1) rapid

exhumation of metamorphic rocks and associated pegmatites located to the NE of Ndulukuni area, and (2) late stretching and consequent NE−SW faulting along Kimathane – Yamumu syncline and (3) Stretching and shearing along Tiva River which has contributed significantly to the formation of magnetite deposit.

SUB-CHAPTER 4.4: REMOTE SENSING INVESTIGATIONS AND IRON MINERALISATION OF MUTOMO-IKUTHA AREA

The remotely sensed raw data of the studied areas are included in Landsat-7 Enhanced Thematic Mapper Plus (ETM+) data scenes number 167/61 (Path/Row) and covers Mutomo – Ikutha area. Subsets of the digital ETM+ imagery covering the studied areas were obtained. The image processing techniques were applied in this work using ENVI 4.8, ArcGIS 10 and PCI, GeoAnalyst software-package. Geometric correction has been done for the digital data of the ETM+ bands of the study areas. Raw digital satellite data usually includes geometric distortions due to sensor geometry, scanner, platform instabilities, earth rotation, earth curvature, etc. and it was necessary to correct and adapt them (e.g. Mather, 1987, Lillesand *et al*., 2004, Richards, 1995). The georeferencing was carried out using ground control points selected from topographic sheets of scale 1:50,000 (175/1 of Ikutha, 164/3 of Mutomo, 164/4 of Mutha and 172/2 of Ithumba).The root mean square error (RMS) in the geometric processing was 0.54. The following parameters were used in the registration procedures: UTM Projection, Zone 37S, and Arc 1960 Datum. Image enhancement techniques were applied to the selected subset of the ETM+ data for the study area. The achievement of the goal of the application of remote sensing techniques on the studied gneisses led to identify and characterize the studied iron ore bearing gneisses based on the different remote sensing processes of ETM+ data such as colour composite image, principal component and band ratio images.

4.4.1 Colour composite images of ETM data

Digital images are typically displayed as additive colour composites using the three primary colours, red, green and blue (RGB). Different spectral bands of ETM+ data have been selected and combined in RGB colour system to make colour composite images for the studied areas. These combinations were used to select the best colour composite ETM image to be useful in extracting meaningful information about visual lithological discrimination of the studied hornblende gneiss rocks such as combination of ETM bands 7, 4 and 2 (Figure 4.73).

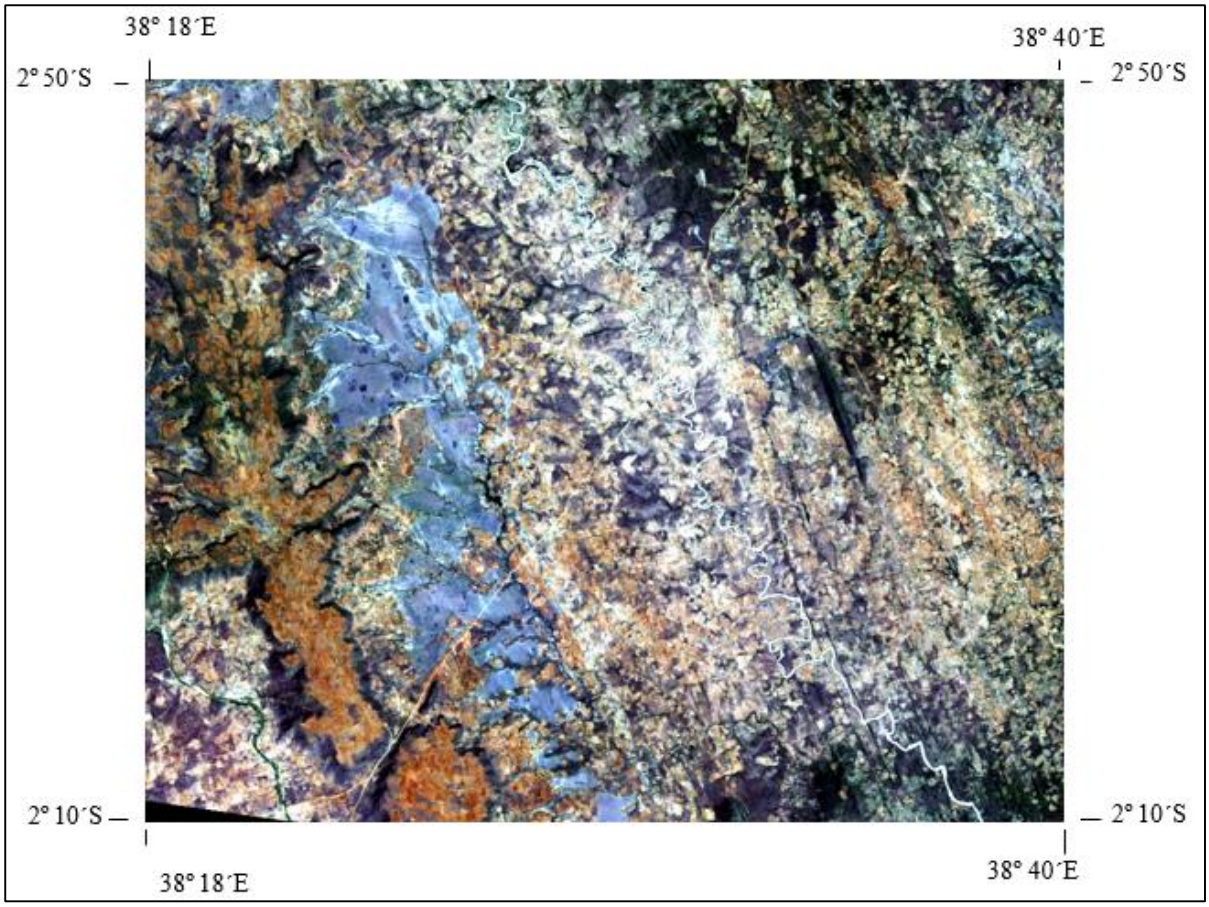

Figure 4.73: Landsat thematic mapper colour composite of Ikutha regional area. ETM+ bands 7 4 2 = RGB.

4.4.2 Principal component analysis of ETM+ data

Different bands of multispectral data are often correlated and thus contain similar information i.e. have similar visual appearances. This correlation means that there is redundancy of information. The principal components (PC) transformation is used, to reduce this data redundancy, by compressing multispectral data sets and calculating a new coordinate system. The application of the PC on the present data is to compress all of the information contained in an original n-channel (band) data set, into fewer number of channels or components, that could be displayed separately as single stretched PC-images, or as component in color composite PC-image . The false colour composite image of principal components PC1, PC2 and PC3 for the studied areas successfully distinguish and characterize the studied gneisses (Figure 4.74).

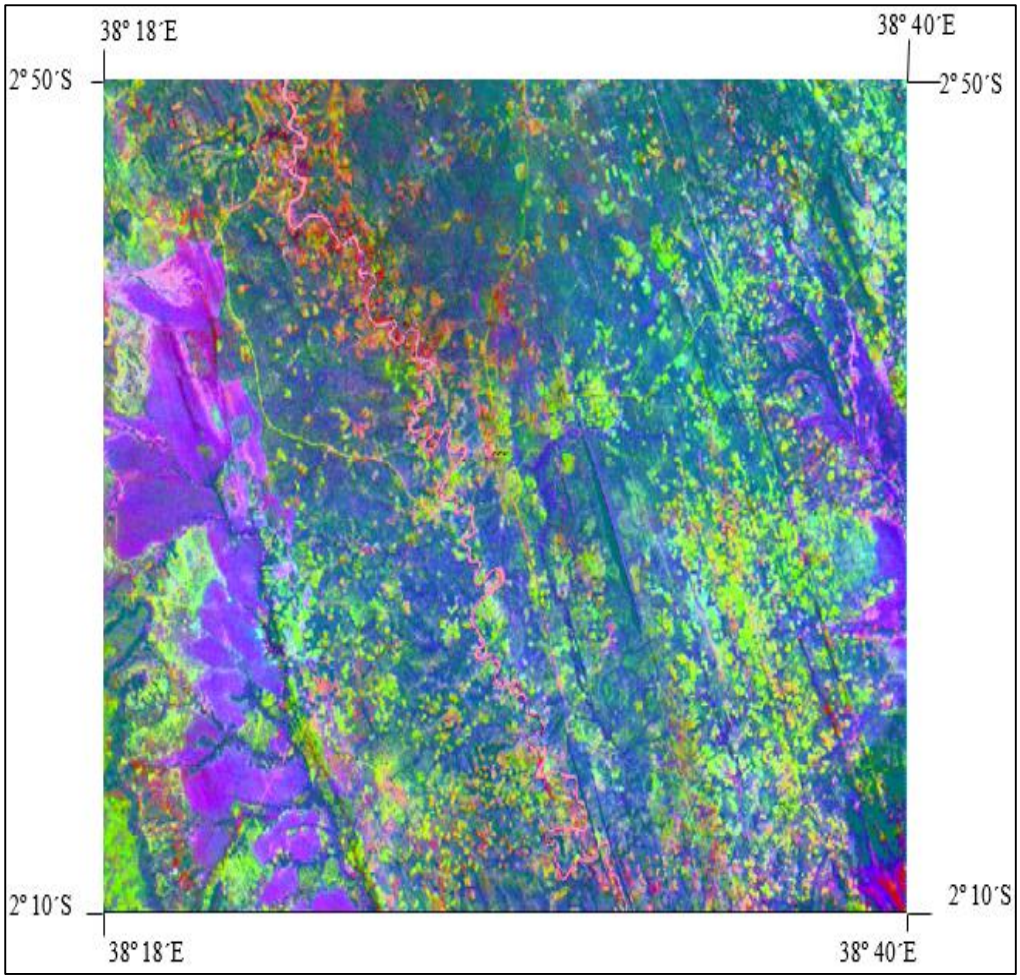

Figure 4.74: False colour composite image of principal components PC1, PC2, PC3 displayed in RGB for Mutomo – Ikutha area

4.4.3 Band ratios of ETM+ data

Addition, subtraction, multiplication and division of the pixel brightness from two bands of image data to form a new image are particularly simple transformations to apply in image processing technique. Multiplication seems not to be as useful as the others, band differences and ratios being most common. Differences can be used to highlight regions of change between two images of the same area. Ratios of different spectral bands from the same image are found useful in reducing the effect of topography and for enhancing subtle differences in the spectral reflectance characteristics for rocks and soils. The use of the band ratio technique was applied to the satellite ETM+ Landsat 7 digital data for this study area. The reflectance values in band 7 (2.08 to 2.35 μm) of TM data depend mainly on the hydroxyl content of the rocks. The ratio of band 5 to band 7 was used as a measure of the intensity of the hydroxyl absorption (2.2 to

2.4 µm region). This ratio was used because band 5 is not within the confines of the Fe –bearing aluminosilicate related or hydroxyl-related absorption features, whereas band 7 is within the hydroxyl absorption wave lengths. The high value of band 5/7 ratio appears in light tone due to the high content of hydroxyl bearing minerals.

The spectral band ratio is one of the most common powerful techniques applied for mapping the minerals of alteration zones (clay, alunite and iron minerals). Recognition of hydrothermal altered rocks associated with mineral deposits was carried out using image processing techniques such as band ratio images in addition to colour ratio composite images. The spectral bands of ETM+ are well suited for recognizing assemblage of altered minerals. The hydrothermal minerals that were detected by the Landsat image processing of the data of selected areas could be classified into two groups: hydroxyl (clay minerals) and hydrated mineral (sericites) detected by band ratio 5/7 on one hand, and minerals containing iron (magnetite) detected by band ratio 3/1 on the other hand. Applying these techniques led to the recognition of more than three zones of altered rocks within the studied gneisses along Tiva River.

4.4.4 Colour composite ETM+ band ratio images

Colour composite images have been constructed using combination of three ETM band ratios. Different ETM band ratio combinations were carried out to select the optimum colour composite image to use in the visual lithologic discrimination of the investigated area. Some of these combinations are illustrated in (Figure 4.73). The best selected result was the colour composite image produced by the combination of bands 5/7, 4/5 and 5/1 (Figure. 4.75).

This selected image was prepared as shown in which ratio band 5/7 image was assigned by the red component, ratio band 4/5 image by the green component and band 5/1 image by the blue component. The selected colour composite image diagnoses some aspects between the different rock units. For example, it determines and delineates the black cotton soil (purple colour) from the gneisses. The silica rich rocks display red – purple colour in this image and is due to the high band 4/5 ratio. The migmatites appear on this image in blue colour due to the high band 5/1 ratio. The boundaries between the black cotton soil and the older gneisses could be delineated in the western part of the mapped area using the colour composite image of ratio bands (Figure 4.75).

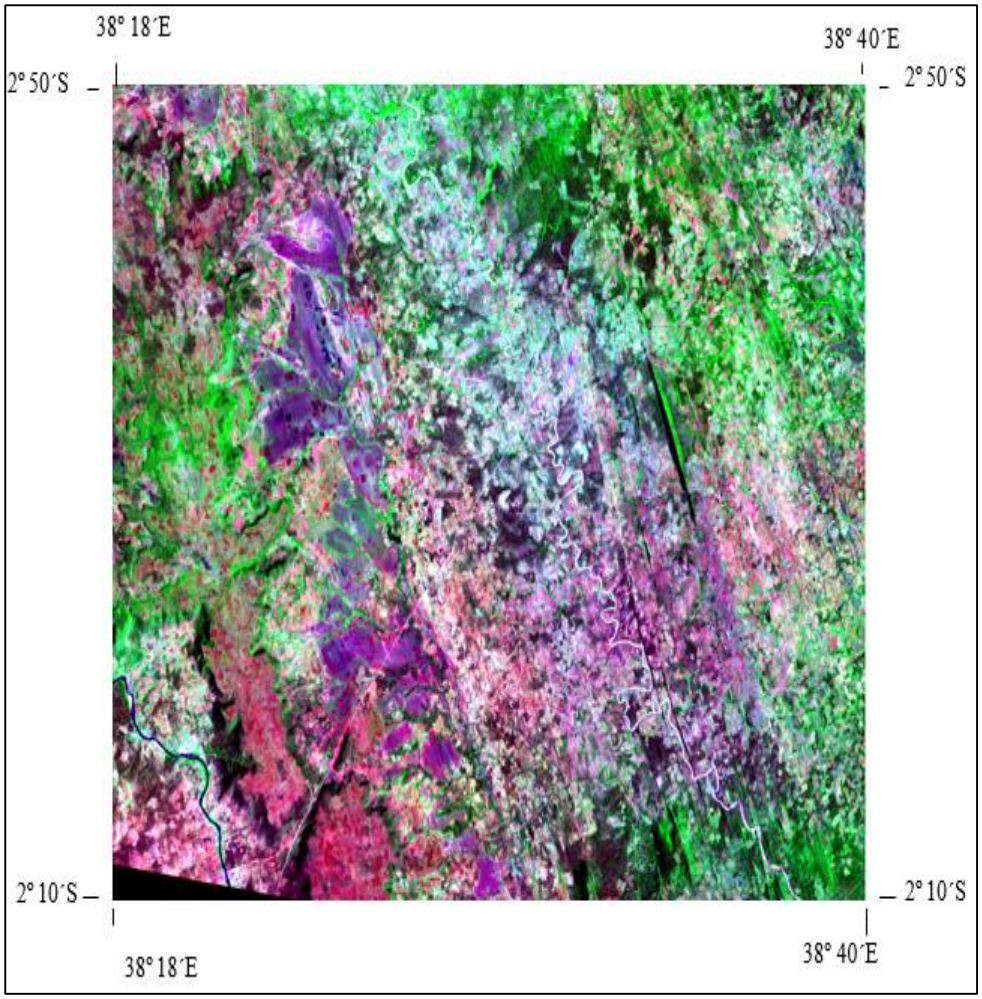

Figure 4.75: Landsat Enhanced Thematic Mapper colour composite of Mutomo - Ikutha area. The colour composite image produced by the combination of bands 5/7, 4/5 and 5/1.

4.4.5 Lineaments extraction

The automatic lineaments extraction from Landsat ETM+ panchromatic band of the study areas was carried out under the default parameters of GeoAnalyst-PCI package. These lineaments have been visually edited to extract only the structural lineaments. The obtained total structural lineaments in Ikutha area were 56. The rose diagram of these lineaments shows that their predominant trend is NNW (Figure 4.76). The zones of high lineament intensities concentrated at the central and eastern part of River Tiva as exemplified in Figure 4.76. The intersected lineaments, on the other hand, are found to be restricted and concentrated only in the southern part of the Ikutha town.

It could be concluded that the alteration zones and/or mineralized zones in the investigated areas, delineated by band ratio images of the studied gneisses (Figure 4.77) coincide more or less with high lineaments intensity and/or lineaments intersection or both.

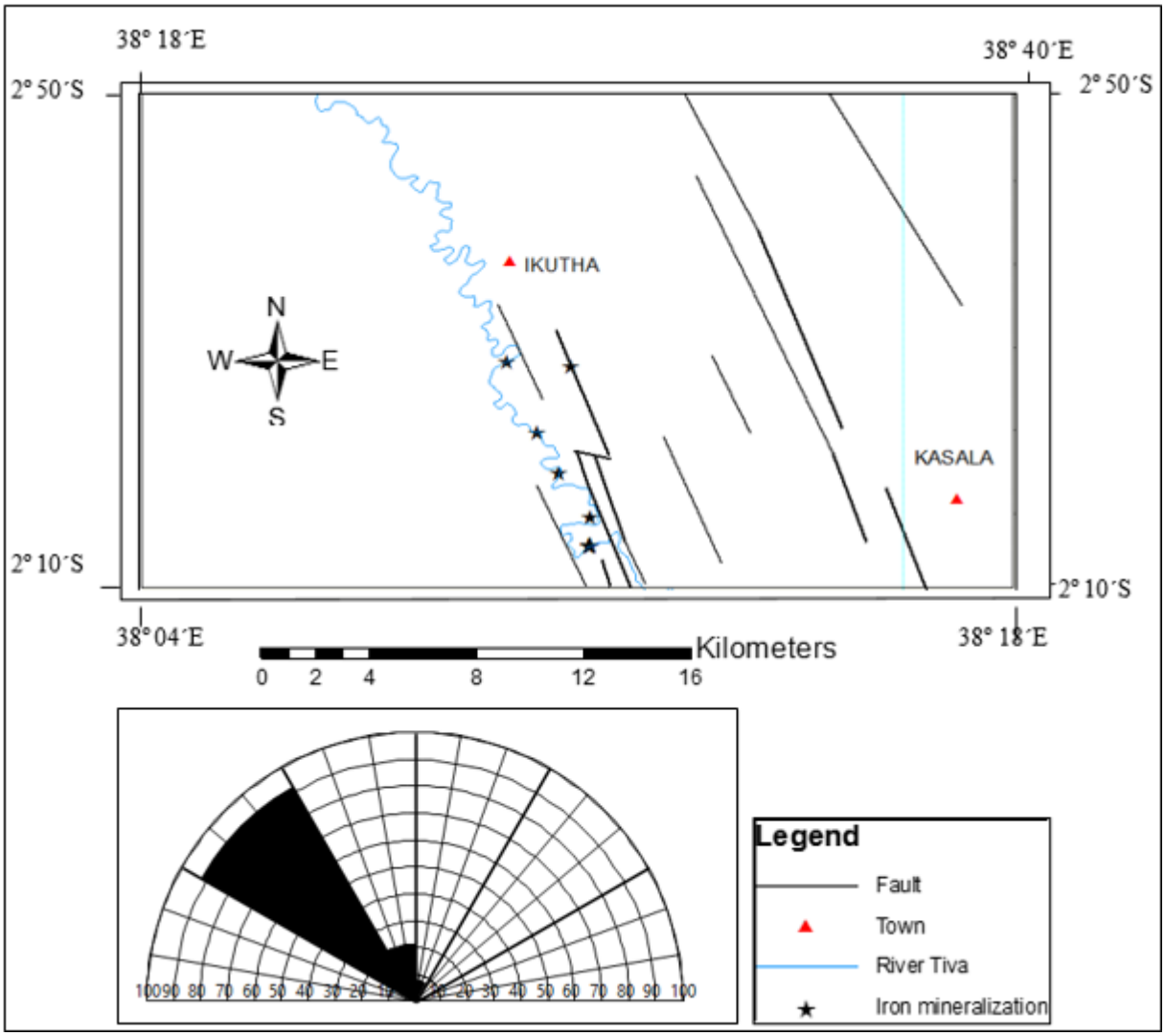

Figure 4.76: Structural lineaments extracted from the Mutomo – Ikutha image and their frequency rose diagram. This lineament rose diagram agree with the rose diagram for the joints.

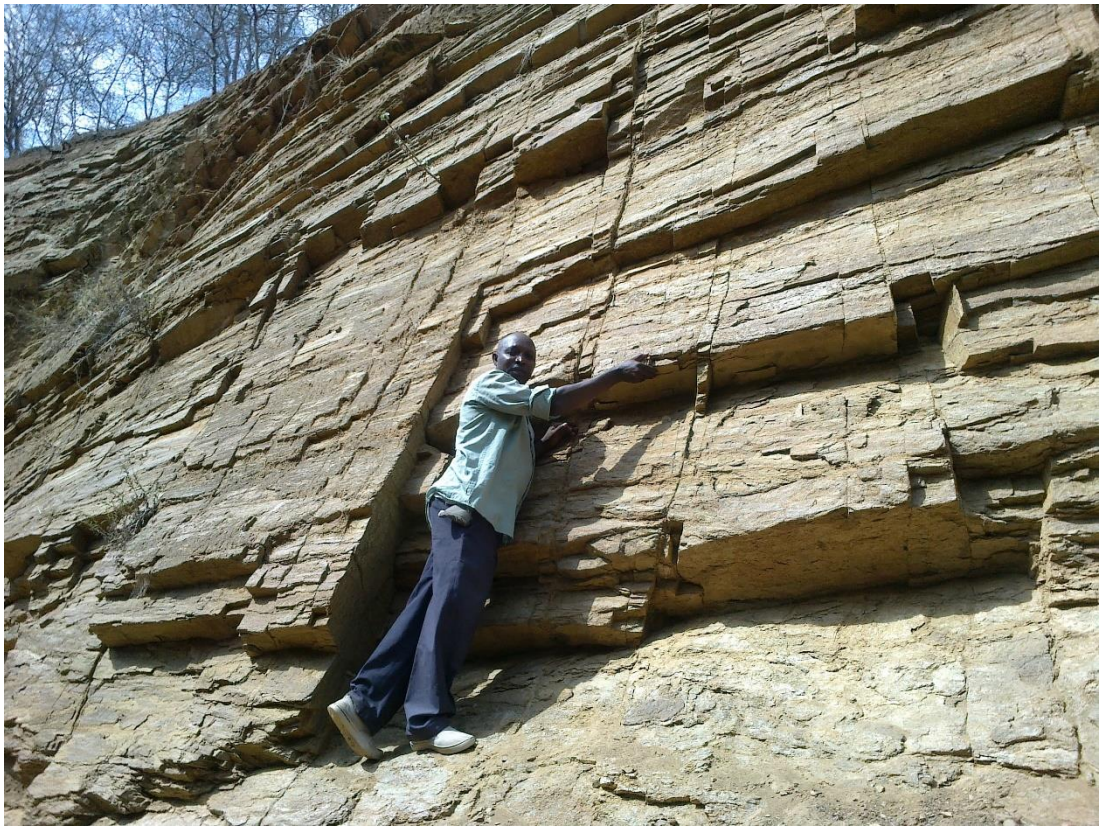

Figure 4.77: Strongly, foliated and jointed hornblende gneisses west of Tiva River.

4.4.6 Iron mineralized zones

From the studied remotely sensed data, it is worth mentioning that there are many criteria of the alteration zones that could be used as a guide for the exploration of Iron mineralization occurring within the gneisses rocks in the study area (Mozambique mobile belt of Kenya). The most important criteria used as a tool to increase the potentiality of the iron mineralization was to distinguish high and low reflectance portions in the study area. Moreover, construction of the alteration map that was derived from image processing helped in the deciphering of new zones of mineralization. Such alteration map could be used in the exploration for iron mineralization in the future.

The methods applied in this work for the exploration of hydrothermal iron ore mineralization using satellite image processing are based on the surface spectral features. The occurrence of hydrothermal altered rock is one of the main features that can be utilized to determine the localization of iron mineralization. By comparing the intensity of the extracted structural lineaments, and their intersections to the altered zones depicted from remote sensing processing

technique it could be recognized that the alteration zones, more or less coincide with the high frequency and intersected lineaments.

The distribution of hydrothermal alteration zones within the processed Landsat images become the key in locating the main outflows of a hydrothermal system, which led, after the field checking, to recognizing high Fe_3O_4 anomalies and mineralized zones within the study area. Therefore, many locations are delineated in this work as altered zones, whether by clay minerals or sericite (Figure 4.78). Iron oxides are frequently observed in the outcrops of hydrothermally altered gneisses. Therefore their identification is a useful key in defining areas related to deeply mineralized zones.

Figure 4.78: Hornblende gneiss that has undergone hydrothermal alteration (sericitization) south of Ikutha town.

4.4.7 Ground truthing with laboratory investigations

Extensive geological, field proving and geochemical investigations were carried out for the alteration zones (Figure 4.79), delineated in the studied gneisses by the Landsat image processing. During the field works, the geochemical investigations revealed that the Fe_3O_4 is relatively high in the sheared gneisses as well as altered gneisses. The four locations discovered as high geochemical anomalies with some iron mineralization, are mainly connected to the hornblende gneisses and hornblende biotite gneiss of Tiva group. These locations include Timboni, Muangeni, Kitambasye and Mutuluni in Ikutha area .The mineralized zones of Ikutha formation are found to be mainly connected or hosted by the hornblende gneisses that follow

the direction of the strong and nearly vertical shear zone striking N320^{o}W-S140^{o}E in the western part of Ikutha town.

The Fe_3O_4 anomaly at the northern part of Timboni, is mainly connected and hosted by highly altered and weathered gneisses and structurally controlled by NNW- SSE shear zone. One of the striking feature of this anomaly is its association with high content sericite unlike the anomalies of Timboni area which are associated with apatite.

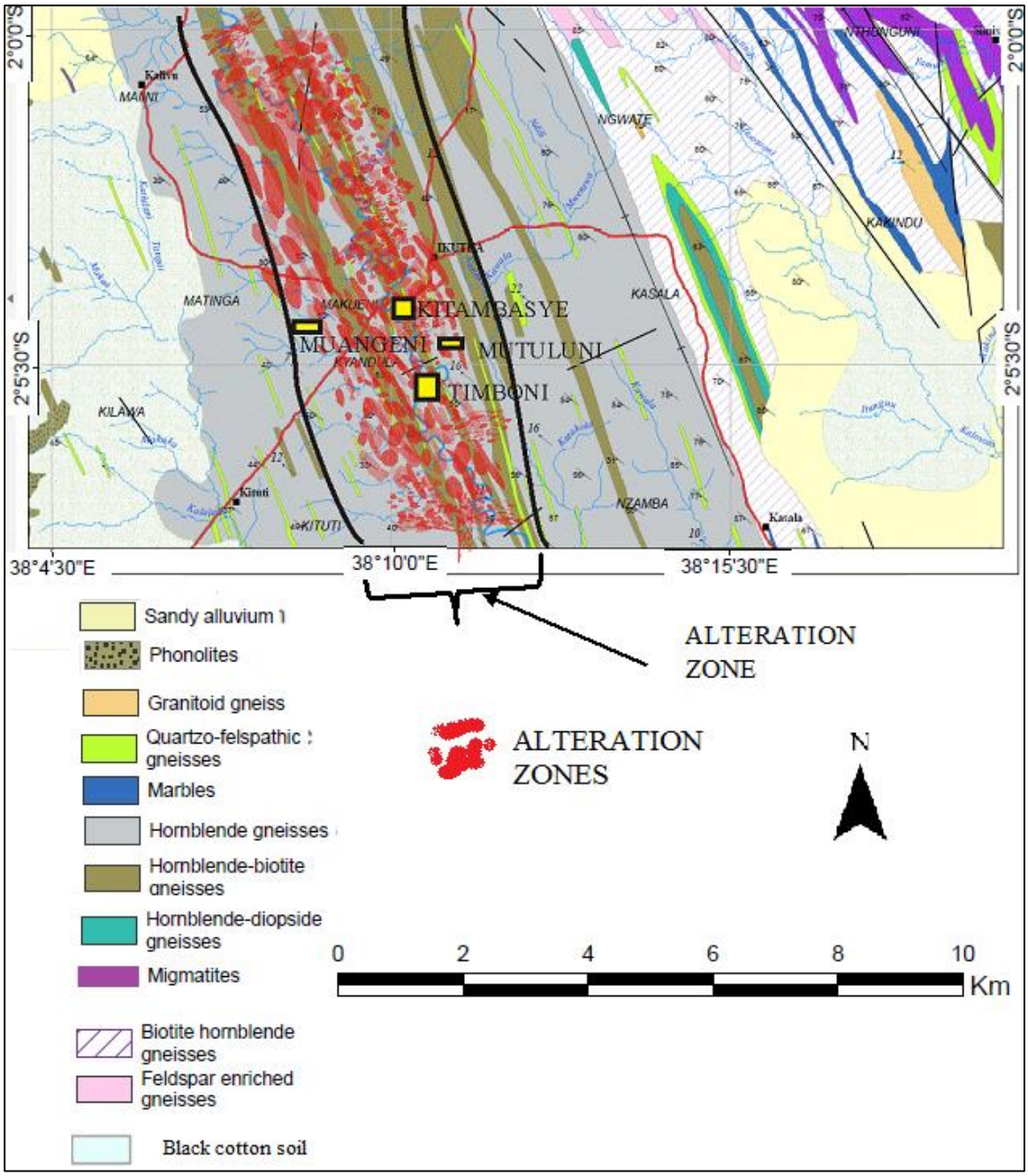

Figure 4.79: Hydrothermal alterations map of Ikutha area, interpreted from the Landsat ETM images and field works.

4.4.8 Discussion on remote sensing and iron mineralisation

This study aimed to use the capability of remote sensing techniques integrated with geological investigations to characterize the iron bearing gneisses and to detect hydrothermal alteration zones, and their associated structures suitable for iron mineralization. Recognition of hydrothermal altered rocks associated with mineral deposits was carried out using image processing technique such as band ratio images, in addition to colour ratio composite images. The spectral bands of ETM+ are well suited for recognizing assemblage of altered minerals. The hydrothermal minerals that were detected by the Landsat image processing of the data of selected areas could be classified into two groups: Hydroxyl (sericite minerals) and hydrated mineral/ detected by band ratio 5/7 on one hand, and minerals containing iron (magnetite) detected by band ratio 3/1 on the other hand. Applying these techniques led to recognition of more extended zone of altered rocks within the studied gneisses. The association of hornblende gneisses, shearing and faulting along river Tiva in Ikutha area appear to have play an important role in the distribution and localization of the mineralization.

Image processing techniques were applied to the digital subset ETM+ data of the studied areas. These techniques generated several products of enhanced satellite imagery such as colour composite images, ratio images and principal components. These techniques have been successfully used in the lithological discrimination of iron bearing gneisses. The capabilities of remote sensing data to characterize the iron bearing gneisses in addition to characterization and mapping of the hydrothermal alteration zones usually help in localization of iron mineralization.

Extensive field geologic and geochemical investigations to the zones delineated by the image processing technique led to the discovery of four locations of high Fe_2O_3 anomalies (Figure 4.79) with some iron mineralization, mainly connected to the studied gneisses. These location include Timboni, Muangeni, Kitambasye and Mutulini (East of Timboni). This work showed the important criteria that can be considered as tools to increase the potentiality of the iron discovery in Mutomo – Ikutha area. Moreover, construction of the alteration map of the different studied gneisses interpreted from the image processing can be applied in the discovery of new zones of mineralization. This technique can be used in exploration for iron

mineralization in the future elsewhere in the Mozambique mobile belt having similar conditions.

Saggerson (1957) classified the gneisses under the metamorphosed calcareous sediments which is contrary to the IUGS classification. He had also left a gap on the southern part of the area he had mapped (see figure 4.78 for the missing rock units in Saggerson (1957)). The lithology on the geological map produced by Walsh (1963) and Saggerson do not merge at their adjacent boundaries (see figure 4.80). These gaps were addressed during this research work by using satellite image and geological field investigation.

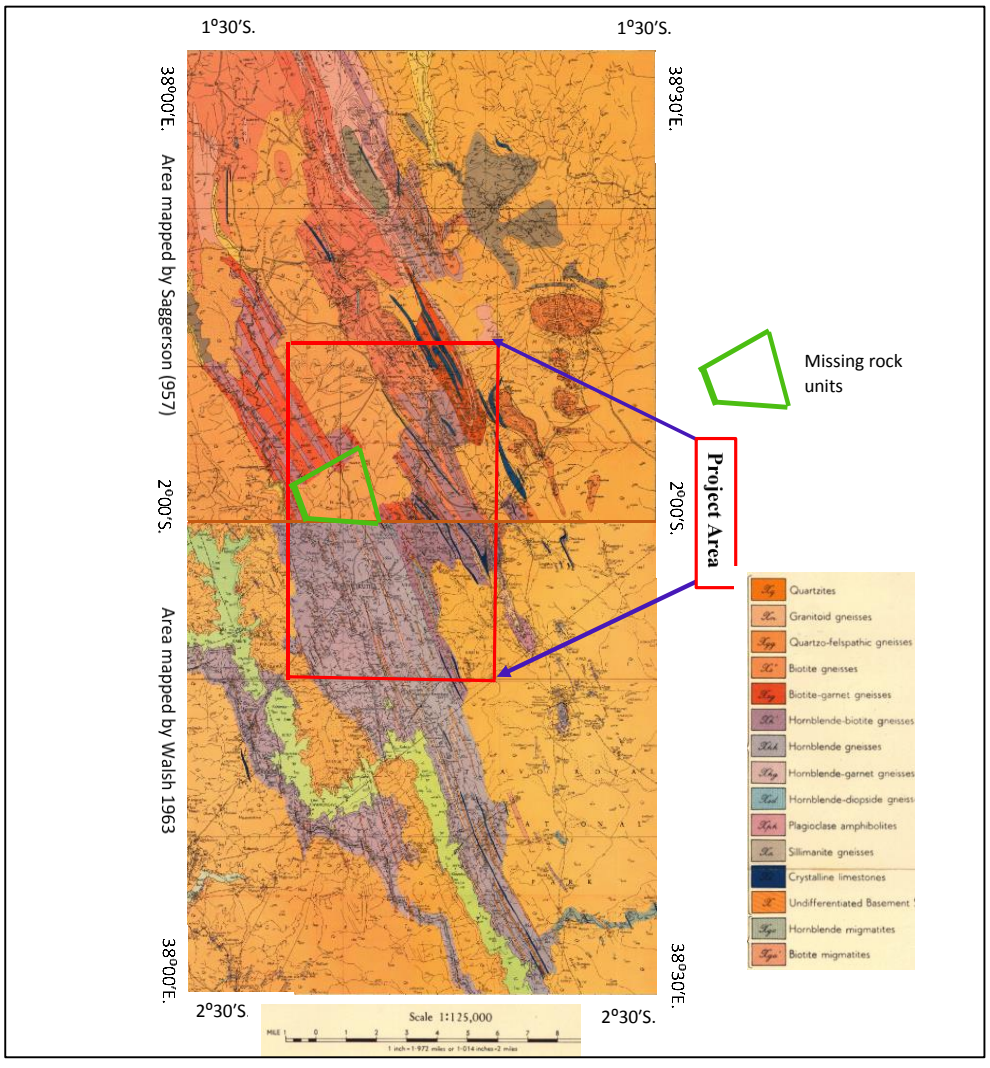

Figure 4.80: The geology maps of the study area according to Saggerson (1957) and Walsh (1963). The two maps have been joined together to establish the continuity of geology and the gaps.

SUB-CHAPTER 4.5: GEOCHEMISTRY AND GENESIS OF IRON ORE DEPOSITS OF MUTOMO-IKUTHA AREA

This section describes the geochemistry for the rock units occurring in Mutomo – Ikutha area aiming at supplementing their petrographic classification and elucidate on their petrogenesis. It also describes the possible mechanism of the genesis of iron ore in the study area. The study adopts multi-elemental variation diagrams to highlight the geochemical nature, origin and petrological relationships between the different rock units. The geochemical diagrams have been plotted using geochemistry extension of Oasis Montaj software, Microsoft Excel and WinRock.

4.5.1. Geochemical results

Representative analytical data for the major element composition of the Mutomo – Ikutha iron ore and its host rocks are shown in Table 4.17. Other results are presented in the Appendix A. The results were processed as explained and discussed in the following sections.

The sampling grid map (Figure 3.6) for these particular study is presented in chapter 3 of this thesis. The geochemical distribution intensity map of the Fe_2O_3 content in this area is graphically presented in Figure 4.81. High content of Fe_2O_3 occur in hornblende gneiss on the western part of the area sampled (Figure 4.81). The concentration of Fe_2O_3 (56.6 % - 82.3%) display a linear trend of north to south. Low values of Fe_2O_3 (7% - 13.2) occur mainly on the eastern, south-eastern and southwestern part of the area.

(a) Correlation of Fe_2O_3 with other elements in host rock

Iron ore is hosted mainly in the hornblende gneisses (see Figure 4.2 and Figure 4.79) found in the western part of the study area and trending in the NW – SE direction. Pearson correlation coefficient was used to test the dependence of each element. The chemical results shown in Table 4.17 and appendix A were plotted using SSP software and Oasis Montaj software. It is noted that Al_2O_3 correlates positively with SiO_2 (Table 4.18) while CaO correlates positively with SiO_2 and Al_2O_3. MgO correlates positively with SiO_2, Al_2O_3, and CaO as shown in Table 4.18. Na_2O correlates positively with SiO_2, Al_2O_3, CaO and MgO. It is also observed that K_2O

has a positive correlation with SiO_2, Al_2O_3, and Na_2O but near zero correlation with CaO and MgO. Positive correlation among these elements indicate that their mode of delivery into the study area is similar. TiO_2 and MnO have near zero correlation with SiO_2, Al_2O_3, CaO, MgO and K_2O, which shows that their mode of delivery into the area was not the same. Fe_2O_3 correlates negatively with SiO_2, Al_2O_3, CaO, MgO and K_2O but positively with P_2O_5 (see Figure 4.82A – H). There is a weak correlation between Fe_2O_3 with TiO_2 and MnO (Figure 4.82F) which indicates their different mode of delivery into the study area.

MgO shows a positive correlation of R = 0.61 with CaO (Table 4.18 and 4.19) but shows negative correlation with Fe_2O_3 where R = -0.05. It also has weak correlation with Na_2O. Its correlation with other elements is null. This pattern suggests that most Ca and Mg are hosted by carbonate minerals in Mutomo – Ikutha area. The lack of positive correlation of carbonates with Fe_2O_3 implies that the carbonate component is entirely unrelated to the processes involved in supplying Fe_2O_3 to these rocks.

The relationships of these compounds (SiO_2, Al_2O_3, CaO, MgO, K_2O, Fe_2O_4, P_2O_5, TiO_2 and MnO) elements points to an overwhelming component of orthochemical iron. Considering that typical detrital material has low Fe concentrations, a likely source for the Fe is hydrothermal fluids whose source is magmatic.

P_2O_5 shows little or weak correlation with other elements apart from iron with R = 0.77(Table 4.18 and Figure 4.82H). Given the lack of correlation with Al, detrital P_2O_5 should only account for a minimal fraction of the total concentration. Furthermore, P_2O_5 correlates negatively with other enriched elements (SiO_2, and MnO), implying that it may not be having a similar origin with them. The only correlation that exists for phosphorus is a positive correlation with respect to Fe_2O_4 which indicates that both elements came in through the same delivery mechanism.

Table 4.17: Chemical analysis results of the samples collected along the ground magnetic profiles in the study area. Analyzed by Atomic absorption spectrophotometry (AAS) in wt. %

REF .No.	Long.	Lat.	SiO_2	Al_2O_3	CaO	MgO	Na_2O	K_2O	TiO_2	MnO	Fe_2O_3 T	P_2O_5	LOI	TOTAL	Lithology-Mineral/rock type
	(UTM)	(UTM)	Wt.%	Wt.%	Wt.%	Wt.%	Wt.%	Wt.%	Wt.%	Wt.%	Wt. %	Wt.%	Wt.%	Wt.%	
TA-0	408000	9770000	43	22.8	13	5	3.87	0.59	0.96	0.6	6.2	<0.05	3.71	99.73	Amphibolite
T1-1	409000	9770000	2.91	0.6	8.4	0.24	0.17	0.03	0.05	0.4	81.3	5.7	<0.05	99.8	Magnetite +Apt+Di
T1-2	408000	9769000	3.83	0.76	3.77	0.2	0.14	0.03	0.3	0.4	86.1	4.1	<0.05	99.63	Magnetite +Apt
T2-1	410000	9770000	6.97	1.47	0.99	0.19	0.17	0.03	0.18	0.4	88.3	1	<0.05	99.7	Magnetite
T2-2	409000	9769000	4.05	0.33	0.25	0.3	0.12	0.03	1.5	0.6	89	3	<0.05	99.18	Magnetite +Apt
T2-3	408020	9768020	1.72	0.67	5.22	0.27	0.14	0.02	<0.05	0.4	85	5.9	<0.05	99.34	Magnetite
T2-4	408000	9768000	4.78	0.11	0.6	0.47	0.11	0.03	1.7	0.6	90.7	0.5	<0.05	99.6	Magnetite +Apt
T3-1	411000	9770000	41	22.8	13	5	4.87	0.59	0.96	0.6	7.2	<0.05	3.71	99.73	Altered gneiss
T3-2	410000	9769000	6.21	1.52	0.5	0.23	0.24	0.04	0.46	0.4	89.6	0.2	<0.05	99.4	Magnetite

T = Total Fe

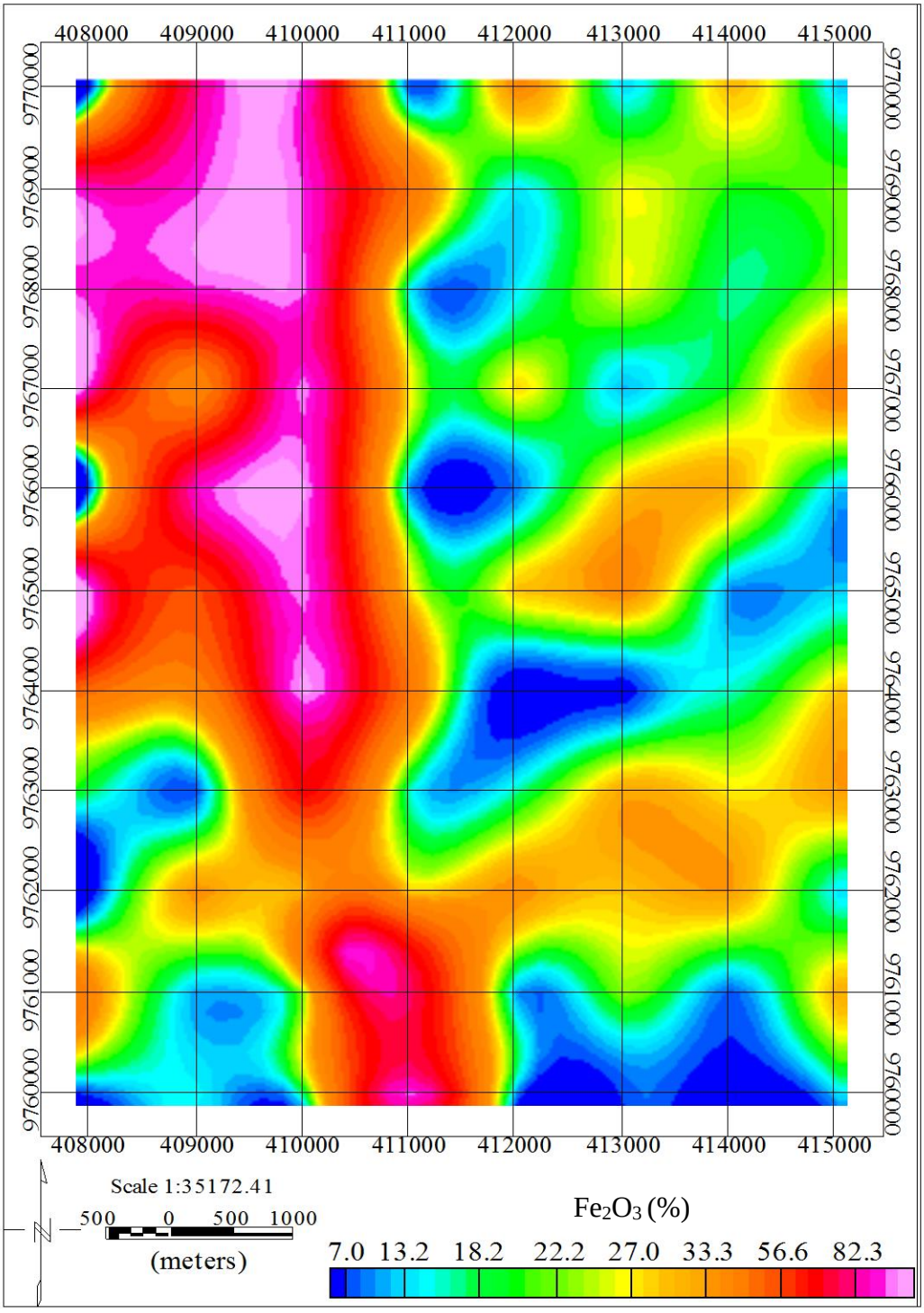

Figure 4.81: Geochemical intensity Map showing distribution of Fe_2O_3 in the study area. High concentration of Fe_2O_3 occurs on the western part of the area trending in the N – S direction.

Table 4.18: Pearson correlation and its graphical presentation of the elements from the iron ore host rocks.

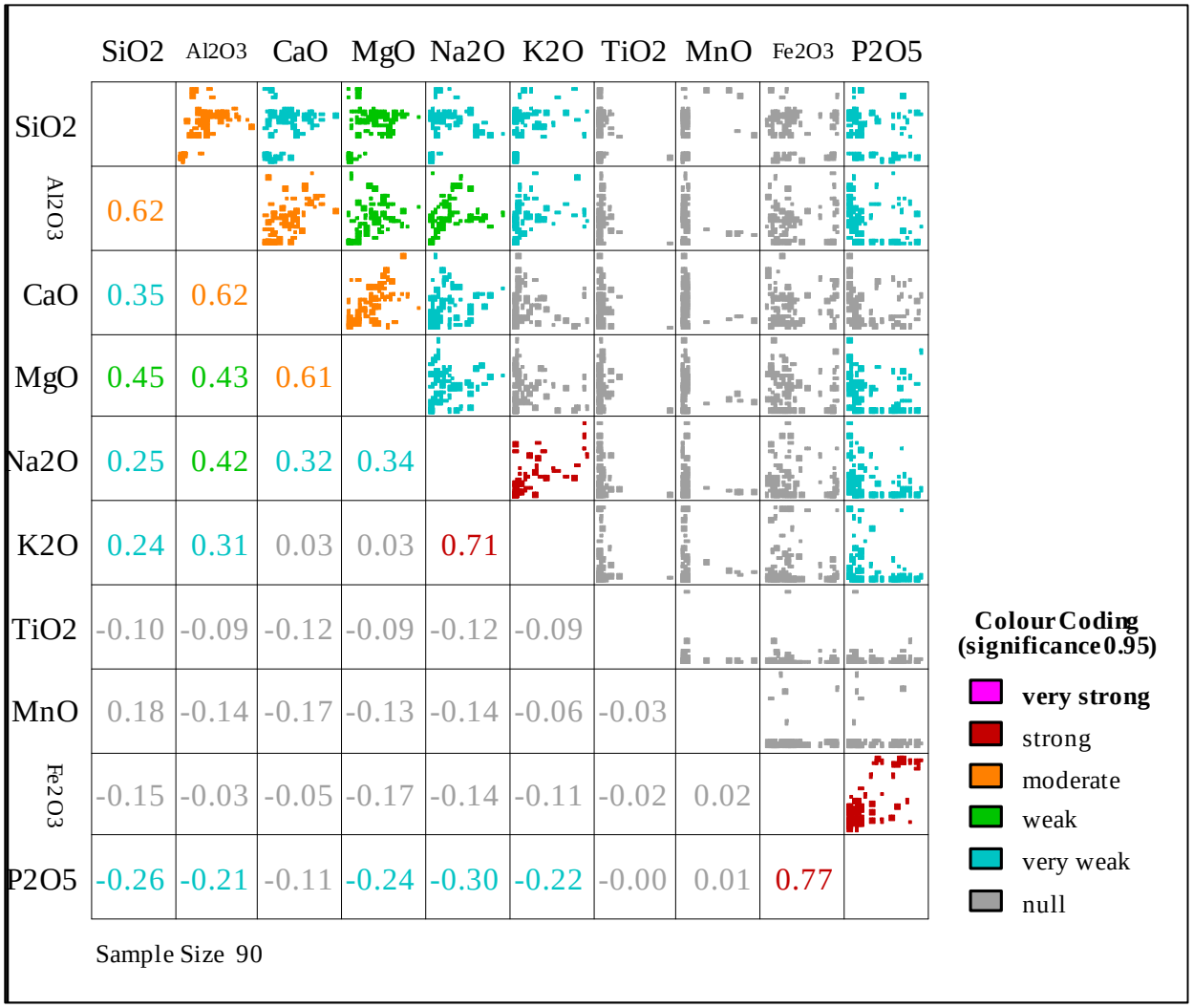

Table 4.19. Pearson correlation significance of the elements from the iron ore host rocks

		SiO2	Al2O3	CaO	MgO	Na2O	K2O	TiO2	MnO	Fe2O3	P2O5
SiO2	Pearson Correlation	1	.624**	.352**	.453**	.247*	.243*	-.104	.179	-.152	-.257*
	Sig. (2-tailed)	.	.000	.001	.000	.019	.021	.328	.092	.152	.015
	N	90	90	90	90	90	90	90	90	90	90
Al2O3	Pearson Correlation	.624**	1	.617**	.431**	.422**	.314**	-.088	-.144	-.031	-.211*
	Sig. (2-tailed)	.000	.	.000	.000	.000	.003	.408	.176	.769	.046
	N	90	90	90	90	90	90	90	90	90	90
CaO	Pearson Correlation	.352**	.617**	1	.608**	.316**	.032	-.120	-.166	-.048	-.110
	Sig. (2-tailed)	.001	.000	.	.000	.002	.767	.260	.118	.656	.301
	N	90	90	90	90	90	90	90	90	90	90
MgO	Pearson Correlation	.453**	.431**	.608**	1	.341**	.034	-.091	-.129	-.173	-.240*
	Sig. (2-tailed)	.000	.000	.000	.	.001	.752	.396	.224	.103	.023
	N	90	90	90	90	90	90	90	90	90	90
Na2O	Pearson Correlation	.247*	.422**	.316**	.341**	1	.711**	-.117	-.141	-.139	-.300**
	Sig. (2-tailed)	.019	.000	.002	.001	.	.000	.272	.184	.191	.004
	N	90	90	90	90	90	90	90	90	90	90
K2O	Pearson Correlation	.243*	.314**	.032	.034	.711**	1	-.085	-.062	-.109	-.220*
	Sig. (2-tailed)	.021	.003	.767	.752	.000	.	.423	.564	.304	.038
	N	90	90	90	90	90	90	90	90	90	90
TiO2	Pearson Correlation	-.104	-.088	-.120	-.091	-.117	-.085	1	-.027	-.016	-.002
	Sig. (2-tailed)	.328	.408	.260	.396	.272	.423	.	.803	.884	.983
	N	90	90	90	90	90	90	90	90	90	90
MnO	Pearson Correlation	.179	-.144	-.166	-.129	-.141	-.062	-.027	1	.022	.012
	Sig. (2-tailed)	.092	.176	.118	.224	.184	.564	.803	.	.838	.913
	N	90	90	90	90	90	90	90	90	90	90
Fe2O3	Pearson Correlation	-.152	-.031	-.048	-.173	-.139	-.109	-.016	.022	1	.768**
	Sig. (2-tailed)	.152	.769	.656	.103	.191	.304	.884	.838	.	.000
	N	90	90	90	90	90	90	90	90	90	90
P2O5	Pearson Correlation	-.257*	-.211*	-.110	-.240*	-.300**	-.220*	-.002	.012	.768**	1
	Sig. (2-tailed)	.015	.046	.301	.023	.004	.038	.983	.913	.000	.
	N	90	90	90	90	90	90	90	90	90	90

**. Correlation is significant at the 0.01 level (2-tailed).

*. Correlation is significant at the 0.05 level (2-tailed).

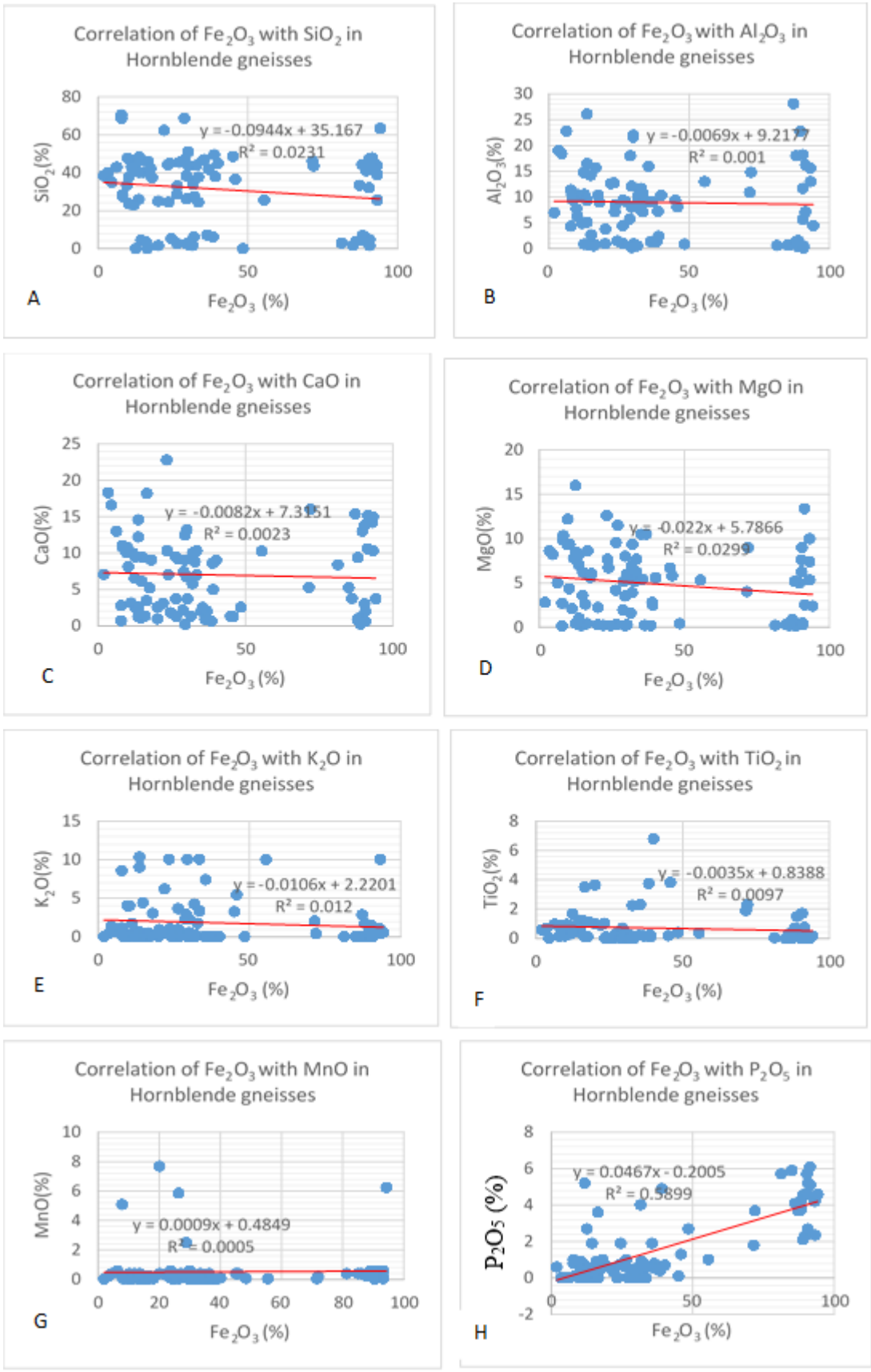

Figure 4.82: Correlation of Fe_2O_3 with SiO_2, Al_2O_3, CaO, MgO, K_2O, Fe_2O_4, P_2O_5, TiO_2 and MnO in the iron ore host rocks.

(b) Elemental association of iron (Fe) in Mutomo – Ikutha area and its correlation with other elements

A total of 180 iron ore samples were analysed using XRF and some of their results tabulated in Table 4.20 and appendix B. The analytical results show that other than Fe, the ore is composed of V, Ti, Mn, Cr, Co, Ni, Cu, Zn, Zr, Nb, Mo, Ag, Sn, Sb, W, and Pb. Pearson coefficient correlation was performed to determine the relationship of genesis among elements.

Negative correlation of Iron to V, Ti, Mn, Cr, Co, Ni, Cu, Zn, Zr, Nb, Mo, Ag, Sn, Sb, W, and Pb as tabulated in Table 4.21 indicates that the mode of their delivery into the ore was not the same. Or as the conditions favoured the formation of iron, the same condition did not favour, Vanadium, Titanium, Manganese, Chromium, Cobalt, Nickel, Copper, Zinc, Zirconium, Niobium, Molybdenum, Silver, Tin, Antimony, Tungsten, and lead. The formation of copper and chromite does not affect the formation of iron and hence are negatively correlated (Figure 4.83). Summary of the elemental correlation is tabulated in Table 4.21.

Iron and has a negative correlation with manganese. Manganese in its Mn^{2+} oxidation state is stable at higher oxidizing potentials than Fe (Glasby and Schulz, 1999) and thus this enrichment may occur either during late stages of iron formation deposition during the progression of an iron-rich plume or during deposition in shallower, more oxidizing environments. Alternatively, it may represent diagenetic mobilization of Mn, which has been documented in modern metalliferous deposits (Gurvich, 2006). This negative correlation indicates that iron deposit in the study area formed from hydrothermal mechanism which was independent of the mechanisms that led to the deposition of manganese and silica in the study area.

Table4.20: Analytical results of the magnetite ore from Mutomo – Ikutha area using x-ray fluorescence method. Elements expressed in weight percentage.

No.	Long. (UTM)	Lat. (UTM)	Ti Wt. %	V Wt. %	Cr Wt. %	Mn Wt. %	Fe Wt. %	Co Wt. %	Ni Wt. %	Cu Wt. %	Zn Wt. %	Zr Wt. %	Nb Wt. %	Mo Wt. %	Ag Wt. %	Sn Wt. %	Sb Wt. %	W Wt. %	Pb Wt. %	Iron Ore elements association
1	408391	9768300	0.698	0.354	0.241	2.447	88.197	0.889	0.845	2.826	< 0.03	< 0.03	< 0.03	1.295	< 0.03	< 0.03	< 0.03	0.661	<0.03	Fe+(Ti, Mn,Co,Ni,Cu,Mo, W)
2	408445	9768322	0.694	0.282	0.453	3.071	84.517	0.907	0.793	4.674	<0.03	<0.03	<0.03	1.857	<0.03	<0.03	<0.03	0.456	<0.03	Fe+(Ti, Mn,Co,Ni,Cu,Mo, W)
3	408486	9768324	0.554	0.323	0.291	3.225	86.295	0.811	0.736	3.502	<0.03	<0.03	<0.03	1.419	<0.03	<0.03	<0.03	0.681	<0.03	Fe+(Ti, Mn,Co,Ni,Cu,Mo, W)
4	408434	9768321	0.771	0.613	0.69	1.897	83.678	0.566	2.958	3.13	< 0.03	< 0.03	< 0.03	0.3	< 0.03	< 0.03	< 0.03	0.984	<0.03	Fe+(Ti,Cr, V,Mn,Co,Ni,Cu, W)
5	408583	9768317	0.679	0.685	0.603	2.285	83.841	0.697	2.901	2.952	<0.03	<0.03	<0.03	0.271	<0.03	<0.03	<0.03	0.995	<0.03	Fe+(Ti, CrV,Mn,Co,Ni,Cu, W)
6	408594	9768263	0.408	0.823	0.448	0.631	86.757	0.109	2.073	1.977	<0.03	<0.03	<0.03	0.146	<0.03	<0.03	<0.03	0.976	<0.03	Fe+(Ti,V,Mn,Ni,Cu, W)
7	408538	9768262	0.996	0.71	0.539	0.849	83.562	0.306	2.737	2.964	< 0.03	< 0.03	< 0.03	0.165	< 0.03	< 0.03	< 0.03	0.888	<0.03	Fe+(Ti,V,Cr,Mn,Ni,Cu, W)
8	408497	9768248	0.542	0.017	0.267	0.4	96.073	<0.03	0.988	0.02	<0.03	<0.03	<0.03	0.072	<0.03	<0.03	<0.03	0.589	<0.03	Fe+(Ti,V,Ni,Cu, W)
9	408447	9768232	0.101	0.26	1.103	3.354	79.641	0.928	4.278	5.524	<0.03	<0.03	<0.03	0.346	<0.03	<0.03	<0.03	<0.03	<0.03	Fe+(Ti,Mn,Cr,Co,V,Ni,Cu,)
10	408397	9768222	0.5	0.652	1.828	4.244	73.289	1.498	5.509	9.639	< 0.03	< 0.03	< 0.03	0.617	< 0.03	< 0.03	< 0.03	<0.03	<0.03	Fe+(Ti,Mn,Mo,Cr,Co,V,Ni,Cu,)
11	408422	9768174	0.82	0.972	1.323	3.175	78.045	1.095	5.291	7.358	<0.03	<0.03	<0.03	0.423	<0.03	<0.03	<0.03	<0.03	<0.03	Fe+(Ti,Mn,Cr,Co,V,Ni,Cu,)
12	408463	9768186	0.034	0.23	<0.03	3.724	69.556	2.509	6.748	4.769	<0.03	<0.03	0.446	1.286	<0.03	<0.03	<0.03	7.511	<0.03	Fe+(Ti,V,Mn,Co,Ni,Cu,Mo,W)
13	408509	9768197	0.656	0.754	2.114	3.478	73.213	1.216	5.772	9.973	< 0.03	< 0.03	<0.03	0.595	< 0.03	< 0.03	< 0.03	<0.03	<0.03	Fe+(Ti,Mn,Mo,Cr,Co,Fe,V,Ni,Cu,)
14	408562	9768209	0.45	0.827	<0.03	6.341	73.266	2.428	3.584	4.71	<0.03	<0.03	0.359	0.774	<0.03	<0.03	<0.03	5.578	<0.03	Fe+(Ti,V,Mn,Co,Ni,Cu,Mo,W)
15	408611	9768209	0.666	0.03	1.172	5.069	77.66	1.393	4.358	6.369	<0.03	<0.03	<0.03	0.246	<0.03	<0.03	<0.03	<0.03	<0.03	Fe+(Ti,V,Mn,Cr,Ni,Cu)
16	408632	9768166	0.492	0.596	0.49	2.337	83.091	0.444	2.597	2.205	< 0.03	<0.03	<0.03	0.076	< 0.03	< 0.03	< 0.03	0.804	<0.03	Fe+(Ti,V<Mn,Ni,Cu,W)
17	408577	9768161	0.111	0.602	0.549	2.503	80.228	0.681	2.878	2.856	<0.03	<0.03	<0.03	0.116	<0.03	<0.03	<0.03	0.843	<0.03	Fe+(Ti,V,Cr,Mn,Co,Ni,Cu,W)
18	408531	9768135	0.759	0.463	0.851	4.143	77.839	0.899	3.656	4.658	<0.03	<0.03	<0.03	0.144	<0.03	<0.03	<0.03	0.063	<0.03	Fe+(Ti,V,Cr,Mn,Co,Ni,Cu)
19	408482	9768119	0.757	0.011	0.962	3.201	82.818	0.349	2.727	3.041	< 0.03	<0.03	<0.03	0.013	< 0.03	< 0.03	< 0.03	0.733	<0.03	Fe+(Ti,V,Cr,Mn,Ni,Cu,W)
20	408440	9768095	0.242	0.906	<0.03	3.999	67.424	2.824	5.987	3.163	<0.03	<0.03	0.5	1.717	<0.03	<0.03	<0.03	9.856	<0.03	Fe+(Ti,V,Mn,Co,Ni,Cu,Nb,Mo,W)
21	408454	9768050	0.866	0.19	<0.03	3.622	67.428	3.328	4.481	2.627	<0.03	<0.03	0.466	2.146	<0.03	<0.03	<0.03	9.358	<0.03	Fe+(Ti,V,Mn,Co,Ni,Cu,Mo,W)
22	408496	9768077	0.651	0.304	<0.03	3.939	66.959	3.35	5.807	2.521	< 0.03	<0.03	0.479	1.704	< 0.03	< 0.03	< 0.03	10.483	<0.03	Fe+(Ti,V,Mn,Fe,Co,Ni,Cu,Mo,W)
23	408449	9768091	0.041	0.791	<0.03	3.915	60.789	3.563	5.847	3.556	<0.03	<0.03	0.535	1.957	<0.03	<0.03	<0.03	9.19	<0.03	Fe+(Ti,V,Mn,Co,Ni,Cu,Nb,Mo,W)
24	408600	9768111	0.571	0.625	<0.03	3.963	61.603	4.721	6.007	0.958	<0.03	<0.03	0.372	2.106	<0.03	<0.03	<0.03	10.036	<0.03	Fe+(Ti,V,Mn,Co,Ni,Cu,Mo,W)

Table 4.21: Pearson correlation and its graphical presentation of the elements from Magnetite ore in Mutomo – Ikutha area

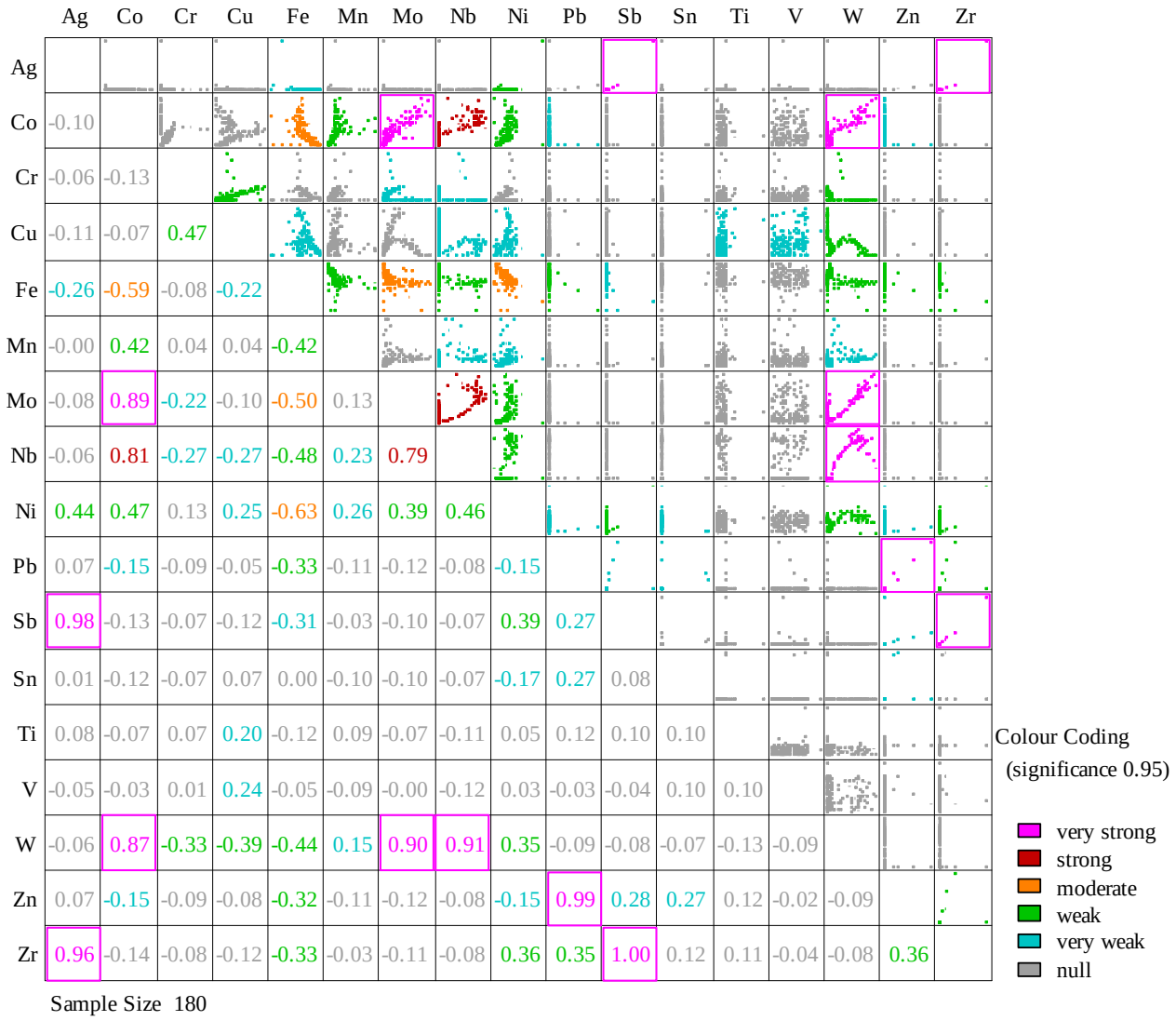

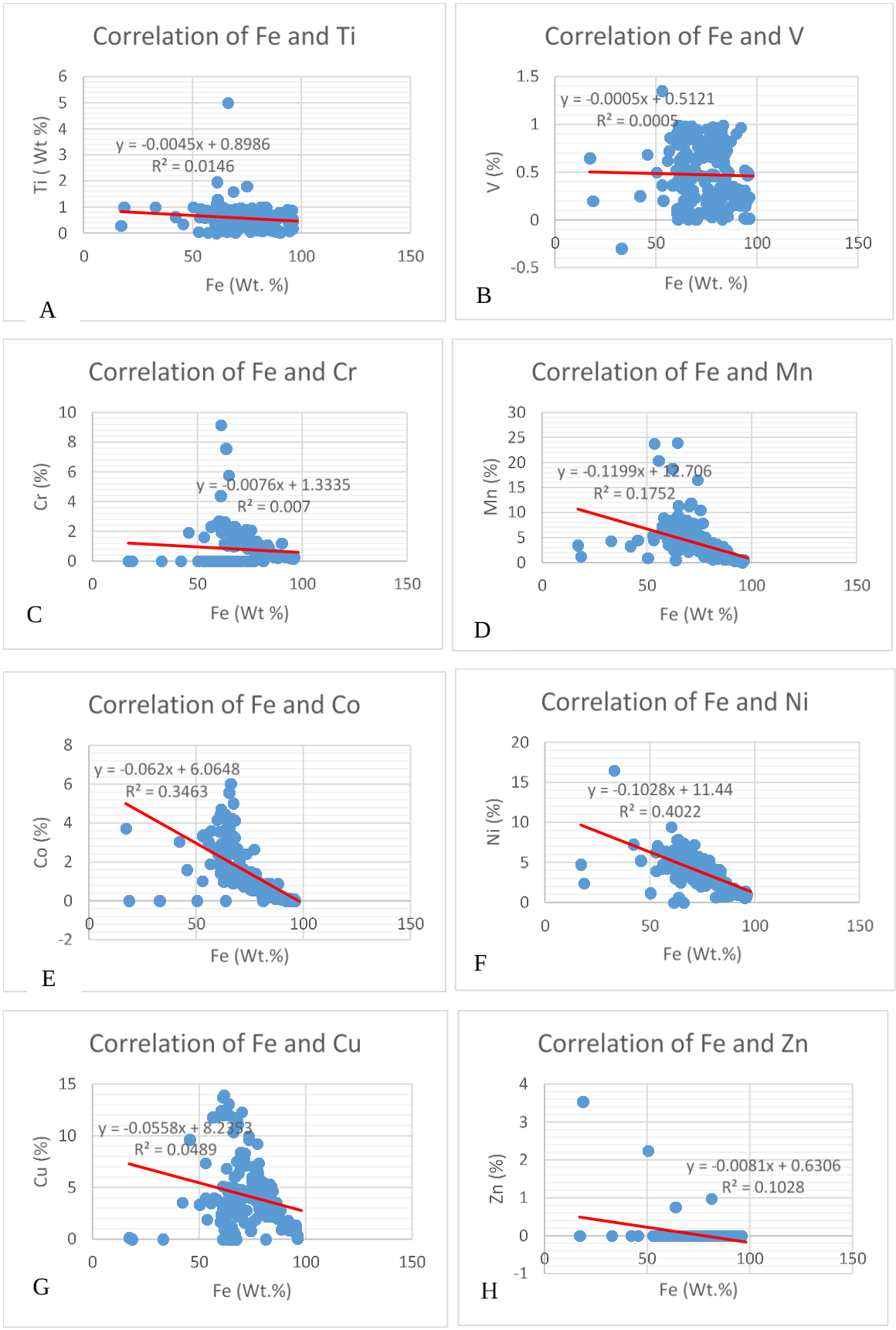

Figure 4.83: Correlation of Fe with V, Ti, Mn, Cr, Co, Ni, Cu, Zn, Zr, Nb, Mo, Ag, Sn, Sb, W, and Pb in Magnetite Ore. (This figure continues on the next page)

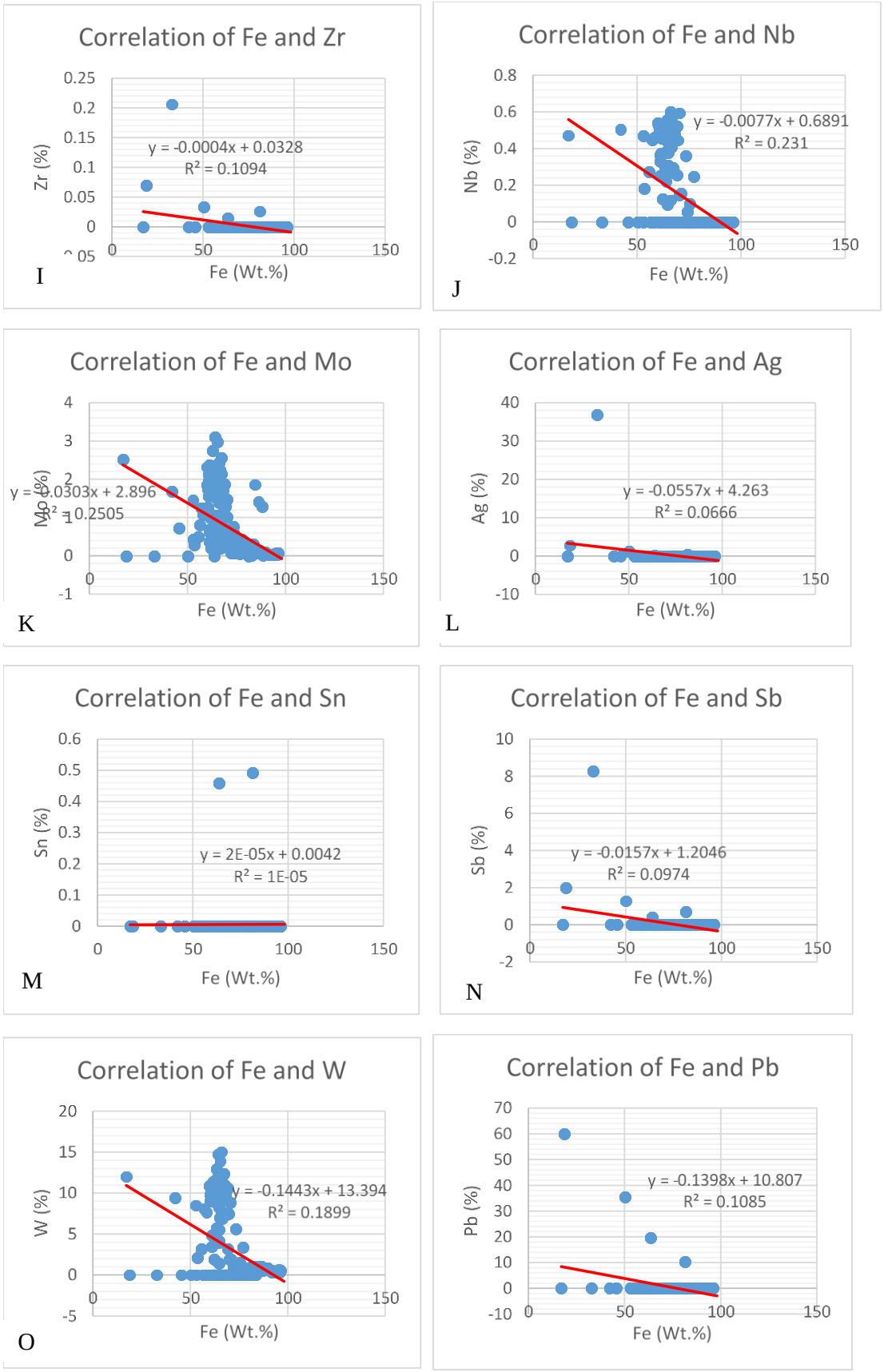

Figure 4.83: Correlation of Fe with V, Ti, Mn, Cr, Co, Ni, Cu, Zn, Zr, Nb, Mo, Ag, Sn, Sb, W, and Pb in Magnetite Ore.

4.5.2. Classification of the Mutomo – Ikutha rocks based on petrochemistry.

- ***Based on the protolith model***

The gneisses can be conveniently separated into two compositional groups. The groups are basic gneisses (SiO_2 = 48-50%) and intermediate to felsic gneisses (SiO_2 = 57-70%). In order to determine whether the protolith of the gneisses were igneous or sedimentary, the discriminatory function *(DF)* of Shaw (1972) was applied. The function is given by the relation:

$DF = 1.44 - 0.21SiO_2 - 0.32Fe_2O_3$ (total Fe) $- 0.98MgO + 0.55CaO + 1.46Na_2O + 0.54K_2O$

The equation is applicable to rocks with MgO < 6% and SiO_2 < 90%. In general positive *DF* values suggest an igneous parentage and negative values are associated with sedimentary precursors. The negative DF values for samples imply sedimentary parentage for majority of the rocks which was the case with the gneisses of Mutomo – Ikutha area (discussed in section 4.1.1. of this thesis and exemplified by Table 4.22).

Table 4.22: Characterization of metamorphic rocks of Mutomo – Ikutha area based on protolith model. The Negative DF values indicate the rocks are of sedimentary origin.

	SiO_2	Al_2O_3	CaO	MgO	Na_2O	K_2O	TiO_2	MnO	Fe_2O_3	LOI	DF
AWK1	72.31	13.16	1.11	0.31	2.92	7.8	ND	0.02	0.61	0.27	-23.1346
AWK2	70.53	15.22	1	0.31	3.62	8.2	ND	0.01	0.76	0.07	-23.9383
AWK3	67	16.97	1.48	0.68	4.01	6.5	0.28	0.09	1.84	0.06	-23.475
AWK4	42	12.27	11.8	5.61	2.23	0.55	2.87	0.3	20.2	1.09	-22.9206
AWK4A	41	13.34	12.3	5.68	2.4	0.56	2.65	0.2	20.8	0.28	-23.3078
AWK5	66.3	8.47	0.6	0.98	0.08	0.12	ND	3.3	18.1	0	-13.955
AWK6	73.59	14.86	0.56	0.35	3.2	4.2	ND	0.03	2.49	0.31	-21.6049

- ***Based on the tectonic model***

Tectonic model has five suites in which rocks can be classified (Figure 4.81). These suites include;

- Mid oceanic ridge basalt (MORB)
- Spreading center island
- Island arc and active continental margins
- Ocean island
- Continental

Most of the Meta basalts of Mutomo – Ikutha area plot in the ocean island and in the mid oceanic ridge (MORB) as shown by Figure 4.84.

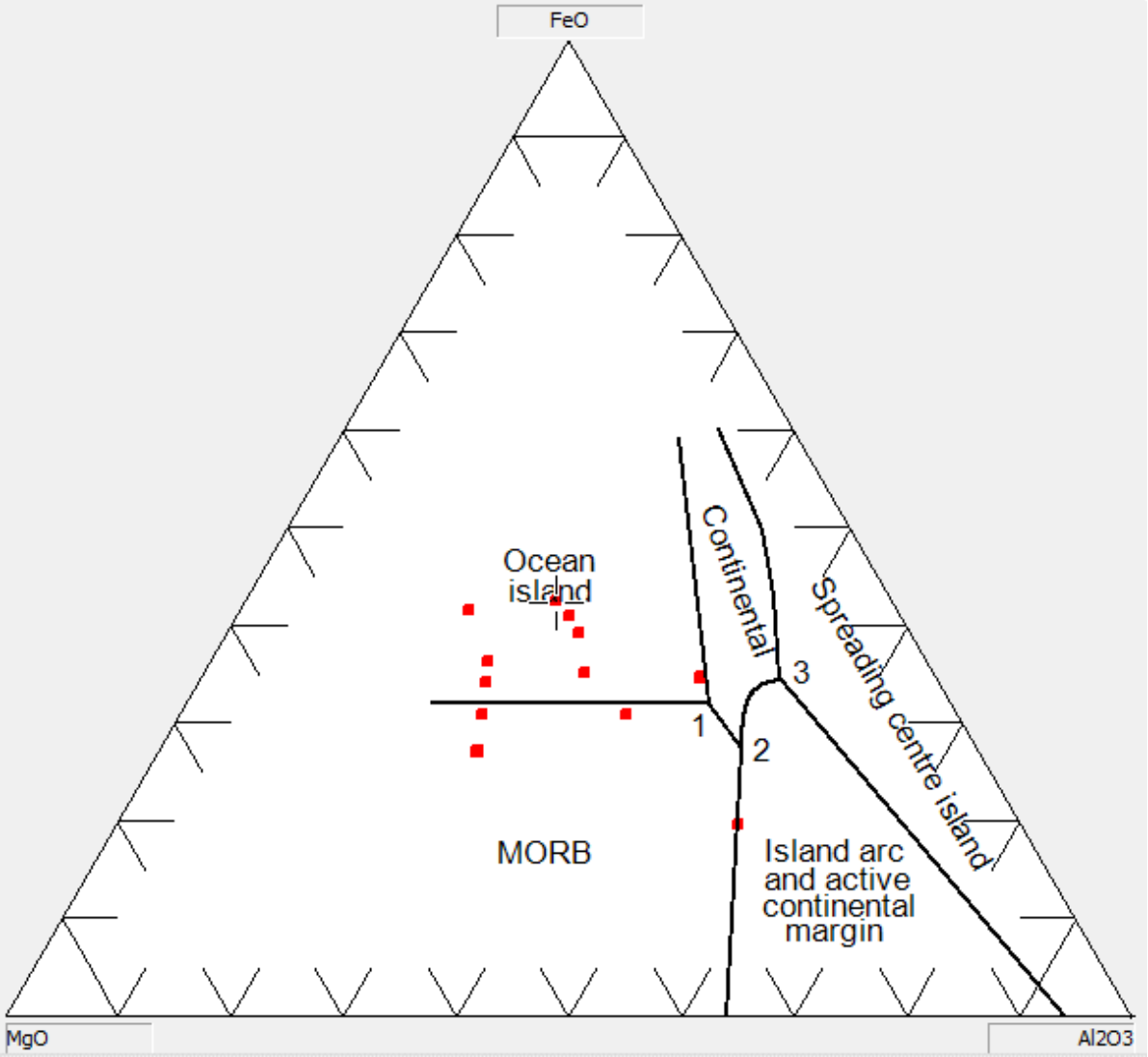

Figure 4.84: Al_2O_3 - FeO – MgO Ternary diagram of Meta basalts. Most of the Metabasalts plot at the Ocean Island and MORB suite. Red box represent 12 readings of the analysis Metabasalts.

4.5.3. The chemistry of mafic rocks of Mutomo – Ikutha area

I. Meta-basalts

Mutomo – Ikutha area has been petrographically identified to be composed of highly deformed pillow basalts. These pillow basalts have been affected by metamorphism and also undergone deformation (Figure 4.85). The meta-basalts were analyzed using AAS (atomic absorption spectrophotometer) and part of the results are as indicated in Table 4.23.

Table 4.23: Chemical composition (wt. %) of Meta – Basalt

Sample #	SiO_2	TiO_2	Al_2O_3	Fe_2O_3	MnO	MgO	CaO	Na_2O	K_2O	P_2O_5	H_2O+	TOTAL
B1	50.38	1.15	17.65	8.58	0.15	9.78	4.05	1.95	0.25	0.05	5.69	99.68
B2	49.58	1.01	17.25	8.35	0.17	9.51	6.46	1.85	0.03	0.04	5.35	99.6
B3	49.91	1.7	14.66	7.56	0.19	6.35	10.37	2.29	0.15	0.1	5.75	99.03
B4	49.65	0.99	7.14	8.2	0.26	13.4	10.6	1.15	0.25	0.3	7.3	99.24
B5	47.6	1.13	7.75	9.51	0.25	12.2	10.8	1.28	0.3	0.2	8.2	99.22
B6	47.7	0.61	16.5	8.14	0.17	8.2	12.6	2.12	0.64	0.5	2.1	99.28
B7	47.9	0.76	16.2	13.2	0.27	2.54	9.6	2.59	0.32	0.5	5.3	99.18
B8	51	0.67	21.6	7.9	0.6	9.8	3.73	1.8	0.04	0.3	2.1	99.54
B9	47.6	1.13	7.75	9.9	0.25	12.2	10.8	1.28	0.3	0.1	7.9	99.21
B10	50.3	0.62	15.6	13.6	0.2	7.4	5.56	2.19	0.38	0.4	2.9	99.15
B11	49.6	1.13	7.75	8.26	0.25	12.2	10.8	1.28	0.3	0.2	7.8	99.57
B12	51.5	0.62	15.6	13.6	0.2	7.4	5.7	2.19	0.38	0.4	2.4	99.99

The analytical data was used to plot classification diagrams according to; TAS-Middlemost, 1994; TAS – le Bas (1986); Jensen Cation (1976); Mullen, 1983; Pearce et.al (1977) and AFM. The sample results clustered in the basalt regions in all the diagrams (Figures 4.86 and 4.87). Figure 4.83 showed that the mafic rocks plotted were basaltic in nature. Figure 4.84 indicate that the rocks belong to Island Arc Tholeiite and mid oceanic ridge.

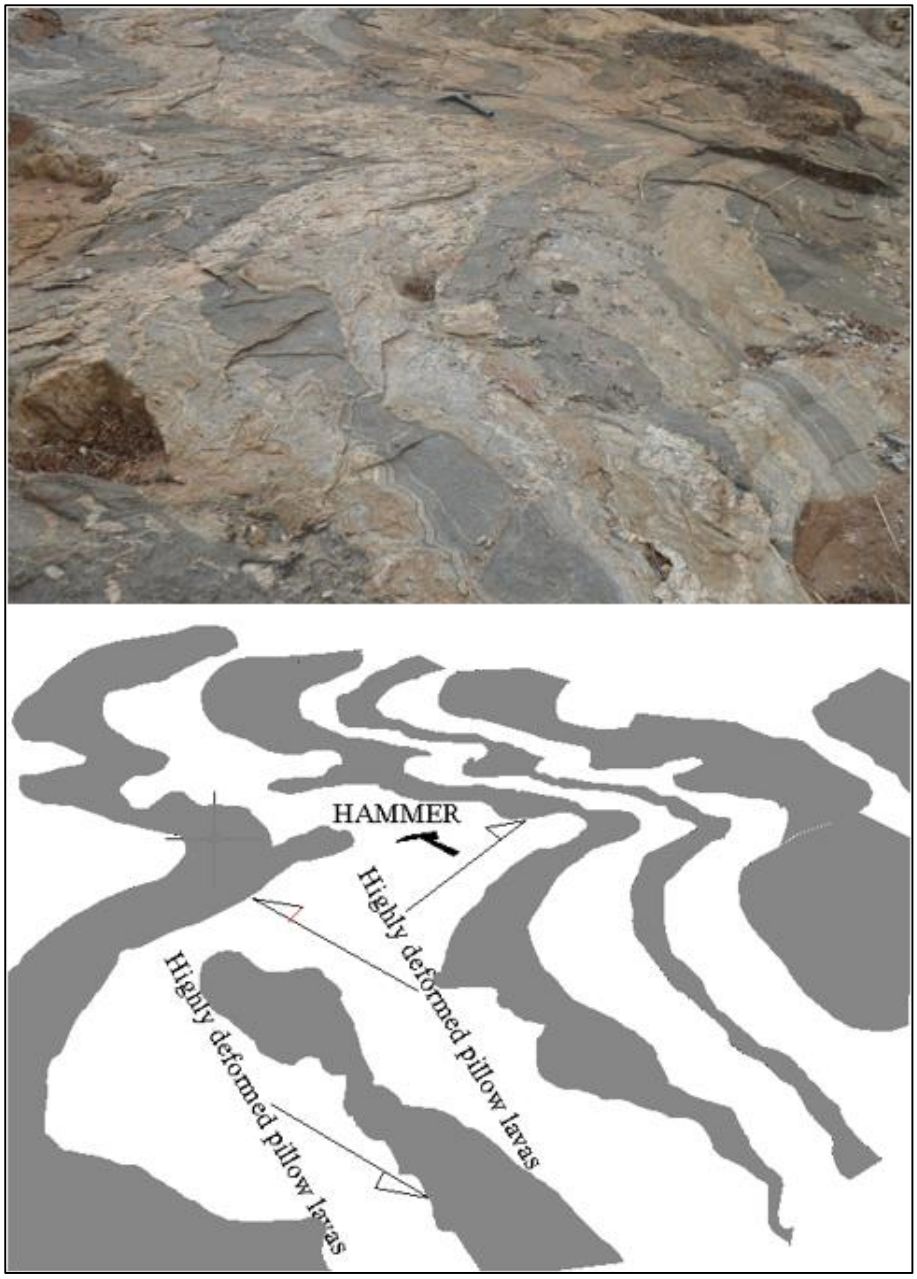

Figure 4.85: Metamorphosed pillow basalts which have undergone intense tectonic deformation on the eastern part of Mutomo town. The mafic (pillow lavas) have undergone progressive metamorphism, ductile flowage and folding. These pillow lavas are hosted in the gneissses in Mutomo – Ikutha area

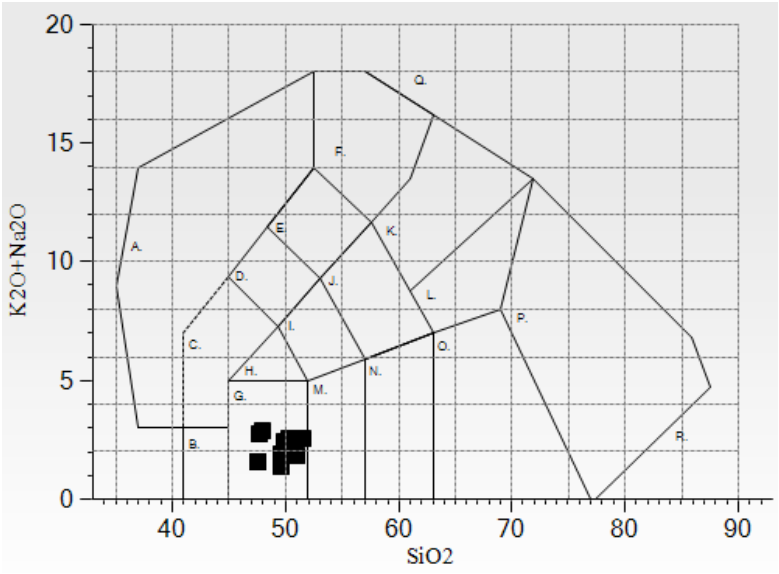

Figure 4.86: Classification of the Metabasalts of Mutomo – Ikutha using Total alkali silica diagram after Middlemost (1994) for volcanic rocks. ■ = Metabasalt, they have plotted in G.

A = Foidite; B = Picrobasalt; C = Basanite (Olivine > 10%), Tephrite (Olivine < 10%); D = Phonotephrite; E = Tephriphonolite; F = Phonolite, G = Basalt; H = Trachybasalt; I = Basaltic Trachyandesite; J = Trachyandesite; K = Trachyte (Quartz < 20%); L = Trachydacite; M = Basaltic Andesite; N = Andesite; O = Dacite; P = Rhyolite; Q = Sodalitite, Nephelinolith, Leucitolith; R = Silexite

Figure 4.84: Classification of the Mutomo – Ikutha area Metabasalts using Total alkali silica diagram after le Bas et al (1986). ■ = Metabasalt plots in G.
A = Foidite; B = Picrobasalt; C = Basanite (Olivine > 10%), Tephrite (Olivine < 10%); D = Phonotephrite; E = Tephriphonolite**;** F = Phonolite; G = Basalt; H = Trachybasalt; I = Basaltic Trachyandesite; J = Trachyandesite; K = Trachyte (Quartz < 20%), Trachydacite (Quartz > 20%); L = Basaltic Andesite; M = Andesite; N = Dacite; O = Rhyolite

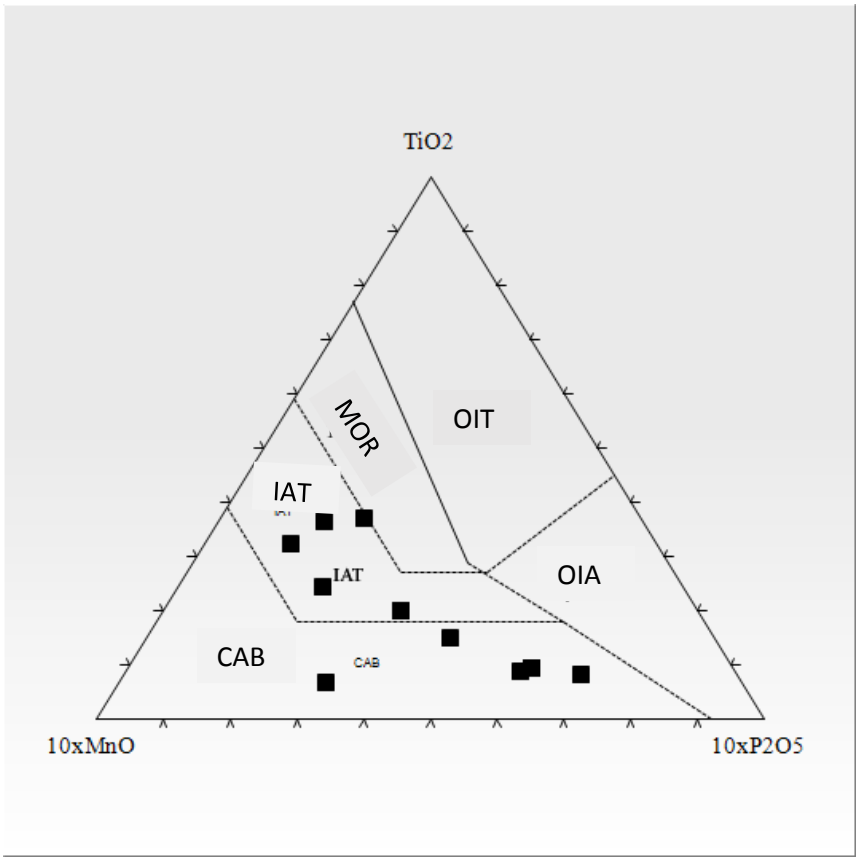

Figure 4.87: Classification of Mutomo – Ikutha Metabasalts using TiO_2 – (10XMnO) – ($10XP_2O_5$) ternary diagram after Mullen (1983). ■ = Metabasalt.

IAT = Island Arc Tholeiite, MORB = Mid Ocean Ridge Basalt, OIT = Ocean Island Tholeiite, CAB = Calc Alkaline Basalt, OIA = Ocean Island Alkali Basalt

II. Meta-gabbro

The mafic rocks that cut across other rock units (Figure 4.88) were analyzed and their results tabulated in Table 4.24. The analysis data was plotted on Total alkali – silica diagram for Plutonic, Middlemost diagram (Figure 4.89) and found to plot in the Gabbroic section.

Table 4.24: Chemical analysis (wt. %) results for Gabbroic samples.

Sample #	SiO_2	TiO_2	Al_2O_3	Fe_2O_3	MnO	MgO	CaO	Na_2O	K_2O	P_2O_5	H_2O+	TOTAL
G1	45.91	0.25	15.57	10.8	0.23	9.07	9.21	2.5	3.51	0.15	2.5	99.7
G2	46	0.15	16.07	9.56	0.47	8.86	9.54	2.1	3.55	0.05	3.15	99.5
G3	45.91	0.15	15.27	9.28	0.95	8.16	9.87	2.3	3.25	0.05	1.42	96.61
G4	46.2	1.6	17.8	9.68	1.02	8.42	7.24	2.1	3.24	0.01	2.25	99.56
G5	45.97	1.13	11.75	8.26	0.25	12.2	9.8	2.28	3.22	0.2	4.8	99.86
G6	47.01	0.62	12.6	13.6	0.2	7.4	9.2	2.19	3.23	0.4	3.2	99.65

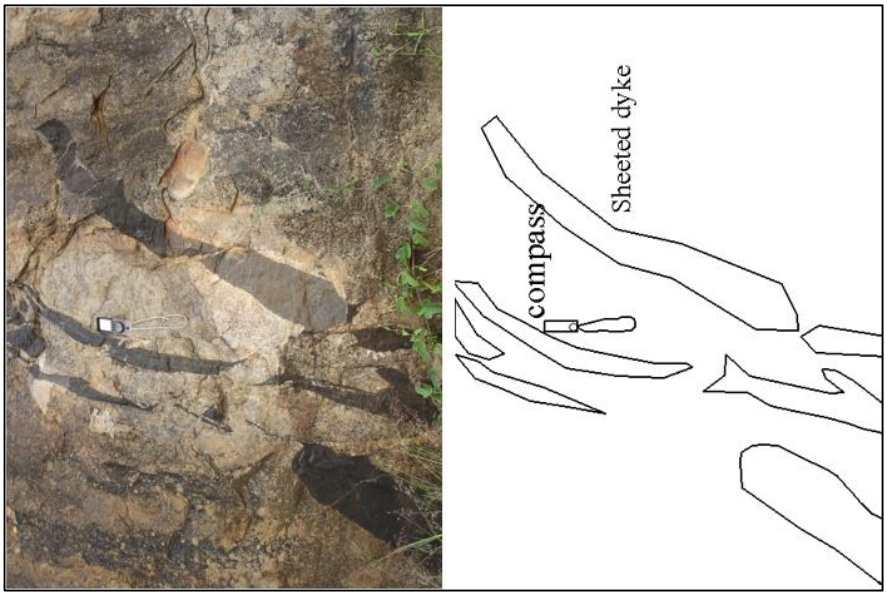

Figure 4.88: Sheeted dykes near Mutomo town at way point 377

(Coordinates 412810/9795302).

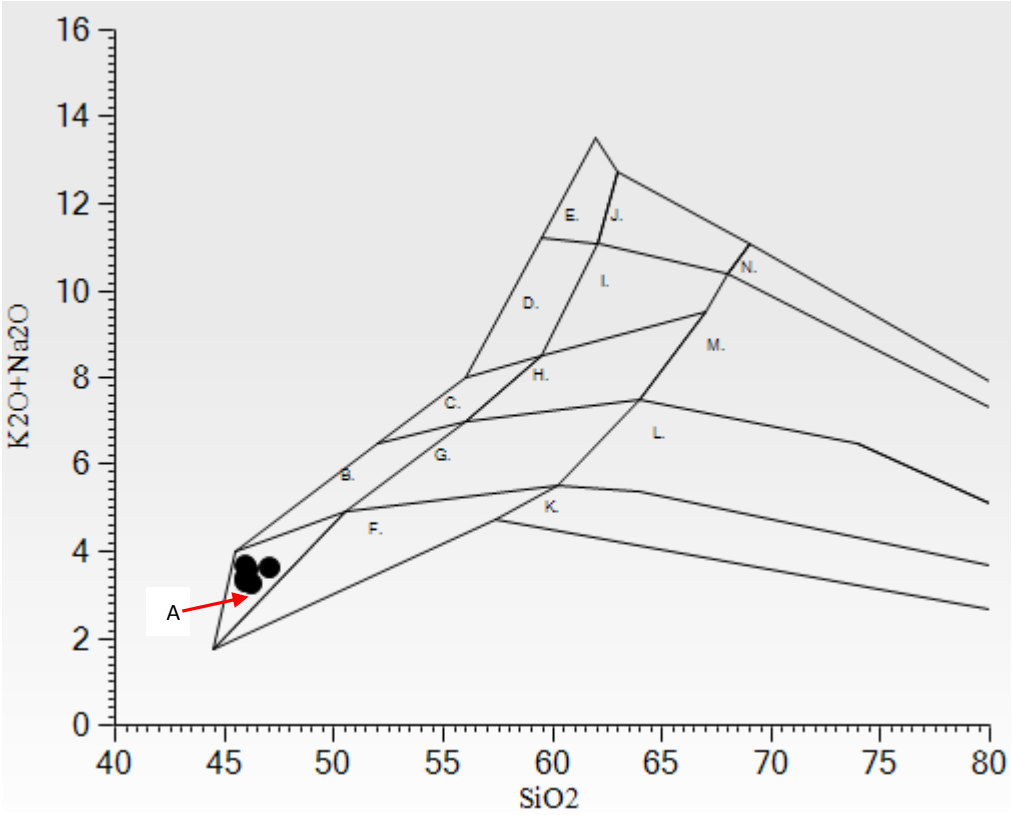

Figure 4.89: Classification of Mutomo Ikutha Meta-gabbro using Total alkali silica diagram after Middlemost (1994) for plutonic rocks. ● = Meta-gabbro.
A = Gabbro, B = Monzodiorite, C = Monzonite, D = Syenite, E = Alkali Feldspar Syenite F = Quartz Diorite, G = Quartz Monzodiorite, H = Quartz Monzonite, I =Quartz Syenite J = Alkali Felds. Qtz. Syenite, K = Tonalite, L = Granodiorite, M = Granite
N = Alkali Feldspar Granite

4.5.4 Discussion on petrochemistry, mineral geochemistry and ore genesis

(i) Mutomo – Ikutha Iron ore mineralization and classification

Mutomo – Ikutha area contains an iron deposit that is controlled by structures, stratigraphy and metamorphism. The analyses show that this deposit is of magnetite variety having between 48 – 93 % Fe_2O_3, 0.2 -5.9 % P_2O_5, 0.05 – 1.9 % TiO_2 and 0.007 % - 1.3 % V resembling the Apatite – Iron ores of Kiruna type. Iron ore in Mutomo – Ikutha area occur inform of veins, dikes, sills, and pod forms (see ground magnetic results). It is also structurally controlled by shear zone and hosted in hornblende gneiss as observed from the results of satellite imagery interpretation under remote sensing section.

Magnetite whole ore geochemistry display a range of composition in terms of trace element content that can be related to the mineral deposit type from which they formed (Loberg and Horndahl, 1983; Beaudoin *et al*., 2007). Discriminant diagrams such as V versus Ti or (Ni+Ca)/(Cr+Mn) versus Ti/V are useful tools to distinguish iron oxides formed in IOCG deposits from those in Kiruna-type, BIF, and orthomagmatic or titaniferous iron ore deposits (Beaudoin *et al*., 2007). Similar diagrams were used in Bafiq district, central Iran to discriminate different Iron ores as indicated in figure 4.90 (Torab, 2008).
The V verses Ti diagram was used to characterize the Mutomo – Ikutha iron ore deposit. The Mutomo – Ikutha iron ores have low Ti (5745 ppm), low V (4768 ppm) and low Cr (7844 ppm), Ni (40644 ppm) and Mn content (40315 ppm) as exemplified by appendix B. Discriminant diagram such as V versus Ti was adopted to characterise the deposit according to the objective of this research. When this trace elements were plotted on discriminant diagrams, they plotted into Kiruna type which excluded them from magmatic titanomagnetite and BIF deposits (Figure 4.91).

Correlation of Fe_2O_3 with Al_2O_3, SiO_2, CaO, Na_2O and K_2O, in rocks hosting Iron ore is negative but correlates positively with P_2O_5. The negative correlation shows that Iron ore and phosphorus in the project area was not related to the formation of the host rocks themselves. The material that formed host rocks originated from clastic materials while Fe_2O_3 came from hydrothermal/ magmatic source.

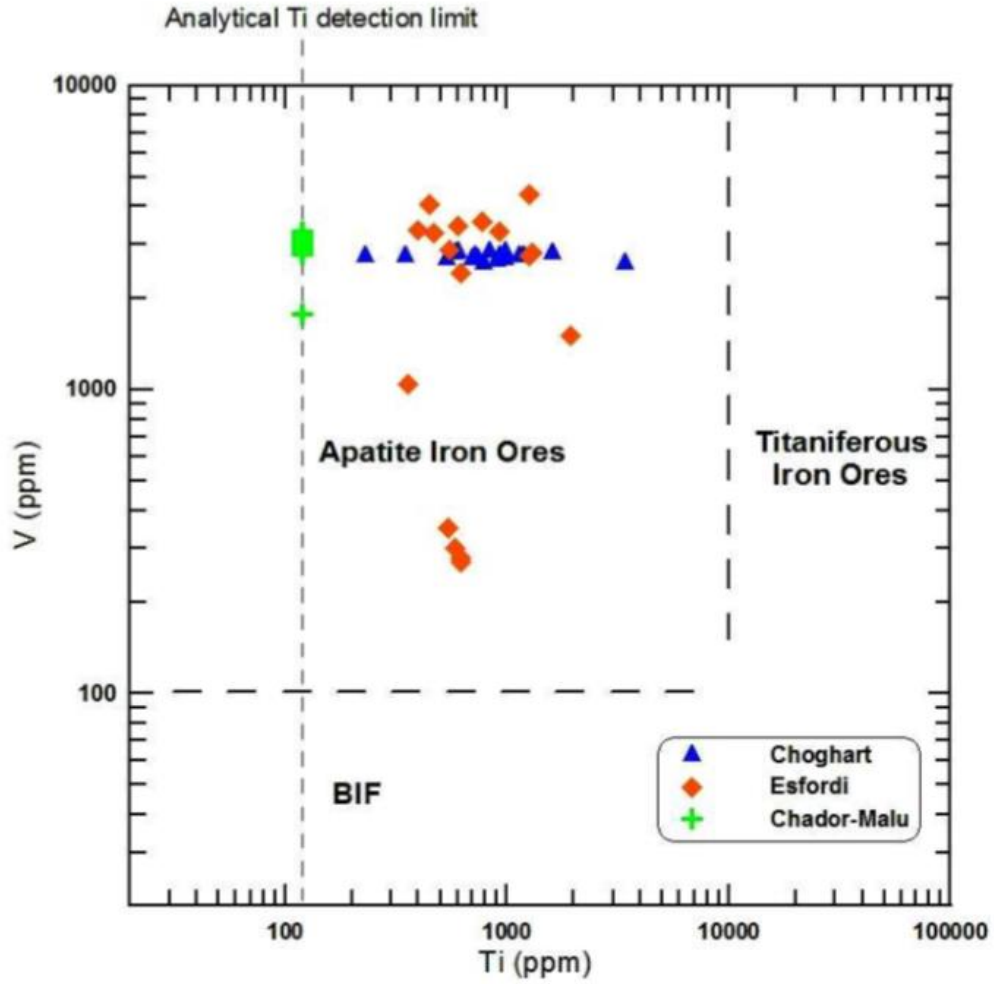

Figure 4.90: Magnetite composition in the Ti versus V discriminant diagram. Reference fields according to Beaudoin *et al*. (2007) and modified by Torab (2008) for magnetite deposit of Bafq mining district in central Iran.

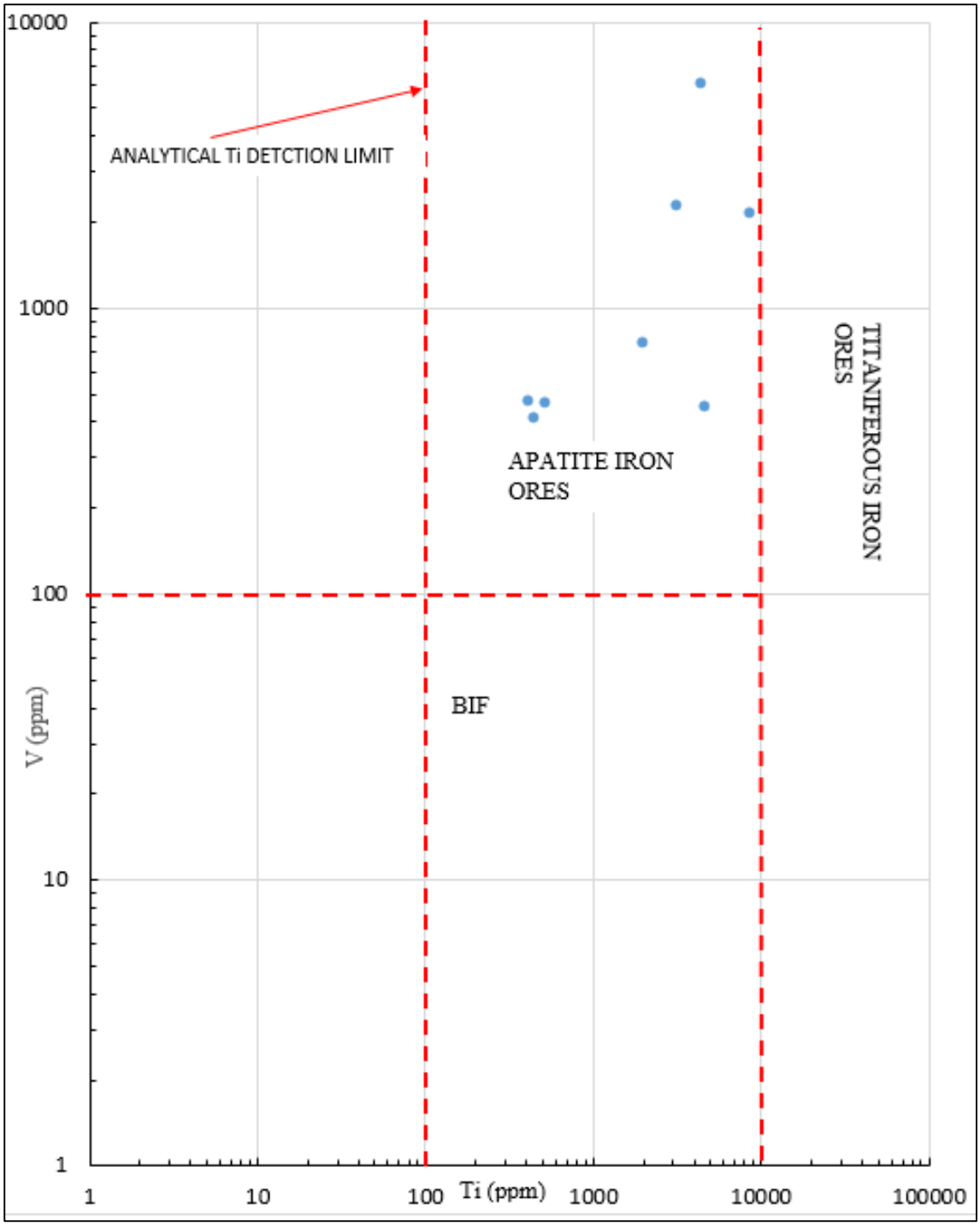

Figure 4.91: Mutomo - Ikutha Magnetite composition in the Ti versus V discriminant diagram. Reference fields according to Loberg and Horndahl (1983).

(ii) Apatite-iron ores of Kiruna type characteristics

Geijer (1931) defined the "Kiruna type" iron ores as "all those deposits that are, in their geological features, closely comparable to those at Kiruna". Hitzman *et al*. (1992) later included apatite-iron ores as a "subgroup" of IOCG (Iron ore – copper ± Gold) deposits. The focus has in the last decade been on the El Laco deposit in Chile since it maybe best preserved magnetite-apatite ore of Kiruna type (Henríquez *et al*., 2003; Henríquez and Nyström, 1998; Naslund *et al*., 2002; Rhodes and Oreskes, 1999; Rhodes *et al*., 1999; Sillitoe and Burrows, 2002).

Kiruna type apatite – iron ore deposits are characterized by the following;

1. The age of apatite-iron ores varies from Paleoproterozoic (Kiirunavaara) to Pliocene (El Laco). No Archaean examples are known (Frietsch and Perdahl, 1995).

2. The emplacement of apatite-iron ores is related to regional fault zones (Frietsch and Perdahl, 1995) either in intracratonic settings (e.g. Kiirunavaara) or subduction zones (e.g. El Laco).

3. The host rock comprises calc-alkaline to alkaline volcanic rocks (andesite to rhyolite) (e.g. Frietsch and Perdahl, 1995; Geijer, 1931; Rhodes *et al*., 1999; Treloar and Colley, 1996).

4. The morphology of the ore bodies includes disk-like, concordant bodies, vein systems, and impregnations (Frietsch and Perdahl, 1995). At the El Laco deposit the ore also occur as lava flows and pyroclastic material (e.g. Naslund *et al*., 2000).

5. The ore mineralogy is simple with magnetite and/or hematite occurring as ore minerals (Martinsson and Wanhainen, 2004). The amount of gangue minerals is low but F-rich apatite, amphibole or pyroxene often occur (Geijer, 1931).

6. Alterations are generally not as prominent a feature in apatite-iron ores as in for example porphyry copper and IOCG systems. Where alterations occur, they generally include silicification, sericitisation, albitisation, and epidotisation, with actinolite, scapolite, tourmaline, biotite, and carbonates as less common constituents (Martinsson and Wanhainen, 2004; Treloar and Colley, 1996).

(iii) Genesis of apatite-iron ores of Kiruna type model and its application to Mutomo – Ikutha iron ore deposit.

The genesis of apatite-iron ores of Kiruna iron ore deposit type has been subject of discussion for many years, with the main focus on magmatic or hydrothermal origins. The magmatic model explains the formation of this type of deposit to have formed from high temperature, volatile-rich iron oxide melts, and is mainly based on textural magmatic features like columnar and dendritic magnetite, igneous structures, and the relation between the ores and their host rocks (Henríquez *et al*., 2003; Henríquez and Nyström, 1998; Naslund *et al*., 2002; Nyström and Henríquez, 1994; Park, 1961). Chemical data from magnetite and apatite is also used to support this magmatic model (Frietsch and Perdahl, 1995; Naslund *et al*., 2002; Nyström and Henríquez, 1994). Broman *et al*. (1999) interpreted fluid inclusion data from pyroxene and apatite at El Laco to have formed from a late-magmatic remnant fluid gradually becoming lower in temperature and salinity.

The hydrothermal model, on the other hand, favors metasomatic replacement from Fe-rich hydrothermal hypersaline fluids as a model for the formation of these types of deposits (Hildebrand, 1986; Hitzman *et al*., 1992; Rhodes *et al*., 1999; Sillitoe and Burrows, 2002). Based on theoretical reasons the existence of iron oxide magmas was questioned by Hildebrand (1986), whereas Rhodes and Oreskes (1999) used oxygen isotopes as evidence to support the replacement theory. Barton and Johnson (1996) proposed a model for the formation of Fe-oxide deposits by hydrothermal processes involving evaporitic ligand sources. Although apatite-iron ores have common characteristics, there is a large variation in alteration and mineralization style between deposits. Many authors have concluded that all deposits of such type didn't form by one process. Magmatic and hydrothermal mechanisms were both involved in their formation (Barton and Johnson, 1996; Martinsson, 2004).

The two model are applied here to explain the genesis of the Mutomo – Ikutha iron ore. The magmatic and hydrothermal mechanisms were involved in the formation of Mutomo – Ikutha iron ore. Mineral chemistry discriminant diagrams justify different modes of elemental delivery into the project study area. A clear spatial relationship has been observed between some apatite iron and copper-gold deposits indicating a possible genetic link between them. It has important implications for the ore genetic model of apatite-iron and copper (-gold) deposits as well as for exploration purposes if this genetic link can be established.

(iv) Relationship between mineralization and tectonic processes in the Ikutha- Mutomo area.

Having information about when and where the deposits formed is important for understanding the ore genesis. It also generates a wider understanding about a relatively new deposit type that has a big economical potential not only in Ikutha, but worldwide. The study area has undergone faulting, shearing, folding and metamorphism which offered an ideal environment for iron mineralization. The suture zone of the east-west Gondwanaland passes through this area and extends to mid Galana then to Madagascar. The Athi shear zone also passes on the western part of the study area.

The project integrated geological-geophysical study, which has made it possible to illustrate some of the tectonic processes that have occurred in this area. This was intended to identify the type of ore deposit from several perspectives and identify features possible useful as exploration tools. The geochemical analysis and its interpretation show that this deposit is apatite-iron deposit.

(v) Comparison of Mutomo - Ikutha iron deposit with other iron deposits in Kenya

The Bukura and Mbesa massive sulphides described by Ichang'i (1983) are examples of hydrothermal deposits. Ichangi observed that the ore consisted of pyrite, pyrrhotite, chalcopyrite and sphalerite. He suggested that hydrothermal fluids associated with the adjacent Mumias Granite were responsible for the mineralization. Huddleston (1954) also described the Bukura massive sulphide and observed that the body had been traced over a distance of about one and a half kilometers. He estimated that the ore reserve was about 17 million tonnes down to a depth of 90 metres but suggested that it may exceed this figure since lateral extensions are known to exist.

Magnetite deposits associated with amphibolite bodies similar to the Wanjala deposit in Taita-Taveta are likely to occur in the West Pokot area where similar tectonic environment prevailed during the Proterozoic. In this area, Vearncombe (1983) described a dismembered ophiolite sequence, including podiform chromites, the root zone of a possible sheeted dyke complex and manganiferous metacherts in the Marich-Ortum region. Associated with the ophiolite are andesitic agglomerates, crystalline limestones, mica schists and psammites which are all indicative of island arc and continental margin environment. The lithological association shows that oceanic crust and an island arc existed to the east of the Tanzanian-Congo craton

(continent). The ocean closed during the Neoproterozoic time, and ophiolite emplaced on the west, to its present position sub-parallel to the craton boundary.

The Kurase Group in the Taita-Taveta area comprises miogeosynclinal lithologies such as marble,quartzite,graphite, sillimanite and kyanite-gneiss and schists; biotite-hornblende gneiss; and amphibolites. Amphibolites of the Mwatate formation reveal the characteristics of within-plate tholeiites or transitional within-plate tholeiites as they occur at continental margins near spreading centers (Nyamai *et al*., 2003).

Pohl and Horkel (1980) suggested that the Wanjala magnetite deposit is a metamorphosed submarine exhalative mineralisation associated with basic volcanics. Deposits in this group have formed by hydrothermal fluid exhalation. The fluids derived from sub-surface magmas or circulating sea or connate waters above zones of a high geothermal gradient form volcanic associated massive sulphide deposits (VMS) and sedimentary basins (SEDEX).

Typically Fe, Mn, B, P, Ni, Cr, Mo and Zn indicate a hydrothermal-exhalative source and Al and Ti a clastic source. Thus, Fe/Ti, Fe/Ni, Mn/Ti and Fe/P ratios and increasing concentrations of ore and associated elements (e.g., Cu, Zn, Ag, As, Cr, Cd, Co, W, Mo, Ni, Sb, and Ti) are suggested as useful geochemical indicators to ore proximity. Metamorphosed hydrothermal alteration zones show metamorphic mineral assemblages that reflect the elemental composition of the original protolith. For example, where there has been medium to high-grade metamorphism, zones of sericitic alteration may be preserved.

Kenya has been known to have iron ore deposits in several parts of the country in places such as Taita-Taveta, Meru, Kitui, Embu, Homa Bay, Machakos, Lolgorien, Migori, Samburu, Samia Hills and Mrima Hill, among others. These deposits occur either as oxides: (magnetite, hematite, martite, goethite and limonite); carbonates (siderite and ankerite) or sulphides (pyrite and pyrrhotite).

Ochieng (1993) described large bodies of titanium-vanadium-magnetite-bearing layered norite-gabbro suite to the S.E. of Mt. Kenya in the Marimante area. He analyzed the ilmenomagnetite and found it to contain between 31.2 and 58.61% Iron oxide (Fe_2O_3), 14.2 to 35.16% titanium (TiO_2) and 0.84 to 0.88% V_2O_5.

(vi) Comparison of Mutomo - Ikutha iron deposit with other world class iron deposits

The Mutomo-Ikutha apatite bearing magnetite deposit in Kitui County may have originated from magmatic hydrothermal solutions which deposited the magnetite in shear zone similar to the origin of Posht-e-Badam Block in Iran. Mokhtari and Emami, 2013, suggested rifting and shearing to have played a role in formation of such deposit of Iron ore. He observed apatite in different deposits of Posht-e-Badam Block in Iran. Iron-apatite ores showed an affinity to alkaline and sub-alkaline magmas and rifting environment. The alkaline host rocks of Central Iran and the iron-apatite ores are clearly related to an extensional setting where rifting was important (SSE–NNW fault lines). The same phenomena is observed in Mutomo - Ikutha where shearing and faulting has taken place in the SSE – NNW direction.

The probable source for this large scale ore forming process is relatively low partial melting of mantle rocks. The ores originated by magmatic differentiation as a late phase in the magmatic evolution forming sub-surface injections. The high phosphorous content and the so-called alkali-iron effect fluxed the immiscible melt and kept iron in solution at temperatures significantly lower than the melting point of magnetite at rather shallow depth. The iron ore formed during magmatism as immiscible liquids (silicate and Fe-P-rich magmatic liquids) which separated from strongly differentiated magmas coupled by a large volatile and alkali element content. Separation of magnetite melt and the ensuing hydrothermal processes dominated by alkali metasomatism could have both been involved to different degrees in the formation of the Ikutha iron ore deposits. Mokhtari and Emami (2013) proposed that the separation of an iron oxide melt and the ensuing hydrothermal processes dominated by alkali metasomatism were both involved to different degrees in the formation of Posht-e-Badam Block iron-apatite deposits.

According to Mokhtari and Emami (2013), the iron-apatite ores of Posht-e-Badam Block were probably formed by magmatic differentiation of an alkaline magma rich in Fe and incompatible elements which were derived by partial melting of upper mantle. Deep seated faults caused transferring of parent magma and replacement in the upper parts of the crust. In this magma reservoir, the high phosphorous and alkali content probably led to the formation of a Fe–F, CO_2–H_2O–P–Na dominated immiscible melt which separated from a silica-rich melt.

The role of other volatile constituents such as CO_2 and F is also important in this process. Hydrothermal ore deposits can be broadly divided into: -

(i) Vein/stockwork systems, in which solutions have deposited ore minerals in brittle structures or cavities.

(ii) Replacement deposits in which solutions have reacted with host rocks, leading to the replacement of carbonates and siliceous material by new gangue and ore minerals.

Primary dispersion patterns associated with these kind of deposits are related to the movement of hydrothermal fluids through the host rocks. Transfer of elements to the host rocks is by fluid related diffusion, fluid flow through the fractures/pore spaces, or a combination of these processes. A high percentage of the iron ore mined in the world currently comes from large deposits of massive hematite formed by the in situ enrichment in iron, most commonly from banded iron formations (BIFs). Most significant resources are the Banded Iron Formation (BIF) preserved in the remnants of old Archean basins. The global distribution of Palae-oproterozoic BIFs marks a unique period in Earth's geological history. The formation of banded ironstone in geologic time is recorded in Middle to Late Archean (3.2 – 2.6BY). These occurred as shelf type sedimentation which also yielded carbonates, quartzites and meta-pelitic schist (Gross, 1993).

Examples include BIFs in the Hamersley Basin in Western Australia (Trendall, 1983), Lake Superior Region in North America, Transvaal Region in South Africa, Krivoy Rog Region in the Ukraine and Minas Gerais Region in Brazil.

Apatite-bearing magnetite deposits constitute an important mineralization type of iron. Deposits of this type, like Pýnarbaþý Apatite-bearing magnetite deposit of Sweden have great economic importance, which constitute the most important source of the Swedish steel industry, and are termed as "Kiruna-type iron deposits"(Wright, 1986). Other important apatite-bearing magnetite deposits are Cerro de Mercado (Mexico), El Laco (Chile), Avnik (Turkey), Ünaldý (Turkey) and Bafq (Iran) (Mücke and Younessi, 1994; Förster and Jafarzadeh, 1994).

In their studies on Magmatic Ti-Fe±V oxide deposits in British Columbia, Gross *et al*., (1998) found that such deposits occur as Ilmenite, hemo-ilmenite or titaniferous magnetite accumulations as cross-cutting lenses or dike-like bodies, layers or disseminations within anorthositic/gabbroic/noritic rocks. Minerals are usually hosted by massive, layered or zoned

intrusive complexes - anorthosite, norite, gabbro, diorite, diabase, quartz monzonite and hornblende pyroxenite, and can be subdivided into an ilmenite subtype (anorthosite-hosted titanium-iron) and a titaniferous magnetite subtype (gabbro-anorthosite-hosted iron-titanium, commonly associated with anorthosite-gabbro-norite-monzonite (mangerite)-charnockite granite (AMCG) suites that are conventionally interpreted to be anorogenic and/or extensional.

Some of the iron-titanium deposits occur at continental margins related to island arc magmatism followed by an episode of orogenic compression. In layered intrusions the titaniferous magnetite seams are commonly within the upper stratigraphic levels and in marginal zones of complex intrusive bodies. Titaniferous magnetite deposits are commonly associated with magnesian, labradorite phases of anorthositic intrusions or gabbroic phases near the margins of the stock. Progressive differentiation of liquids residual from anorthosite-norite magmas leads to late enrichment in Fe and Ti. Typically plagioclase crystallization results in concentration of Fe and Ti in residual magmas which typically crystallize to form ferrodiorites and ferrogabbros. Layers form by crystal settling and accumulation on the floors of magma chambers and the disseminated deposits are believed to have formed in-situ.

Defant and Drummond (1990) studied the geochemistry and petrology of the Southern Luzon Arc, Philippines and observed that the volcanic rocks have typical volcanic arc phenocryst mineralogies: olivine, clinopyroxene, plagioclase, and titanomagnetite in the most mafic rocks and clinopyroxene, plagioclase, orthopyroxene, titanomagnetite, ± amphibole in the more felsic samples where complex zoning, sieve textures, and decoupling of incompatible trace elements suggest that processes such as assimilation have taken place.

Titanium-magnetite ores are among the leading types of commercial iron ore deposits and the main provider of vanadium. The ilmenite-titanium-magnetite variety is an important source of titanium. The ore belong to the late magmatic class of magmatogenetic deposits and have been explored in many countries. Russia has 50% of the world reserves; more than 40 deposits have been discovered in Karelia, on the Kola Peninsula, in the Urals, and Siberia. The ores of the titanium-magnetite deposits are complex, with Fe, V and Ti whose proportions vary over a wide range; they may be essentially titaniferous or typically iron-vanadium ones.

According to Gross *et al*., (1998), titaniferous magnetite deposits can be considerably large, ranging up to a billion tonnes with grades between 1 to 40% Fe, 15 to 20% TiO_2 and less than 10% apatite with V contents averaging 0.25%.

SUB-CHAPTER 4.6: GEOPHYSICAL INVESTIGATION OF IRON ORE DEPOSITS OF MUTOMO – IKUTHA AREA

This sub-chapter gives the results of ground magnetic survey carried out in order to delineate the iron mineralized zone. The results are both for 3D and 2D Euler deconvolution. 3 D Euler deconvolution utilizes XYZ (X = length along X axis, Y = length along Y axis, Z = length along the Z axis) values to provide the subsurface geophysical information. 2D data interpretation gives information along a designated profile and the depth.

Euler deconvolution is based on the Euler homogeneity equation which could be written in the form,

$$(x-x_0)\frac{\partial T}{\partial x}+(y-y_0)\frac{\partial T}{\partial y}+(z-z_0)\frac{\partial T}{\partial z}+\eta T=0 \qquad (4.1)$$

Where T = total magnetic field anomaly due to the magnetic source located at (x_0, y_0, z_0)

η = is the structural index related to the simple source geometry.

Equation (4.1) can be solved in a least-square fashion to obtain the source coordinates and its geometry. However, direct application of equation (4.1) to the observed data is not useful because the absolute value of the anomalous field (T) is rarely known. Equation (4.1) does not account for the regional or background magnetic field due to nearby sources, as a result the exact solution is unreliable and erratic (Thompson, 1982).

In general, the unknown regional field (B) can be approximated using Taylor series equation given as,

$$B(x,y,)=B_0+x\frac{\partial B}{\partial x}+y\frac{\partial B}{\partial y}+0\,(2) \qquad (4.2)$$

Where B_0 is the constant background at the centre of the specified window and O(2) represents higher-order terms in the Taylor series expansion. The anomalous field (T) can now be expressed as the difference between the observed (F) and regional (B) fields,

$$T = F - B. \qquad (4.3)$$

The modified Euler equation is obtained by substituting T into equation (4.1),

$$(x-x_0)\frac{\partial(F-B)}{\partial x}+(y-y_0)\frac{\partial(F-B)}{\partial y}+(z-z_0)\frac{\partial(F-B)}{\partial z}+\eta(F-B)=0 \qquad (4.4)$$

The use of magnetic data is a geophysical exploration technique based on mapping the subsurface distribution of magnetic minerals (oxides or sulphides). This technique can be a valid approach to mineral exploration either directly for mineral deposits containing magnetic minerals (e.g. magnetite, hematite, pyrrhotite) or indirectly for the ones spatially associated with, for example faults. Advances in spatial controls using global positioning systems (GPS) have not only reduced the survey costs but also increased data accuracy.

Total magnetization of rock is a vector sum of the two components: (1) induced magnetization (proportional in magnitude and generally parallel to the earth's ambient field), and (2) remnant magnetization (which has direction and intensity dependent on the origin and geological history of the rock). The intensity of induced magnetization is related to the ambient field through the magnetic susceptibility of the rock considered (Hildenbrand *et al*., 2001; Reid, 1990). This magnetic susceptibility constant is directly proportional to the modal mineral composition and chemistry of the rock.

In this method, a significant formula that shows the relations between the fields and the magnetization within materials (Telford *et al*., 1990) is expressed by equation (4.5):

$$B = \mu_o (H + M) \qquad (4.5)$$

Where B, the magnetic induction is the total flux of magnetic field lines through a cross-sectional area of a material, μ_o is the permeability of free space (4π x 10^{-7} Wb/Am^{-1}), H is the magnetic field applied to the material and M is magnetization or response of the material to the applied magnetic field. Magnetic susceptibility (k) is another important parameter, the relationship between magnetic induction B, magnetizing force H and susceptibility k (Reynolds, 1997) is given as:

$$B = \mu_o H (1 + k) \qquad (4.6)$$

Where B is in tesla, μ_o is free space permeability, H is given in amperes/meters and k is dimensionless in SI units.

The magnetic survey in this particular study was aimed at outlining the structural framework of the subsurface, delineates features and estimates the depths. Different algorithms were applied that enables easier identification of shear zone, fracture and contact features in the area (Hood and Teskey, 1989; Aboud *et al*., 2005; Falebita *et al*., 2011; Riddihough, 1971). The result made possible the demarcation of subsurface structures that control iron ore mineralization.

Rocks have widely varying magnetic properties (Carmichael, 1982; Clark, 1997). At the regional scale, magnetic highs are commonly associated with major igneous provinces in crystalline basement. By contrast, magnetic lows often occur in areas dominated by thick sedimentary basins (Hildenbrand *et al*., 2001) or where for example, igneous rocks are altered and magnetite was replaced by hematite when hydrothermal fluids have migrated along faults. Grant, (1985) emphasized that magnetic response observed in magnetic anomaly maps is influenced by the geometry and depth of the magnetic bodies, their azimuth with regard to magnetic north, and the inclination of the magnetic field at the latitude of the survey. In the neighbourhood of mineral deposits, mineralogical variety and thermal history related to mineral deposit can subsequently affect magnetic properties. The degree of oxidation, alteration, weathering, and metamorphism also affects the magnetic properties of the rock (Hildenbrand *et al*., 2001). All these combined factors concur to generate complex sections of magnetic properties for ground magnetic survey in Mutomo – Ikutha area.

4.6.1 Spatial distribution of Iron in Mutomo-Ikutha area

Qualitatively, the corrected total magnetic intensity and IGRF (International Geomagnetic Reference Field) removed map (Figure 4.92 and 4.93) shows the magnetic field amplitude, which reaches 1000 nT i.e. ranges in amplitude from 250 nT to 1000 nT. This is relatively high compared with its spatial distribution of the survey, and the acute variation in its magnetic intensity may be an indication of the variations in either lithology or basement topography (Dobrin and Savit, 1988). These high amplitude defines the location occupied by iron ore in survey area.

The contours become close on the western part of area trending in the NW – SE direction (Figure 4.92). The closeness of the contours indicate high values of the magnetic anomaly. Further investigations by trenching and pitting revealed that that this area with high anomaly contained Magnetite (see Figure 4.94). The area occupied by anomalies widens towards the

north from the south. The results were plotted into 3D (Figure 4.92) to visualise the magnetic anomaly in the XYZ format.

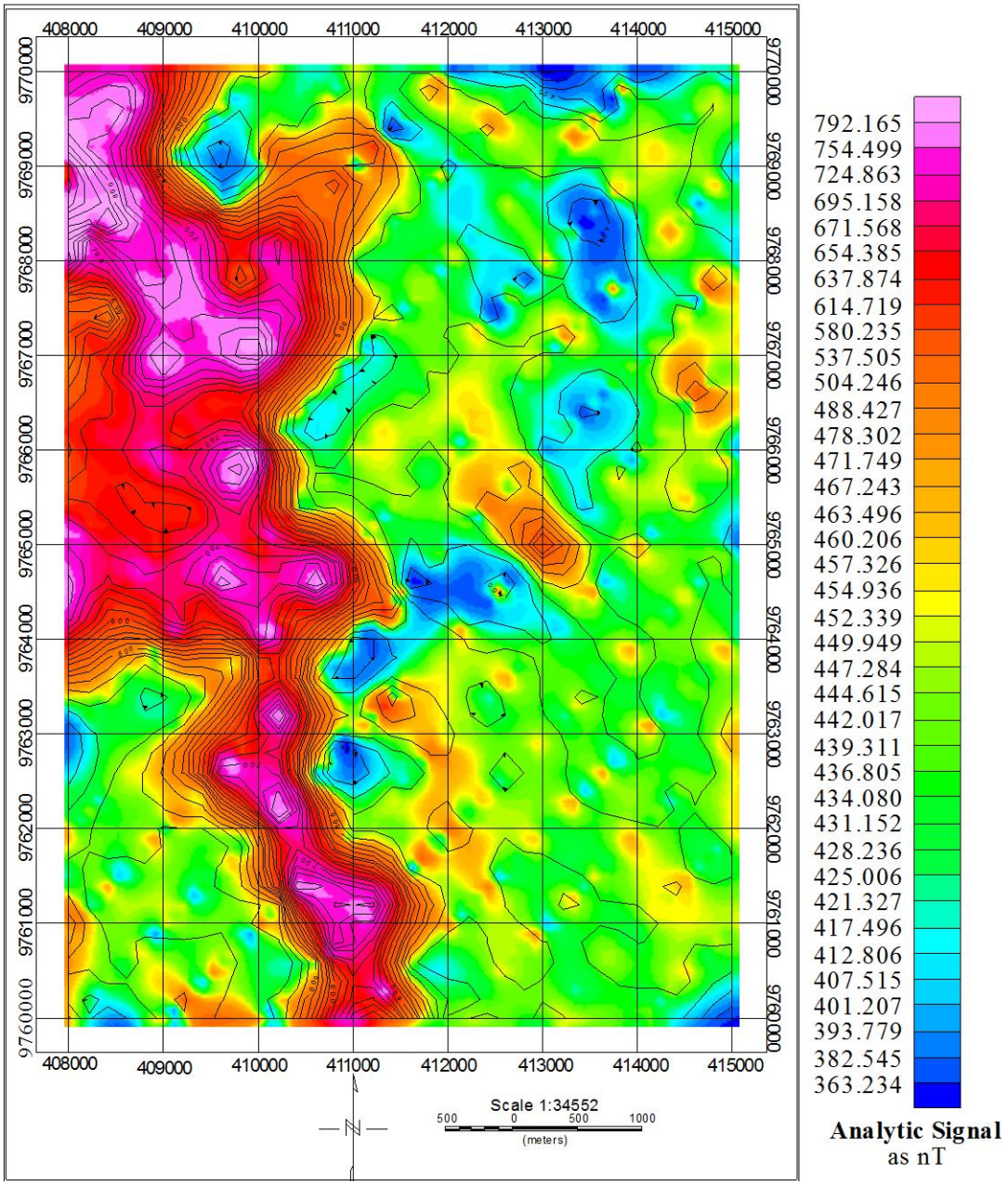

Figure 4.92: Display of magnetic field amplitude showing the trend of Iron ore mineralization in Mutomo – Ikutha area. The boundary of the iron rich rocks is marked by the brown colour.

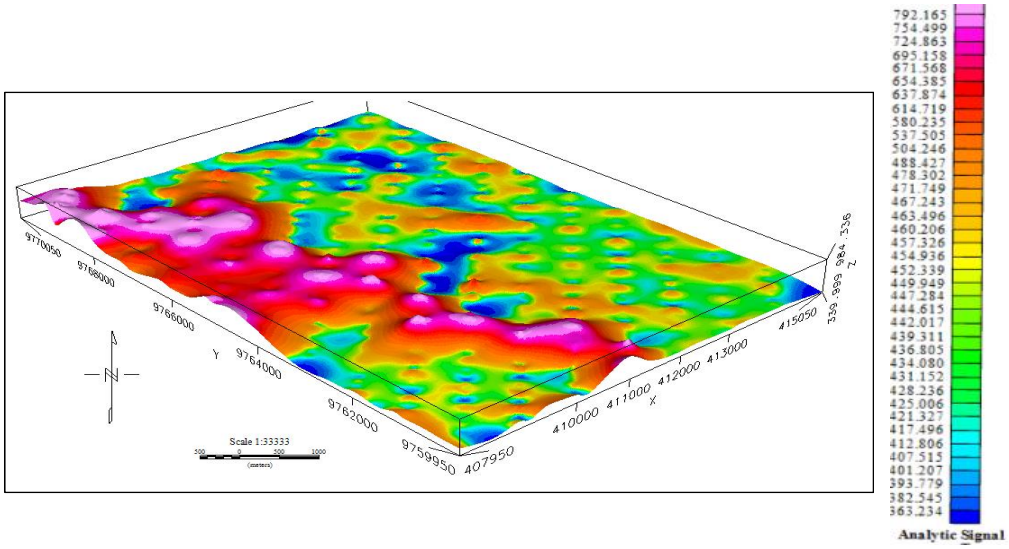

Figure 4.93: The figure showing the trend of Iron ore mineralization in Mutomo – Ikutha area in 3D. The boundary of the iron rich rocks is marked by the red colour

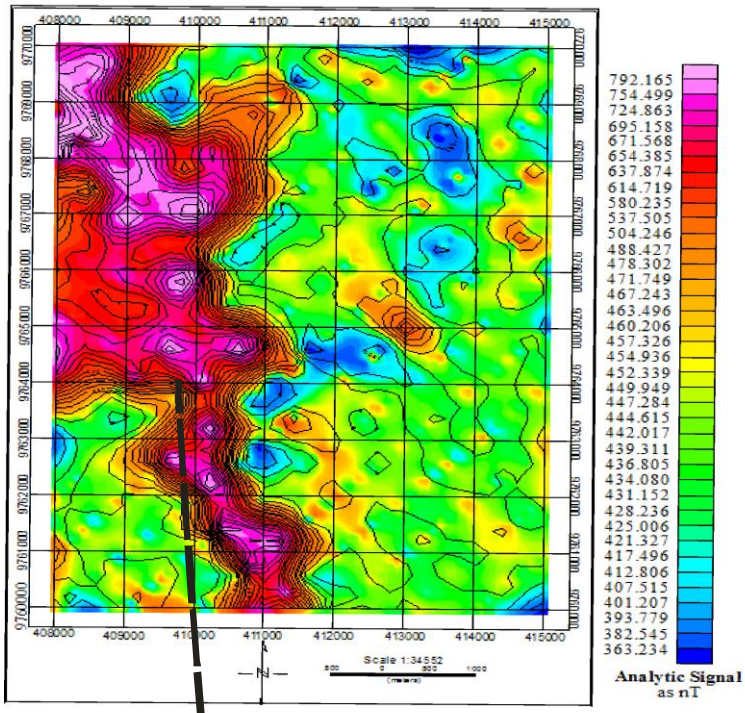

Figure 4.94: The magnetic amplitude contour map showing the trend of Iron ore mineralization in Mutomo – Ikutha area. The boundary of the iron rich rocks is marked by the tightly spaced contours on the western part of the research area.

4.6.2 Delineation of the shear and Iron ore Mineralized zone using Euler convolution

The summary of magnetic anomalies along the profiles is tabulated in Table 4.25. High magnetic anomaly is observed from 0 - 100 meters below the surface along profile T3-T'3 (Figure 4.95). This high magnetic anomaly indicates that iron ore body occurs below the surface. Mineralization of Iron along this profile varies from 0 - 10 meters. This iron ore occurs in form of pod form, dike, sill and in disseminated form as observed from the structural index figure. The ore is hosted in non-magnetic body (hornblende gneiss). The abrupt discontinuities of the structural index plots indicates that the area has undergone shearing and faulting as noted along the profiles; T1-T'1 to profile T16-T'16 (see Figures A1 – A16 in Appendix C).

The first fault plane occur between 200 meters and 400 meters along the profile, while the second fault is at 800 meters along profile T1-T'1 (Figure A1 in Appendix C). Faulting is at 200, 380, 450, 1200, 1600, and 1750 meters along profile T2-T'2. Mineralization occurs at the surface to 50 meters depth. Brittle shearing is observed from the pseudo-section. Mineralization occur inform of pod forms, veins, dike and sill, some of which are blind deposits that are not observed on the surface. Along profile T3-T'3 (Figure 4.95), mineralization is up to 80 meters deep from the surface. Again mineralization is in form of pod forms, veins, dikes and sills. Blind deposits were observed along the same profile. Profile T4 – T4' shows that area is sheared and faulted. Shearing is more pronounced towards T′4. Mineralization occurs from the surface to 150 meters below the surface. Brittle shearing was noted along the profile. Mineralization is in form of pod forms, stockwork, dikes and sills. Blind deposit observed along the profile.

Discontinuities along profile T5-T′5 indicate brittle shearing has taken place in this area. Mineralization from the surface to 170 meters below the surface. Mineralization in form of stockwork, pod form, veins, dikes and sills. Intense shearing is towards T′5 (Figure A5 in appendix C). Mineralization starts from the surface to 125 meters along profile T6-T'6 (Figure 4.96). This Mineralization is in form of veins, pod forms, dike and sill. Shearing is intense towards T′6 (see Figure A6 in appendix C). Pseudo-section of profile T7-T'7 shows that iron ore mineralization begins from the surface to 160 meters below the surface (Figure 4.97). Mineralization occurs in form of veins, stock work, pod form, sill and dike. The ore is more disseminated towards T7 (Figure 4.97 and Appendix C).

Profile T8-T’8 pseudo – section shows that the area is sheared and faulted. Intense shearing at 4000 meters to 5500 meters along the profile (Figure 4.98 and Appendix C). Mineralization is from the surface to 150 meters below the surface. Mineralization is in form of veins, dikes, sills, podiform, and stockwork. Profile T9 – T’9 pseudo – section shows that mineralization occur from the surface to 75 meters below surface. Intense shearing that has opened up fractures are 4500 meters to 6000 meters along the profile T9 - T′9 (Figure A9 in Appendix C). Mineralization in form of veins, pod form, dikes and sills are observed along the profile. The same scenario is observed on profiles 10 (see Figure 4.99), 11,12,13,14 and 15 (see Figure 4.100 for Traverse 14). Pseudo – section of profile T16-T’16 less mineralization noted at 400 and 980 meters along the profile compared to other profiles. Mineralization occurs at a depth of 20 meters in form of podform (Figure A16 in Appendix C).

Table 25: Magnetic interpretation of the ground magnetic data

Profile	**Structural interpretation**	**Mineralization depth**	**Mineralization type**
T1 – T1’	Brittle shearing along the profile	From the surface to 25 m below the surface	Podform and dykes
T2 –T2’	Brittle shearing towards T2. Semi brittle shearing towards T’2	From the surface to 20 m below the surface	Sills and podform
T3 – T3’	Brittle shearing is prominent along the profile	From surface to 100 m	Podform, dyke, sill, disseminated form
T4 – T4’	Brittle to semi brittle shearing	From the surface to 160 meters	Sills, dykes, and podform
T5 – T5’	Brittle shearing is prominent	From surface to 160 m below the surface	Stockwork, Podform, Vein, dyke and Sills
T6 – T6’	Shearing prominent towards T6’	From the surface to 100 m below the surface	Veins, Podform, dyke and sills
T7 – T7’	Prominent shearing along the profile	From surface to 160 m	Veins, stockwork, podform, sill and dyke. Disseminated mineralization intense towards T7
T8 – T8’	Sheared and faulted along the profile	From surface to 150 below surface	Dykes, podform and disseminated mineralisation
T9 – T9’	Intense shearing that has opened fracture at distance from 4500 m – 6000 m along the profile.	From surface to 75 m below the surface	Sills, dykes and podform
T10 –T10’	Shearing and faulting along the profile	From the surface to 100 m below the surface	Dykes and podform are prominent. .
T11 – T11’	Shearing and faulting prominent along the profile	From the surface to 100 m below the surface.	Dykes, podform and disseminated mineralization
T12 – T12’ T13 – T13’ T14 – T14’ T15 – T15’ T16 – T16’	Shearing and faulting prominent	From the surface to 100 m below the surface	Sills, dykes and podform

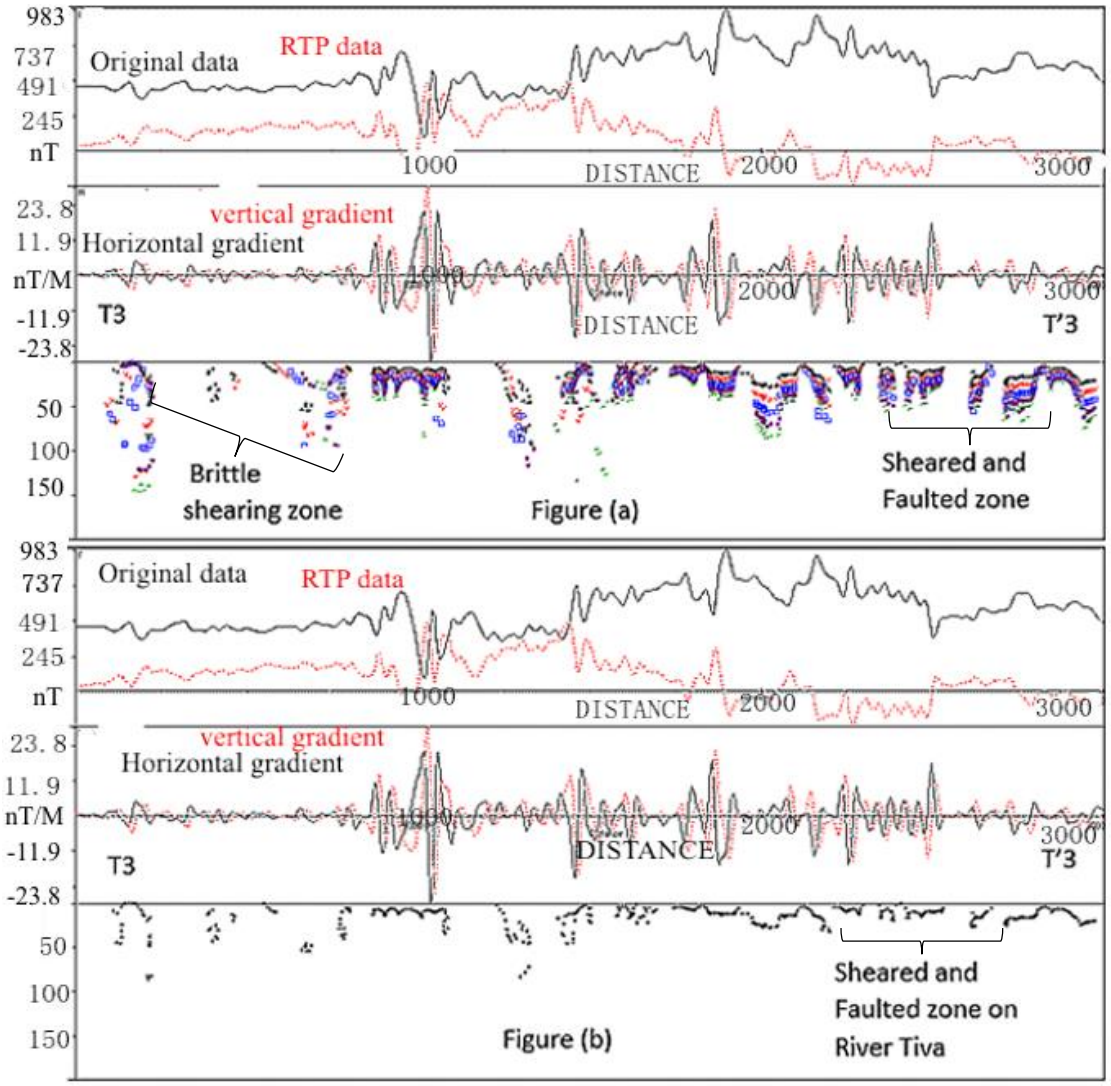

Figure 4.95: (a) Schematic section of profile T3 - T′3 through a sheared and faulted zone showing the underlying mineralization. (b); structural index pseudo -section showing faulting and shearing zones.

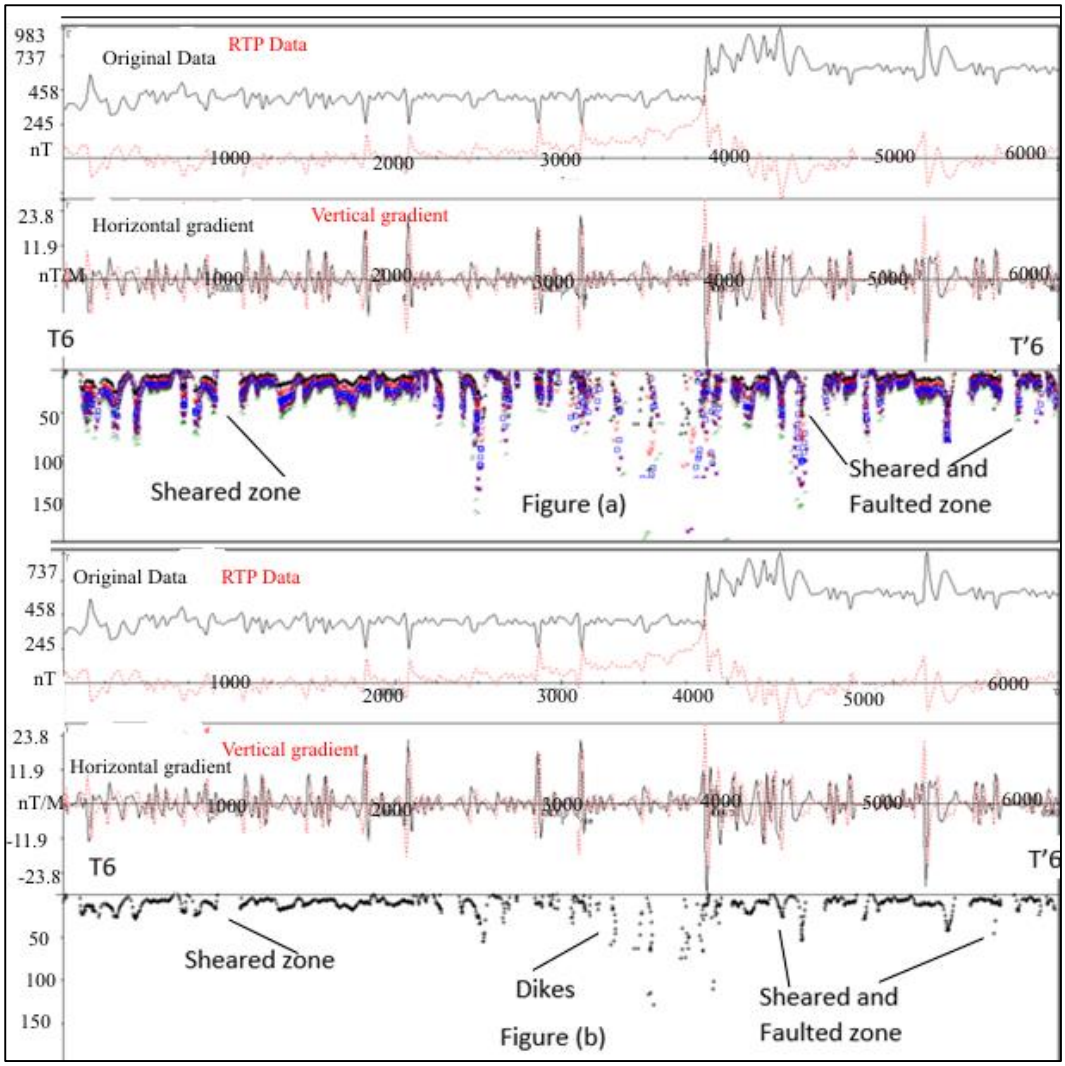

Figure 4.96: (a); Schematic section of profile T6 - T′6 through a sheared and faulted showing the underlying mineralization. (b); structural index pseudo -section showing faulting and shearing.

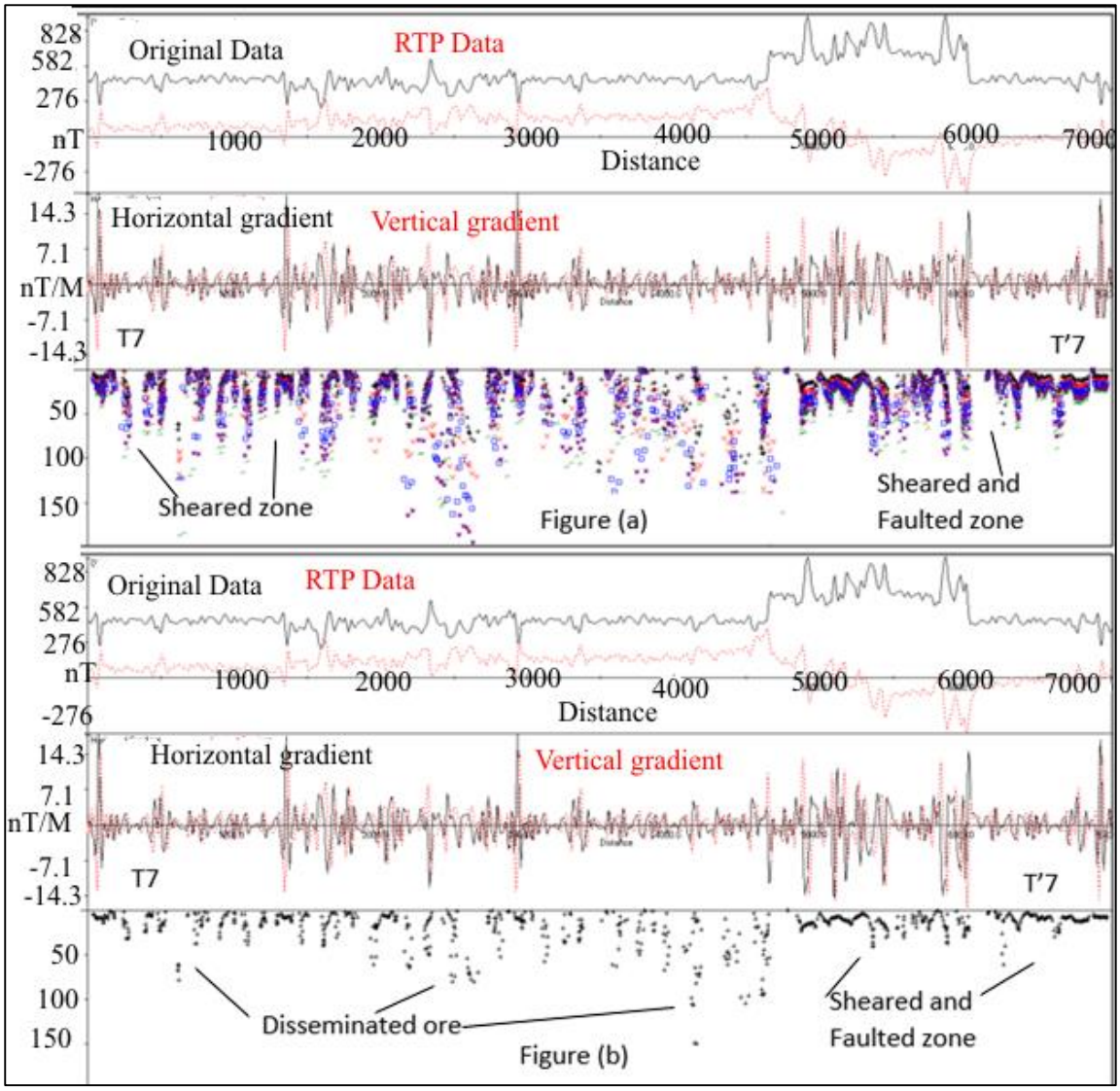

Figure 4.97 : (a); Schematic section of profile T7 - T′7 through a sheared and faulted showing the underlying mineralization. (b); structural index pseudo -section showing faulting and shearing.

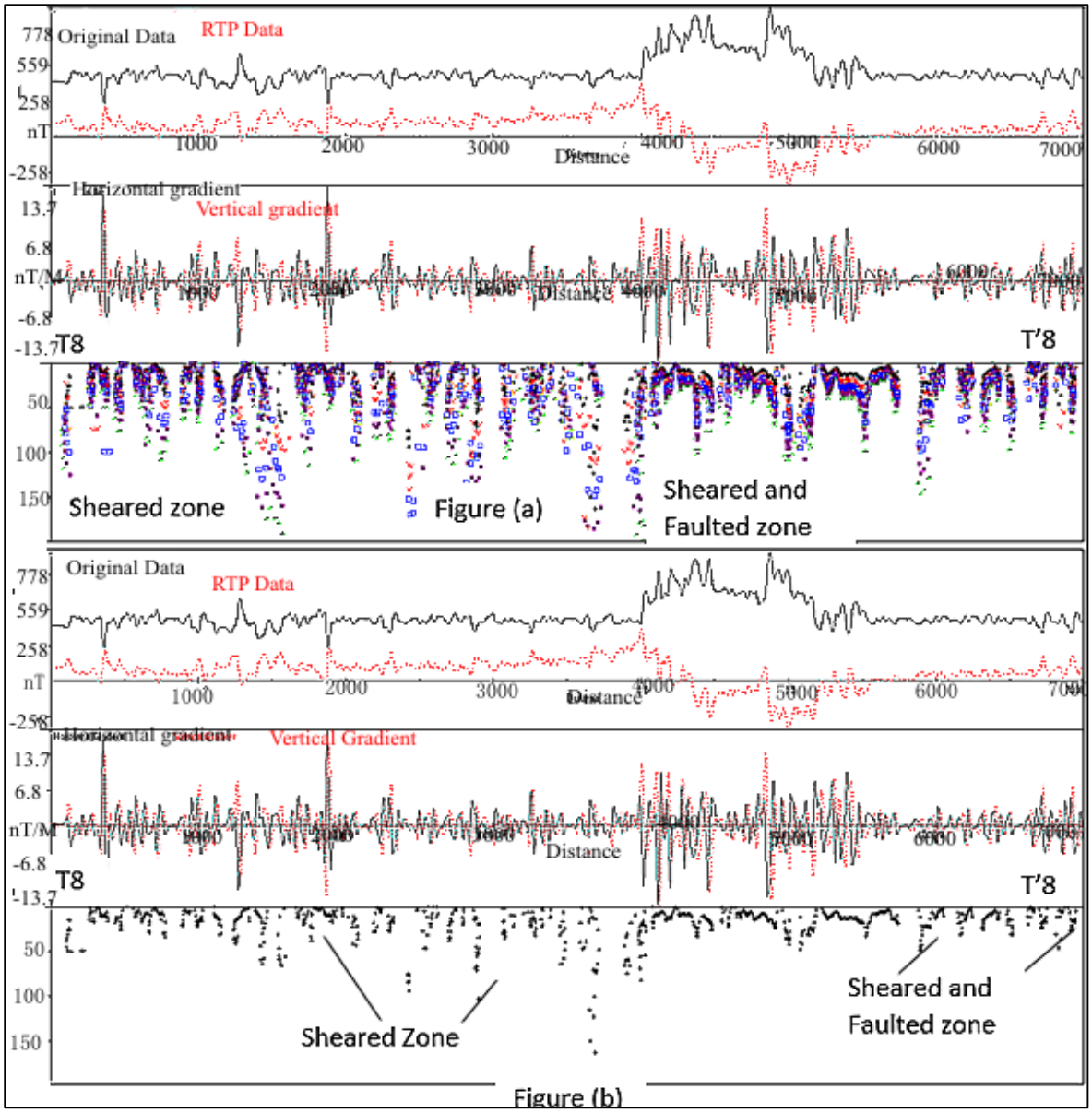

Figure 4.98: (a); Schematic section of profile T8 - T′8 through a sheared and faulted showing the underlying mineralization. (b); structural index pseudo -section showing faulting and shearing.

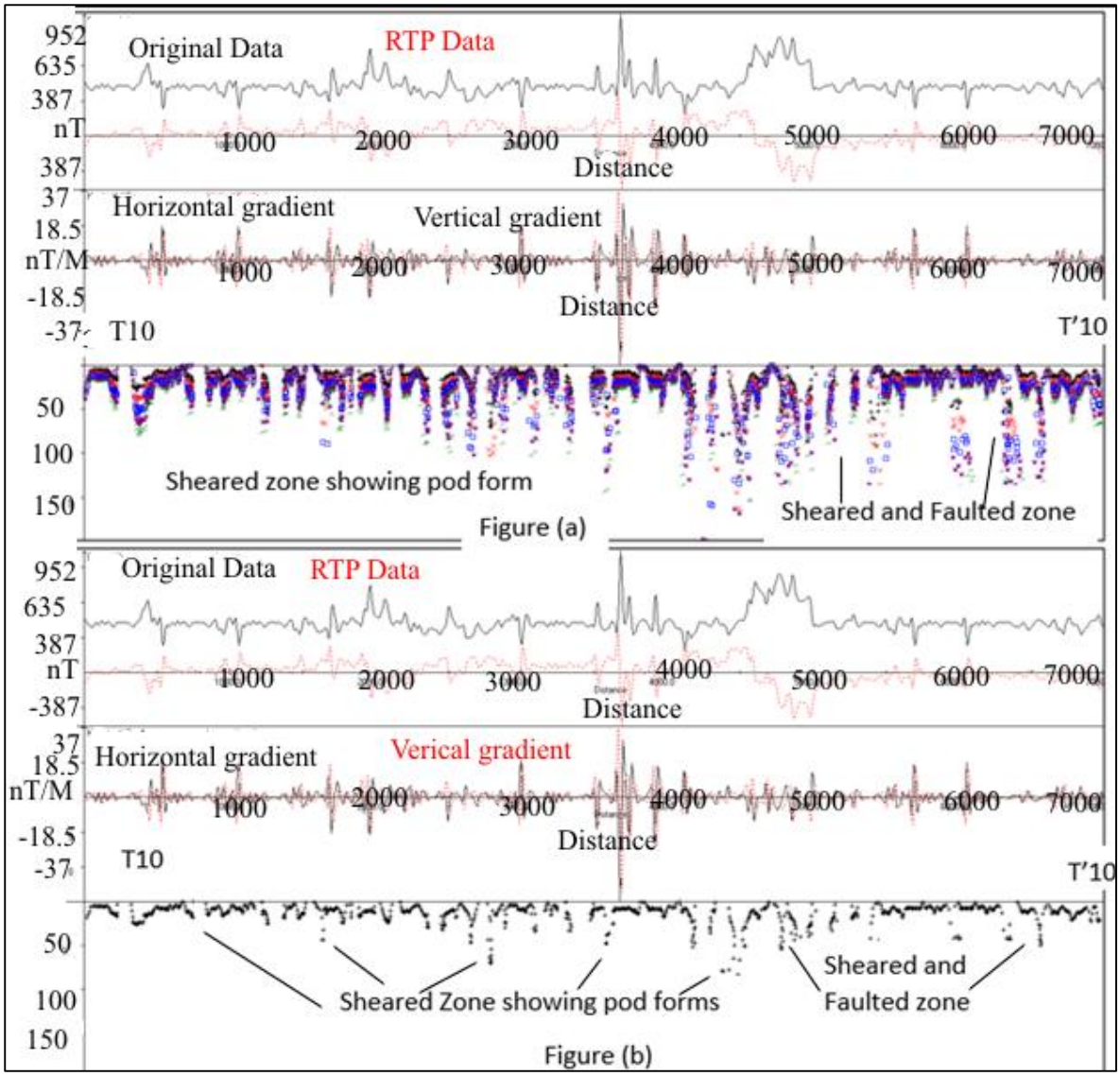

Figure 4.99: (a); Schematic section of profile T10 - T′10 through a sheared and faulted showing the underlying mineralization. (b); structural index pseudo -section showing faulting and shearing.

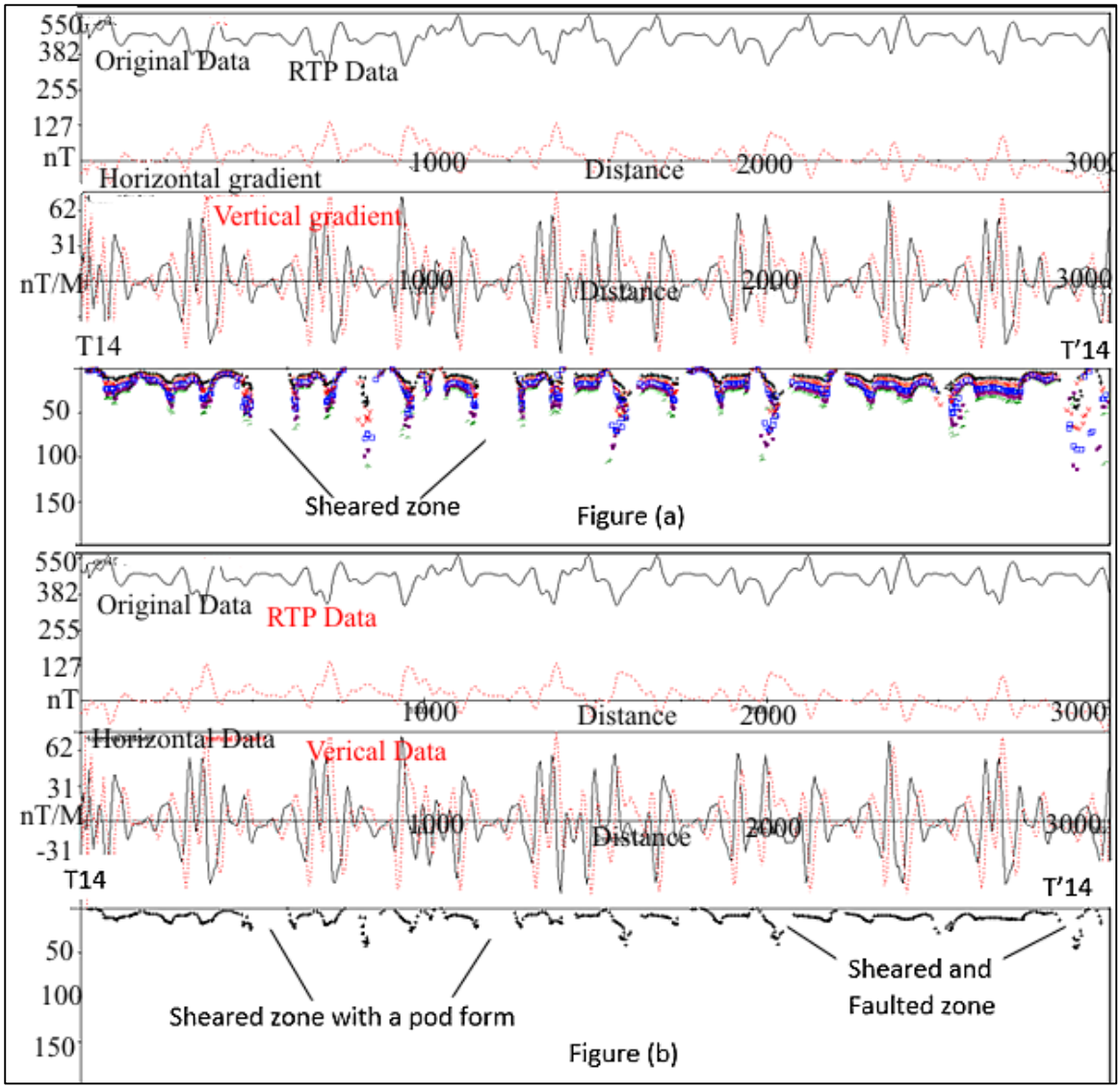

Figure 4.100: (a); Schematic section of profile T14 - T′14 through a sheared and faulted showing the underlying mineralization. (b); structural index pseudo -section showing faulting and shearing.

4.6.3 Discussion on geophysical investigation of Mutomo – Ikutha area iron ore

Geophysical survey which involved magnetic survey carried out along the profiles T1 – T16 show high magnetic anomalies on the western part of the area. The anomalies trend in the N – S direction. This shows that bodies that are magnetic in nature are located around this part of the area of study. The anomalies were detected by Euler 2D convolution to a depth of 160 meter below the surface, which indicates that magnetite ore occurs up to this depth. The Euler 2D also shows the discontinuities along the profiles. These discontinuities mark the faults and shear zones in the area plus pod form nature of the deposits.

4.6.4 Ore quantity assessment

Iron ore reserve estimation was done to find out the quantity of iron ore that might be mined economically in Mutomo – Ikutha area. The surface area hosting iron ore deposit was estimated using ArcGIS 10.10 software indicate and was found to cover about 15 km^2. This area was also confirmed on the ground using magnetic survey, geochemical survey, and geological mapping. The iron ore depth estimation was done using ground magnetic survey which showed that the area is mineralized with Iron to a depth of 160 meters. Safe open cast mining will be done up to 20 meters.

In calculating the reserve potential of a deposit, formula 5-1 was used.

$$T = Th \times BD \times A \qquad (5\text{-}1)$$

Where

T = Tonnage (in metric tonnes)

Th = Thickness of the deposit within the area of influence in meters

BD = bulk density ($kg/m^{3)}$

A = area of influence on a plan (m^2)

Using formula 5-1, Tonnage of Mutomo – Ikutha iron ore is

20 m x 2500 ($kg/m^{3)}$ x 5,000,000 (m^2)

= 250,000,000,000 kg

= 250,000,000,000/1000

= 250 million tons.

CHAPTER FIVE: SUMMARY, CONCLUSIONS AND RECOMMENDATIONS

In this thesis, evidence backed by petrologic, petrochemistry, remote sensing data, and ground magnetic studies bearing information on the formation of iron ores in the Neoproterozoic Mozambique mobile belt rocks of south-eastern Kenya have been presented. Various potential models explaining these data have been discussed. The aim of this final chapter is to provide the conclusion, contribution to knowledge, projected contribution to the economy of Kenya and recommendations.

5.1 CONCLUSION

The conclusion of this thesis is based on the four objectives of this research and are explained as follows;

(1) The first objective of this research was to investigate the petrology and geochemistry of the rocks hosting the iron ore and associated minerals in order to characterize their tectonic setting. From the research carried out, it has been ascertained from the petrology studies that Mutomo – Ikutha area contains metasediments, metabasalts and meta gabbros, and marbles. Metasediments represent a thick sequence of sedimentary rocks. The entire sequence was marked by the alternation of thin pelitic, psammitic and limey layers, together with minor thin basic volcanic and intrusive rocks. Paragneissic rocks in the belt were deposited under deep marine conditions. Iron mineralization is within the rocks having mineral assemblage of Hornblende + Quartz + Biotite + Magnetite + Apatite ± Plagioclase and microcline found in the mesocratic rocks. Petrological studies have also revealed that Mutomo – Ikutha area occurs on an ophiolitic suite. This was realized from the discovery of the occurrence of ophiolitic suite sequence which includes; Meta – sediments (para-gneisses, and marbles), sheeted gabbro dykes, dunite, peridotites, meta-basalts (metamorphosed pillow basalts), and serpentinite. The wholesome association and composition of these rocks show that they were part of the oceanic crust which has undergone obduction during the collision of the East and West Gondwanaland. The trend of the rocks in the NW – SE orientation shows that there was compression on these rock units from NE and SW.

(2) (a) Geochemical evidence indicate that the iron ore deposit of Mutomo – Ikutha area contain between 48 – 93 % Fe_2O_3, 0.2-5.9% P_2O_5, and 0.05 – 1.9 % TiO_2. This deposit

also contain 0.007% - 1.3% of vanadium, resembling the Apatite – Iron ores of Kiruna type. Geochemical evidence has also shown that Fe_2O_3 has positive correlation with P_2O_5 and negative correlation with other elements found within the host rock. This shows that the mode of delivery of the two minerals into the area were similar. Fe_2O_3 and P_2O_5 were deposited into the area by hydrothermal/ magmatic fluids while other minerals in the host rocks got into Mutomo – Ikutha area through detrital process. Correlation of the elements in the mineral chemistry data show that iron and phosphorus were delivered in the area through the same medium. This stipulates that phosphates and iron equilibrated during the late stage of magmatism. Correlation of the elements show that Na_2O, K_2O, and Al_2O_3mostly originated from the detrital material. Magmatic and hydrothermal fluids contributed to the formation of the main reef of iron ore trending from N – S and the one in the pegmatites.

(2) (b) The second objective of this research was to determine the surface and subsurface extent of the iron deposits in the project area and associated alteration zones so as to establish their quantity and economic potential. This objective was accomplished using ground magnetic survey. Ground magnetic survey carried out in Ikutha area has revealed that iron ore deposit trends in the N – S direction. Mineralization was noted from the surface to the subsurface depth of 160 meters. The ore deposit is wide in the northern part and narrows down towards the south. This survey has also shown that iron ore mineralization is associated with shearing and faulting. The deposit occurs in pod forms, veins and disseminated form. From the analysis of the total magnetic data, it is noted that the deposit occupies a total area of 5,000,000 square meters. This data has been used to work out an approximate iron ore reserve which is estimated to be 250 million tons.

(3) The third objective of this research was to identify major and minor geological structures occurring in the project area in order to establish the deformation history and tectonic controls of the iron deposits. This research has established that the meta-sediments, meta-basalts and meta-gabbros were subjected to multiple phases of successive deformation and metamorphism. Three phases of folding (F1, F2, and F3) accompanied by medium- to high-grade amphibolite-facies metamorphic conditions were identified. The lower-crustal rocks suffered partial anatexis, yielding granitoid rocks and migmatites, which outcrop in the Mutomo formation; regional folding may control their distribution. Subsequently, magmatic bodies (olivine norite, south of

Ikutha, gabbros and peridotite of Kenze area) and later dike swarms (gabbro dykes) in Kapoponi group) were emplaced before and after the end of metamorphism. The dykesthat formed after metamorphism were controlled by the NE–SW fracture zones. Post-folding brittle structures cut rock units in Mutomo – Ikutha area.

Structural studies have shown that Mutomo – Ikutha rock units have gone through 3 deformational stages: D1, D2, and D3. Early stages of D1 deformation produced NW-trending isoclinal folds F1, which were refolded by D2 to produce SE-trending F2 recumbent folds, reorientation of the metamorphic foliations, and formation of migmatites at the late stages of this event. D3 was the last stage of deformation and it led to the F3 folding and shearing of the hornblende gneisses hosting the iron ore. The first two folding and transposition events can be related with initial offscraping and folding of the metasediments possibly in an accretionary prism environment. Open folds and brittle structures around Ikutha represent the second (D2) stage. The analyses of planar and linear structural elements from the Mutomo – Ikutha area clearly show the presence of three generations of folds (F1, F 2, and F3). The mean attitude of F1 hinges plunges between 10^0 and 25^0 to N320^0W, F2 plunges 12^0 and 70^0 to S140^0E, and F3 plunges 15^0 and 25 to 270^0 W. From these data, it is apparent that the F1 and F2 had dominantly NW–SE striking axial surfaces, with gently plunging hinges, whereas the superimposed F3 folds generally have W-E orientations. The geometrical relationships between D1 and D2 suggest that the Mutomo – Ikutha structures were mainly developed in response to a NE–SW compressional stress. This compressional stress may be related to oblique collision between the East and the West Gondwana at ~750–550Ma. However, the youngest, cross-cutting faults probably relate to the post- and syn- tectonic forces that operated in the NE – SW trend. These forces could have been accompanied by brittle and ductile shearing. It is therefore concluded that extensional ductile deformation in Mutomo – Ikutha area was accompanied and/or alternated with an approximately NE−SW-directed horizontal shortening perpendicular to the stretching direction during the later stages of extensional shear zone deformation. Extensive geological investigations and remote sensing technics led to the discovery of shear zone and mineral alteration zone in Mutomo – Ikutha area. Remote sensing investigations showed that lineaments in this are trend in the NW – SE direction.

(4) The fourth objective of this research was to investigate the tectono-metamorphic setting and genesis of the iron deposit occurring in the Mutomo-Ikutha area and compare it with other similar deposits elsewhere around the World. It has been revealed that the Pan-African tectonothermal events in Mutomo – Ikutha area were marked by penetrative and progressive deformation and metamorphism up to the amphibolite facies, resulting in the formation of migmatites and iron ore mineralization. The deformation sequence indicates that iron mineralization is controlled by tectonics and metamorphism. Hydrothermal fluids from late magmatism carrying ferrous metal deposited iron in the fractured zone that were created by brittle shearing along the western part of the area, especially within Tiva gneisses. This is atypical scenario in which Kiruna type Iron ore deposits form (Torab, 2008). Iron vein trending in the North - South direction on the south western part of the survey area occurs within the shear zone as identified from petrological studies. Field observations of the shearing and faulting of the mafic rocks within the gneisses indicate that mafic rocks came in before the end of metamorphic period. Metamorphism was accompanied by shearing, faulting and folding during the D3 stage.The second phase or iron ore mineralization took place during the metasomatism where iron ore formed in the pegmatites. This kind of ore is low in the phosphate content compared to the main reef of iron that is found within the shear zone. Other minerals found within the hornblende gneisses include manganese and copper. Industrial minerals like graphite, magnesite, calcite, garnets, and vermiculite occur within Kapoponi group.

The main research objective of this project was to investigate the petrology, tectonometamorphic setting and the genesis of the iron deposit in the Mutomo – Ikutha area with a view to understanding the geological processes that led to the formation of such a deposit and compare it with other similar deposits elsewhere around the world. From the evidence described above, it can be concluded that the iron ore deposit in the project study area occurs in high – grade metamorphic rock unit that has been affected by a series of tectonic events. This deposit formed by late magmatic/hydrothermal processes and resembles the Kiruna apatite – iron ore type.

5.2 RECOMMENDATION

- This study recommends that drilling and assay works should be done to establish the proved tonnage and quality of the iron deposit in this area.
- It is recommended that more research on the minerals associated with Iron ore should be carried out to establish their quantities and grade.
- Feasibility should be carried out on the extraction and utilization of magnetite
- The study recommends that more geophysical survey using gravity method should done to compare the results with magnetic data obtained.

5.3 CONTRIBUTION TO KNOWLEDGE

This research has shown that iron ore can form in the Neoproterozoic Mozambique mobile belt of Kenya that has undergone shearing and high grade metamorphism followed by late stage magmatism/hydrothermal activity. The research has shown that, other than magmatic processes that form Kiruna type iron ore, hydrothermal processes can also contribute to the formation of such deposits.

It has been proven by this research that tectonic structures can control iron ore mineralization. Ikutha iron ore occurs in the shear zone meaning that shear zones can be the major targets during iron ore deposits exploration.

It has also shown that remote sensing can be used to map alteration zones, geology and lineaments that control mineralization and hence be used in the discovery of iron ore deposits. This has been realized by successful delineation of alteration zones associated with iron ore mineralization.

It has also been realized from this research that Iron ore in Mutomo – Ikutha area and any other areas can be explored using the integrated model of remote sensing, geological mapping, ground magnetic mapping and geochemical mapping (see Figure 5.1). All the four methods have revealed the same focal location (western part of the study area) where iron ore deposit is located.

This research has also filled the gap that had been left by Saggerson (1957) (shown in Figure 4.78).The new geological map (Figure 4.2) developed during this research has shown that hornblende biotite gneisses and hornblende gneiss occur in the gap that had been left by Saggerson (1953). The new geological map produced has harmonized the geological units that were not matching from Saggerson (1957) and Walsh (1963).

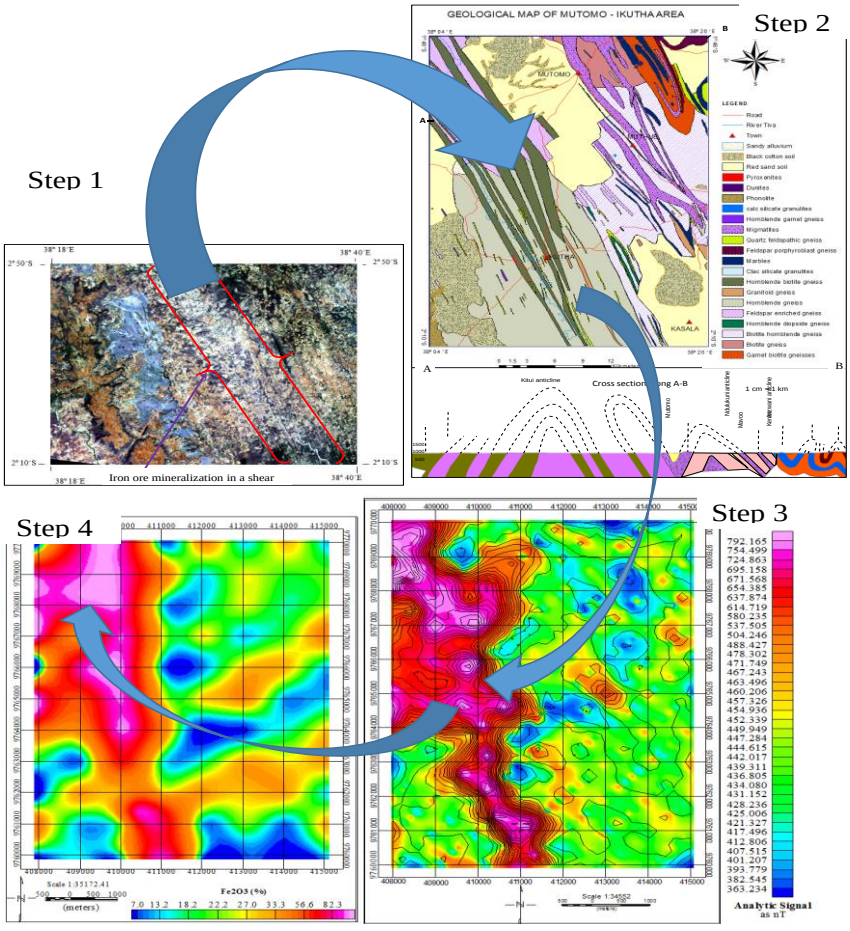

Figure 5.1: An intergraded iron ore exploration model. Step 1-remote sense, Step 2 – Geological mapping, Step 3 – Magnetic survey, Step 4 – Geochemical mapping.

5.4 CONTRIBUTION TO ECONOMYOF KENYA

The research has shown that Mutomo – Ikutha area has huge deposit of iron which can be used to put up a steel mill. This research has also managed to discover Manganese, Garnets, Copper, Magnesite, Graphite and marbles in the project area. Other minerals like tungsten, chromite, molybdenum, and nickel associated with Iron ore have also been identified. Mining and trading in this minerals will bring a great economic growth in Kenya and the lives of the people of Kitui County will improve significantly. Iron and Manganese can be used in making steel for construction industry as per the plan of vision 2030. Magnesite can be used to make furnace bricks and as a constituent in fertilizers. Marbles can be used in the manufacture of cement and as fillers in paint manufacturing. Garnets found in Mutomo – Ikutha area are of Gem quality and therefore can be used for ornamental purposes.

REFERENCES

Aboud, E., Goussev, S., Hassan, H., Supriyanto, S. and Ushijima, K., 2005. Horizontal gradient and band-pass filter of aeromagnetic data image the subsurface structure; Example from Esh El Mellaha Area, Gulf of Suez, Egypt. Proceedings of the SEG/EGS/EPEX/EPA International Conference, Cairo 2005: Imaging the Future May 16-19.

Ashworth, J.R., . 1985. Migmatites. New York, Chapman and Hall, 268 pp.

Barton, M.D. and Johnson, D.A., 1996. Evaporitic-source model for igneous-related Fe oxide-(REE-Cu-Au-U) mineralization. Geology **24**: 259-262.

Beaudoin, G., Dupuis, C., Gosselin, P. and Jebrak, M., 2007. Mineral chemistry of iron oxides: application to mineral exploration. In: C.J. Andrew (Editor), Ninth Biennial SGA meeting, SGA, Dublin, pp. 497-500.

Behre, S., 1990. Ophiolites in north-east and east Africa: implications for Proterozoic crustal growth. Journal of the Geological Society of London, **147**, pp. 41-57.

Biyajima, K., Suswa, K. and Miyakawa, K., 1975. Mantled gneiss dome in the Mozambique belt around Machakos area, Kenya, Preliminary Report. African Studies, Nagoya University, pp. 6 – 13.

Blumenfeld, P. and Bouchez J.L., 1988. Shear criteria in granite and migmatite deformed in the magmatic and solid states, Journal of Structural Geology, **4**, 361–372

Boger, S.D., and Miller, J.M., 2004. Terminal suturing of Gondwana and the onset of the Ross–Delamerian Orogeny: the cause and effect of an Early Cambrian reconfiguration of plate motions. Earth and Planetary Science Letters **219**, 35–48.

Brown, M. and Rushmer, T., 1997. The role of deformation in the movement of granitic melt: views from the laboratory and the field, in Deformation-Enhanced Melt Segregation and Metamorphic Fluid Transport, Mineral SocietyServices, vol. **8**, edited by M. Holness, pp. 111 – 144, Chapman and Hall, London.

Broman, C., Nyström J.O., Henríquez, F. and Elfman, M., 1999. Fluid inclusions in magnetite-apatite ore from a cooling magmatic system at El Laco, Chile. GFF 121: 253-267.

Burke, K. and Derwey, J., 1972. Orogeny in Africa. 3rded. Ibadan University Press, pp. 583-608.

Cahen, L. and Snelling, N.J., 1966. The geochronology of equatorial Africa. North – Holland, Amsterdam, 195 p.

Cahen, L., Snelling, N.J., Delhal, J., Vail, J.R., Bonhomme, M. and Ledent, D., 1984. The Geochronology and Evolution of Africa. Clarendon Press, Oxford, 512 pp.

Carmichael, R.S., 1982. Magnetic properties of minerals and rocks. In: CRC Handbook of Physical Constants for Rocks. Boca Raton, FL, pp. 229–287

Cartier L.E., 2009. Livelihoods and production cycles in the Malagasy artisanal ruby sapphire trade: a critical examination. Resources Policy, **34**, 80-86.

Clark, D.A. 1997. Magnetic petrophysics and magnetic petrology: aids to geological interpretation of magnetic surveys. AGSO Journal of Australian Geology and Geophysics **17**, 83-103.

Collins, A.S., 2006. Madagascar and the amalgamation of central Gondwana. Gondwana Research **9**, 3–16.

Collins, A.S. and Pisarevsky, S.A., 2005. Amalgamating eastern Gondwana: the evolution of the circum-Indian orogens. Earth Science Reviews **71**, 229–270.

Davies, G.F., 1992. On the emergence of plate tectonics. Geology **20**: 963-66

Davis, G.H. and Reynolds, S.J., 1996. Structural geology of rocks and regions, 2nd edition. John Wiley, New York, 864 pp.

Defant, M.J. and Drummond, M.S., 1990. Derivation of some modern arc magmas by melting of young subducted lithosphere. Nature **347**, 662–665

Dobrin, M.B. and Savit, C.H., 1988. Introduction to geophysical prospecting. McGraw-Hill Book Co. Inc. New York. Pp 152-190, 498-578, 691- 745 pp.

Drury, S.A., 1993. Image Interpretation in Geology, 3rd Edition. Allen and Unwin, London, 590 pp.

Eckstrand, O.R., 1984. Canadian mineral deposit types: geological synopsis. Geol. Surv. Canada Econ. Rep **36**, Ottawa.

Evans, A.M., 1993. Ore geology and industrial minerals – An introduction. Blackwell Scientific Publication, Oxford, 389 pp.

Environmental Protection Agency (EPA), 1994 "Extraction and beneficiation of ores and minerals, technical resource document, Iron," vol. **3**, pp. 56 -64.

Falebita, D. E., Olorunfemi, M.O. and Ojo, J. S., 2011. An appraisal of the geologic structure beneath the Ikogosi warm spring in south-western Nigeria using integrated surface geophysical methods. Earth Sciences Research Journal **15**(1): 27-34

Fleuty, M. J., 1964. The description of folds. Proc. Geol. Assoc. England, **75**, pp. 461-492.

Förster, H. and Jafarzadeh, A., 1994. The Bafq Mining District in Central Iran - a Highly Mineralized Infracambrian Volcanic Field. EconomicGeology **89**, 1697-1721.

Frietsch, R. and Perdahl, J.A., 1995. Rare earth elements in apatite and magnetite in Kiruna-type iron ores and some other iron ore types. Ore Geology Review 9: 489-510.

Gaciri, S.J., Altherr, R., Nyamai, C.M. and Mathu, E.M., 1993. Distribution of elements in mineral pairs from Mozambique belt rocks of Matuu area, central Kenya. In: Opiyo-Akech, N., 1984 edition, Proceedings of the 5th Conference on the Geology of Kenya - Geology for Sustainable Development, pp. 57-62. UNEP/ UNESCO, Nairobi.

Gass, I., 1977. The evolution of the Pan African crystalline basement in NE Africa and Arabia. Journal of the Geological Society of London, **134**, pp. 129-138.

Geijer, P., 1931. The iron ores of the Kiruna type, geographical distribution, geological characters and origin. Sverigesgeologiskaundersökning, C**367**, pp. 1-39.

Glasby, G.P. and Schulz, H.D., 1999, EH, pH diagrams for Mn, Fe, Co, Ni, Cu and As under seawater conditions: Application of two new types of EH, pH diagrams to the study of specifi c problems in marine geochemistry: Aquatic Geochemistry, v. **5**, p. 227– 248, doi: 10.1023/A: 1009663322718.

Goldstein, J.I., Newburry, D.E., Echlin, P., Joy, D.C., Fiori, C.E and Lifshin, E., 1981. Scanning electron microscopy and X – ray Microanalysis, New York, 143 pp.

Government of Kenya, 2007. Ministry of state for planning, National development, and vision 2030 in the office of the right Honourable Prime Minster and Ministry of finance, Nairobi, Kenya.

Grant, F.S., 1985. Aeromagnetics, geology and ore environments, 1, Magnetite in igneous, sedimentary and metamorphic rocks: An overview.Geoexploration, **23**, 303-333.

Gross, G.A., Gower, C.F. and Lefebure, D.V., 1998. Magmatic Ti-Fe±V Oxide Deposits, in Geological Fieldwork 1997, British Columbia Ministry of Employment and Investment, Paper -1, pages 24J-1 to 24J-3.

Gross, G. A., 1993. Industrial and genetic models for iron ore in iron formations; In: Mineral Deposit Modelling; Geol. Assoc. Canada, Spec. Paper 40 151–170.

Gurvich, E.G., 2006. Metalliferous sediments of the world ocean: Springer, Berlin, 416pp.

Hackman, B.D., Charsley, T.J., Kagasi J., Key, R.M., Siambi, W.S. and Wilkinson, A.F., 1989. Geology of the Isiolo Area Report. Geological Survey of Kenya, No.**103**, 88 pp.

Henríquez, F. and Nyström, J.O., 1998 - Magnetite bombs at El Laco volcano, Chile, *GFF* 120, 269-271.

Henríquez, F., Naslund, H.R., Nyström, J.O., Vivallo, W., Aguirre, R., Dobbs, F.M. and Lledó, H., 2003. New field evidence bearing on the origin of the El Laco magnetite deposit, northern Chile - A. Discussion: Econ. Geol., v. **98**, 1497-1500.

Hildebrand, R.S., 1986. Kiruna-type deposits: their origin and relationship to intermediate subvolcanic plutons in the Great Bear Magmatic Zone, Northwest Canada. Econ. Geol. **81**, 640–659.

Hildenbrand, T.G., Stuart, W.D. and Talwani, P., 2001. Geological Structures Related to New Madrid Earthquakes near Memphis, Tennessee, Based on Gravity and Magnetic Interpretations. Environment Geology, **62**, 105-121.

Hitzman, M.W., Oreskes, N. and Einaudi, MT.1992. Geological characteristics and tectonic setting of Proterozoic iron oxide (Cu-U-Au-REE) deposits. Precamb Res 58: 241-287.

Holmes, A., 1951. The sequence of Precambrian orogenic belts in Southern and Central Africa. XVIII International Geological Congress, 14, pp. 254-269

Hood, P.J. and Teskey, D.J., 1989, Aeromagnetic gradiometer program of the Geological Survey of Canada: Geophysics, v. **54**, 1012-1022.

Horkel, A., Pohl, W., Niedermayr, G., Okelo, R., Wachira, K., and Nauta, J., 1979. Geology of the Taita Hills. Degree sheet 6^0 SE (Sheet 189/4). Geological Survey of Kenya Report **102**, 46 pp.

Huddleston, A. 1954. Geology of Kakamega district. Rept. No. **28**, Geological Survey of Kenya, 59p.

Hudleston, P. J., 1973. Fold morphology and some geometrical implications of theories of fold development: Tectonophysics, v. **16**, p. 1-46.

Hudleston, P. J. and Lan, L., 1993. Information from fold shapes. Journal of Structural Geology **15**, 253-264

Hutchison, C.S., 1974. Laboratory Handbook of Petrographic techniques, Wiley, New York.

Ichangi, D.W., 1993. Lithostratigraphic setting of mineralization in the Migori segment of the Nyanza Greenstone Belt. [In: Aketch, N.O.: Proceedings of the 5th Conference on the geology of Kenya. Geology for sustainable development. UNEP/UNESCO

Jensen, L.S., 1976. A new cation plot for classifying sub – alkali rocks: Ontario division of mines, miscellaneous paper **66**,22p.

Jones, M.P., 1987. Applied Mineralogy. Graham and Trotman, London, 468 pp.

ISSSC, 1976. International sub-commission on stratigraphic classification –International stratigraphic guide, Hedberg, H.D (Ed), John Wiley and Sons, N.Y., 200p.

Kazmin, V., 1972. Some aspects of Precambrian development in East Africa. Nature, **237**, pp. 158-160.

Kennedy, W., 1964. The structural differentiation of Africa in the Panafrican tectonic episode. 8th Annual Report of the Research Institute for African Geology. University of Leeds, pp. 48-49.

Key, R., Charsley, T.J., Hackman, B.D., Wilkinson, A.F. and Rundle, C.C., 1989. Superimposed Upper Proterozoic Collision controlled Orogenies in the Mozambique Belt of Kenya. Precambrian Research **44**, pp. 197-225.

Key, R. and Hill, P.G., 1989. Further evidence for the controls on the growth of vanadium grossular garnets in Kenya. Journal of Gemology **21**(7), pp. 412-422.

Kröner, A., 1977. Precambrian mobile belts of southern and eastern Africa- Ancient sutures of ensialic mobility; a case for crustal evolution towards plate tectonics. Tectonophysics **40**, pp. 101-135.

Kröner, A., 1984. Late Precambrian plate tectonics and orogeny: a need to redefine the term Pan African. In J. Klerkx, JMichot (eds.), African geology, pp. 23-27, Tervuren, Belgium

Kröner, A., 1991. African linkage of Precambrian Sri Lanka. Geological Research **80**(2), pp. 429-440.

Kusky, T.M., Bradley, D.C., Haeussler, P., and Karl, S., 1997, Controls on accretion of flysch and mélange belts at convergent margins: Evidence from the Chugach Bay thrust and Iceworm mélange, Chugach Terrane, Alaska: Tectonics, v. **16**, p. 855–878

Kusky, T.M., and Bradley D.C., 1999. Kinematic analysis of melange fabrics: examples and applications from the McHugh Complex, Kenai Peninsula, Alaska. Journal of Structural Geology. **21**, P.1773-1796.

Laajoki, K., 1991. Stratigraphy of the northern end of the early Proterozoic (Larelian) Kainuu schist belt and associated gneiss complexes, Finland. Bull. No. **358**, Geo. Surv. Finland, 105p.

Le Bas, M. J., LeMaitre, R., Streckeisen, A.H. and B. Zanet.1986. A chemical classification of volcanic rocks based on the total alkali-silica diagram. /. Petrol, **27**,745-750.

Leitch, A.M., Weinberg, R.F., 2002. Modelling granite migration by mesoscale pervasive flow. Earth Planet. Sci. Lett. 200, 131 – 146.

Lichte, F.E., Meier, A.L., and Crock, J.G., 1987. Determination of the rare-earth elements in geological materials by inductively coupled plasma mass spectrometry. Analytical Chemistry, **59**, pp. 1150-1157.

Lillesand, T.M. and Keifer, R.W., 1979. Remote sensing and image interpretation. Wiley, New York.

Lillesand, T.M., Kiefer, R.W. and Chipman, J.W., 2004. Remote sensing and image interpretation. 5th ed., John Wiley and sons Inc. New York, ISBN 0-471-25515-7,763P.

Loberg B and Horndahl A. 1983. Ferride geochemistry of Swedish Precambrian iron ores. MineraliumDeposita. **18**, 487-404.

Marchildon, N. and Brown, M., 2003. Spatial distribution of melt-bearing structures in anatectic rocks from Southern Brittany, France: implications for melt transfer at grain- to orogen-scale. Tectonophysics **364**, 215–235.

Martinsson, O. and Wanhainen, C., 2004. Cu-Au Deposits in the Gällivare Area In: Allen RL, Martinsson O, Weihed P (eds) Svecofennian Ore-Forming Environments: Volcanic-Associated Zn-Cu-Au-Ag, Intrusion- Associated Cu-Au, Sediment-Hosted Pb-Zn, and Magnetite-Apatite Deposits of Northern Sweden. Society of Economic Geologists, Guidebook Series, Vol. **33**, pp 161-165.

Mather, P.M., 1987. Computer processing of remotely sensed images, an introduction, John Wiley and sons, ISMN: 0-471-9064-4.

Mathu, E.M., 2000. Petrology and tectonic evolution of Archean and Neoproterozoic rocks of Kakamega – Kapsabet belt area, western Kenya. Unpublished Ph.D. thesis, University of Nairobi.

Mathu, E.M., 1992. The Mutito and Ikoo faults in the Pan – African Mozambique belt, Eastern Kenya. In: Mason, R. (Ed.), Basement Tectonics, Kluwer Academic publishers, Netherlands. pp 61 – 69

Mathu, E.M. and Tole M.P., 1984. Geology of the Ithanga Hills area. Journal of African Earth Sciences, **2**, pp. 1-16.

Mathu, E.M., Ngecu, W.M., Nyamai C.M. and Davies, T.C., 1991. Proterozoic island tectonism in the Kenyan Mozambique belt east of Nairobi. In: Muhongo, S. (Ed.) Proceedings of the International Geological Field Conference on the Mozambique belt in East Africa, Tanzania. **8**, pp.59 UNESCO, Nairobi, Kenya.

Maxwell, J.A., 1968. Rock and Minerals analysis, Jhon Wiley and Sons, N. Y., 584p.

McWilliams, M.O., 1981. Palaeomagnetism and Precambrian tectonic evolution of Gondwana. In Precambrian Plate Tectonics, Ed. A Kroner, pp. 649-87. Amsterdam: Elsevier

Meert, J.G., 2003. A synopsis of events related to the assembly of eastern Gondwana. Tectonphysics**362**, 1–40.

Meert, J.G., 2007. Testing the Neoproterozoic glacial models. Gondwana Research **11**, 573–574 pp.

Mehnert, K.R., 1968. Migmatites and the origin of granitic rocks. Elsevier, Amsterdam, pp 405

Middlemost, E. A. K., 1994. The basalt clan. Earth Sci. Rev., **11**, 337-364 pp.

Mokhtari, M.A.A. and Emami, M.H., 2013. REE patterns and REE mineralization in apatite-magnetite deposits of Bafq-Saghand District (Central Iran). Geosciences, Scientific Quarterly Journal, Special Issue, V. **17**, N. 1, P. 161-168.Journal of Tectonophysics , **221**, pp. 223-250.

Mosley, P.N. 1993. Geological evolution of the late Proterozoic "Mozambique Belt "of Kenya. Tectonophysics, 221:223-355.

Mücke, A. and Younessi, R., 1994. Magnetite-apatite deposits (Kiruna-type) along the SanandejSirjan zone and in the Bafq area, Iran, associated with ultramafic and calcalkaline rocks carbonatites. Mineralogy and Petrology **50**, 219-244.

Muhongo, S., 1994. Late Proterozoic collision tectonics in the Mozambique belt of East Africa: Evidence from ulunguru mountains (Tanzania). Journal of African Earth Sciences **19**, pp 103 – 108.

Muhongo, S., Hauzenberg, C. and Sommer, H., 2003. Vestiges of the Mesoproterozoic events in the Neoproterozoic Mozambique belt: the east African perspective in the Rodina puzzle. Gondwana Research, **6** (3): 409-416.

Mullen, E. D., 1983. $Mn/TiO_2/ P_2O_5$: A minor element discriminant for basaltic rocks of oceanic environments and its implications for petrogenesis. Earth Planet. Sci. Lett.,**62**, 53-62.

Naslund, H.R., Aguirre, R., Dobbs, F.M., Henriquez, F.J. and Nystrom, J.O., 2000. The origin, emplacement and eruption of ore magmas. IX CongresoGeologicoChilenoActas, Chile, V. **2**, P. 135-139.

Naslund, H.R., Henríquez, F., Nyström, J.O., Vivallo, W., and Dobbs, F.M., 2002. Magmatic iron ores and associated mineralization: examples from the Chilean High Andes and Coastal Cordillera. In: Porter, T.M. (Ed.), Hydrothermal Iron Oxide Copper– Gold and related deposits: A Global Perspective. Porter Geoscience Consultancy Publishing, Adelaide, pp. 207–228.

Nicol, A.W., 1995. Physicochemical methods of mineral analysis. New York: Plenum press, 508 pp.

Nureki, T.K., Suwa, K., Biyajima, Y., Saka and., Yusa,Y., 1977. Tectonic evolution of the Mozambique belt area south east of Machakos, Kenya. 2nd Prelim. Rept. African studies, Nagoya University. (Earth sciences **2**), 13 – 38.

Nyamai, C.M., Mathu, E.M., and Ngecu, W.M., 1993. A review of the geology of the Mozambique Belt in Kenya. In: Proceedings of the 9th International Geological Conference of the Geological Society of Africa – Regional Trends in African Geology, Accra, Ghana, pp 334 – 347.

Nyamai C.M., 1995. Petrography and Geochemical of Mozambique belt rocks of the Matuu area, Central Kenya. In: UNESCO, *Geology for Sustainable Development, Newsletter/Bulletin* 10, pp 154 – 155.

Nyamai, C.M., Opiyo-Akech, N., Gaciri, S.J. and Fujimaki, H., 1999. Geochemistry and tectonomagmatic affinities of the Mozambique belt intrusive rocks in Matuu-Masinga area, central Kenya. Gondwana Research, **2**, pp. 387-399.

Nyamai, C.M., Opiyo-Akech, N., Gaciri, S.J. and Fujimaki, H., 2000a. Structures, metamorphism and Geochronology of the Mozambique belt metamorphic and intrusive

rocks from Matuu-Masinga area, central Kenya. Journal of African Science Technology and Engineering Series **1**, pp. 47-55.

Nyamai, C.M., Opiyo-Akech, N., Gaciri, S.J., Johansson, B. and Sato, Y., 2000b. Petrography, mineral chemistry and thermobarometry of the Neoporoterozoic Mozambique belt rocks of Matuu-Masinga area, central Kenya. In: Mukhopadhaya, D., Ghosh, S.S., Chakrabarti, B.K., Sanyai, S. and Gupta, S.D. (Eds.),proceedings of the International seminar on Precambrian crust in Eastern and Central India, UNESCO-IUGS-IGCP-368, Journal of Geological Survey of India Special Publication, **57**, pp. 296-316.

Nyamai, C.M., Gaciri, S.J., Opiyo-Akech, N., Johansson, B. and Sato, Y., 2002. Conditions of pyroxene crystallization and thermobarometry of the Neoproterozoic Mozambique belt intrusive rocks of Matuu-Masinga area, central Kenya. In: Nyamai, C.M. and Maimba, M. (Eds.) Proceedings of the 8th and 9th Regional Conference of the Geology of Kenya, Geological Society of Kenya, pp. 116 -122.

Nyamai, C.M., Mathu, E.M., Opiyo-Akech, N., and Wallbrecher, E., 2003. A reappraisal of the geology, geochemistry, structures and tectonics of the Mozambique belt in Kenya, east of the rift system. African Journal of Science and Technology Science and Engineering Series, **4**, pp. 51-71.

Nyambok, I.O., Chorowicz, J., and Mathu E.M., 1993. The Late ProterozoicYatta shear zone: a possible lateral ramp across the Kenya Rift. In: Opiyo-Akech, N., (Ed.) Proceedings of the 5th Conference on the Geology of Kenya- Geology for Sustainable Development, UNEP/ UNESCO, Nairobi. pp. 69-77.

Nyström, J., and Henriquez, E., 1994. Magmatic features of iron ores of the Kiruna type inChile and Sweden: ore textures and magnetite geochemistry. Economic Geology,**89**,820–839.

Nystuen, 1989. Rules and recommendations for naming geological units in Norway. Norweigian Committee on Stratigraphy (NorskGeologiskTidsskrifft 69, Suppl. 1, 1-111)

Ochieng, J.O. 1993. Petrology of the gabbroic suite of rocks occurring south-east of Kenya. In: Opiyo-Akech, N. (Ed.) Proceedings of the 5th Conference of the Geology of Kenya - Geology for Sustainable Development, UNEP/ UNESCO, Nairobi pp. 33-36.

Opiyo-Akech, N. and Nyambok, I.O., 1984. Precambrian geology of the Ishiara area, Kenya. Journal of African Earth Sciences, **2**, pp. 61-65.

Park, C. F. Jr., 1961 - A magnetite "flow" in northern Chile, Economic Geology 56, 431-441.

Pearce, T.H., Gorman, B. E., and Birkett, T. C. 1977. The relationship between major element geochemistry and tectonic environment of basic and intermediate volcanic rocks. Earth and Planetary Science Letters **36**, 121–132.

Pearce, J.A., Harris, N.B.W., and Tindle, A.G., 1984. Trace element discrimination diagrams for the tectonic interpretation of granitic rocks: Journal of Petrology, v. **25**, p. 956-983.

Peters, W.C., 1983. The use of Multispectral Satellite imagery in exploration for petroleum and minerals. Philosophical Transactions of the Royal Society of London **A309**, pp. 243 – 255.

Pitcher, W.S., 1979.The nature, ascent and emplacement of granitic magmas, Journal of the Geological Society, v. **136**, p. 627-662.

Pohl, W. and Niedermayr, G., 1979. Geology of the Mwatate Quadrangle and the vanadium grossularite deposits of the area. Geological Survey of Kenya Report **101**, 56 pp.

Pohl, W. and Horkel, A., 1980. Notes on the geology and mineral resources of the Mtito Andei – Taita area (southern Kenya). Mitteilung der Oesterreich Geologische Gesellschaft, 73, pp. 135-152.

Pohl, W. and Prochaska W., 1983. Petrochemistry of some mafic and ultramafic rocks from the Mozambique belt, Northern Tanzania. Journal of African Earth Sciences, **1**, pp. 183-191.

Pryer, L.L., 1993. Microstructures in feldspars from a major crustal thrust zone: the Grenville front, Ontario, Canada Journal of Structural Geology, **15**, 21-36

Ramsay, J. G. 1962. Interference patterns produced by the superposition of folds of similar types. Journal of Geology. **70**: 466–481

Ramsay, J. G., 1967. Folding and Fracturing of Rocks. McGraw-Hill, New York. 568 pp

Ramsay, J.G. and Huber, M.I., 1987. The Techniques of modern structural geology, Volume **2**, Folds and fractures. Academic Press, London

Reid, A. B., Allsop, J. M., Granser, H., Millett, A. J. and Somerton, I. W., 1990. Magnetic interpretation in three dimensions using Euler deconvolution. Geophysics, **55**, pp. 80-91.

Reynolds, J.M. 1997. An Introduction to Applied and Environmental Geophysics, John Wiley and Sons Ltd, Chichester, 796 pp, first edition.

Rhodes, A.L. and Oreskes N., 1999. Oxygen Isotope Composition of Magnetite Deposits at El Laco, Chile: Evidence of Formation from Isotopically Heavy Fluids In: Skinner BJ (ed) Geology and Ore Deposits of the Central Andes. Society of Economic Geologists, Special Publication 7, pp 333-351.

Rhodes, A.L., Oreskes, N. and Sheets, S., 1999. Geology and rare earth element geochemistry of magnetite deposits at El Laco, Chile In: Skinner BJ (ed) Geology and ore deposits of the Central Andes. Society of Economic Geologists, **17**, pp 299-332.

Richards, J.A., 1995. Remote sensing, digital Image processing, and introduction, Sec. Ed., Springer, P.340.

Riddihough, R.P., 1971. Diurnal corrections to magnetic surveys. an assessment of errors. Geophysical Prospecting **19**, 551-567.

Roberts, R. G. and Sheahan, P. A., 1989.Ore Deposit Models" (Geoscience Canada Reprint Series, 3). St Johns, Newfoundland (Geological Association of Canada), 194 pp.

Rose, A.W., Hawkes, H.E. and Webb, J.S., 1979. Geochemistry in mineral exploration. Academic press, London. 586 pp.

Sanders, L.D., 1954. Geology of Kitui Area, Report 30. Geological Survey of Kenya, 53 pp.

Sanders, L.D. 1965. Geology of the contact between the Nyanza Shield and the Mozambique belt in western Kenya. Rept. Geol. Surv. Kenya, No.7

Saggerson, E.P., 1957. Geology of south Kitui area, Report 37. Geological Survey of Kenya, 57 pp.

Schissel and Aro, P., 1992. The early Proterozoic sedimentary iron and manganese deposits and their tectonic setting. Economic Geology, **97**(5), 1367-1374.

Schlüter, T., 1997. Geology of East Africa, Gebrüder Borntraeger. Berlin, Stuttgart, 484 pp

Schoeman, J. J., 1948."A geological reconnaissance of the area west of Kitui Township". Report No. **11**, Geol. Surv. Kenya.

Shackleton, R.M., 1976. Possible late – Precambrian ophiolites in Africa and Brazil. Ann. Report Res. Institute of African Geology, **20**: 3-7

Shackleton, R.M., 1986. The final collision zones between East and West Gondwana: where is it? J. African Earth science, **23**(3): 271- 287

Shaw, H.R., 1972. Viscosities of magmatic silicate liquids: An empirical method of prediction. American Journal of Science,**272**:870-893

Sillitoe, R.H. and Burrows, D.R., 2002. New field evidence bearing on the origin of the El Laco magnetite deposit, Northern Chile. Economic Geology,**97**, 1101–1109.

Simonet, C., 2000. Geology of the Yellow Mine (Taita- Taveta District, Kenya) and other yellow tourmaline deposits in East Africa. Journal of Gemology, **27**, pp.11-29.

Stern, J.R., 1994. Arc assembly and continental collision in the Neoproterozoic East African Orogeny: Implication for the consolidation of Gondwanaland, Annual Review in Earth Planet Sciences, **22**, pp. 319 – 351.

Stern, J.R., 2002. Crustal evolution in the East African Orogen: a neodymium isotopic perspective. Journal of African Earth Science.**34**(3-4): 109-117.

Stern, J.R., 2008. Neoproterozoic crustal growth: The solid earth system during a critical episode of earth history, Gondwana research, **14** (1-2): 33-50

Suleiman, A., 1999. Colored stones in Africa and Madagascar. Journal of Gems and Gemology, **35**(3), pp. 66-67.

Survey of Kenya, 1980. Agro – climatic zone maps, 1980, 156 pp.

Suwa, K., Suzuki, K, Miyakawa, K. and Agata, T., 1979. Vanadium and vanadium grossulars from the Mozambique metamorphic rocks, Mgama Ridge, Kenya. 4th Preliminary Report of African Studies, Nagoya University, pp. 87-96.

Suwa, K., 1981. Petrological studies on the African continent. 6th Preliminary Report of African Studies, Nagoya University, pp. 3-13.

Telford, W.M., Geldart, L.P. and Sheriff, R.E., 1990. Applied geophysics, 2nd edition, Cambridge University Press, Cambridge, 792p.

Thompson, D. T., 1982.EULDEP: A new technique for making computer-assisted depth estimates from magnetic data. Geophysics, **47**: 31-37.

Torab, F.M. 2008. Geochemistry and metallogeny of magnetite-apatite deposits of the Bafq Mining District, Central Iran. Unpublished PhD thesis, Clausthal University of Technology.

Treloar, P.J. and Colley, H., 1996. Variations in F and Cl contents in apatites from magnetite-apatite ores in northern Chile, and their ore- genetic implications. Mineral Magazine**60**: 285-301.

Trendall, A.F., 1983. The Hamersley Basin. In: Trendall, A.F. & Morris, R.C. (editors), Iron-formation: facts and problems. 69- 129. Elsevier, Amsterdam.

Twiss, R.J., 1988. Description and classification of folds in single surfaces. Journal of Structural geology **10**,607-623.

USGS (http:/www.earthexplorer.gov).Valid on 12th October 2011.

USGS (U.S. Geological Survey), 2014. Mineral commodity summaries-Iron ore, p. 83-90.

Vigneresse, J.L., Barbey, P. and Cuney, M., 1996. Rheological transitions during partial melting and crystallization with application to felsic magma segregation and transfer. Journal of Petrology,**37**, 1579 – 1600.

Vearncombe, J.R., 1983.A dismembered ophiolite from the Mozambique Belt, West Pokot, Kenya. Journal of African Earth Sciences, **1**, pp. 133-143.

Vernon, R., 2000. Review of microstructural evidence of magmatic and solid-state flow. Electronic Geosciences **5** (2), 1436e2511

Walsh, J., 1963. Geology of Ikutha Area, Report **56**. Geological Survey of Kenya, 78pp.

Weinberg, R.F., and Mark, G., 2008. Magma migration, folding, and disaggregation of migmatites in the Karakoram shear zone, Ladakh, NW India. In: Geological Society of America Bulletin, vol. **120**. http://dx.doi.org/10.1130/B26227.1, pp. 994e1009.

Whitney, D., Teyssier, C., and Vanderhaeghe, O., 2004. Gneiss domes and crustal flow. In: Geological Society of America Special Papers, vol. **380**. http://dx.doi.org/ 10.1130/0-8137-2380-9.15, pp. 15e33.

Winchester, J.A., 1972. The petrology of Moinian calc-silicate gneisses from Fannich Forest and their significance as indicators of metamorphic grade, Journal of Petrology, 13, 405-424.

Winchester, J.A., 1974, The zonal pattern of regional metamorphism in the Scottish Caledonies, Journal of the Geological Society, London, **130**, 509-524.

Williams, H.; Turner, F. J. & Gilbert, C. M. 1982. Petrography. An introduction to the study of rocks in thin sections (2nd Ed.). W.H. Freeman and Company, S. Francisco, 626 pp

Wilson, C.J.L., 1980. Shear zones in a pegmatite: a study of albite-mica-quartz deformation, Journal of Structural Geology, **2**, 203-209

Wright, S. F., 1986. On the origin of iron ores of the Kiruna Type - An additional discussion. Economic Geology,**81**, 192-206.

Yardley, B.W.D.1989. An introduction to metamorphic petrology. Longman, Essex, 248 pp.

Zwart, H. J., 1967. The duality of orogenic belts. Geology of Mijnbouw. **46**, 283-309.

PAPERS PUBLISHED IN PEER REVIEWED JOURNALS

iii. Waswa A.K, Nyamai C.M., Mathu E.M, and Ichang'i D.W, 2015. Application of Magnetic Survey in the Investigation of Iron Ore Deposits and Shear Zone Delineation: Case Study of Mutomo-Ikutha Area, SE Kenya. International Journal of Geological sciences, 6, 729-740.

iv. Waswa A.K., Nyamai C.M., Mathu E.M. and Ichang'i, D.W. 2015. Integration of Geological Mapping and Remote Sensed Studies for the Discovery of Iron—Ore Mineralization in Mutomo—Ikutha Area, SE Kenya. *Universal Journal of Geoscience*, 3, 39-50.

LIST OF APPENDICES

APPENDIX A: CHEMICAL ANALYSIS OF IRON ORE AND HOST ROCKS.

Chemical analysis of the iron ore and host rocks. Analysis done using atomic absorption spectrophotometer (AAS). Elements expressed in weight percent (Wt. %).

REF.NO.	Longitude (UTM)	Latitude (UTM)	SiO_2 Wt.%	Al_2O_3 Wt.%	CaO Wt.%	MgO Wt.%	Na_2O Wt.%	K_2O Wt.%	TiO_2 Wt.%	MnO Wt.%	Fe_2O_3 Wt.%	P_2O_5 Wt.%	LOI Wt.%	TOTAL Wt.%	Lithology-Mineral/rock type
TA-0	408000	9770000	43.00	22.80	13.00	5.00	3.87	0.59	0.96	0.60	6.20	<0.05	3.71	99.73	Amphibolite
T1-1	409000	9770000	2.91	0.60	8.40	0.24	0.17	0.03	0.05	0.40	81.30	5.70	<0.05	99.80	Magnetite +Apt+Di
T1-2	408000	9769000	3.83	0.76	3.77	0.20	0.14	0.03	0.30	0.40	86.10	4.10	<0.05	99.63	Magnetite +Apt
T2-1	410000	9770000	6.97	1.47	0.99	0.19	0.17	0.03	0.18	0.40	88.30	1.00	<0.05	99.70	Magnetite
T2-2	409000	9769000	4.05	0.33	0.25	0.30	0.12	0.03	1.50	0.60	89.00	3.00	<0.05	99.18	Magnetite +Apt
T2-3	408020	9768020	1.72	0.67	5.22	0.27	0.14	0.02	<0.05	0.40	85.00	5.90	<0.05	99.34	Magnetite
T2-4	408000	9768000	4.78	0.11	0.60	0.47	0.11	0.03	1.70	0.60	90.70	0.50	<0.05	99.60	Magnetite +Apt
T3-1	411000	9770000	41.00	22.80	13.00	5.00	4.87	0.59	0.96	0.60	7.20	<0.05	3.71	99.73	Altered gneiss
T3-2	410000	9769000	6.21	1.52	0.50	0.23	0.24	0.04	0.46	0.40	89.60	0.20	<0.05	99.40	Magnetite
T3-3	409000	9768000	5.38	1.25	0.70	0.22	0.20	0.03	0.14	0.40	89.90	1.70	<0.05	99.92	Magnetite
T3-4	408000	9767000	7.14	1.35	0.89	0.22	0.19	0.03	0.25	0.40	88.00	0.80	<0.05	99.27	Magnetite
T4-1	412000	9770000	36.52	8.05	1.25	5.83	4.43	5.48	0.18	0.40	36.35	1.30	<0.05	99.79	Magnetite+Apt +Hbl
T4-2	411000	9769000	32.02	5.66	0.63	9.00	1.05	0.27	3.80	0.60	45.80	0.70	<0.05	99.53	Magnetite+Hbl gneiss
T4-3	410000	9768000	6.16	1.35	0.62	0.21	0.24	0.04	0.27	0.04	90.50	0.40	<0.05	99.83	Magnetite+Apt +Hbl
T4-4	409000	9767000	26.01	5.10	12.20	7.00	0.95	0.47	3.74	0.40	38.40	5.20	<0.05	99.93	Hbl +Pyx (Di+Hyp) gneiss
T4-5	408000	9766000	47.70	16.50	14.60	8.20	2.12	0.64	0.61	0.17	8.00	<0.05	0.67	99.21	Hbl +Pyx (Di+Hyp) gneiss
T5-1	413000	9770000	47.90	16.20	15.20	2.54	2.59	0.32	0.76	0.27	13.20	<0.05	0.46	99.44	Hbl +Pyx (Di+Hyp) gneiss
T5-2	412000	9769000	33.50	28.10	15.40	0.92	0.25	2.86	0.84	0.28	13.60	0.30	3.16	99.21	Hbl +Pyx (Di+Hyp) gneiss
T5-3	411000	9768000	44.02	15.60	14.20	7.40	2.19	0.38	0.62	0.20	15.60	<0.05	0.21	99.42	Hbl +Pyx (Di+Hyp) gneiss
T5-4	410000	9767000	1.64	0.55	1.99	0.27	0.13	0.04	0.76	0.05	91.50	2.70	0.00	99.63	Magnetite + Apt
T5-5	409000	9766000	2.06	0.93	3.67	0.27	0.11	0.02	<0.05	0.08	87.20	5.20	<0.05	99.54	Magnetite + Apt
T5-6	408100	9765100	2.57	0.98	1.30	0.34	0.14	0.02	<0.05	0.06	93.10	1.00	<0.05	99.51	Magnetite

Chemical analysis of the iron ore and host rocks. Analysis done using atomic absorption spectrophotometer (AAS). Elements expressed in weight percent (Wt. %).

REF.NO.	Longitude (UTM)	Latitude (UTM)	SiO_2 Wt.%	Al_2O_3 Wt.%	CaO Wt.%	MgO Wt.%	Na_2O Wt.%	K_2O Wt.%	TiO_2 Wt.%	MnO Wt.%	Fe_2O_3 Wt.%	P_2O_5 Wt.%	LOI Wt.%	TOTAL Wt.%	Lithology-Mineral/rock type
T5-7	408000	9765000	4.58	0.73	1.08	0.21	0.14	0.04	0.29	0.02	90.70	1.90	<0.05	99.69	Magnetite
T6-1	414000	9770000	33.01	9.40	9.45	9.57	3.20	3.67	<0.05	0.05	30.25	1.00	<0.05	99.60	Magnetite +Apt
T6-2	413000	9769000	25.57	12.98	10.30	5.34	8.14	10.02	<0.05	0.06	26.40	1.00	<0.05	99.81	Magnetite +Apt
T6-3	412000	9768000	39.00	15.60	15.00	10.00	2.17	1.01	0.42	0.60	15.40	<0.05	<0.05	99.20	Hbl +Pyx (Di+Hyp) gneiss
T6-4	411000	9767000	25.57	12.98	10.30	5.34	8.14	10.02	<0.05	0.06	26.40	1.00	<0.05	99.81	Qtz-Feldspar gneiss +Mn
T6-5	410040	9766040	<0.05	0.85	2.55	0.42	0.11	0.02	<0.05	0.07	93.20	2.70	<0.05	99.92	Magnetite +Apt
T6-6	409980	9765980	<0.05	0.85	2.55	0.42	0.11	0.02	<0.05	0.07	93.20	2.70	<0.05	99.92	Magnetite +Apt
T6-7	409000	9765000	25.10	3.76	2.56	2.24	0.65	0.94	0.36	7.68	55.50	0.60	<0.05	99.39	Hbl+Pyx+Bt+Magnetite
T6-8	408000	9764000	28.75	4.42	3.71	4.20	0.73	1.00	0.39	5.86	48.40	0.60	1.53	99.59	Magnetite
T7-1	415000	9770000	68.80	5.71	2.15	1.97	1.43	2.31	0.65	2.50	12.60	0.30	1.32	99.74	Biotite gneiss
T7-2	414000	9769000	45.90	7.14	10.60	13.40	1.15	0.25	0.99	0.26	20.10	<0.05	0.14	99.93	hornblende gneiss
T7-3	413000	9768000	45.01	10.35	9.02	5.56	2.04	0.03	<0.05	0.09	26.35	0.70	<0.05	99.15	Biotite gneiss
T7-4	412000	9767000	37.50	9.05	9.02	6.06	5.07	3.05	0.24	0.06	28.80	1.00	<0.05	99.85	Hbl +Pyx (Di+Hyp) gneiss
T7-5	411000	9766000	62.40	12.60	3.11	0.23	4.37	6.20	0.76	0.30	9.30	0.30	0.15	99.72	Mag+Apt+Hbl+Di +Sphene
T7-6	410000	9765000	<0.05	0.79	3.49	0.41	0.10	0.01	<0.05	0.06	91.40	3.60	<0.05	99.86	Magnetite +Sphene
T7-7	409000	9764000	23.00	4.89	10.00	7.80	1.00	0.25	6.80	0.40	40.02	5.20	0.50	99.86	Magnetite+apt+hbl
T7-8	408000	9763000	47.60	7.75	10.80	12.20	1.28	0.30	1.13	0.25	18.00	<0.05	0.50	99.81	Qtz-Feldspar gneiss +Mn
T8-1	415000	9769000	45.52	9.23	9.20	11.50	0.55	0.07	0.90	0.40	22.00	<0.05	<0.05	99.37	Qtz-Feldspar gneiss +Mn
T8-2	414000	9768000	63.47	4.48	3.70	2.40	0.71	0.59	0.15	6.24	16.40	<0.05	1.46	99.60	Hbl +Pyx gneiss
T8-3	413000	9767000	68.74	4.32	2.79	2.73	0.82	1.16	0.30	5.08	11.80	1.00	1.14	99.88	biotite hornblende gneiss
T8-4	412000	9766000	40.20	19.00	18.30	8.60	2.08	0.40	0.17	0.22	9.80	<0.05	0.50	99.27	Diopside +Magnetite
T8-5	411000	9765000	45.04	8.56	7.02	6.70	2.05	1.05	0.30	0.60	27.04	0.70	<0.05	99.06	Amphibolite
T8-6	410000	9764000	1.58	0.91	0.96	0.28	0.14	0.04	0.16	0.40	94.20	0.60	<0.05	99.27	Magnetite
T8-7	409000	9763000	44.00	22.00	13.20	6.00	3.79	0.56	0.92	0.06	7.80	<0.05	0.86	99.19	hornblende gneiss
T8-8	408000	9762000	51.00	21.60	6.73	5.80	6.80	2.34	0.67	0.60	3.40	0.30	0.50	99.74	diopside
T9-1	415000	9768000	48.50	9.35	1.34	6.68	6.35	3.25	0.10	0.40	23.80	0.10	<0.05	99.87	biotite hornblende gneiss
T9-2	414000	9767000	46.06	10.90	5.29	4.03	6.85	2.05	3.65	0.05	20.05	0.80	<0.05	99.73	biotite hornblende gneiss
T9-3	413000	9766000	46.78	9.02	2.01	10.50	0.12	0.04	0.19	0.04	30.08	0.60	<0.05	99.38	Magnetite + Hbl gneiss
T9-4	412000	9765000	49.50	7.20	8.60	2.80	0.30	0.04	0.26	0.02	30.02	0.50	<0.05	99.24	Hbl +Pyx (Di+Hyp) gneiss

Chemical analysis of the iron ore and host rocks. Analysis done using atomic absorption spectrophotometer (AAS). Elements expressed in weight percent (Wt. %).

REF.NO.	Longitude (UTM)	Latitude (UTM)	SiO_2 Wt.%	Al_2O_3 Wt.%	CaO Wt.%	MgO Wt.%	Na_2O Wt.%	K_2O Wt.%	TiO_2 Wt.%	MnO Wt.%	Fe_2O_3 Wt.%	P_2O_5 Wt.%	LOI Wt.%	TOTAL Wt.%	Lithology-Mineral/rock type
T9-5	411000	9764000	38.05	2.42	4.97	2.50	1.08	0.05	0.18	0.06	45.00	4.90	<0.05	99.21	Magnetite +Apt
T9-6	410000	9763000	6.06	7.80	5.80	3.90	1.43	0.26	1.90	0.29	71.52	<0.05	0.41	99.37	Magnetite
T9-7	409000	9762000	41.90	9.02	2.01	10.50	0.12	0.04	0.19	0.04	35.05	0.50	<0.05	99.37	magnetite + biotite gneiss
T9-8	408000	9761000	38.47	6.97	7.07	2.80	0.16	0.03	0.24	0.03	38.80	4.60	<0.05	99.17	Magnetite in sandy
T10-1	415000	9767000	40.24	2.71	9.40	6.20	0.54	0.37	0.12	0.20	39.00	0.02	0.59	99.39	hornblende biotite gneiss
T10-2	414000	9766000	34.00	9.50	9.09	6.95	3.06	4.25	0.00	0.06	32.00	0.90	<0.05	99.81	biotite hornblende gneiss
T10-3	413000	9765000	43.02	10.10	3.16	2.10	1.40	1.70	0.17	0.03	36.86	0.80	<0.05	99.34	Hbl +Pyx (Di+Hyp) gneiss
T10-4	412000	9764000	70.60	11.40	0.71	0.14	3.18	8.60	0.57	0.20	2.91	0.80	0.68	99.79	silica sand
T10-5	411000	9763000	43.30	14.70	6.53	16.00	1.18	0.25	0.62	0.16	15.00	<0.05	1.41	99.15	Amphibolite
T10-6	410000	9762000	37.85	6.25	8.13	4.35	1.95	0.02	0.25	0.40	31.75	8.90	<0.05	99.85	Hbl +Pyx gneiss
T10-7	409000	9761000	35.00	18.40	16.60	8.20	3.16	1.37	0.89	0.40	11.20	<0.05	4.55	99.77	Amphibolite
T10-8	408000	9760000	45.91	15.70	18.20	8.60	2.10	0.51	0.15	0.23	7.80	<0.05	0.42	99.62	Amphibolite
T11-1	415000	9766000	47.00	18.00	7.41	5.20	4.10	2.89	1.67	0.40	12.40	0.20	0.40	99.67	Amphibolite
T11-2	414000	9765000	43.00	18.20	13.80	7.60	3.60	1.44	0.77	0.40	10.20	<0.05	0.71	99.72	Amphibolite
T11-3	413000	9764000	44.19	12.70	22.80	12.60	0.73	0.32	<0.05	0.15	4.47	<0.05	1.45	99.41	Amphibolite
T11-4	412000	9763000	46.45	14.20	6.13	3.60	3.10	4.41	3.50	0.12	16.60	1.00	0.74	99.85	biotite hornblende gneiss
T11-5	411000	9762000	41.57	10.53	9.46	8.45	0.10	0.03	<0.05	0.08	29.05	0.60	<0.05	99.87	Hbl +Pyx (Di+Hyp) gneiss
T11-6	410360	9761360	3.61	0.55	1.33	2.60	0.11	0.03	<0.05	0.06	90.40	0.90	<0.05	99.59	Magnetite+Apt
T11-7	410000	9761000	43.78	11.70	8.80	5.20	3.38	1.77	1.03	0.20	23.20	<0.05	0.40	99.46	Hbl +Pyx (Di+Hyp) gneiss
T11-8	409000	9760000	47.06	16.00	2.51	5.40	3.28	7.40	1.24	0.17	14.80	1.90	0.00	99.76	Hbl +Pyx (Di+Hyp) gneiss
T12-1	415000	9765000	43.54	14.80	16.00	9.00	2.40	0.44	0.55	0.18	12.60	<0.05	0.30	99.81	hornblende gneiss
T12-2	414000	9764000	44.32	18.00	9.40	5.20	3.28	1.76	1.23	0.21	15.90	<0.05	0.42	99.72	biotite hornblende gneiss
T12-3	413000	9763000	42.18	10.32	5.20	5.62	0.13	0.11	2.25	0.17	32.80	0.50	<0.05	99.28	Magnetite
T12-4	412000	9762000	38.45	8.03	9.05	3.50	1.80	0.04	2.31	0.05	35.50	0.50	<0.05	99.23	Magnetite +Hbl gneiss
T12-5	411000	9761000	2.52	0.24	0.22	0.18	0.15	0.07	23.00	0.40	72.00	0.40	<0.05	99.18	Magnetite
T12-6	410980	9760980	5.23	1.47	1.81	0.20	0.19	0.03	0.70	0.04	88.10	1.90	<0.05	99.67	Magnetite+Apt
T12-7	410000	9760000	26.40	12.10	12.52	8.02	12.50	10.07	0.10	0.40	17.50	<0.05	<0.05	99.61	Diopside+hbl gneiss
T13-1	415000	9764000	47.25	11.67	3.02	6.25	0.19	0.03	0.70	0.04	29.42	0.50	<0.05	99.07	biotite hornblende gneiss
T13-2	414020	9763020	24.40	7.10	10.31	7.70	10.32	10.07	0.10	0.40	29.50	<0.05	<0.05	99.90	Amphibolite

Chemical analysis of the iron ore and host rocks. Analysis done using atomic absorption spectrophotometer (AAS). Elements expressed in weight percent (Wt. %).

REF.NO.	Longitude (UTM)	Latitude (UTM)	SiO_2 Wt.%	Al_2O_3 Wt.%	CaO Wt.%	MgO Wt.%	Na_2O Wt.%	K_2O Wt.%	TiO_2 Wt.%	MnO Wt.%	Fe_2O_3 Wt.%	P_2O_5 Wt.%	LOI Wt.%	TOTAL Wt.%	Lithology-Mineral/rock type
T13-3	414000	9763000	37.70	10.67	7.02	6.25	9.19	3.35	0.01	0.04	24.50	0.60	<0.05	99.33	Magnetite + Clay
T13-4	413000	9762000	24.40	12.00	9.68	7.90	7.30	10.02	0.10	0.40	28.00	<0.05	<0.05	99.80	Magnetite+ biotite gneiss
T13-5	412000	9761000	1.61	0.55	1.33	1.60	0.11	0.03	<0.05	0.06	90.40	4.02	<0.05	99.71	Magnetite
T14-6	411000	9760000	27.50	10.46	10.02	9.35	7.80	0.03	<0.05	0.06	33.45	0.90	<0.05	99.57	Magnetite + Apt
T14-1	415000	9763000	23.50	10.46	10.02	9.35	7.80	4.03	<0.05	0.06	33.45	0.90	<0.05	99.57	Magnetite+Apt +Sphn+Hbl
T14-2	414000	9762000	33.50	10.46	10.02	9.35	7.80	4.03	<0.05	0.06	23.45	0.90	<0.05	99.57	Magnetite
T14-3	413000	9761000	28.50	10.46	11.02	9.80	7.80	0.03	<0.05	0.06	31.45	0.10	<0.05	99.22	Mag+Apt +Spn+Hbl+Di
T15-1	415000	9761000	27.50	9.50	10.80	10.35	8.85	0.04	<0.05	0.06	32.05	0.10	<0.05	99.25	Hbl +Pyx (Di+Hyp) gneiss
T15-2	414980	9760980	48.30	9.35	2.56	1.02	6.90	10.35	0.95	0.05	10.36	0.00	9.50	99.34	Hbl +Pyx (Di+Hyp) gneiss
T15-3	413000	9760000	40.25	26.10	1.25	0.92	5.20	9.02	0.84	0.28	9.60	0.30	6.20	99.96	Hbl +Pyx (Di+Hyp) gneiss
T15-4	412000	9760000	47.50	23.20	1.50	1.25	2.65	5.48	0.70	0.09	8.20	<0.05	9.34	99.91	Hbl +Pyx (Di+Hyp) gneiss
T16-1	415000	9762000	49.01	21.50	2.50	1.10	2.57	6.53	0.21	0.01	8.25	<0.05	7.45	99.13	Hbl +Pyx (Di+Hyp) gneiss
T16-2	414000	9761000	33.50	28.10	15.40	0.92	0.25	2.86	0.84	0.28	13.60	0.30	3.16	99.21	Hbl +Pyx (Di+Hyp) gneiss
T16-3	414000	9760000	32.00	2.02	30.01	8.08	<0.05	<0.05	<0.05	<0.05	<0.05	<0.05	27.09	99.20	Hbl +Pyx (Di+Hyp) gneiss
TB-0	415000	9760000	33.50	28.10	15.40	0.92	0.25	2.86	0.84	0.28	13.60	0.30	3.16	99.21	Hbl +Pyx (Di+Hyp) gneiss
		Min.	**1.58**	**0.11**	**0.22**	**0.14**	**0.10**	**0.01**	**0.00**	**0.01**	**1.91**	**0.00**	**0.00**		
		Max.	**70.60**	**28.10**	**30.01**	**16.00**	**12.50**	**10.35**	**23.00**	**7.68**	**94.20**	**8.90**	**27.09**		
		Aver.	**32.86**	**9.61**	**7.30**	**4.78**	**2.53**	**1.91**	**1.16**	**0.51**	**38.48**	**1.52**	**2.54**		

APPENDIX B: CHEMICAL ANALYSIS OF MAGNETITE ORE.

Chemical analysis of magnetite ore. Analysis done using the X-ray fluorescence (XRF) method. Elements expressed in weight percent (wt. %).

No.	Long. (UTM)	Lat. (UTM)	Ti Wt. %	V Wt. %	Cr Wt. %	Mn Wt. %	Fe Wt. %	Co Wt. %	Ni Wt. %	Cu Wt. %	Zn Wt. %	Zr Wt. %	Nb Wt. %	Mo Wt. %	Ag Wt. %	Sn Wt. %	Sb Wt. %	W Wt. %	Pb Wt. %	Iron Ore elements association
1	408391.000	9768300.000	0.698	0.354	0.241	2.447	88.197	0.889	0.845	2.826	< 0.03	< 0.03	< 0.03	1.295	< 0.03	< 0.03	< 0.03	0.661	<0.03	Fe+(Ti, Mn,Co,Ni,Cu,Mo, W)
2	408445.000	9768322.000	0.694	0.282	0.453	3.071	84.517	0.907	0.793	4.674	<0.03	<0.03	<0.03	1.857	<0.03	<0.03	<0.03	0.456	<0.03	Fe+(Ti, Mn,Co,Ni,Cu,Mo, W)
3	408486.000	9768324.000	0.554	0.323	0.291	3.225	86.295	0.811	0.736	3.502	<0.03	<0.03	<0.03	1.419	<0.03	<0.03	<0.03	0.681	<0.03	Fe+(Ti, Mn,Co,Ni,Cu,Mo, W)
4	408434.000	9768321.000	0.771	0.613	0.690	1.897	83.678	0.566	2.958	3.130	< 0.03	< 0.03	< 0.03	0.300	< 0.03	< 0.03	< 0.03	0.984	<0.03	Fe+(Ti,Cr, V,Mn,Co,Ni,Cu, W)
5	408583.000	9768317.000	0.679	0.685	0.603	2.285	83.841	0.697	2.901	2.952	<0.03	<0.03	<0.03	0.271	<0.03	<0.03	<0.03	0.995	<0.03	Fe+(Ti, CrV,Mn,Co,Ni,Cu, W)
6	408594.000	9768263.000	0.408	0.823	0.448	0.631	86.757	0.109	2.073	1.977	<0.03	<0.03	<0.03	0.146	<0.03	<0.03	<0.03	0.976	<0.03	Fe+(Ti,V,Mn,Ni,Cu, W)
7	408538.000	9768262.000	0.996	0.710	0.539	0.849	83.562	0.306	2.737	2.964	< 0.03	< 0.03	< 0.03	0.165	< 0.03	< 0.03	< 0.03	0.888	<0.03	Fe+(Ti,V,Cr,Mn,Ni,Cu, W)
8	408497.000	9768248.000	0.542	0.017	0.267	0.400	96.073	<0.03	0.988	0.020	<0.03	<0.03	<0.03	0.072	<0.03	<0.03	<0.03	0.589	<0.03	Fe+(Ti,V,Ni,Cu, W)
9	408447.000	9768232.000	0.101	0.260	1.103	3.354	79.641	0.928	4.278	5.524	<0.03	<0.03	<0.03	0.346	<0.03	<0.03	<0.03	<0.03	<0.03	Fe+(Ti,Mn,Cr,Co,V,Ni,Cu,)
10	408397.000	9768222.000	0.500	0.652	1.828	4.244	73.289	1.498	5.509	9.639	< 0.03	< 0.03	< 0.03	0.617	< 0.03	< 0.03	< 0.03	<0.03	<0.03	Fe+(Ti,Mn,Mo,Cr,Co,V,Ni,Cu,)
11	408422.000	9768174.000	0.820	0.972	1.323	3.175	78.045	1.095	5.291	7.358	<0.03	<0.03	<0.03	0.423	<0.03	<0.03	<0.03	<0.03	<0.03	Fe+(Ti,Mn,Cr,Co,V,Ni,Cu,)
12	408463.000	9768186.000	0.034	0.230	<0.03	3.724	69.556	2.509	6.748	4.769	<0.03	<0.03	0.446	1.286	<0.03	<0.03	<0.03	7.511	<0.03	Fe+(Ti,V,Mn,Co,Ni,Cu,Mo,W)
13	408509.000	9768197.000	0.656	0.754	2.114	3.478	73.213	1.216	5.772	9.973	< 0.03	< 0.03	<0.03	0.595	< 0.03	< 0.03	< 0.03	<0.03	<0.03	Fe+(Ti,Mn,Mo,Cr,Co,Fe,V,Ni,Cu,)
14	408562.000	9768209.000	0.450	0.827	<0.03	6.341	73.266	2.428	3.584	4.710	<0.03	<0.03	0.359	0.774	<0.03	<0.03	<0.03	5.578	<0.03	Fe+(Ti,V,Mn,Co,Ni,Cu,Mo,W)

Chemical analysis of magnetite ore. Analysis done using the X-ray fluorescence (XRF) method. Elements expressed in weight percent (wt. %).

No.	Long. (UTM)	Lat. (UTM)	Ti Wt. %	V Wt. %	Cr Wt. %	Mn Wt. %	Fe Wt. %	Co Wt. %	Ni Wt. %	Cu Wt. %	Zn Wt. %	Zr Wt. %	Nb Wt. %	Mo Wt. %	Ag Wt. %	Sn Wt. %	Sb Wt. %	W Wt. %	Pb Wt. %	Iron Ore elements association
15	408611.000	9768209.000	0.666	0.030	1.172	5.069	77.660	1.393	4.358	6.369	<0.03	<0.03	<0.03	0.246	<0.03	<0.03	<0.03	<0.03	<0.03	Fe+(Ti,V,Mn,Cr,Ni,Cu)
16	408632.000	9768166.000	0.492	0.596	0.490	2.337	83.091	0.444	2.597	2.205	< 0.03	<0.03	<0.03	0.076	< 0.03	< 0.03	< 0.03	0.804	<0.03	Fe+(Ti,V<Mn,Ni,Cu,W)
17	408577.000	9768161.000	0.111	0.602	0.549	2.503	80.228	0.681	2.878	2.856	<0.03	<0.03	<0.03	0.116	<0.03	<0.03	<0.03	0.843	<0.03	Fe+(Ti,V,Cr,Mn,Co,Ni,Cu,W)
18	408531.000	9768135.000	0.759	0.463	0.851	4.143	77.839	0.899	3.656	4.658	<0.03	<0.03	<0.03	0.144	<0.03	<0.03	<0.03	0.063	<0.03	Fe+(Ti,V,Cr,Mn,Co,Ni,Cu)
19	408482.000	9768119.000	0.757	0.011	0.962	3.201	82.818	0.349	2.727	3.041	< 0.03	<0.03	<0.03	0.013	< 0.03	< 0.03	< 0.03	0.733	<0.03	Fe+(Ti,V,Cr,Mn,Ni,Cu,W)
20	408440.000	9768095.000	0.242	0.906	<0.03	3.999	67.424	2.824	5.987	3.163	<0.03	<0.03	0.500	1.717	<0.03	<0.03	<0.03	9.856	<0.03	Fe+(Ti,V,Mn,Co,Ni,Cu,Nb,Mo, W)
21	408454.000	9768050.000	0.866	0.190	<0.03	3.622	67.428	3.328	4.481	2.627	<0.03	<0.03	0.466	2.146	<0.03	<0.03	<0.03	9.358	<0.03	Fe+(Ti,V,Mn,Co,Ni,Cu,Mo,W)
22	408496.000	9768077.000	0.651	0.304	<0.03	3.939	66.959	3.350	5.807	2.521	< 0.03	<0.03	0.479	1.704	< 0.03	< 0.03	< 0.03	10.483	<0.03	Fe+(Ti,V,Mn,Fe,Co,Ni,Cu,Mo, W)
23	408449.000	9768091.000	0.041	0.791	<0.03	3.915	60.789	3.563	5.847	3.556	<0.03	<0.03	0.535	1.957	<0.03	<0.03	<0.03	9.190	<0.03	Fe+(Ti,V,Mn,Co,Ni,Cu,Nb,Mo, W)
24	408600.000	9768111.000	0.571	0.625	<0.03	3.963	61.603	4.721	6.007	0.958	<0.03	<0.03	0.372	2.106	<0.03	<0.03	<0.03	10.036	<0.03	Fe+(Ti,V,Mn,Co,Ni,Cu,Mo,W)
25	408640.000	9768129.000	1.295	0.372	<0.03	3.711	61.461	2.911	<0.03	2.596	<0.03	<0.03	0.487	1.932	<0.03	<0.03	<0.03	10.474	<0.03	Fe+(Ti,V,Mn,Co,Cu,Mo,W)
26	408664.000	9768078.000	0.815	0.362	<0.03	8.078	58.268	2.701	6.054	3.845	<0.03	<0.03	0.460	1.236	<0.03	<0.03	<0.03	7.717	<0.03	Fe+(Ti,V,Mn,Co,Ni,Cu,Mo,W)
27	408684.000	9768028.000	0.111	0.007	1.273	2.831	69.636	0.973	4.376	7.771	<0.03	<0.03	<0.03	0.363	<0.03	<0.03	<0.03	<0.03	<0.03	Fe+(Ti,V,Cr,Mn,Co,Ni,Cu)
28	408664.000	9768084.000	0.228	0.114	<0.03	3.491	60.274	2.495	5.894	3.563	<0.03	<0.03	0.476	1.737	<0.03	<0.03	<0.03	9.057	<0.03	Fe+(Ti,V,Mn,Co,Ni,Cu,Mo,W)
29	408630.000	9768047.000	0.624	0.784	<0.03	4.264	63.550	3.617	6.185	<0.03	<0.03	<0.03	0.297	2.326	<0.03	<0.03	<0.03	12.902	<0.03	Fe+(Ti,Mn,V,Co,Ni,Mo,W)
30	408593.000	9768019.000	0.331	0.307	0.965	3.384	75.922	0.985	4.022	5.762	<0.03	<0.03	<0.03	0.248	<0.03	<0.03	<0.03	<0.03	<0.03	Fe+(Ti,V,Cr,Mn,Co,Ni,Cu)
31	408545.000	9767992.000	1.800	0.178	1.130	3.938	74.915	0.976	3.690	5.606	<0.03	<0.03	<0.03	0.274	<0.03	<0.03	<0.03	<0.03	<0.03	Fe+(Ti,V,Cr,Mn,Co,Ni,Cu)
32	408501.000	9767970.000	1.956	0.950	2.158	4.109	61.222	1.793	4.829	13.694	<0.03	<0.03	<0.03	0.692	<0.03	<0.03	<0.03	<0.03	<0.03	Fe+(Ti,V,Cr,Mn,Co,Ni,Cu,Mo, W)
33	408536.000	9767934.000	0.215	0.024	<0.03	3.364	64.688	2.927	5.712	4.644	<0.03	<0.03	0.559	1.510	<0.03	<0.03	<0.03	8.228	<0.03	Fe+(Ti,V,Mn,Co,Ni,Cu,Nb,Mo, W)
34	408584.000	9767951.000	0.062	0.756	0.745	2.566	76.532	0.774	2.962	3.708	<0.03	<0.03	<0.03	0.178	<0.03	<0.03	<0.03	0.648	<0.03	Fe+(Ti,V,Cr,Mn,Co,Ni,Cu,W)
35	408628.000	9767967.000	0.093	0.330	2.627	4.952	62.908	2.076	4.694	12.222	<0.03	<0.03	<0.03	0.975	<0.03	<0.03	<0.03	<0.03	<0.03	Fe+(Ti,V,Cr,Mn,Co,Ni,Cu,Mo)
36	408668.000	9767993.000	0.181	0.673	1.612	4.778	71.149	1.545	7.202	7.752	<0.03	<0.03	<0.03	0.564	<0.03	<0.03	<0.03	<0.03	<0.03	Fe+(TI,V,Cr,MnCo,Ni,Cu,Mo)
37	408709.000	9768025.000	0.579	0.320	<0.03	4.926	65.370	3.755	5.215	3.490	<0.03	<0.03	0.536	1.968	<0.03	<0.03	<0.03	9.549	<0.03	Fe+(Ti,Mn,V,Co,Ni,Cu,Nb,Mo, W)

Chemical analysis of magnetite ore. Analysis done using the X-ray fluorescence (XRF) method. Elements expressed in weight percent (wt. %).

No.	Long. (UTM)	Lat. (UTM)	Ti Wt. %	V Wt. %	Cr Wt. %	Mn Wt. %	Fe Wt. %	Co Wt. %	Ni Wt. %	Cu Wt. %	Zn Wt. %	Zr Wt. %	Nb Wt. %	Mo Wt. %	Ag Wt. %	Sn Wt. %	Sb Wt. %	W Wt. %	Pb Wt. %	Iron Ore elements association
38	408727.000	9767978.000	0.414	0.937	<0.03	2.828	70.317	2.102	4.828	3.919	<0.03	<0.03	0.594	1.476	<0.03	<0.03	<0.03	8.875	<0.03	Fe+(Ti,V,Mn,Co,Ni,Cu,Nb,Mo,W)
39	408685.000	9767952.000	0.773	0.135	<0.03	4.742	64.773	3.369	6.133	3.175	<0.03	<0.03	0.499	1.705	<0.03	<0.03	<0.03	9.682	<0.03	Fe+(Ti,V,Mn,Co,Ni,Cu,Mo,W)
40	408645.000	9767927.000	0.916	0.113	<0.03	5.010	63.672	4.434	5.919	0.742	<0.03	<0.03	0.471	2.338	<0.03	<0.03	<0.03	11.825	<0.03	Fe+(Ti,V,Mn,Co,Ni,Cu,Mo,W)
41	408606.000	9767890.000	0.685	0.483	<0.03	4.696	64.018	3.749	4.057	<0.03	<0.03	<0.03	0.219	3.096	<0.03	<0.03	<0.03	14.740	<0.03	Fe+(Ti,V,Mn,Co,Ni,Cu,Mo,W)
42	408573.000	9767851.000	0.838	0.205	7.567	3.382	63.597	1.905	6.340	4.612	<0.03	<0.03	0.302	0.479	<0.03	<0.03	<0.03	4.055	<0.03	Fe+(Ti,V,Cr,Mn,Co,Ni,Cu,W)
43	408471.000	9768636.000	0.347	0.361	4.397	3.539	61.050	2.252	6.507	5.116	<0.03	<0.03	0.331	0.617	<0.03	<0.03	<0.03	4.788	<0.03	Fe+(Ti,V,Cr,Mn,Co,Ni,Cu,W)
44	408471.000	9768638.000	0.189	0.739	0.000	4.156	77.159	2.658	3.538	3.957	<0.03	<0.03	0.246	0.438	<0.03	<0.03	<0.03	3.417	<0.03	Fe+(Ti,V,Mn,Co,Ni,Cu,W)
45	408434.000	9768604.000	0.467	0.077	1.454	6.106	71.320	1.677	5.171	8.334	<0.03	<0.03	<0.03	0.510	<0.03	<0.03	<0.03	<0.03	<0.03	Fe+(Ti,V,Cr,Mn,Co,Ni,Cu,Mo)
46	408400.000	9768568.000	0.178	0.885	1.253	3.291	66.845	1.089	4.177	6.110	<0.03	<0.03	<0.03	0.196	<0.03	<0.03	<0.03	<0.03	<0.03	Fe+(Ti,V,Cr,Mn,Co,Ni,Cu)
47	408364.000	9768526.000	0.954	0.458	1.131	7.873	72.090	1.642	2.436	2.832	<0.03	<0.03	<0.03	0.084	<0.03	<0.03	<0.03	0.818	<0.03	Fe+(Ti,V,Cr,Mn,Co,Ni,Cu,W)
48	408329.000	9768491.000	0.042	0.292	<0.03	4.665	65.858	4.182	4.959	0.762	<0.03	<0.03	0.433	2.224	<0.03	<0.03	<0.03	11.339	<0.03	Fe+(Ti,V,Mn,Co,Ni,Cu,Mo,W)
49	408282.000	9768488.000	0.754	0.007	<0.03	4.329	65.937	2.763	7.380	4.826	<0.03	<0.03	0.463	1.399	<0.03	<0.03	<0.03	7.516	<0.03	Fe+(Ti,V,Mn,Co,Ni,Cu,Mo,W)
50	408284.000	9768537.000	0.414	0.448	<0.03	4.279	61.669	2.705	5.299	1.799	<0.03	<0.03	0.455	2.124	<0.03	<0.03	<0.03	11.412	<0.03	Fe+(Ti,V,Mn,Co,Ni,Cu,Mo,W)
51	408314.000	9768576.000	0.715	0.010	<0.03	5.360	60.759	2.790	5.389	3.551	<0.03	<0.03	0.500	1.552	<0.03	<0.03	<0.03	9.330	<0.03	Fe+(Ti,V,Mn,Co,Ni,Cu,Nb,Mo,W)
52	408346.000	9768615.000	0.084	0.884	<0.03	4.234	67.782	4.145	4.623	2.193	<0.03	<0.03	0.491	1.747	<0.03	<0.03	<0.03	10.970	<0.03	Fe+(Ti,V,Mn,Co,Ni,Cu,Mo,W)
53	408302.000	9768528.000	0.432	0.993	<0.03	3.894	61.246	4.422	6.026	0.000	<0.03	<0.03	0.364	2.371	<0.03	<0.03	<0.03	9.750	<0.03	Fe+(Ti,V,Mn,Co,Ni,Mo,W)
54	408341.000	9768562.000	0.495	0.801	0.629	1.968	81.910	0.432	2.571	2.343	<0.03	<0.03	<0.03	0.085	<0.03	<0.03	<0.03	0.924	<0.03	Fe+(Ti,V,Cr,Mn,Ni,Cu,W)
55	408373.000	9768597.000	0.317	0.072	1.143	3.021	74.900	1.114	4.319	5.984	<0.03	<0.03	<0.03	0.175	<0.03	<0.03	<0.03	<0.03	<0.03	Fe+(Ti,V,Cr,Mn,Co,Ni,Cu,)
56	408414.000	9768626.000	0.220	0.724	0.631	2.944	78.169	0.695	2.800	3.226	<0.03	<0.03	<0.03	0.089	<0.03	<0.03	<0.03	0.670	<0.03	Fe+(Ti,V,Cr,Mn,Ni,Co,Cu,Mo,W)
57	408452.000	9768661.000	0.783	0.660	0.614	2.974	78.804	0.702	2.709	2.982	<0.03	<0.03	<0.03	0.113	<0.03	<0.03	<0.03	0.857	<0.03	Fe+(Ti,V,Cr,Mn,Co,Ni,Cu,W)
58	408416.000	9768697.000	1.119	0.410	0.000	8.399	60.827	4.295	4.909	2.425	<0.03	<0.03	0.480	2.121	<0.03	<0.03	<0.03	10.472	<0.03	Fe+(Ti,V,Mn,Co,Ni,Cu,Mo,W)
59	408383.000	9768662.000	0.143	0.475	0.935	3.418	79.060	0.896	3.453	5.127	<0.03	<0.03	<0.03	0.158	<0.03	<0.03	<0.03	0.000	<0.03	Fe+(Ti,V,Cr,Mn,Co,Ni,Cu,W)
60	408346.000	9768621.000	0.890	0.240	<0.03	10.544	75.356	1.288	2.352	1.732	<0.03	<0.03	0.099	0.145	<0.03	<0.03	<0.03	1.481	<0.03	Fe+(Ti,V,Mn,Co,Ni,Cu,W)
61	408317.000	9768589.000	0.292	0.011	<0.03	11.288	70.202	1.720	2.916	2.435	<0.03	<0.03	0.145	0.220	<0.03	<0.03	<0.03	1.969	<0.03	Fe+(Ti,V,Mn,Co,Ni,Cu,W)

Chemical analysis of magnetite ore. Analysis done using the X-ray fluorescence (XRF) method. Elements expressed in weight percent (wt. %).

No.	Long. (UTM)	Lat. (UTM)	Ti Wt. %	V Wt. %	Cr Wt. %	Mn Wt. %	Fe Wt. %	Co Wt. %	Ni Wt. %	Cu Wt. %	Zn Wt. %	Zr Wt. %	Nb Wt. %	Mo Wt. %	Ag Wt. %	Sn Wt. %	Sb Wt. %	W Wt. %	Pb Wt. %	Iron Ore elements association
62	408285.000	9768552.000	0.654	0.889	1.515	5.127	70.049	1.713	4.589	12.302	<0.03	<0.03	<0.03	1.007	<0.03	<0.03	<0.03	<0.03	<0.03	Fe+(Ti,V,Cr,Mn,Co,Ni,Cu,Mo,)
63	408242.000	9768586.000	0.752	0.310	<0.03	3.695	68.262	2.424	4.795	4.714	<0.03	<0.03	0.507	1.307	<0.03	<0.03	<0.03	7.598	<0.03	Fe+(Ti,V,Mn,Co,Ni,Cu,Nb,Mo, W)
64	408274.000	9768610.000	0.915	0.727	0.641	2.438	81.003	0.401	2.641	2.434	<0.03	<0.03	<0.03	0.081	<0.03	<0.03	<0.03	0.841	<0.03	Fe+(Ti,V,Cr,Mn,Ni,Cu,W)
65	408247.000	9768581.000	0.256	0.993	0.809	3.760	83.268	0.900	3.268	4.010	<0.03	<0.03	<0.03	0.105	<0.03	<0.03	<0.03	0.412	<0.03	Fe+(Ti,V,Cr,Mn,Co,Ni,Cu)
66	408284.000	9768614.000	0.423	0.895	1.021	2.691	80.350	0.781	4.037	5.085	<0.03	<0.03	<0.03	0.223	<0.03	<0.03	<0.03	<0.03	<0.03	Fe+(Ti,V,Cr,Mn,Co,Ni,Cu)
67	408320.000	9768645.000	0.346	0.220	0.988	2.019	77.998	0.609	3.907	5.392	<0.03	<0.03	<0.03	0.214	<0.03	<0.03	<0.03	<0.03	<0.03	Fe+(Ti,V,Cr,Mn,Co,Ni,Cu)
68	408357.000	9768686.000	0.554	0.082	<0.03	5.082	66.559	4.207	5.155	4.134	<0.03	<0.03	0.552	1.411	<0.03	<0.03	<0.03	7.706	<0.03	Fe+(Ti,V,Mn,Co,Ni,Cu,Nb,Mo, W)
69	408387.000	9768726.000	0.170	0.940	2.459	5.672	61.612	1.992	3.982	13.923	<0.03	<0.03	<0.03	0.992	<0.03	<0.03	<0.03	<0.03	<0.03	Fe+(Ti,V,Cr,Mn,Co,Ni,Cu,Mo)
70	410642.000	9763052.000	0.153	0.075	<0.03	4.860	60.171	2.665	9.448	2.378	<0.03	<0.03	0.525	1.840	<0.03	<0.03	<0.03	9.778	<0.03	Fe+(Ti,V,Mn,Co,Ni,Cu,Nb,Mo, W)
71	410667.000	9763092.000	0.813	0.478	0.926	3.070	77.686	0.748	3.880	5.469	<0.03	<0.03	<0.03	0.227	<0.03	<0.03	<0.03	<0.03	<0.03	Fe+(Ti,V,Cr,Mn,Co,Ni,Cu)
72	410701.000	9763128.000	0.128	0.940	1.865	4.560	68.026	1.579	5.494	11.075	<0.03	<0.03	<0.03	0.741	<0.03	<0.03	<0.03	<0.03	<0.03	Fe+(Ti,V,Cr,Mn,Co,Ni,Cu,Mo)
73	410733.000	9763164.000	0.219	0.522	0.981	4.078	67.139	0.911	3.927	4.897	<0.03	<0.03	<0.03	0.335	<0.03	<0.03	<0.03	<0.03	<0.03	Fe+(Ti,V,Mn,Cr,Co,Ni,Cu)
74	410766.000	9763198.000	0.691	0.852	2.410	8.961	57.984	2.734	4.269	11.848	<0.03	<0.03	<0.03	1.071	<0.03	<0.03	<0.03	<0.03	<0.03	Fe+(Ti,V,Cr,Mn,Co,Ni,Cu)
75	410798.000	9763234.000	0.051	0.362	<0.03	5.362	52.890	3.347	6.230	3.981	<0.03	<0.03	0.469	1.452	<0.03	<0.03	<0.03	8.482	<0.03	Fe+(Ti,V,Mn,Co,Ni,Cu,Mo,W)
76	410763.000	9763268.000	0.954	0.979	1.029	6.777	64.318	1.536	3.860	5.004	<0.03	<0.03	<0.03	0.292	<0.03	<0.03	<0.03	<0.03	<0.03	Fe+(Ti,V,Cr,Mn,Co,Ni,Cu)
77	410734.000	9763230.000	0.355	0.685	1.927	4.465	45.613	1.593	5.210	9.620	<0.03	<0.03	<0.03	0.724	<0.03	<0.03	<0.03	<0.03	<0.03	Fe+(Ti,V,Cr,Mn,Co,Ni,Cu,Mo)
78	410702.000	9763194.000	0.619	1.350	1.610	4.497	53.025	1.025	3.932	7.346	<0.03	<0.03	<0.03	0.436	<0.03	<0.03	<0.03	<0.03	<0.03	Fe+(Ti,V,Cr,Mn,Co,Ni,Cu)
79	410673.000	9763159.000	0.282	0.650	<0.03	3.475	17.091	3.736	4.736	0.129	<0.03	<0.03	0.472	2.513	<0.03	<0.03	<0.03	12.018	<0.03	Fe+(Ti,V,Mn,Co,Ni,Cu,Mo,W)
80	410645.000	9763121.000	0.623	0.251	<0.03	3.310	42.107	3.051	7.273	3.522	<0.03	<0.03	0.504	1.685	<0.03	<0.03	<0.03	9.462	<0.03	Fe+(Ti,V,Mn,Co,Ni,Cu,Nb,Mo, W)
81	410613.000	9763080.000	0.789	0.249	0.348	0.902	89.870	0.211	1.841	1.572	<0.03	<0.03	<0.03	0.080	<0.03	<0.03	<0.03	0.675	<0.03	Fe+(Ti,V,Mn,Ni,Cu,W)
82	410579.000	9763080.000	0.880	0.500	0.265	0.100	95.500	0.102	1.383	1.334	<0.03	<0.03	<0.03	0.068	<0.03	<0.03	<0.03	0.608	<0.03	Fe+(Ti,V,Mn,Ni,Cu,W)
83	410613.000	9763113.000	0.146	0.949	0.595	0.920	82.431	0.245	2.346	2.924	<0.03	<0.03	<0.03	0.059	<0.03	<0.03	<0.03	0.645	<0.03	Fe+(Ti,V,Cr,Mn,Ni,Cu,W)
84	410646.000	9763144.000	0.081	0.900	0.599	0.885	82.010	0.103	2.143	2.524	<0.03	<0.03	<0.03	0.055	<0.03	<0.03	<0.03	0.727	<0.03	Fe+(Ti,Mn,V,Cr,Ni,Cu,W)

Chemical analysis of magnetite ore. Analysis done using the X-ray fluorescence (XRF) method. Elements expressed in weight percent (wt. %).

No.	Long. (UTM)	Lat. (UTM)	Ti Wt. %	V Wt. %	Cr Wt. %	Mn Wt. %	Fe Wt. %	Co Wt. %	Ni Wt. %	Cu Wt. %	Zn Wt. %	Zr Wt. %	Nb Wt. %	Mo Wt. %	Ag Wt. %	Sn Wt. %	Sb Wt. %	W Wt. %	Pb Wt. %	Iron Ore elements association
85	410679.000	9763179.000	0.408	0.935	0.793	2.116	76.006	0.538	3.357	3.823	<0.03	<0.03	<0.03	0.144	<0.03	<0.03	<0.03	0.541	<0.03	Fe+(Ti,V,Mn,Cr,Co,Ni,Cu,W)
86	410746.000	9763287.000	0.657	0.885	0.605	1.829	79.961	0.454	2.561	3.198	<0.03	<0.03	<0.03	0.153	<0.03	<0.03	<0.03	0.734	<0.03	Fe+(Ti,V,Cr,Mn,Ni,Cu,W)
87	410719.000	9763330.000	0.749	0.655	1.177	2.533	62.788	0.986	4.772	6.811	<0.03	<0.03	<0.03	0.440	<0.03	<0.03	<0.03	<0.03	<0.03	Fe+(Ti,VMn,Cr,Co,Ni,Cu)
88	410688.000	9763295.000	1.000	0.300	<0.03	4.318	32.922	<0.03	16.478	<0.03	<0.03	0.206	<0.03	<0.03	36.903	<0.03	8.269	<0.03	<0.03	Fe+(Mn,Ni,Ag,Sb)
89	410656.000	9763261.000	0.884	0.790	2.220	6.151	63.660	2.263	4.537	12.015	<0.03	<0.03	<0.03	1.049	<0.03	<0.03	<0.03	<0.03	<0.03	Fe+(Ti,V,Cr,Mn,Co,Ni,Cu,Mo)
90	410625.000	9763227.000	0.744	0.275	0.000	3.603	67.980	3.259	4.932	3.235	<0.03	<0.03	0.477	1.707	<0.03	<0.03	<0.03	9.686	<0.03	Fe+(Ti,V,Mn,Co,Ni,Cu,Mo,W)
91	410596.000	9763190.000	0.625	0.458	0.540	2.365	79.366	0.748	3.274	2.972	<0.03	<0.03	<0.03	0.083	<0.03	<0.03	<0.03	0.804	<0.03	Fe+(Ti,V,Cr,Mn,Co,Ni,Cu,W)
92	410566.000	9763153.000	0.538	0.265	0.929	2.245	77.983	0.569	4.745	2.965	<0.03	<0.03	<0.03	0.105	<0.03	<0.03	<0.03	0.785	<0.03	Fe+(Ti,V,Cr,Mn,Co,Ni,Cu,W)
93	410528.000	9763186.000	0.117	0.398	<0.03	5.930	66.061	6.036	<0.03	<0.03	<0.03	<0.03	0.118	2.431	<0.03	<0.03	<0.03	15.016	<0.03	Fe+(Ti,V,Mn,Co,Mo,W)
94	410564.000	9763222.000	0.791	0.825	<0.03	3.898	62.846	4.280	7.778	0.184	<0.03	<0.03	0.477	2.753	<0.03	<0.03	<0.03	11.371	<0.03	Fe+(Ti,V,Mn,Co,Ni,Mo,W)
95	410595.000	9763256.000	0.088	0.280	0.402	0.609	87.196	0.380	1.922	2.682	<0.03	<0.03	<0.03	0.094	<0.03	<0.03	<0.03	0.569	<0.03	Fe+(Ti,V,Mn,Ni,Cu,W)
96	410625.000	9763292.000	0.512	0.920	1.291	1.721	77.400	1.188	4.941	9.203	<0.03	<0.03	<0.03	0.298	<0.03	<0.03	<0.03	<0.03	<0.03	Fe+(Ti,V,Cr,Mn,Co,Ni,Cu)
97	410654.000	9763329.000	0.936	0.735	1.081	2.145	77.069	0.562	4.239	6.677	<0.03	<0.03	<0.03	0.338	<0.03	<0.03	<0.03	<0.03	<0.03	Fe+(Ti,V,Cr,Mn,Co,Ni,Cu)
98	410690.000	9763368.000	0.919	0.702	<0.03	2.492	65.181	1.658	7.224	4.637	<0.03	<0.03	0.416	1.060	<0.03	<0.03	<0.03	6.942	<0.03	Fe+(Ti,V,Mn,Co,Ni,Cu,Mo,W)
99	410655.000	9763402.000	0.224	0.301	<0.03	7.587	64.860	2.575	7.419	3.871	<0.03	<0.03	0.307	0.552	<0.03	<0.03	<0.03	4.142	<0.03	Fe+(Ti,V,Mn,Co,Ni,Cu,Mo,W)
100	410626.000	9763368.000	0.732	0.323	2.094	5.406	75.700	1.508	5.122	4.730	<0.03	<0.03	<0.03	0.221	<0.03	<0.03	<0.03	<0.03	<0.03	Fe+(Ti,V,Cr,Mn,Co,Ni,Cu)
101	410591.000	9763333.000	0.047	0.860	<0.03	7.200	57.075	3.599	6.366	3.986	<0.03	<0.03	0.448	1.238	<0.03	<0.03	<0.03	8.037	<0.03	Fe+(Ti,V,Mn,Co,Ni,Cu,W)
102	410555.000	9763301.000	0.708	0.244	<0.03	8.439	69.071	1.850	4.228	3.622	<0.03	<0.03	0.255	0.422	<0.03	<0.03	<0.03	3.207	<0.03	Fe+(Ti,V,Mn,Co,Ni,Cu,W)
103	410523.000	9763263.000	0.953	0.178	0.809	2.135	77.261	0.931	3.016	4.359	<0.03	<0.03	<0.03	0.088	<0.03	<0.03	<0.03	0.277	<0.03	Fe+(Ti,V,Cr,Mn,Co,Ni,Cu)
104	410496.000	9763303.000	0.369	0.422	<0.03	4.257	63.486	2.117	7.840	3.800	<0.03	<0.03	0.379	0.822	<0.03	<0.03	<0.03	5.751	<0.03	Fe+(Ti,V,Mn,Co,Ni,Cu,Mo,W)
105	410530.000	9763335.000	0.431	0.737	1.666	2.305	74.549	0.663	4.236	4.649	<0.03	<0.03	<0.03	0.269	<0.03	<0.03	<0.03	0.126	<0.03	Fe+(Ti,V,Cr,Mn,Co,Ni,Cu)
106	410562.000	9763371.000	0.510	0.397	0.826	4.234	73.955	1.001	3.140	4.041	<0.03	<0.03	<0.03	0.118	<0.03	<0.03	<0.03	0.423	<0.03	Fe+(Ti,V,Cr,Mn,Co,Ni,Cu)
107	410594.000	9763406.000	0.501	0.405	<0.03	6.243	66.120	3.350	3.849	3.510	<0.03	<0.03	0.599	1.821	<0.03	<0.03	<0.03	9.784	<0.03	Fe+(Ti,V,Mn,Co,Ni,Cu,Nb,Mo,W)
108	410626.000	9763441.000	0.214	0.640	<0.03	4.488	69.144	2.685	4.103	2.708	<0.03	<0.03	0.523	1.881	<0.03	<0.03	<0.03	10.579	<0.03	Fe+(Ti,V,Mn,Co,Ni,Cu,Nb,Mo,W)

Chemical analysis of magnetite ore. Analysis done using the X-ray fluorescence (XRF) method. Elements expressed in weight percent (wt. %).

No.	Long. (UTM)	Lat. (UTM)	Ti Wt. %	V Wt. %	Cr Wt. %	Mn Wt. %	Fe Wt. %	Co Wt. %	Ni Wt. %	Cu Wt. %	Zn Wt. %	Zr Wt. %	Nb Wt. %	Mo Wt. %	Ag Wt. %	Sn Wt. %	Sb Wt. %	W Wt. %	Pb Wt. %	Iron Ore elements association
109	410591.000	9763471.000	0.098	0.012	0.284	0.386	94.367	0.000	0.974	0.798	<0.03	<0.03	<0.03	0.052	<0.03	<0.03	<0.03	0.483	<0.03	Fe+(Ti,V,Mn,Ni,Cu)
110	410557.000	9763434.000	0.724	0.150	0.265	0.357	91.835	0.039	0.906	1.797	<0.03	<0.03	<0.03	0.033	<0.03	<0.03	<0.03	0.295	<0.03	Fe+(Ti,V,Cr,Mn,Ni,Cu)
111	410522.000	9763401.000	0.644	0.953	1.030	2.259	75.111	0.602	4.366	5.076	<0.03	<0.03	<0.03	0.338	<0.03	<0.03	<0.03	<0.03	<0.03	Fe+(Ti,V,Cr,Mn,Co,Ni,Cu)
112	410506.000	9763440.000	0.898	0.020	2.084	3.954	66.688	1.703	5.059	11.717	<0.03	<0.03	<0.03	0.891	<0.03	<0.03	<0.03	<0.03	<0.03	Fe+(Ti,V,Cr,Mn,Co,Ni,Cu,Mo)
113	410541.000	9763474.000	0.074	0.036	0.000	3.849	65.310	5.579	3.397	<0.03	<0.03	<0.03	0.491	2.975	<0.03	<0.03	<0.03	13.890	<0.03	Fe+(Ti,V,Mn,Co,Ni,Mo,W)
114	410539.000	9763544.000	0.607	0.665	0.812	1.262	77.117	0.563	3.800	4.112	<0.03	<0.03	<0.03	0.235	<0.03	<0.03	<0.03	0.551	<0.03	Fe+(Ti,V,Cr,Mn,Co,Ni,Cu,W)
115	410506.000	9763508.000	0.304	0.149	0.643	1.140	80.772	0.232	2.861	4.080	<0.03	<0.03	<0.03	0.127	<0.03	<0.03	<0.03	0.408	<0.03	Fe+(Ti,V,Cr,Mn,Ni,Cu)
116	410486.000	9763486.000	0.776	0.418	0.636	1.054	84.212	0.353	2.332	2.767	<0.03	<0.03	<0.03	0.077	<0.03	<0.03	<0.03	0.743	<0.03	Fe+(Ti,V,Cr,Mn,Ni,Cu,W)
117	410466.000	9763533.000	0.495	0.729	0.556	0.911	85.190	0.202	2.454	2.245	<0.03	<0.03	<0.03	0.106	<0.03	<0.03	<0.03	0.945	<0.03	Fe+(Ti,V,Cr,Mn,Ni,Cu,W)
118	410498.000	9763574.000	0.952	0.928	0.468	0.843	82.306	0.219	2.251	2.233	<0.03	<0.03	<0.03	0.106	<0.03	<0.03	<0.03	0.973	<0.03	Fe+(Ti,Mn,V,W,Co,Cu,Ni)
119	410533.000	9763616.000	0.794	0.148	0.748	1.201	79.336	0.577	3.768	3.535	<0.03	<0.03	<0.03	0.228	<0.03	<0.03	<0.03	0.843	<0.03	Fe+(Ti,V,Cr,Mn,Co,Cu,Ni,W)
120	410493.000	9763654.000	0.157	0.129	0.454	0.749	86.370	0.270	2.488	2.227	<0.03	<0.03	<0.03	0.126	<0.03	<0.03	<0.03	1.004	<0.03	Fe+(Ti,Mn,V,Ni,Cu,W)
121	410465.000	9763620.000	0.657	0.078	0.501	3.651	81.503	0.736	2.412	2.210	<0.03	<0.03	<0.03	0.127	<0.03	<0.03	<0.03	1.028	<0.03	Fe+(Ti,Cr,V,Mn,Co,Ni,Cu,W)
122	410441.000	9763594.000	0.818	0.100	2.018	3.056	62.086	1.650	5.338	12.075	<0.03	<0.03	<0.03	0.664	<0.03	<0.03	<0.03	<0.03	<0.03	Fe+(Ti,V,Cr,Mn,Co,Cu,Ni)
123	410409.000	9763631.000	0.343	0.964	0.877	4.014	81.008	0.856	3.749	4.315	<0.03	<0.03	<0.03	0.269	<0.03	<0.03	<0.03	0.385	<0.03	Fe+(Ti,V,Cr,Mn,Co,Ni,Cu)
124	410443.000	9763665.000	0.944	0.205	<0.03	23.743	53.584	3.402	7.071	1.908	<0.03	<0.03	0.180	0.290	<0.03	<0.03	<0.03	2.095	<0.03	Fe+(Ti,V,Mn,Co,Cu,Ni,W)
125	410473.000	9763701.000	0.697	0.050	<0.03	11.904	70.983	1.587	4.074	1.618	<0.03	<0.03	0.154	0.224	<0.03	<0.03	<0.03	1.934	<0.03	Fe+(Ti,V,Mn,Cu,Co,Ni,W)
126	410453.000	9763744.000	0.531	0.491	<0.03	23.967	64.650	1.579	2.504	1.294	<0.03	<0.03	0.095	0.135	<0.03	<0.03	<0.03	1.457	<0.03	Fe+(Ti,Mn,Co,Ni,Cu,W)
127	410418.000	9763707.000	0.889	0.454	<0.03	16.578	74.229	1.422	2.044	0.824	<0.03	<0.03	0.054	0.074	<0.03	<0.03	<0.03	0.870	<0.03	Fe+(Ti,Mn,Ni,Cu,W)
128	410381.000	9763668.000	0.594	0.900	0.392	0.640	89.754	0.087	1.760	1.659	<0.03	<0.03	<0.03	0.098	<0.03	<0.03	<0.03	0.814	<0.03	Fe+(Ti,Mn,Ni,Cu,W)
129	410358.000	9763710.000	0.973	0.550	0.922	1.480	83.813	0.559	3.943	5.127	<0.03	<0.03	<0.03	0.260	<0.03	<0.03	<0.03	<0.03	<0.03	Fe+(Ti,V,Cr,Mn,Co,Cu,Ni)
130	410397.000	9763745.000	0.863	0.851	<0.03	4.254	66.511	2.567	7.225	6.012	<0.03	<0.03	0.514	1.398	<0.03	<0.03	<0.03	6.872	<0.03	Fe+(Ti,V,Mn,Ni,Cu,W)
131	410431.000	9763779.000	0.039	0.156	0.373	0.805	88.767	0.239	1.668	1.792	<0.03	<0.03	<0.03	0.053	<0.03	<0.03	<0.03	0.704	<0.03	Fe+(Ti,V,Mn,Ni,Cu,W)
132	410400.000	9763812.000	0.364	0.464	1.790	3.130	72.062	0.763	5.357	7.114	<0.03	<0.03	<0.03	0.527	<0.03	<0.03	<0.03	<0.03	<0.03	Fe+(Ti,V,Cr,Mn,Co,Ni,Cu,Mo)

Chemical analysis of magnetite ore. Analysis done using the X-ray fluorescence (XRF) method. Elements expressed in weight percent (wt. %).

No.	Long. (UTM)	Lat. (UTM)	Ti Wt. %	V Wt. %	Cr Wt. %	Mn Wt. %	Fe Wt. %	Co Wt. %	Ni Wt. %	Cu Wt. %	Zn Wt. %	Zr Wt. %	Nb Wt. %	Mo Wt. %	Ag Wt. %	Sn Wt. %	Sb Wt. %	W Wt. %	Pb Wt. %	Iron Ore elements association
133	410368.000	9763780.000	0.177	0.250	1.381	2.170	75.600	0.644	5.461	7.024	<0.03	<0.03	<0.03	0.414	<0.03	<0.03	<0.03	<0.03	<0.03	Fe+(Ti,V,Cr,Mn,Co,Ni,Cu)
134	410346.000	9763819.000	0.127	0.502	0.525	1.344	85.702	0.312	2.116	2.146	<0.03	<0.03	<0.03	0.072	<0.03	<0.03	<0.03	0.814	<0.03	Fe+(Cr,Ti,Mn,V,Ni,Cu,W)
135	410384.000	9763854.000	0.872	0.834	1.007	4.348	77.773	1.203	4.159	4.988	<0.03	<0.03	<0.03	0.324	<0.03	<0.03	<0.03	<0.03	<0.03	Fe+(Ti,Mn,V,Cr,Co,Ni,Cu)
136	410417.000	9763887.000	0.651	0.967	0.328	0.489	91.956	<0.03	0.964	0.897	<0.03	<0.03	<0.03	0.039	<0.03	<0.03	<0.03	0.526	<0.03	Fe+(Ti,V,Ni,Cu,W)
137	410412.000	9763930.000	0.450	0.520	0.254	0.357	93.964	<0.03	0.815	1.156	<0.03	<0.03	<0.03	0.041	<0.03	<0.03	<0.03	0.376	<0.03	Fe+(Ti,V,Ni,Cu)
138	406649.000	9770093.000	0.177	0.768	1.298	2.903	70.763	0.941	5.727	7.160	<0.03	<0.03	<0.03	0.534	<0.03	<0.03	<0.03	<0.03	<0.03	Fe+(Ti,V,Cr,Mn,Co,Ni,Cu,Mo)
139.	406573.000	9770182.000	0.638	0.095	1.087	1.482	83.189	0.704	4.115	5.308	<0.03	<0.03	<0.03	0.266	<0.03	<0.03	<0.03	<0.03	<0.03	Fe+(Ti,V,Cr,Mn,Co,Ni,Cu)
140	406584.000	9770158.000	0.139	0.202	0.352	1.100	88.674	0.110	1.182	0.925	<0.03	<0.03	<0.03	0.019	<0.03	<0.03	<0.03	0.726	<0.03	Fe+(Ti,V,Mn,Ni,Cu,W)
141	406595.000	9770143.000	0.888	0.020	0.350	0.491	93.588	0.131	0.949	0.913	<0.03	<0.03	<0.03	0.038	<0.03	<0.03	<0.03	0.429	<0.03	Fe+(Ti,V,Ni,Cu)
142	406610.000	9770127.000	0.656	0.040	1.557	6.806	69.482	1.760	5.096	8.372	<0.03	<0.03	<0.03	0.567	<0.03	<0.03	<0.03	<0.03	<0.03	Fe+(Ti,Mn,Cr,V,Co,Ni,Cu,Mo)
143	406621.000	9770107.000	0.361	0.127	1.954	4.512	61.396	1.431	5.048	11.987	<0.03	<0.03	<0.03	0.674	<0.03	<0.03	<0.03	<0.03	<0.03	Fe+(Ti,V,Mn,Cr,Co,Ni,Cu,Mo)
144	406628.000	9770085.000	0.821	0.303	0.843	2.924	83.142	0.897	3.591	4.814	<0.03	<0.03	<0.03	0.263	<0.03	<0.03	<0.03	0.126	<0.03	Fe+(Ti,V,Cr,Mn,Co,Ni,Cu)
145	406634.000	9770066.000	0.623	0.108	0.802	2.386	75.515	0.591	3.467	4.519	<0.03	<0.03	<0.03	0.244	<0.03	<0.03	<0.03	0.326	<0.03	Fe+(Ti,V,Cr,Mn,Co,Ni,Cu)
146	410529.000	9763339.000	1.000	0.960	<0.03	0.660	81.271	<0.03	0.686	<0.03	0.981	0.026	<0.03	<0.03	0.463	0.491	0.694	<0.03	10.203	Fe+(Mn,Ni,Zn,Sb,Pb)
147	410502.000	9763378.000	1.000	0.500	<0.03	0.921	50.311	<0.03	1.190	3.342	2.249	0.033	<0.03	<0.03	1.168	<0.03	1.281	<0.03	35.500	Fe+(Mn,Ni,Cu,Zn,Sb,Pb)
148	410475.000	9763341.000	0.447	0.037	0.497	1.334	85.360	0.426	2.291	2.336	<0.03	<0.03	<0.03	0.125	<0.03	<0.03	<0.03	0.877	<0.03	Fe+(Ti,V,Mn,Ni,Cu,W)
149	410442.000	9763309.000	1.000	0.600	0<0.03	0.547	63.726	<0.03	0.592	13.074	0.752	0.015	<0.03	<0.03	0.254	0.458	0.432	<0.03	19.519	Fe+(Mn,Ni,Cu,Zn,Pb)
150	410405.000	9763344.000	1.000	<0.03	0<0.03	1.238	18.628	<0.03	2.388	<0.03	3.540	0.069	<0.03	<0.03	2.778	<0.03	1.977	<0.03	60.000	Fe+(Mn,Ni,Zn,Ag,Sb)
151	410443.000	9763379.000	1.585	0.850	1.059	5.490	68.640	1.638	4.202	6.440	<0.03	<0.03	<0.03	0.236	<0.03	<0.03	<0.03	<0.03	<0.03	Fe+(Ti,V,Cr,Mn,Co,Ni,Cu)
152	410476.000	9763413.000	0.172	0.313	0.241	0.316	93.996	<0.03	0.837	1.186	<0.03	<0.03	<0.03	0.042	<0.03	<0.03	<0.03	0.370	<0.03	Fe+(V,Ti,Ni,Cu)
153	410446.000	9763446.000	0.252	0.471	0.179	0.233	95.303	<0.03	0.594	1.024	<0.03	<0.03	<0.03	0.045	<0.03	<0.03	<0.03	0.231	<0.03	Fe+(Ti,V,Ni,Cu)
154	410413.000	9763411.000	0.118	0.147	0.243	0.287	94.376	<0.03	0.799	1.007	<0.03	<0.03	<0.03	0.048	<0.03	<0.03	<0.03	0.359	<0.03	Fe+(Ti,V,Ni,Cu)
155	410377.000	9763371.000	0.939	0.609	1.266	2.210	69.698	1.097	6.400	7.254	<0.03	<0.03	<0.03	0.386	<0.03	<0.03	<0.03	<0.03	<0.03	Fe+(Ti,V,Cr,Mn,Co,Ni,Cu)
156	410342.000	9763405.000	0.747	0.851	<0.03	9.334	64.760	3.024	6.861	4.458	<0.03	<0.03	0.378	0.831	<0.03	<0.03	<0.03	5.538	<0.03	Fe+(Ti,V,Mn,Co,Ni,Cu,W)

Chemical analysis of magnetite ore. Analysis done using the X-ray fluorescence (XRF) method. Elements expressed in weight percent (wt. %).

No.	Long. (UTM)	Lat. (UTM)	Ti Wt. %	V Wt. %	Cr Wt. %	Mn Wt. %	Fe Wt. %	Co Wt. %	Ni Wt. %	Cu Wt. %	Zn Wt. %	Zr Wt. %	Nb Wt. %	Mo Wt. %	Ag Wt. %	Sn Wt. %	Sb Wt. %	W Wt. %	Pb Wt. %	Iron Ore elements association
157	410376.000	9763440.000	0.049	0.323	1.193	1.232	90.189	0.207	1.660	1.149	<0.03	<0.03	<0.03	0.072	<0.03	<0.03	<0.03	0.649	<0.03	Fe+(Ti,V,Mn,Cr,Ni,Cu,W)
158	410411.000	9763473.000	0.188	0.238	0.200	0.557	95.959	<0.03	0.691	0.393	<0.03	<0.03	<0.03	0.041	<0.03	<0.03	<0.03	0.317	<0.03	Fe+(Ti,V,Mn,Ni)
159	410438.000	9763510.000	0.442	0.476	0.192	0.351	95.920	0.085	0.733	0.503	<0.03	<0.03	<0.03	0.047	<0.03	<0.03	<0.03	0.399	<0.03	Fe+(Ti,V,Ni,Cu)
160	410402.000	9763541.000	0.236	0.202	0.258	0.420	94.948	<0.03	0.908	0.676	<0.03	<0.03	<0.03	0.044	<0.03	<0.03	<0.03	0.433	<0.03	Fe+(Ti,V,Ni,Cu)
161	410367.000	9763505.000	0.260	0.040	5.774	11.333	64.850	2.351	5.223	3.095	<0.03	<0.03	0.265	0.443	<0.03	<0.03	<0.03	3.930	<0.03	Fe+(Ti,V,Cr,Mn,Co,Ni,Cu,W)
162	410328.000	9763463.000	0.507	0.040	9.157	8.078	61.114	1.830	5.173	2.950	<0.03	<0.03	0.252	0.367	<0.03	<0.03	<0.03	3.442	<0.03	Fe+(Ti,Mn,V,Cr,Co,Ni,Cu,W)
163	410295.000	9763499.000	0.966	0.030	<0.03	18.752	62.171	1.993	3.040	2.068	<0.03	<0.03	0.126	0.201	<0.03	<0.03	<0.03	1.963	<0.03	Fe+(Mn,V,Ti,Co,Ni,Cu,W)
164	410335.000	9763536.000	0.900	0.083	0.776	7.805	76.504	1.286	2.104	1.946	<0.03	<0.03	<0.03	0.058	<0.03	<0.03	<0.03	0.878	<0.03	Fe+(Ti,V,Cr,Mn,Co,Ni,Cu,W)
165	410372.000	9763574.000	0.128	0.435	<0.03	3.870	66.608	4.245	5.581	0.483	<0.03	<0.03	0.408	2.260	<0.03	<0.03	<0.03	10.866	<0.03	Fe+(Ti,V,Mn,Co,Ni,Mo,W)
166	410403.000	9763614.000	0.597	0.985	2.321	4.750	67.646	1.352	4.574	11.467	<0.03	<0.03	<0.03	1.048	<0.03	<0.03	<0.03	<0.03	<0.03	Fe+(Ti,V,Cr,Mn,Co,Ni,Cu,Mo)
167	410371.000	9763646.000	0.578	0.620	<0.03	20.395	55.588	3.057	4.258	3.489	<0.03	<0.03	0.273	0.500	<0.03	<0.03	<0.03	3.203	<0.03	Fe+(Ti,Cr,Mn,Co,Ni,Cu,Mo,W)
168	410335.000	9763611.000	0.456	0.521	<0.03	4.620	59.892	4.176	5.980	1.679	<0.03	<0.03	0.539	2.320	<0.03	<0.03	<0.03	10.882	<0.03	Fe+(W,Mo,Nb,Ti,V,Mn,Co,Ni,Cu)
169	410302.000	9763571.000	0.596	0.907	2.682	6.472	60.223	2.418	4.296	12.450	<0.03	<0.03	<0.03	1.269	<0.03	<0.03	<0.03	<0.03	<0.03	Fe+(Ti,V,Cr,Mn,Co,Ni,Cu,Mo)
170	410270.000	9763535.000	0.211	0.663	<0.03	3.774	63.130	3.466	4.779	3.573	<0.03	<0.03	0.452	1.695	<0.03	<0.03	<0.03	8.810	<0.03	Fe+(Ti,V,Mn,Co,Ni,Cu,Mo,W)
171	410231.000	9763575.000	5.000	0.932	1.770	3.211	66.129	1.101	5.172	10.356	<0.03	<0.03	<0.03	0.655	<0.03	<0.03	<0.03	<0.03	<0.03	Fe+(Ti,V,Mn,Cr,Co,Ni,Cu,Mo)
172	410268.000	9763611.000	0.868	0.722	2.304	5.879	56.441	1.892	4.766	11.803	<0.03	<0.03	<0.03	0.811	<0.03	<0.03	<0.03	<0.03	<0.03	Fe+(Ti,V,Cr,Mn,Ni,Cu,Co,Mo)
173	410299.000	9763645.000	0.484	0.431	<0.03	3.640	67.370	5.019	3.470	<0.03	<0.03	<0.03	0.293	2.555	<0.03	<0.03	<0.03	12.322	<0.03	Fe+(Ti,V,Mn,Co,Ni,Nb,Mo,W)
174	410332.000	9763687.000	0.468	0.243	<0.03	4.432	65.161	3.746	6.084	1.213	<0.03	<0.03	0.476	2.140	<0.03	<0.03	<0.03	12.163	<0.03	Fe+(Ti,V,Mn,Co,Cu,Ni,W)
175	410358.000	9763712.000	0.669	0.237	0.473	2.538	82.794	0.465	2.500	2.460	<0.03	<0.03	<0.03	0.100	<0.03	<0.03	<0.03	0.846	<0.03	Fe+(Ti,V,Mn,Ni.Cu,W)
176	409250.000	9766596.000	0.744	0.517	1.303	3.662	69.346	1.205	5.423	6.892	<0.03	<0.03	<0.03	0.510	<0.03	<0.03	<0.03	<0.03	<0.03	Fe+(Ti,V,Cr,Mn,Co,Ni,Cu,Mo)
177	409218.000	9766558.000	0.532	0.295	1.495	3.585	67.640	1.012	4.717	7.509	<0.03	<0.03	<0.03	0.527	<0.03	<0.03	<0.03	<0.03	<0.03	Fe+(Ti,V,Cr,Mn,Co,Ni,Cu,Mo)
178	409185.000	9766524.000	0.243	0.342	0.489	2.157	81.924	0.618	2.752	2.640	<0.03	<0.03	<0.03	0.110	<0.03	<0.03	<0.03	0.894	<0.03	Fe+(Ti,V,Mn,Co,Ni,Cu,W)
179	409151.000	9766489.000	0.512	0.854	0.909	2.910	83.418	0.615	3.506	3.949	<0.03	<0.03	<0.03	0.227	<0.03	<0.03	<0.03	0.590	<0.03	Fe+(Ti,Cr,Mn,Co,Ni,Cu,W)
180	409121.000	9766455.000	0.474	0.477	1.228	4.087	69.961	1.315	4.810	6.763	<0.03	<0.03	<0.03	0.322	<0.03	<0.03	<0.03	<0.03	<0.03	Fe+(Ti,Cr,V,Mn,Co,Ni,Cu)

Chemical analysis of magnetite ore. Analysis done using the X-ray fluorescence (XRF) method. Elements expressed in weight percent (wt. %).

No.	Long. (UTM)	Lat. (UTM)	Ti Wt. %	V Wt. %	Cr Wt. %	Mn Wt. %	Fe Wt. %	Co Wt. %	Ni Wt. %	Cu Wt. %	Zn Wt. %	Zr Wt. %	Nb Wt. %	Mo Wt. %	Ag Wt. %	Sn Wt. %	Sb Wt. %	W Wt. %	Pb Wt. %	Iron Ore elements association
	Min		0.034	0.007	0.000	0.100	17.091	0.000	0.592	0.000	0.752	0.015	0.054	0.013	0.254	0.458	0.432	0.000	10.203	
	Max		5.000	1.350	9.157	23.967	96.073	6.036	16.478	13.923	3.540	0.206	0.599	3.096	36.903	0.491	8.269	15.016	60.000	
	Aver.		0.596	0.481	1.213	4.119	72.165	1.716	4.101	4.439	1.969	0.081	0.392	0.736	11.246	0.475	3.051	4.303	32.571	

APPENDIX C: 2D EULER MAGNETIC PROFILE SECTIONS

I. INTERPRETATION FOR PROFILE T1 – T′1

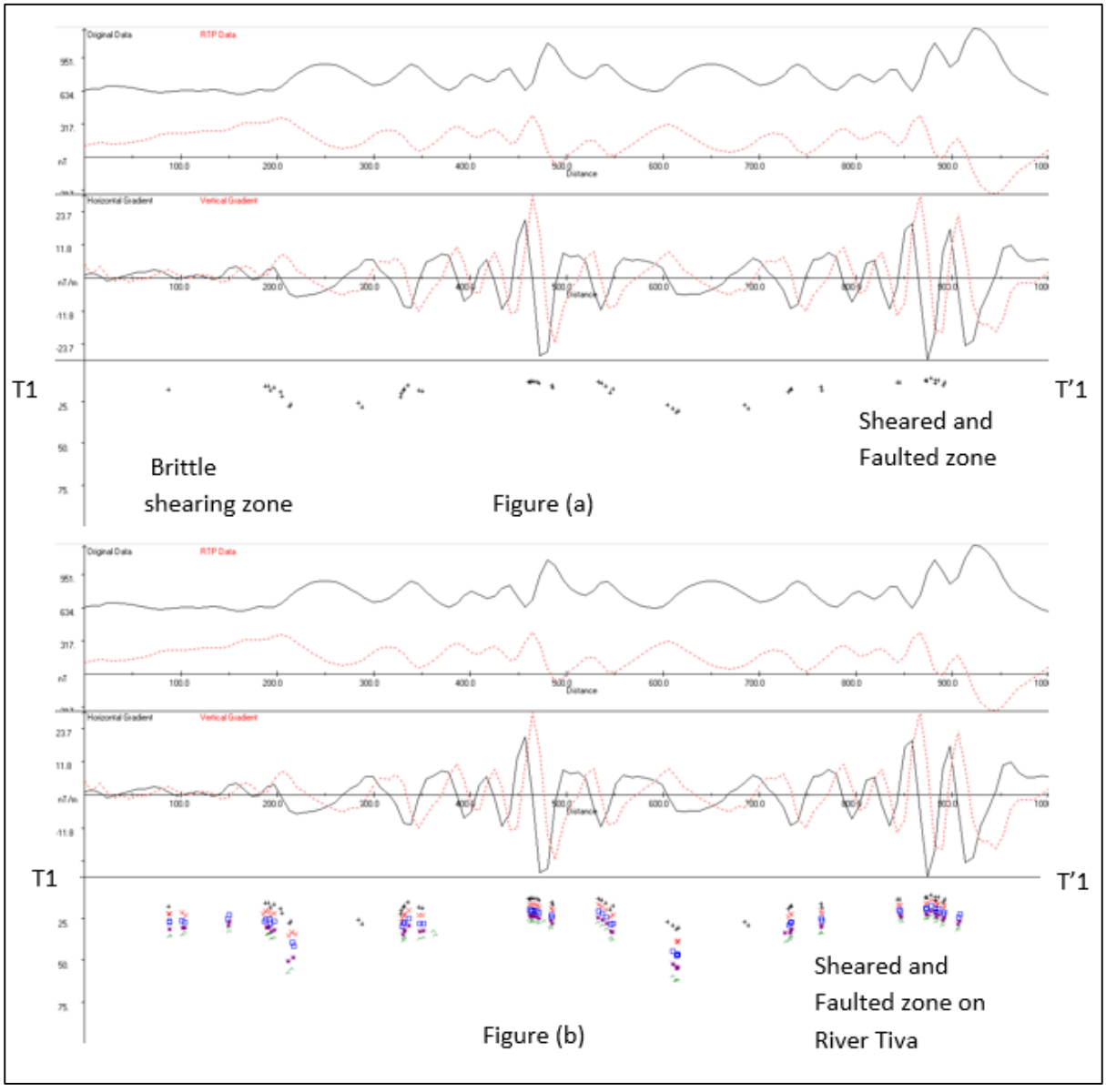

Figure A1: (a); Schematic section of profile T1 - T′1 through a sheared and faulted showing the underlying mineralization. (b); structural index pseudo -section showing faulting and shearing.

II. INTERPRETATION OF PROFILE T2 - T′2

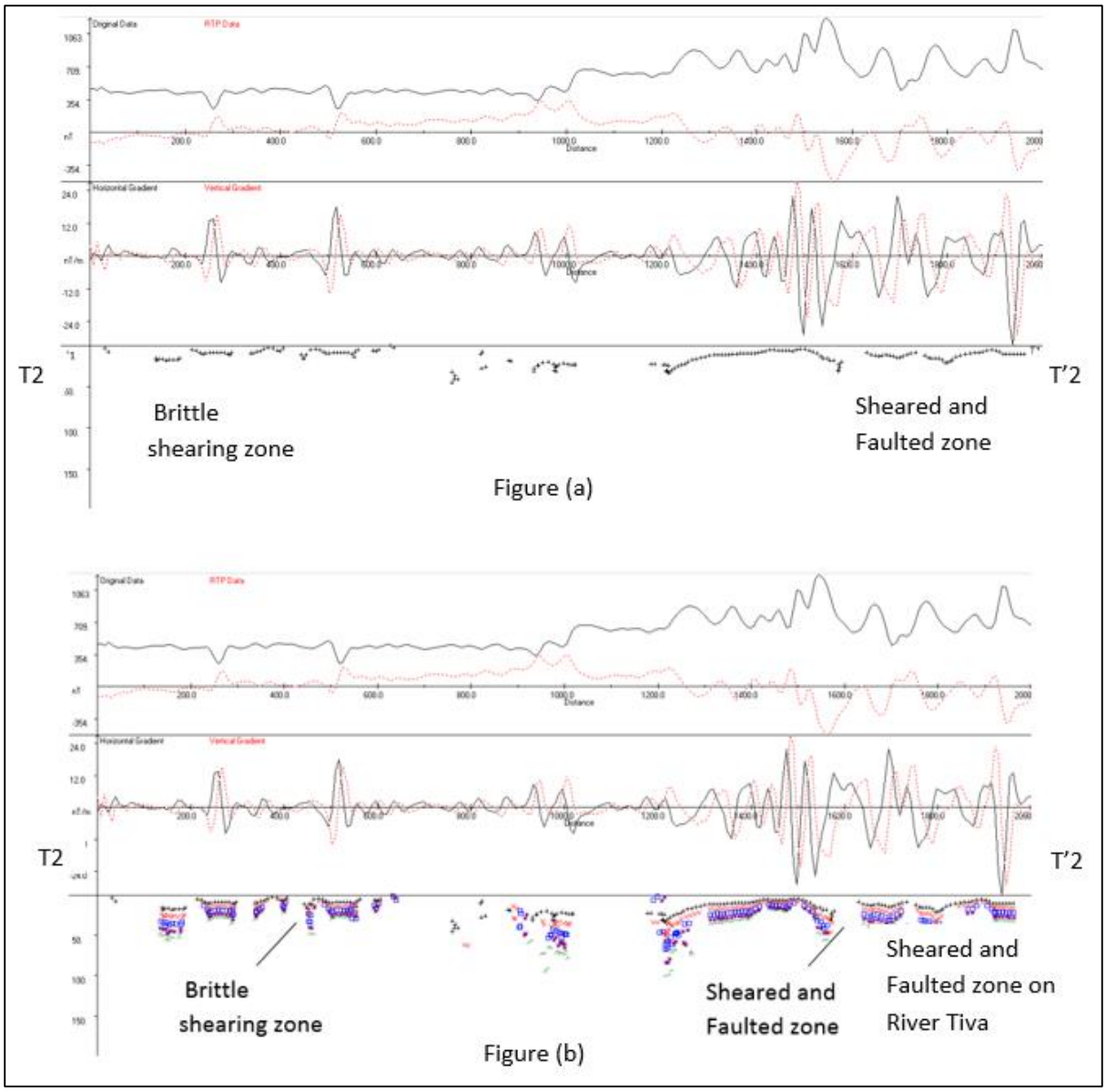

Figure A2: (a); Schematic section of profile T2 - T′2 through a sheared and faulted showing the underlying mineralization. (b); structural index pseudo -section showing faulting and shearing.

III. INTERPRETATION OF PROFILE T3 - T′3

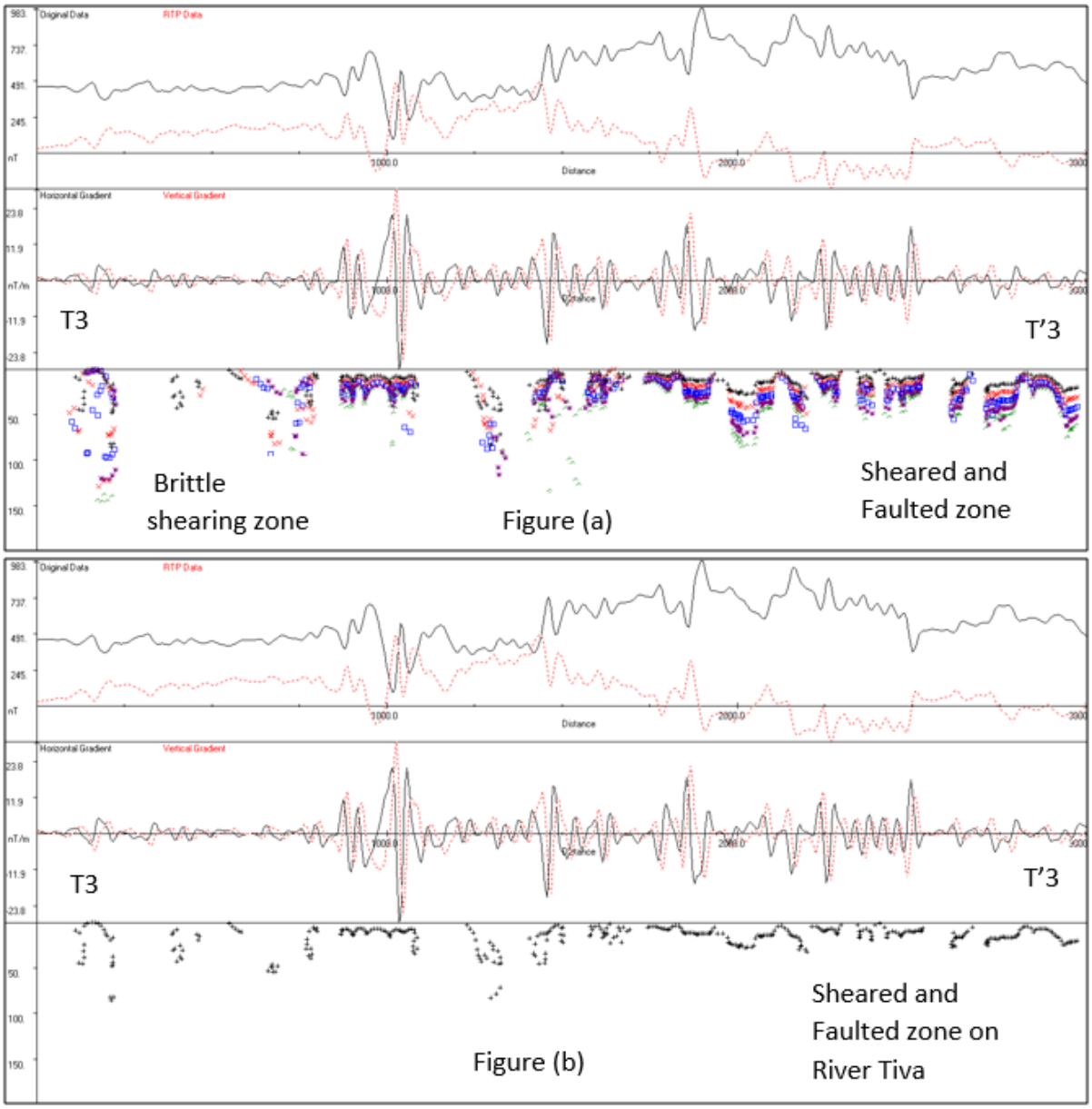

Figure A3: (a); Schematic section of profile T3 - T′3 through a sheared and faulted showing the underlying mineralization. (b); structural index pseudo -section showing faulting and shearing.

IV. INTERPRETATION OF PROFILE T4 - T′4

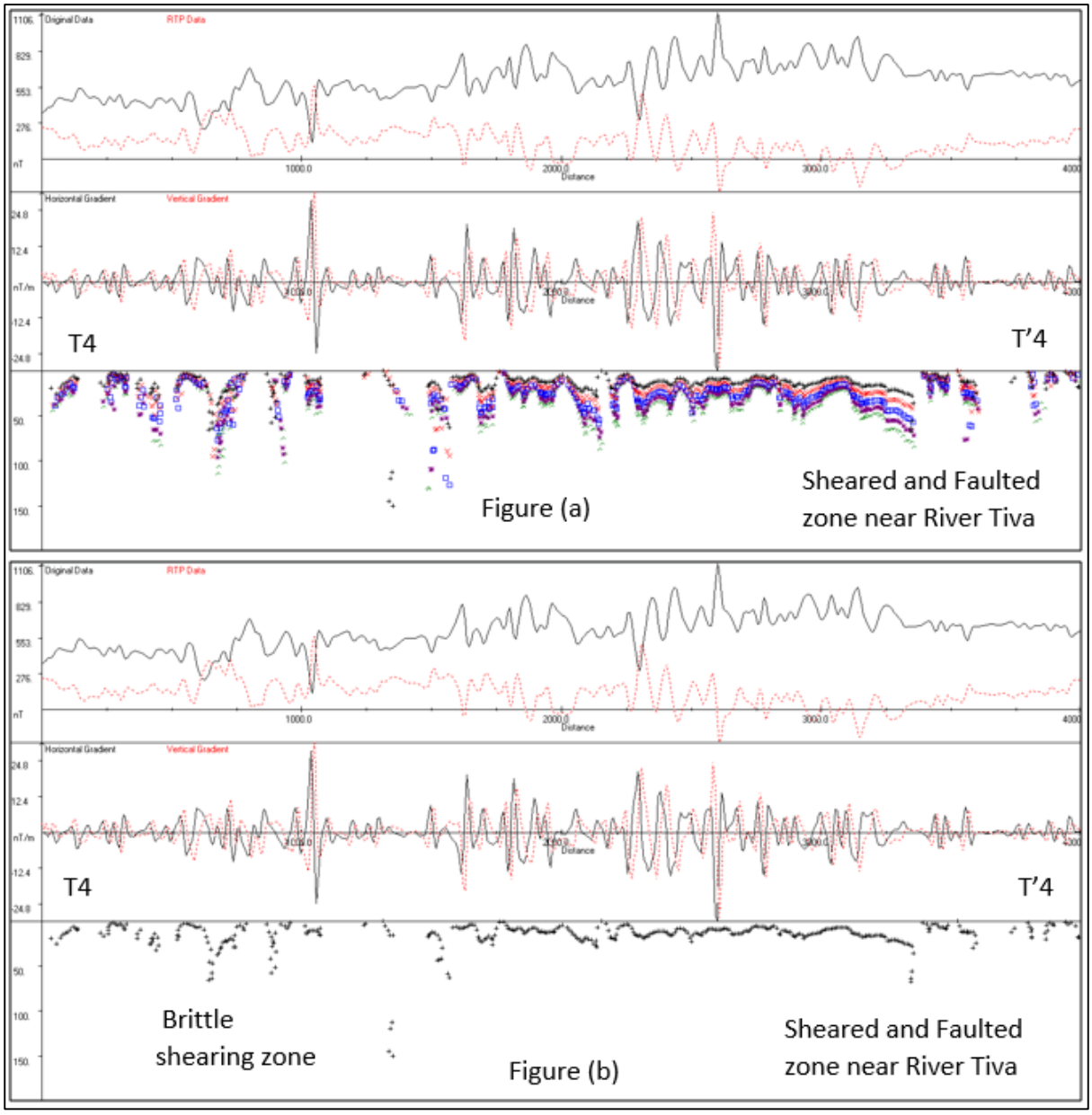

Figure A4: (a); Schematic section of profile T4 - T′4 through a sheared and faulted showing the underlying mineralization. (b); structural index pseudo -section showing faulting and shearing.

V. INTERPRETATION OF PROFILE T5 - T′5

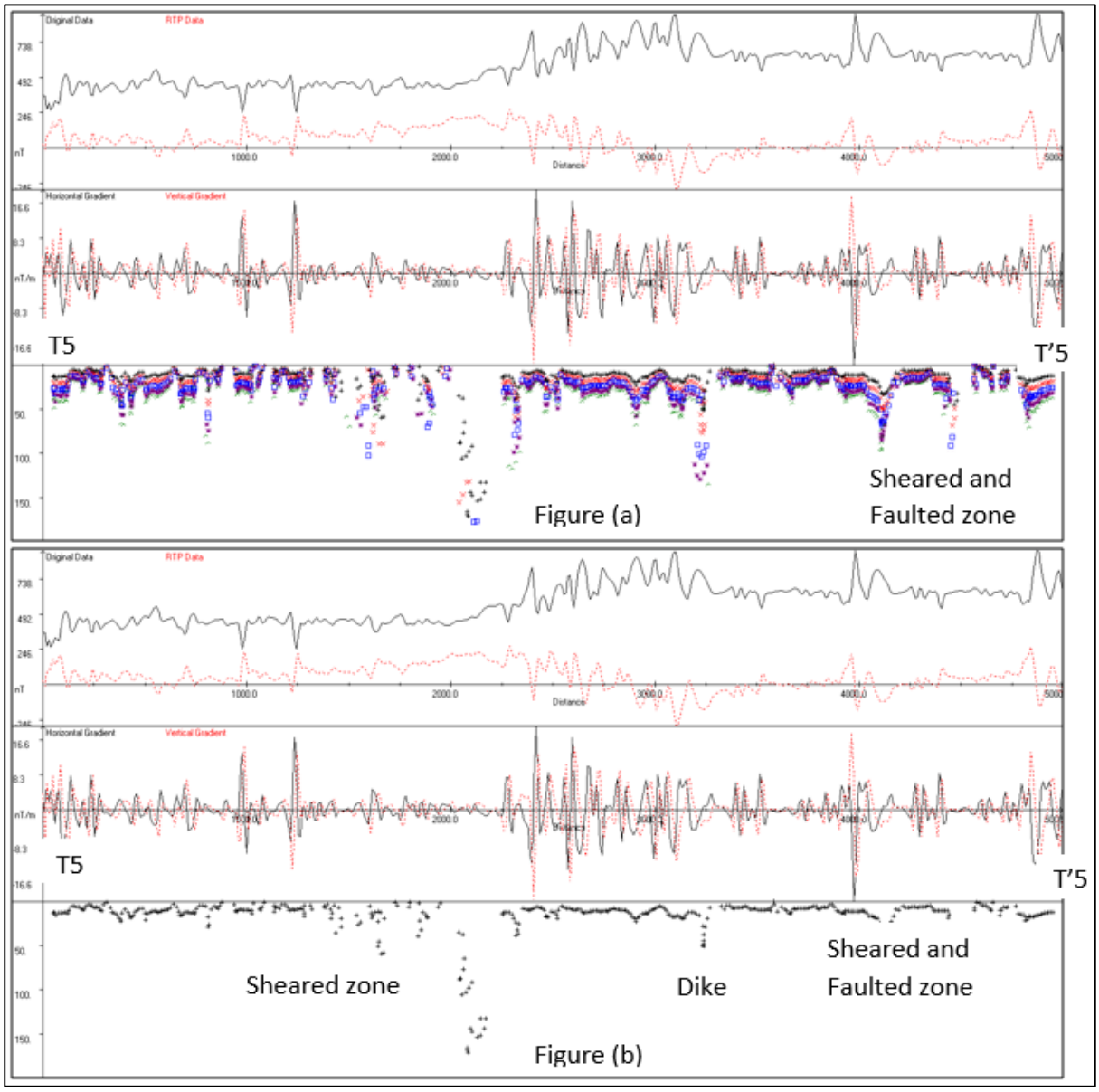

Figure A5: (a); Schematic section of profile T15 - T′15 through a sheared and faulted showing the underlying mineralization. (b); structural index pseudo -section showing faulting and shearing.

VI. INTERPRETATION OF PROFILE T6 - T′6

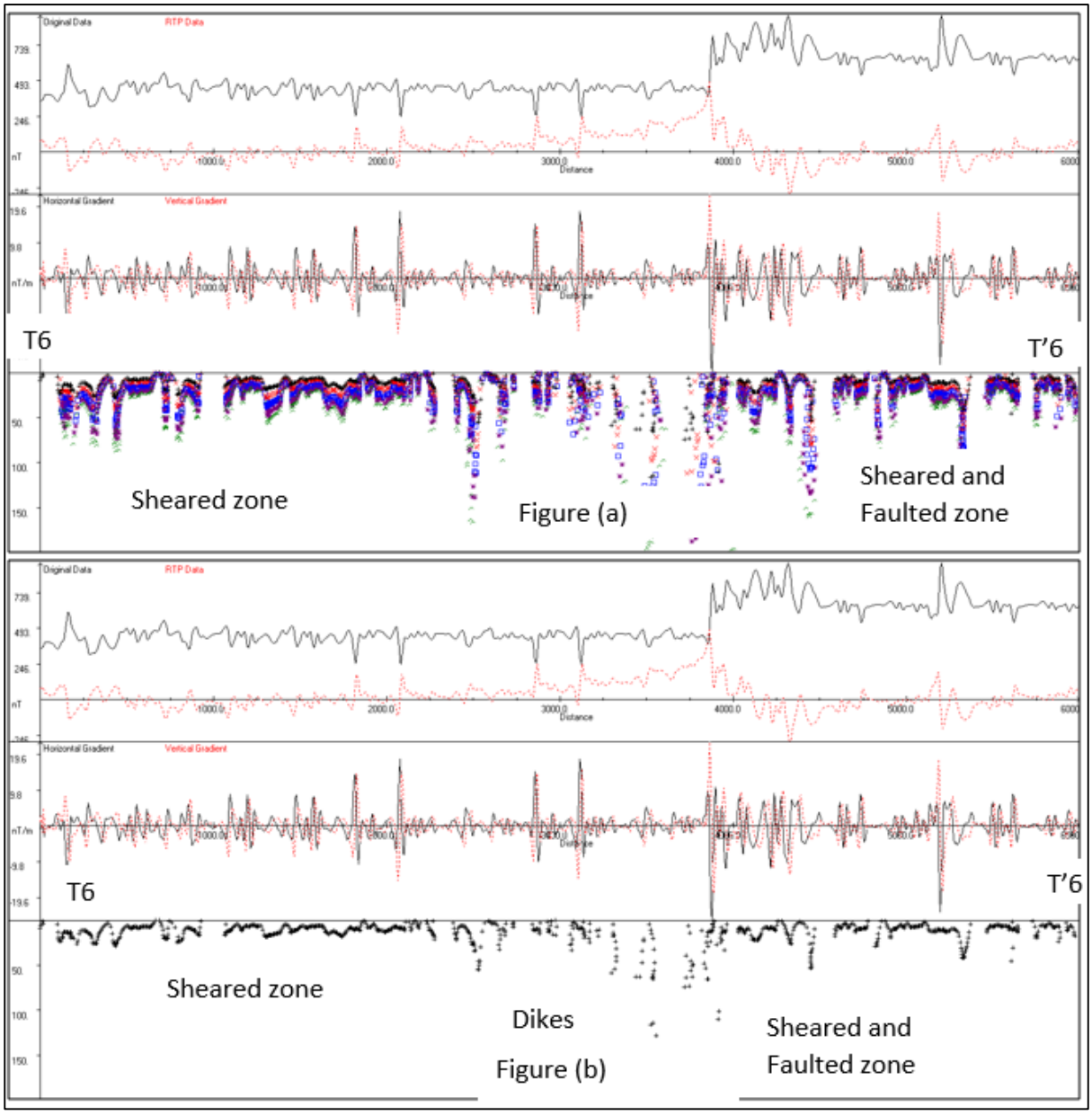

Figure A6: (a); Schematic section of profile T6 - T′6 through a sheared and faulted showing the underlying mineralization. (b); structural index pseudo -section showing faulting and shearing.

VII. INTERPRETATION OF PROFILE T7 - T′7

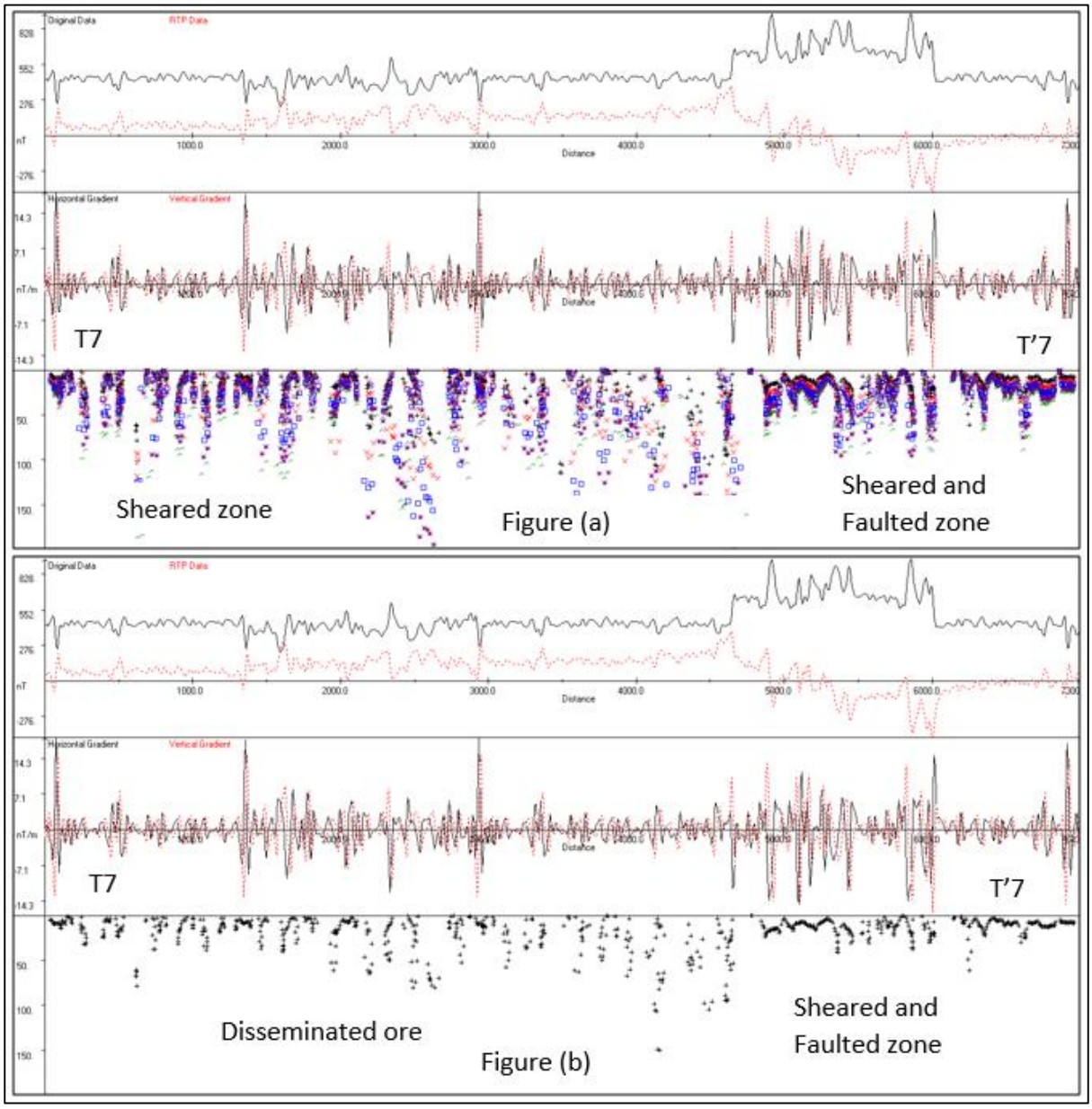

Figure A7: (a); Schematic section of profile T7 - T′7 through a sheared and faulted showing the underlying mineralization. (b); structural index pseudo -section showing faulting and shearing.

VIII. INTERPRETATION OF PROFILE T8 - T′8

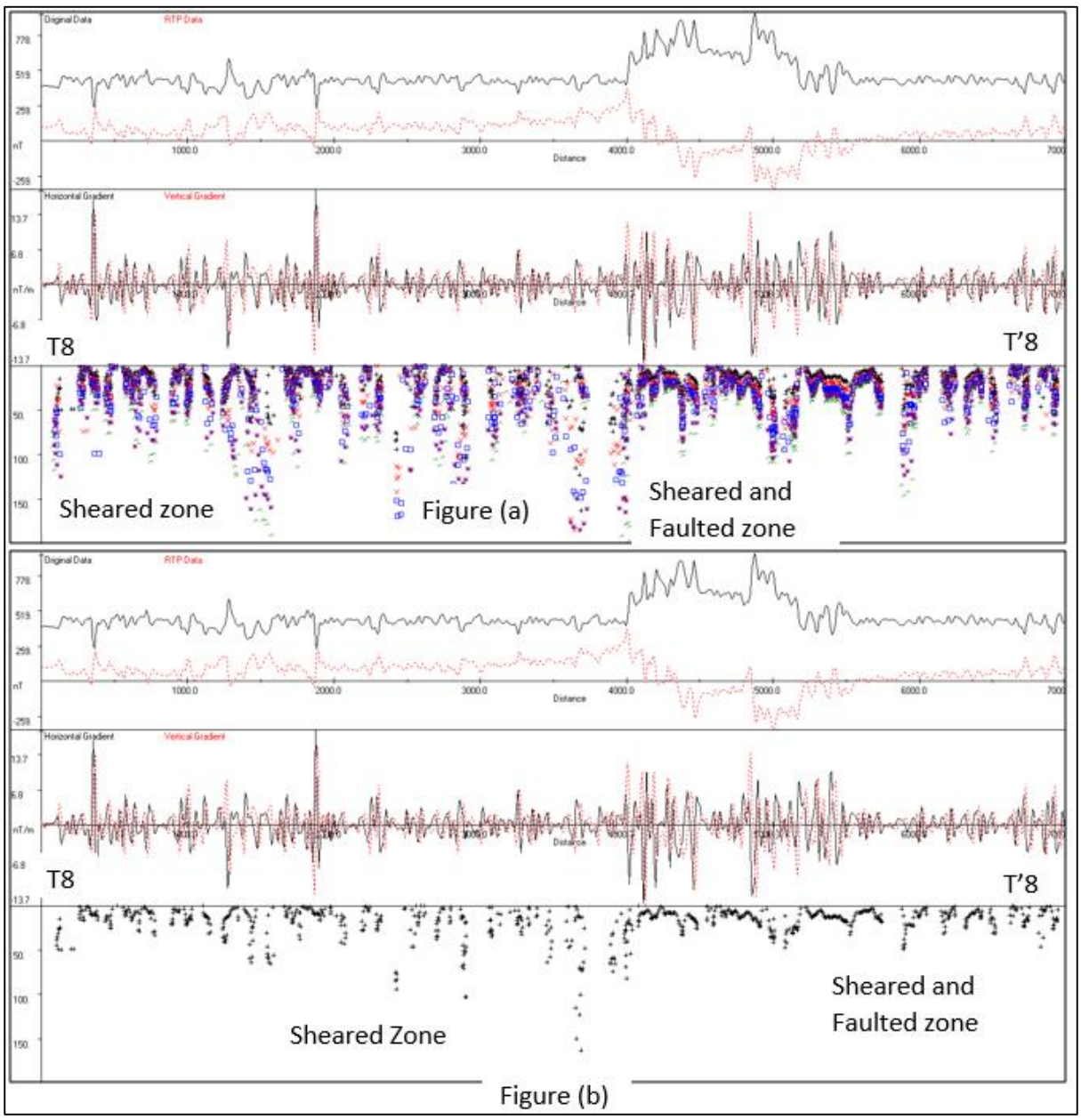

Figure A8: (a); Schematic section of profile T8 - T′8 through a sheared and faulted showing the underlying mineralization. (b); structural index pseudo -section showing faulting and shearing.

IX. INTERPRETATION OF PROFILE T9 - T′9

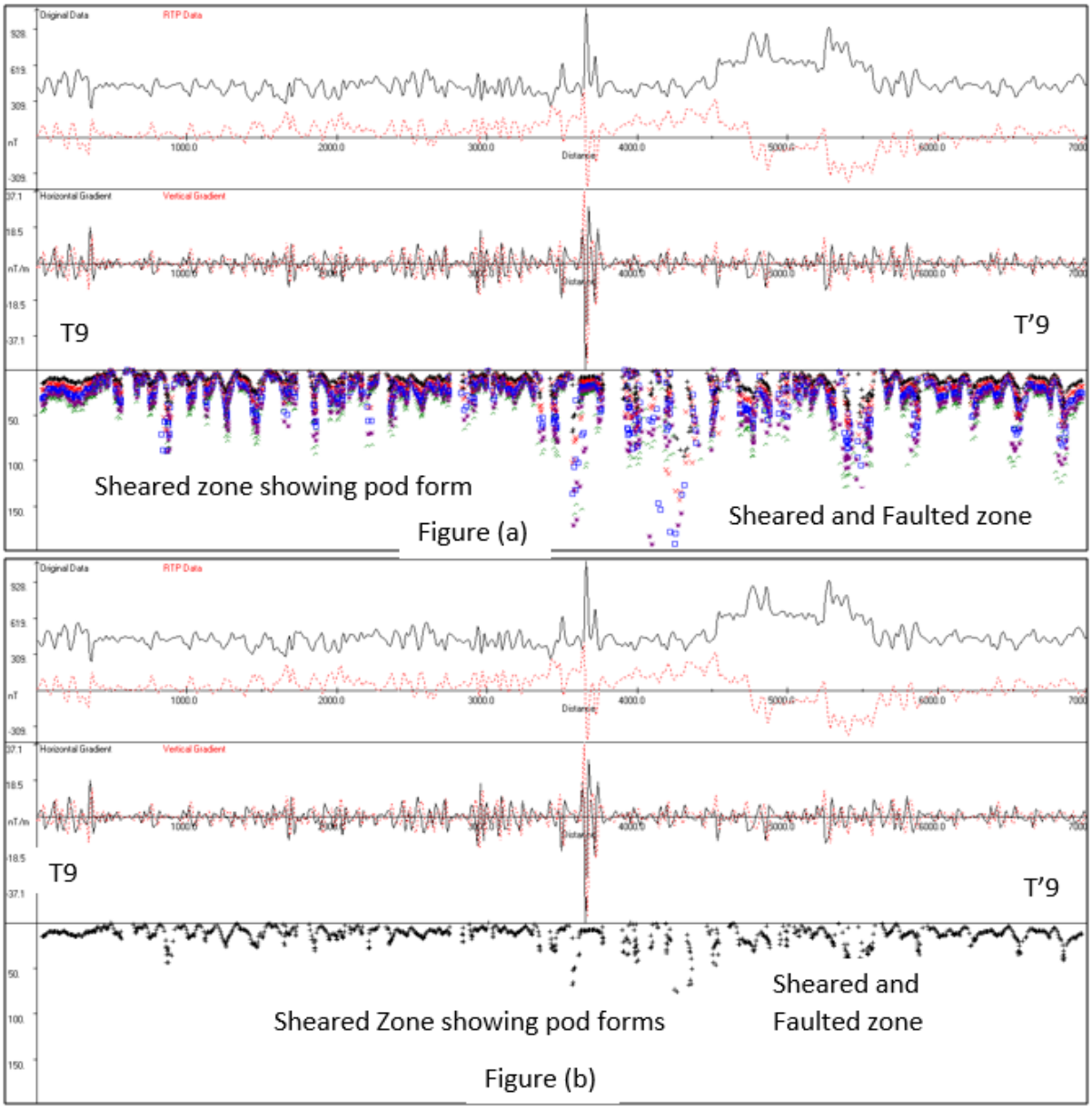

Figure A9: (a); Schematic section of profile T9 - T′9 through a sheared and faulted showing the underlying mineralization. (b); structural index pseudo -section showing faulting and shearing.

X. INTERPRETATION OF PROFILE T10 - T′10

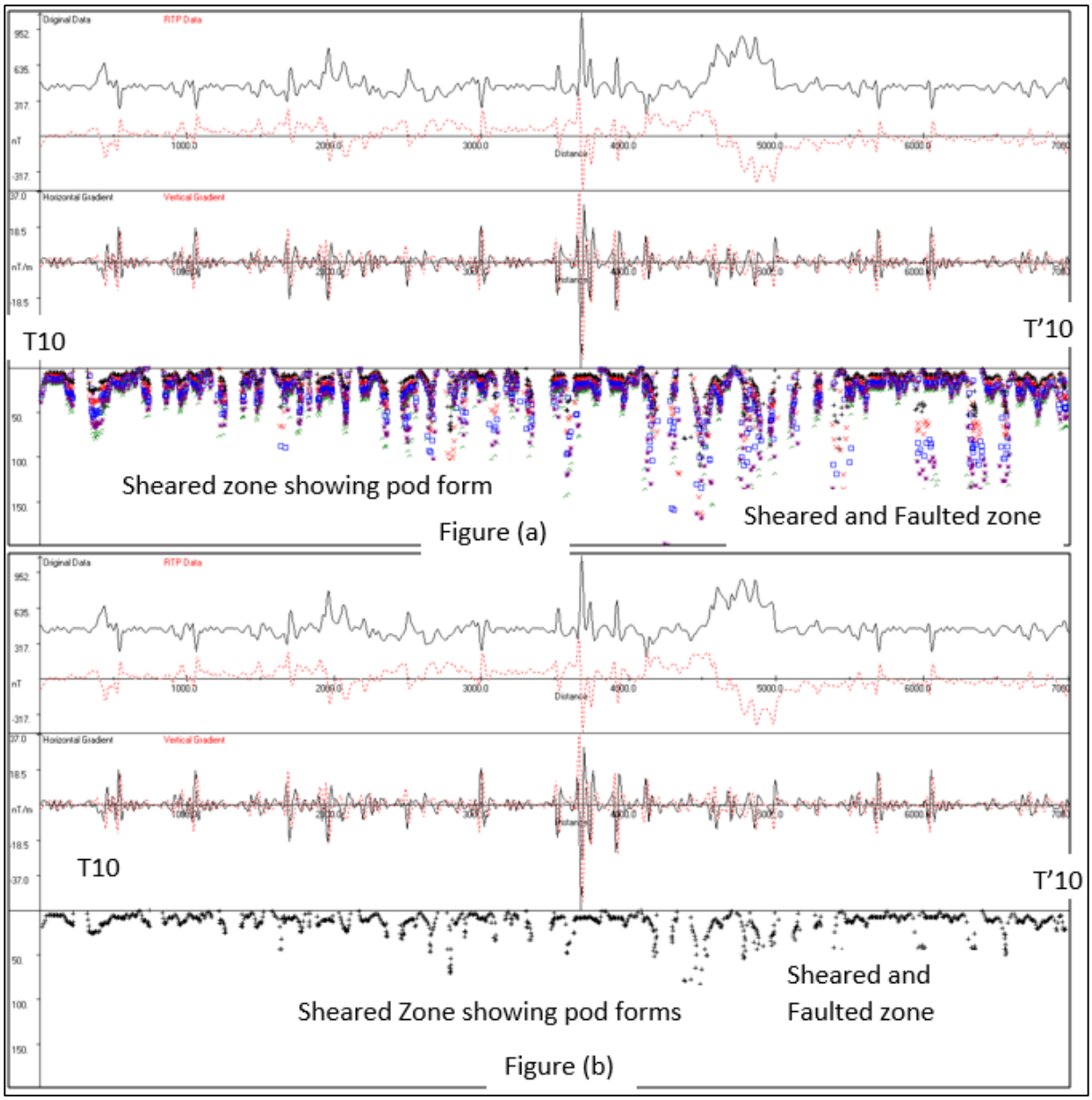

Figure A10: (a); Schematic section of profile T10 - T′10 through a sheared and faulted showing the underlying mineralization. (b); structural index pseudo -section showing faulting and shearing.

XI. INTERPRETATION OF PROFILE T11 - T′11

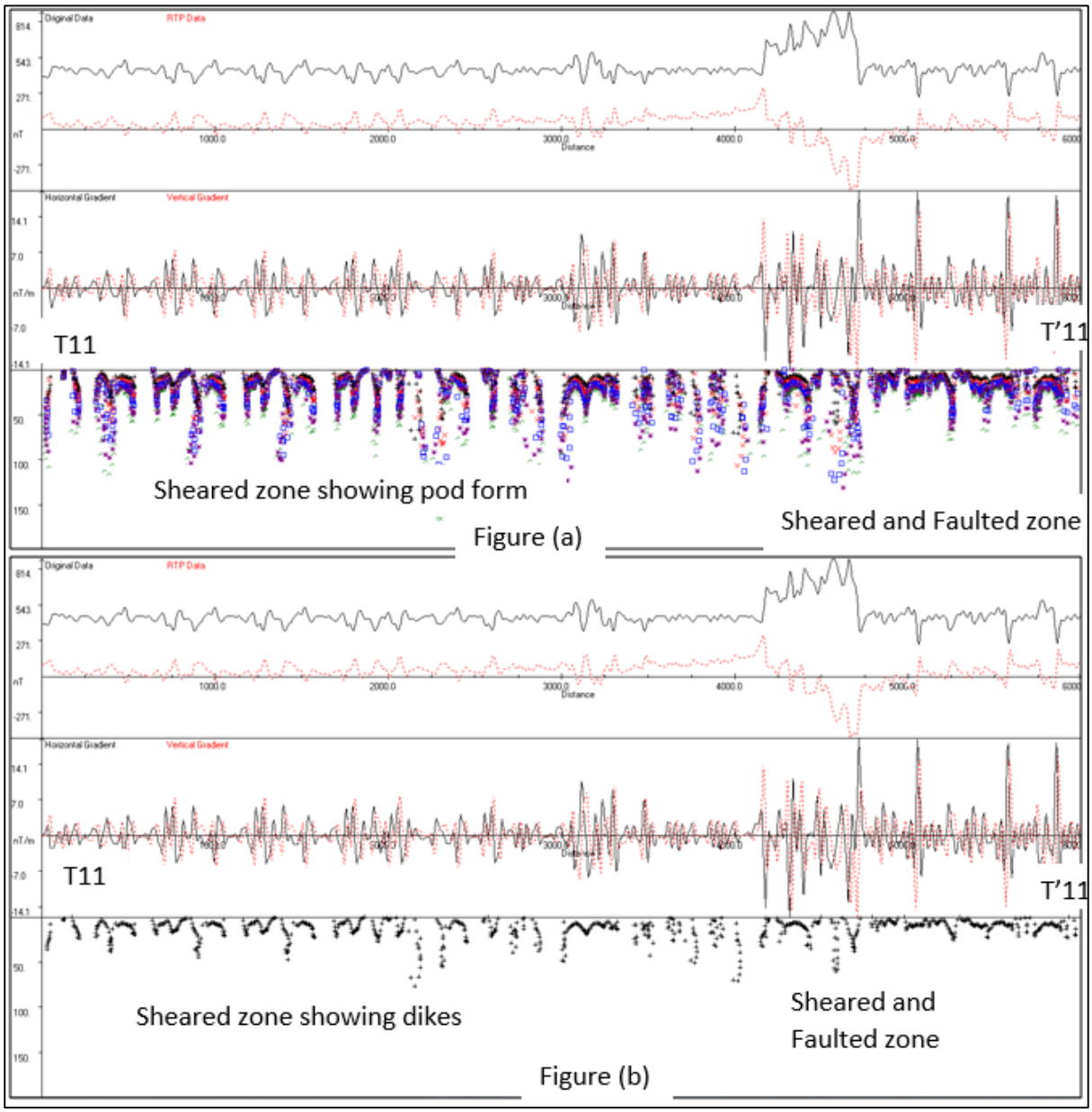

Figure A11: (a); Schematic section of profile T11 - T′11 through a sheared and faulted showing the underlying mineralization. (b); structural index pseudo -section showing faulting and shearing.

XII. INTERPRETATION OF PROFILE T12 - T′12

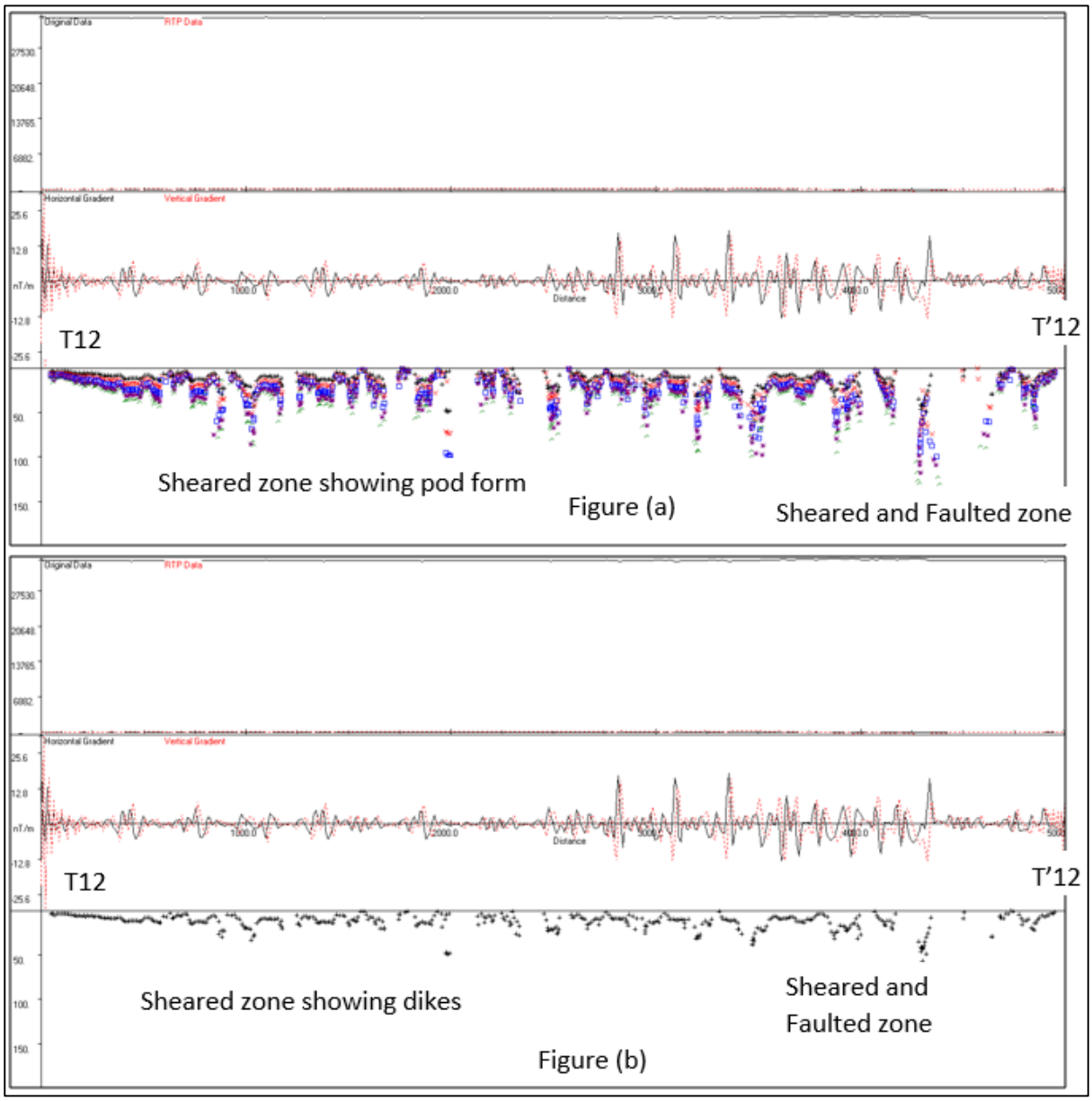

Figure A12: (a); Schematic section of profile T12 - T′12 through a sheared and faulted showing the underlying mineralization. (b); structural index pseudo -section showing faulting and shearing.

XIII. INTERPRETATION OF PROFILE T13 - T′13

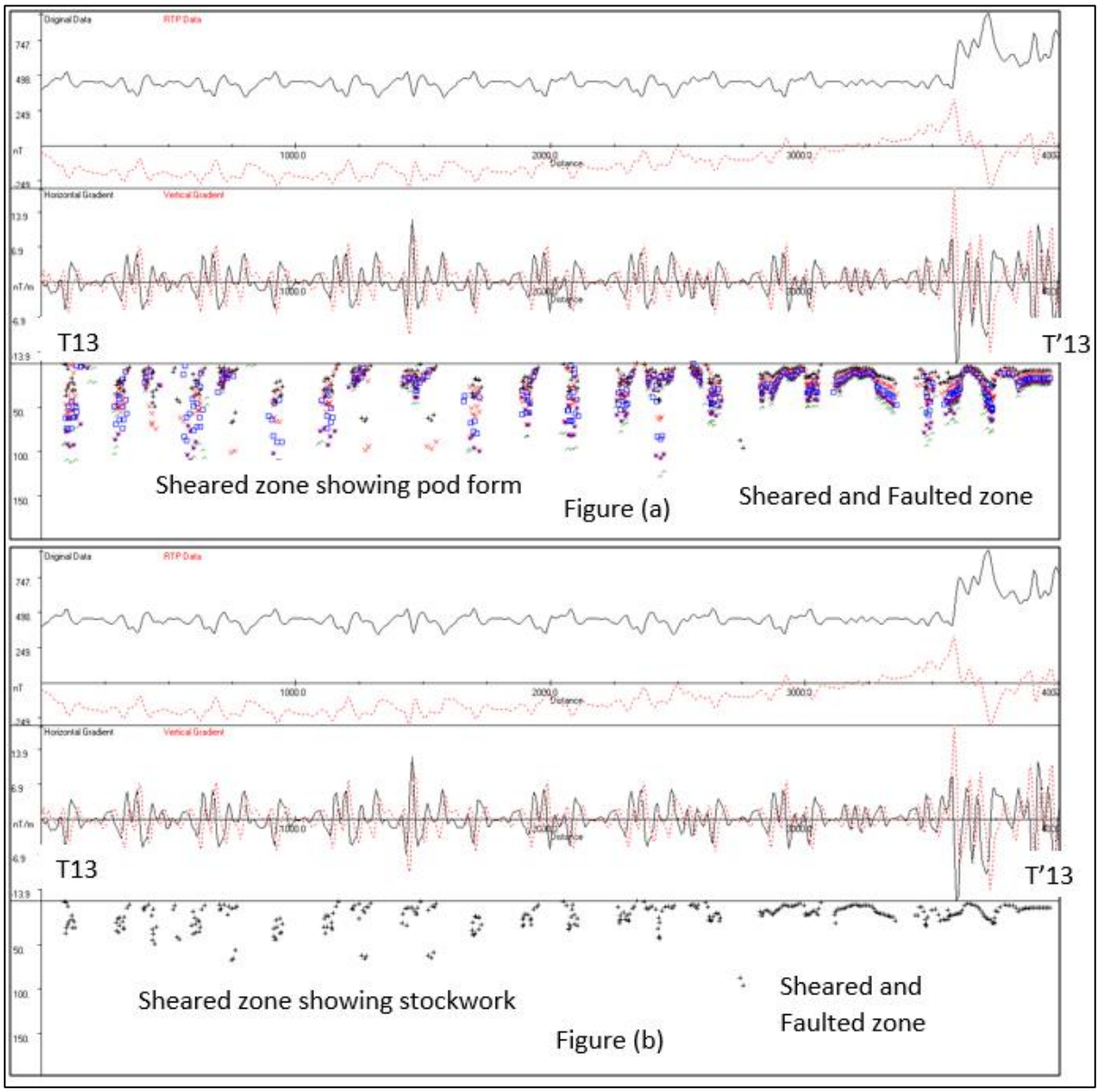

Figure A13: (a); Schematic section of profile T13 - T′13 through a sheared and faulted showing the underlying mineralization. (b); structural index pseudo -section showing faulting and shearing.

XIV. INTERPRETATION OF PROFILE T 14 - T′14

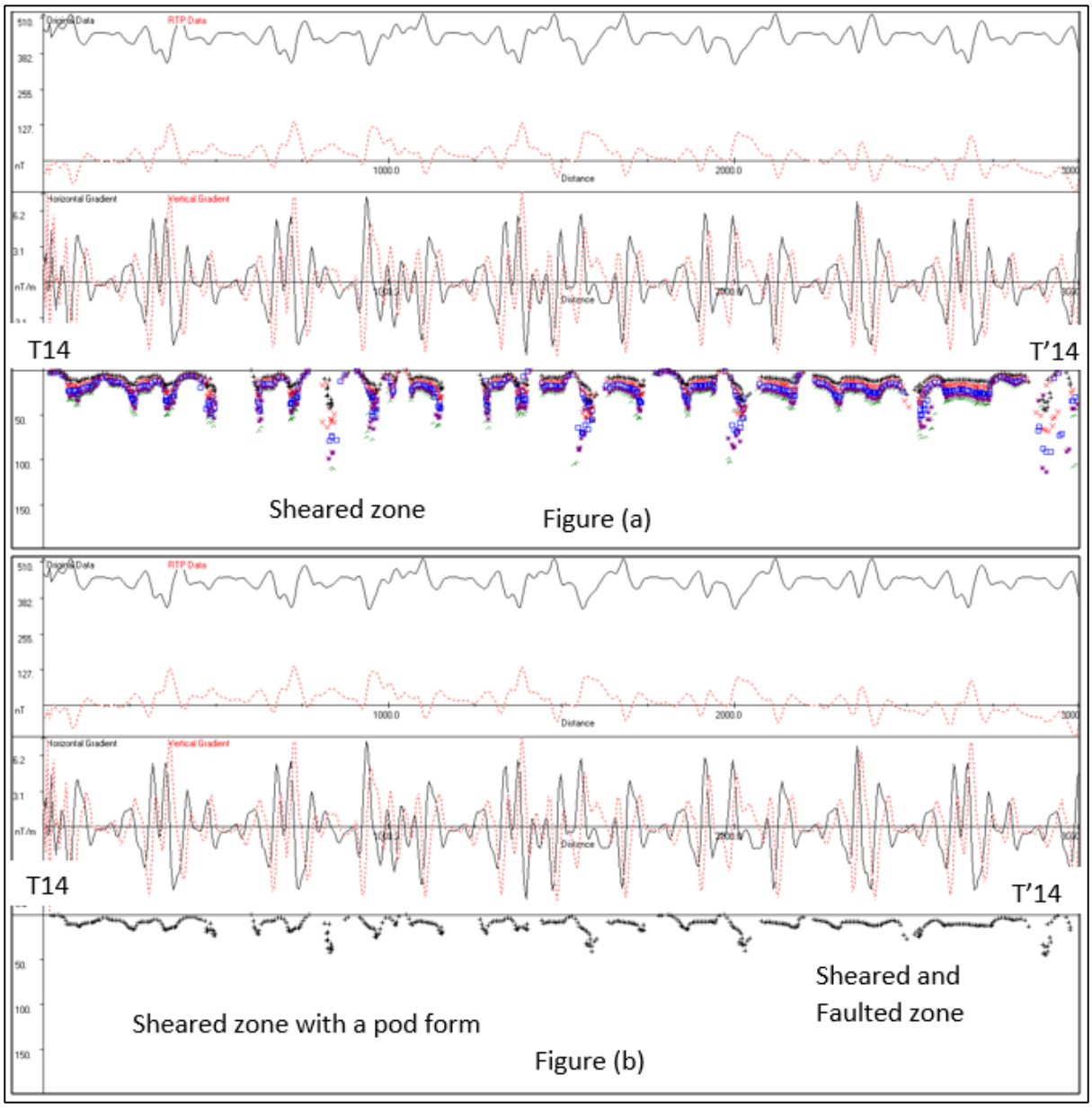

Figure A14: (a); Schematic section of profile T14 - T′14 through a sheared and faulted showing the underlying mineralization. (b); structural index pseudo -section showing faulting and shearing.

XV. INTERPRETATION OF PROFILE T15 - T′15

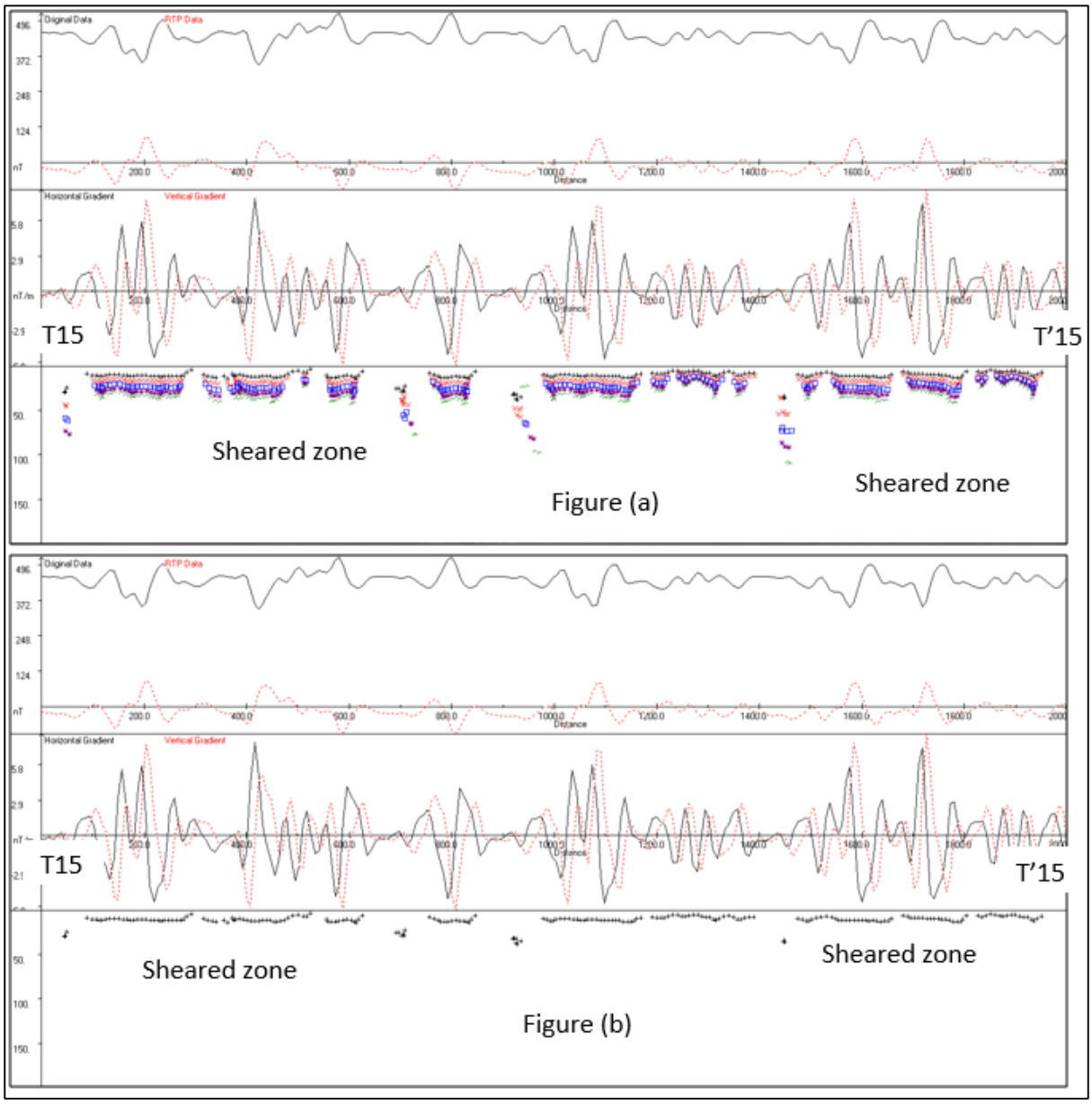

Figure A15: (a); Schematic section of profile T15 - T′15 through a sheared and faulted showing the underlying mineralization. (b); structural index pseudo -section showing faulting and shearing.

XVI. INTERPRETATION OF PROFILE T16 - T′16

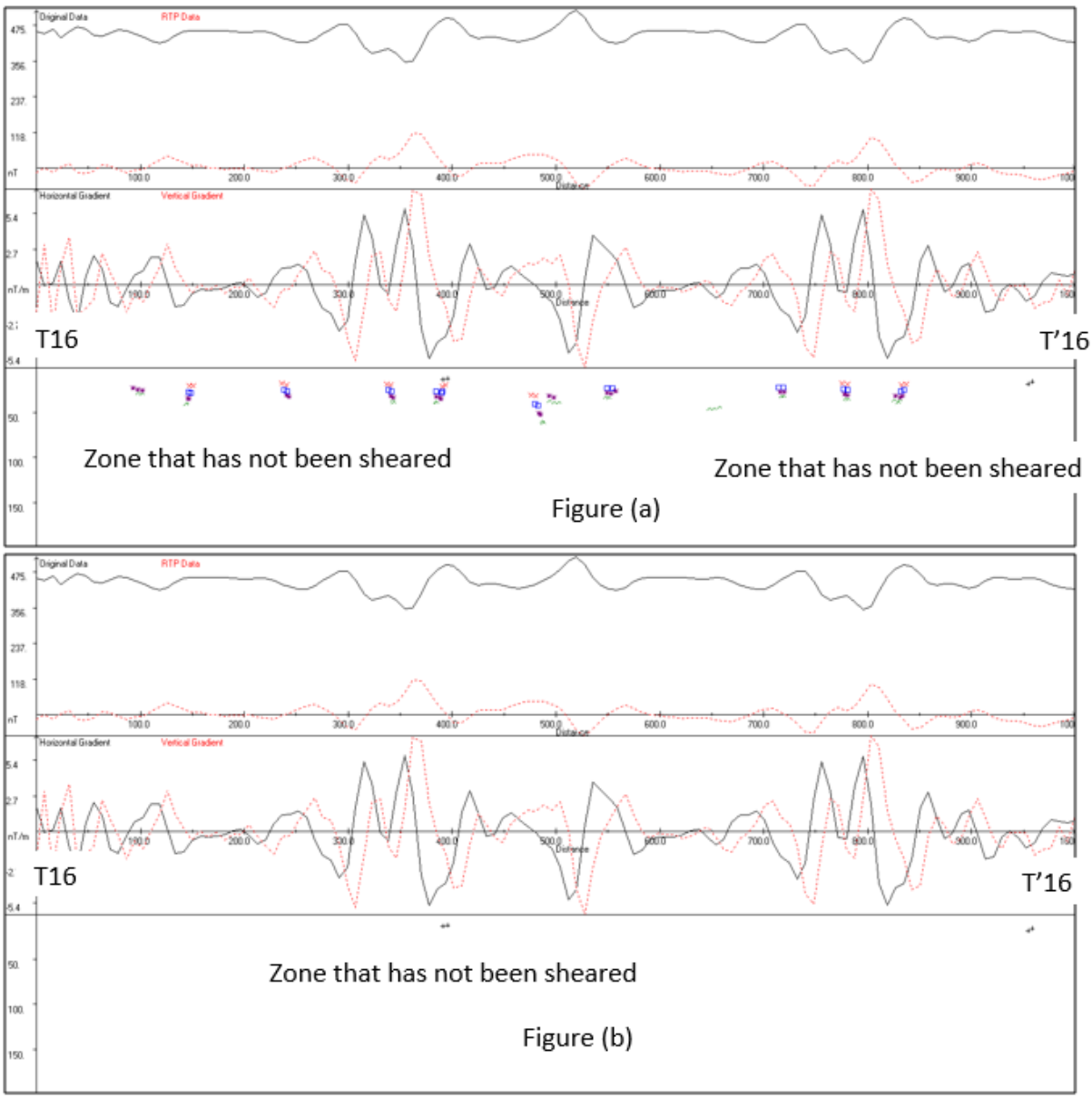

Figure A16: (a); Schematic section of profile T16 - T′16 through a sheared and faulted showing the underlying mineralization. (b); structural index pseudo -section showing faulting and shearing.